Tampere University

HEIDI TEPPOLA-GÜREL

Rodent and Human Neuronal Networks

Analysis of Functional Maturation, Synaptic Transmission, and Spontaneous Activity *in Vitro*

Tampere University Dissertations 576

Tampere University Dissertations 576

HEIDI TEPPOLA-GÜREL

Rodent and Human Neuronal Networks

Analysis of Functional Maturation, Synaptic Transmission, and Spontaneous Activity *in Vitro*

ACADEMIC DISSERTATION
To be presented, with the permission of
the Faculty of Medicine and Health Technology
of Tampere University,
for public discussion online in the auditorium S2
of the Sähkötalo Building, Korkeakoulunkatu 3, Tampere,
on 22 April 2022 at 12 o'clock.

ACADEMIC DISSERTATION
Tampere University, Faculty of Medicine and Health Technology
Finland

Responsible supervisor and Custos	Docent Marja-Leena Linne Tampere University Finland	
Pre-examiners	Professor Emeritus Jaap van Pelt Vrije Universiteit Amsterdam The Netherlands	Professor Raoul-Martin Memmesheimer University of Bonn Germany
Opponent	Professor Maria Victoria Sanchez-Vives University of Barcelona Spain	

The originality of this thesis has been checked using the Turnitin OriginalityCheck service.

Cover design: Roihu Inc.

ISBN 978-952-03-2345-5 (print)
ISBN 978-952-03-2346-2 (pdf)
ISSN 2489-9860 (print)
ISSN 2490-0028 (pdf)
http://urn.fi/URN:ISBN:978-952-03-2346-2

PunaMusta Oy – Yliopistopaino
Joensuu 2022

To Eeli and Ayla

Trust in dreams, for in them is hidden the gate to eternity.
–Khalil Gibran

ACKNOWLEDGEMENTS

The research of this thesis was conducted at the Faculty of Medicine and Health Technology, Tampere University, Finland. The research was started at (previous) Tampere University of Technology in a collaboration with the Department of Cell Biology at the University of Tampere. Part of the research was conducted at Bernstein Center & Department of Microsystems Engineering, Albert-Ludwig University of Freiburg, Germany.

I would like to express my sincere gratitude to my supervisor, Principal Investigator, Group Leader Marja-Leena Linne, PhD, Docent, for her excellent supervision, encouragement, and support for my research. I thank her for introducing me to the fields of neuroscience and computational neuroscience, and for offering several opportunities to develop myself by completing part of this research at the University of Freiburg and attending several international courses and conferences. These opportunities have enhanced my scientific career and experience. Words are not enough to express my gratitude.

The official reviewers of my thesis, Professor Emeritus Jaap van Pelt, PhD, and Professor Raoul-Martin Memmesheimer, PhD, are deeply acknowledged for their careful review and constructive comments. The reviews certainly improved the quality of my thesis.

I greatly acknowledge Professor Emerita Tuula O. Jalonen, PhD, for her long-term collaboration, guidance, and support for scientific thinking and writing, especially in human neuroblastoma research. I want to thank her for the invaluable advice and ideas I have received during this scientific journey.

I cordially thank Professor Ulrich Egert, PhD, for his supervision in rodent MEA recordings and data analysis and for the opportunity to work as a visiting researcher in his electrophysiology laboratory at the University of Freiburg, Germany. I would like to thank Mr. Patrick Pauli and Ms. Ute Riede for their technical support.

I sincerely thank Professor Timo Yli-Komi, MD, PhD, for the opportunity to work in his cell biology laboratory at the University of Tampere, Finland. I wish to thank Ms. Mirja Hyppönen, Ms. Hilkka Mäkinen, and Ms. Paula Helpiölä for their technical assistant.

I am deeply thankful to my co-authors and colleagues Jugoslava Aćimović, PhD, Tuomo Mäki-Marttunen, PhD, Samora Okujeni, PhD, Jertta-Riina Uusimies (née Sarkanen), PhD, Tiina Manninen, PhD, and Mikko Lehtimäki, MSc. This interdisciplinary work would not have been possible without their contributions. My sincere thanks are to Jugoslava and Tuomo for their long-term cooperation, their guidance in data analysis, and their commitment to build computational models based on my experimental data. I cordially thank Riina for her guidance in human cell research. I greatly thank Samora for his guidance in rodent network culturing, MEA recordings, and data analysis. I would also like to thank Tiina, Mikko, and Editor Matthew James for proofreading some parts of my thesis.

Special thanks to my dear colleagues and friends in Tampere and Freiburg; Katri Holm, PhD, Eeva Toivari, PhD, Antti Pettinen, PhD, Pekka Ruusuvuori, PhD, Jyrki Selinummi, PhD, Kaisa-Leena Aho, PhD, Antti Saarinen, PhD, Jukka Intosalmi, PhD, Riikka Havela, MD, MSc, Oliver Weihberger, PhD, Steffen Kandler, PhD, Yury Zaytsev, PhD, Sarah Jarvis, PhD, Matthew Goddard, PhD, Imke Reimer, PhD, Patrick Dini, MSc, and Laura Keto, MSc.

I would like to acknowledge the financial support for the thesis from the Graduate School of Tampere University of Technology, Tampere Graduate School in Information Science and Engineering, Finnish Foundation for Economic and Technology Sciences, Finnish Foundation for Technology Promotion, Finnish Cultural Foundation (Central and Pirkanmaa Regional funds), Brain Research Society of Finland, and Finnish Brain Foundation sr.

I cordially thank my parents, Sari and Pentti, even though he is no longer with us. I thank my mother for always doing her best to support and encourage me. She has demanded the right amount of strength and independence, pushed me towards new challenges, and taken the best care of us. I wish to thank my father who always believed in my ability to succeed. I deeply thank my brother Harri for listening and encouraging me when needed.

I sincerely thank my "foster family" Marja, Pertti, Petteri, and Valtteri for their great support such as dinners, accommodation, transport, scientific drawings, and discussions, as well as the excellent company while working in Tampere.

My friends are greatly acknowledged for sharing the interest on many aspects of life with me. It is a wealth to know you all. With your support I have been able to relax and make this journey a long one. Thank you: Anna, Denis, Dorothea, Essi, Hanna, Hannah, Heidi, Iina, Katja, Kirsi, Maiju, Markus, Miia, Mirjami, Paulina, Piia, Pälvi, Suvi, Terhi, Tero, Tiina A., Tiina T., and Veera. Special thanks to Aki, Ali,

Anne, Esa, Kari, Liisa, Mauri, Mehlika, Nihat, Olli, Pia, Pirjo, Päivi, Riitta, Ritva, Timo, Tiina, and Tuula for their support.

Finally, I would like to deeply acknowledge my family Tayfun, Eeli, and Ayla – for their love and understanding. Thank you Eeli and Ayla for focusing my attention on the little wonders of life with your adorable personalities <3.

Vantaa, March 2022

Heidi Teppola-Gürel

ABSTRACT

The development of neuronal networks is a complex process that occurs during the embryonic and postnatal stages in mammals. Abnormalities in this process are known to lead to neurodevelopmental disorders. Spontaneous network activity, observed as repetitive network-wide bursts (NBs), is a hallmark of the functional maturation of developing neocortical networks in both sensory cortices *in vivo* and dissociated cortical cultures *in vitro*. NBs emerge in parallel with the formation of the network structure and synaptic transmission. Synaptic transmission between neurons is driven by excitatory AMPA (α-amino-3-hydroxy-5-methyl-4-isoxazolepropionic acid) and NMDA (N-methyl-D-aspartate acid) receptors as well as inhibitory $GABA_A$ (γ-amino butyric acid type A) receptors and their neurotransmitters. How these three ionotropic receptors affect the initiation, propagation, and termination of postnatal cortical NBs is not understood in detail.

The first aim of this compilation thesis is to characterize the role of synaptic transmission in spontaneous network activity in postnatal rat cortical networks *in vitro*. The second aim is to reinforce the utilization of multiunit time-series data obtained in the first aim in data-driven *in silico* modeling. The third aim of this thesis is to study the differentiation of human neuroblastoma cells towards neuronal phenotypes and networks and to characterize the key indicators of network structure and synapses.

In this thesis, I first characterized the contributions of synaptic AMPA, NMDA, and $GABA_A$ receptors to the initiation, propagation, and termination of NBs in postnatal rat cortical cultures. I recorded network activity with the microelectrode array (MEA) technique and pharmacologically antagonized synaptic receptors at the end of the third week *in vitro*. I then analyzed the recorded activity using several methods. Furthermore, I developed a data analysis procedure that supports the fitting and validation of computational spiking network models to quantitatively reproduce experimental results and study the effect of synaptic transmission on network dynamics *in silico*. Finally, I assessed the effects of estradiol, cholesterol, brain-derived neurotrophic factor, and retinoic acid on the level of neuronal differentiation in human neuroblastoma cells by analyzing the number of

proliferating nuclei, synaptic vesicles, and neurites in human cell networks at 10 days *in vitro*.

The results of this thesis show that each synaptic receptor type has a specific contribution to the dynamics of spontaneous network activity. Excitatory AMPA receptors initiate bursts by rapidly recruiting cells for network-wide activity, while NMDA receptors maintain the activity that has already been initiated. $GABA_A$ receptors inhibit the early onset phase of AMPA receptor-mediated activity and attenuate the termination phase of NMDA receptor-mediated bursts. The results clearly show an interaction between fast AMPA receptor-mediated excitation and $GABA_A$ receptor-mediated inhibition. In the presence of this interaction, the burst propagation patterns are rich and diverse. In the absence of this interaction, in contrast, bursts originate and propagate along the same pathways. The results of the thesis further describe how multiunit time-series data recorded by the MEA technique on rat cortical networks under pharmacology are analyzed to support the development of spiking network models. The results of this thesis also suggest that human neuroblastoma cells can be morphologically differentiated into neuronal phenotypes. Differentiation of these human cells increases neurite outgrowth and branching, neuron-neuron interactions, and the ability of cells to induce synaptic vesicle recycling. These findings are a prerequisite for the formation of proper neuronal network.

In conclusion, the studies presented in this thesis reveal for the first time how the three main mediators of synaptic transmission AMPA, NMDA, and $GABA_A$ receptors shape the dynamics of network activity, including the initiation, propagation, and termination of bursts in postnatal rat cortical networks *in vitro*. The data analysis presented in this thesis promotes the development of data-driven spiking network models. Such data-driven models can be used to study the complex dynamics of cellular mechanisms in network activity as well as to create and design new hypotheses that can be studied *in vitro* and *in vivo*. Finally, the results on human cell differentiation contribute to future studies comparing human neuroblastoma cell-based neuronal networks to rodent networks.

TIIVISTELMÄ

Hermosoluverkkojen kehittyminen on perustavanlaatuinen prosessi nisäkkäiden alkionaikaisissa ja syntymänjälkeisissä kehityksen vaiheissa. Tiedetään, että poikkeavuudet ja häiriöt tässä prosessissa johtavat hermostollisiin kehityshäiriöihin. Spontaani hermosoluverkon aktiivisuus eli verkon purskeaktiivisuus on tunnusomaista kehittyvien aivokuoren hermosoluverkkojen toiminnalliselle kypsymiselle sekä aistinvaraisessa aivokuoressa *in vivo* että aivokuorelta eristetyistä soluista muodostetussa kortikaalisessa soluviljelmässä *in vitro*. Kortikaalisen verkon purskeaktiivisuus syntyy samanaikaisesti hermosoluverkon rakenteen ja synaptisen viestinvälityksen muodostumisen kanssa. Synaptinen viestinvälitys siirtää tietoa hermosolusta toiseen. Sitä ohjaavat kiihdyttävät välittäjäaineet AMPA ja NMDA sekä estävä välittäjäaine GABA, kaikki omien spesifisten ionotrooppisten reseptoriensa kautta. Vielä ei täysin tiedetä, miten synaptinen viestinvälitys ionotrooppisten reseptorien kautta vaikuttaa kortikaalisen verkon purskeiden alkamiseen, etenemiseen ja päättymiseen vastasyntyneen rotan aivokuorelta eristetyissä hermosoluverkoissa *in vitro*, joten reseptorien vaikutusten parempi karakterisointi on erittäin tärkeää. Hermosoluverkon aktiivisuuden riippuvuutta synaptisesta viestinvälityksestä voidaan tutkia käyttämällä myös datavetoisia laskennallisia hermosoluverkkomalleja, joiden avulla voidaan perustella uusien biologisten hypoteesien ja kokeiden suunnittelua, luomista ja testaamista.

Tämän kokoelmaväitöskirjan tavoitteena on karakterisoida synaptisen viestinvälityksen roolia vastasyntyneen rotan aivokuoren hermosoluverkkojen spontaanissa purskeaktiivisuudessa *in vitro* ja lisätä kokeellisten tulosten hyödyntämistä datavetoisessa laskennallisessa mallinnuksessa *in silico*. Tässä väitöskirjassa kehitän rekisteröimäni datan analysointimenetelmän, joka tukee sekä neurobiologisiin kysymyksiin vastaamista, että keräämäni dataan perustuvien mallien sovittamista ja validointia kokeellisten tulosten toistamiseksi kvantitatiivisesti *in silico*-menetelmillä. Lisäksi yksi väitöskirjan tavoite on erilaistaa ihmisen neuroblastoomasoluja hermosolujen kaltaisiksi soluiksi ja soluverkoiksi.

Tässä väitöskirjassa karakterisoin synaptisten AMPA-, NMDA- ja $GABA_A$-reseptorien osuutta vastasyntyneiden rottien kortikaalisten hermosoluverkkojen purskeaktiivisuuden alkamisessa, etenemisessä ja päättymisessä. Tutkin vaikutuksia

rekisteröimällä sähköistä aktiivisuutta hermosoluverkon solujen ulkopuolelta monielektroditekniikalla ja samanaikaisesti manipuloimalla synaptisten reseptorien toimintaa farmakologisin keinoin kolme viikkoa kypsyneissä viljelmissä *in vitro*. Lisäksi analysoin eri farmakologisissa tilanteissa kortikaalisten verkkojen purskeista rekisteröityä monielektrodiaikasarjadataa usein eri tavoin, mukaan lukien tapa, joka tukee datavetoisen laskennallisen hermosoluverkkomallin sovittamista kokeellisten tulosten tuottamiseksi *in silico*. Lopuksi arvioin ihmisen neuroblastoomasolujen kykyä erilaistua fenotyypiltään hermosoluverkkojen kaltaisiksi estradiolin, kolesterolin, aivoista peräisin olevan neurotrofisen tekijän ja retinoiinihapon avulla. Arvioin näiden yhdisteiden vaikutukset verkon erilaistumiseen määrittämällä tumien ja synaptisen vesikkeleiden lukumäärää ja neuriittien kasvua 10 vuorokautta erilaistetuissa viljelmissä *in vitro*.

Väitöskirjan tulokset korostavat synaptisen viestinvälityksen merkitystä rotan kortikaalisen verkon purskeaktiivisuudessa. Tulokset osoittavat, että jokaisella synaptisella reseptorilla on erityinen vaikutus verkon aktiivisuuden dynamiikkaan. AMPA-reseptorit aloittavat ja osallistavat hermosolut nopeasti osaksi verkonlaajuisia purskeita, NMDA-reseptorit puolestaan ylläpitävät eteneviä purskeita. $GABA_A$-reseptorit estävät AMPA-reseptorivälitteisten verkon purskeiden varhaista vaihetta sekä vaimentavat NMDA-reseptorivälitteisten purskeiden päättymisvaihetta. Tulokset osoittavat ainutlaatuisen AMPA- ja $GABA_A$-reseptorivälitteisen vuorovaikutuksen nopeasti kiihdyttävien ja estävien reseptorien välillä. Vuorovaikutuksen puuttuessa verkon purskeet saavat alkunsa ja etenevät usein samaa reittiä pitkin. AMPA- ja $GABA_A$-reseptorien läsnä ollessa purskeiden aktivointitapa ja etenemisreitit ovat monimuotoisempia. Väitöskirjassa esitetään ensimmäistä kertaa, miten vastasyntyneiden rottien aivokuoren hermosoluverkoista rekisteröityä monielektrodiaikasarjadataa voidaan hyödyntää matemaattisten verkkoaktiivisuusmallien tukena *in silico*. Väitöskirjan tulokset ihmisen soluilla viittaavat siihen, että neuroblastoomasolut voidaan morfologisesti erilaistaa fenotyypiltään hermosolujen kaltaisiksi. Yhdistelmäkäsittely sisältäen estradiolia, kolesterolia ja retinoiinihappoa edesauttaa neuriittien kasvua ja haarautumista, kykyä tuottaa synaptista vesikkelikierrätystä sekä hermosoluverkon muodostumista ihmisen soluviljelmissä.

Yhteenvetona totean, että tässä väitöskirjassa selvitettiin, miten synaptisen viestinvälityksen kolme pääreseptoria muodostivat yksilöllisesti verkon purskeaktiivisuuden ominaisuuksia, kuten purskeiden syntyä, etenemistä ja päättymistä rotan aivokuoresta eristetyissä hermosoluverkoissa. Lisäksi väitöskirjassa esitetty analyysi kokeellisesti rekisteröidyistä aikasarjadatoista edisti datavetoisen

laskennallisen hermosoluverkkomallien kehittämistä, jota voidaan tulevaisuudessa käyttää ymmärtämään solumekanismien ja verkkotoiminnan monimutkaista dynamiikkaa. Väitöskirjassa kehitetty erilaistamismenetelmä mahdollistaa ihmisen soluihin pohjautuvan hermosoluverkon jatkotutkimukset esimerkiksi monielektroditekniikalla.

CONTENTS

List of Figures

List of Tables

ABBREVIATIONS

AMPA	α-amino-3-hydroxy-5-methyl-4-isoxazolepropionic acid
APs	action potentials
BDNF	brain-derived neurotrophic factor
BF	burst frequency
BL	burst length
BS	burst size
CC	correlation coefficient
Ca^{2+}	calcium ion
CAT	center of activity trajectory
cENOs	cortical early network oscillations
cGDPs	cortical giant depolarizing potentials
CHOL	3β-hydroxy-5-cholestene, cholesterol
CO_2	carbon dioxide
CSs	coverslips
CTNF	corrected total neurofilament fluorescence
CTRL	control
D-AP5	D(-)-2-amino-5-phosphonopentanoic acid
DNase	deoxyribonuclease
DI	deionized
DIV	days *in vitro*
E_2	17-β-estradiol
E	embryonic day
eRC	electrode recruitment count
FP	falling phase
FR	firing rate
$GABA_A$	γ-aminobutyric acid type A
GFR	global firing rate
HS	horse serum
IBI	interburst interval

ISI	interspike interval
K^+	potassium ion
LAM	laminin
L-gln	L-glutamine
Mg^{2+}	magnesium ion
MCS	Multi Channel Systems
MEAs	microelectrode arrays
MEM	minimum essential medium
MFR	maximal firing rate
Na^+	sodium ion
NF-68	neurofilament 68 kD
NB	network burst
NBQX	2,3-dioxo-6-nitro-1,2,3,4-tetrahydrobenzo [*f*]quinoxaline-7-sulfonamide
NMDA	*N*-methyl-$_D$-aspartate acid
6-OHDA	neurotoxin-6-hydroxydopamine
PBS	phosphate-buffered saline
P	postnatal day
PEI	polyethylene imine
PTX	picrotoxin
RA	retinoic acid
RB	retinoic acid with BDNF
RC	retinoic acid with CHOL
RCB	retinoic acid with CHOL and BDNF
RCBE	retinoic acid with CHOL, BDNF and E_2
RE	retinoic acid with E_2
RP	rising phase
RT	recruitment time
SD	standard deviation
STD	short-term synaptic depression
TrkB	tropomyosin-related kinase B
TPA	12-*O*-tetradecanoylphorbol-13-acetate

ORIGINAL PUBLICATIONS

Publication I **Teppola, H.**, Okujeni, S., Linne, M.-L., & Egert, U. (2011). AMPA, NMDA and $GABA_A$ Receptor Mediated Network Burst Dynamics in Cortical Cultures *in vitro*. In *Proceedings of the 8th International Workshop on Computational Systems Biology (WCSB2011)*, 8:181-184

Publication II **Teppola, H.**, Aćimović, J., & Linne, M.-L. (2019). Unique Features of Network Bursts Emerge from the Complex Interplay of Excitatory and Inhibitory Receptors in Rat Neocortical Networks. *Frontiers in Cellular Neuroscience*, 13(377). doi:10.3389/fncel.2019.00377

Publication III Aćimović, J., Mäki-Marttunen, T., **Teppola, H.**, & Linne, M.-L (2021). Analysis of Cellular and Synaptic Mechanisms behind Spontaneous Cortical Activity *in vitro*: Insights from Optimization of Spiking Neuronal Network Models. Submitted Manuscript. Available in: doi:10.1101/2021.10.28.466340

Publication IV **Teppola, H.**, Sarkanen, J.-R., Jalonen, T.O., & Linne, M.-L. (2016). Morphological Differentiation Towards Neuronal Phenotype of SH-SY5Y Neuroblastoma Cells by Estradiol, Retinoic Acid, and Cholesterol. *Neurochemical Research*, 41(4):731–747. doi:10.1007/s11064-015-1743-6

Publication V **Teppola, H.**, Sarkanen, J.-R., Jalonen, T.O., & Linne, M.-L. (2018). Impacts of Laminin and Polyethyleneimine Surface Coatings on Morphology of Differentiating Human SH-SY5Y Cells and Networks. In *Proceedings of the International Federation of Medical and Biological Engineering (IFMBE)*, 65:298-231. doi:10.1007/978-981-10-5122-7_75

AUTHOR'S CONTRIBUTION

The author of this thesis contributed to the publications as follows.

Publication I As the first author of Publication I, M.Sc. Heidi Teppola performed all the experiments, including the preparation of primary cell cultures from the postnatal rat prefrontal cortex, maintenance of cell cultures, microelectrode array recordings, and pharmacological experiments. Teppola also analyzed the electrophysiological data, performed interpretation of the results, prepared the figures, and wrote the manuscript. The research was designed, and the manuscript revised together with Dr. Samora Okujeni, Docent Marja-Leena Linne, and Prof. Ulrich Egert.

Publication II As the first author of Publication II, M.Sc. Heidi Teppola developed Matlab scripts to process and analyze the multi-unit spike data which she had recorded using microelectrode arrays and presented in Publication I. Teppola interpreted the results, prepared the figures, and wrote the manuscript. The research was designed, the results were discussed, and the manuscript was revised together with Dr. Jugoslava Aćimović and Docent Marja-Leena Linne.

Publication III As the third author of Publication III, M.Sc. Heidi Teppola reprocessed and analyzed the multi-unit spike data that she had recorded in Publications I and II. Specifically, Teppola had a role in data curation and data analysis, and she provided the statistical measures for the training and validation of the model. The data was re-analyzed to maximally support the fitting of computational modeling of spontaneous network burst dynamics in Publication III. Dr. Jugoslava Aćimović and Dr. Tuomo Mäki-Marttunen developed the models, performed the simulations, and analyzed the modeling results. The simulated results were interpreted and compared to experimental data by all authors. Aćimović was responsible for leading the writing process and wrote the first versions of the manuscript. The research was designed, and the manuscript was revised together with Aćimović, Mäki-Marttunen, and Docent Marja-Leena Linne.

Publication IV As the first author of Publication IV, M.Sc. Heidi Teppola performed the experiments, including the preparation, maintenance,

and differentiation of cell cultures, immunocytochemical stainings, analysis of the image data with ImageJ, CellC, NeuronGrowth, and Matlab, interpretation of the results, preparation of the figures, and writing of the manuscript. The research was designed, and the manuscript revised together with Dr. Jertta-Riina Sarkanen, Prof. Tuula Orvokki Jalonen, and Docent Marja-Leena Linne.

Publication V As the first author of Publication V, M.Sc. Heidi Teppola designed the research, performed the experiments, including the preparation of surface coatings, maintenance, and differentiation of cell cultures, immunocytochemical stainings, analysis of the data, interpretation of the results, preparation of the figures, and writing of the manuscript. The results were discussed, and the manuscript revised together with Dr. Jertta-Riina Sarkanen, Prof. Tuula Orvokki Jalonen, and Docent Marja-Leena Linne.

This thesis work was supervised by Docent Marja-Leena Linne.

1 INTRODUCTION

1.1 Background and motivation

Cognitive functions, such as action planning, working memory, concentration, and decision-making, largely guide the behavior of adult mammals (Fuster et al., 1985; Fuster, 2000; Funahashi, 2017). During these cognitive functions, information is processed in the prefrontal associative cortex (Goldman-Rakic, 1988; Kolk & Rakic, 2021). The proper functioning of the prefrontal cortex depends on the functional maturation of neuronal networks during the late embryonic and early postnatal stages. This, in turn, is guided by the appropriate development of molecular, cellular, and anatomical properties (Reincke & Hanganu-Opatz, 2017). Abnormalities in the functional maturation of cortical networks can lead to neurodevelopmental disorders, including intellectual disabilities (Goldman-Rakic, 1994; Rubenstein, 2011).

Spontaneous synchronized activity of the neurons is a hallmark of the functional maturation of networks in the embryonic and postnatal stages, both *in vivo* and *in vitro* (Feller, 1999; O'Donovan, 1999; Ben-Ari, 2001; Blankenship & Feller, 2010; Egorov & Draguhn, 2013). This early activity forms the basis for the organization of horizontal cortical layers and vertical columns *in vivo*, which promotes the architecture and guidance of thalamocortical and intracortical circuits before the arrival of sensory information (Luhmann et al., 2016). Spontaneous activity synchronizes neurons in networks, influencing developmental processes during corticogenesis, such as neurogenesis, cell migration, programmed cell death, cell differentiation, synaptogenesis, formation of local and long-range axonal connections, synaptic plasticity, and myelination *in vivo* (Molnar et al., 2020). Synchronized activity is observed as repetitive network bursts (NBs) in the prefrontal cortex *in vivo* (Chiu & Weliky, 2001; Crochet et al., 2005; Yang et al., 2009; Wang & Arnsten, 2015), in cortical brain slices *in vitro* (Yuste & Katz, 1991; Garaschuk et al., 2000; Harsch & Robinson, 2000; Sanchez-Vives & McCormick, 2000; Corner et al., 2002; Corlew et al., 2004; Sun & Luhmann, 2007; Allene et al., 2008), and in dissociated cortical cultures *in vitro* (Dichter, 1978; Murphy et al., 1992; Muramoto et

al., 1993; Maeda et al., 1995; Opitz et al. 2002; Marom & Shahaf, 2002; van Pelt et al., 2004; Chiappalone et al., 2006; Eytan & Marom, 2006; Wagenaar et al., 2006; Tetzlaff et al., 2010; Weihberger et al., 2013; Okujeni et al., 2017). In this thesis, the study of the effect of synaptic transmission on spontaneous network burst (NB) activity focuses on dissociated postnatal rat cortical networks at three weeks *in vitro*.

Functional maturation of the network *in vitro* is a complex process in which the network structure and synapses are formed in parallel with the development of activity (Muramoto et al., 1993; Matsumoto et al., 2016). The process begins with neurons autonomously growing neurites and branching dendrites and forming non-functional synaptic contacts during the first week *in vitro* (de Lima et al., 1997; Moutaux et al., 2018). Dissociated cortical neurons first generate spontaneous action potentials (APs) i.e., spikes and intracellular calcium transients at irregular intervals after 3-4 days *in vitro* (DIV)(Marom & Shahaf, 2002; Wagenaar et al., 2006). Next, dendritic branching and the number of synapses increase, synapses begin to transmit information through their excitatory connections, the number of axonal connections increases, and neurons self-organize into a network structure that generates spontaneous synchronized network activity (Ichikawa et al., 1993; Harrill et al., 2015). The first small bursts have been observed at 4-6 DIV and network-wide synchronized bursts at 5-7 DIV (Wagenaar et al., 2006). In the second week *in vitro*, axonal branching begins, and activity-dependent synapse formation, and the firing rate of neurons increase (van Pelt et al., 2005; Wagenaar et al., 2006; Harrill et al., 2015). Inhibitory connections also develop during the second week *in vitro* (Baltz et al., 2010). Finally, cortical networks mature and functionally stabilize to facilitate synaptic transmission and spontaneous synchronized activity across the whole network around three weeks *in vitro* (Kamioka et al., 1996; Marom & Shahaf, 2002; Harrill et al., 2015; Moutaux et al., 2018).

In mature cortical cell cultures, NBs consist of about 0.5-second-long periods of spiking across the culture, separated by silent burst intervals of about 7 seconds (Kuroda et al., 1992; Robinson et al., 1993). These NBs are driven by excitatory synaptic transmission mediated by the action of glutamate on two types of ionotropic receptors (Jimbo et al., 2000), α-amino-3-hydroxy-5-methyl-4-iso-xazolepropionic acid (AMPA) receptors, and N-methyl- D-aspartate (NMDA) receptors (Hollmann & Heinemann, 1994; Dingledine et al., 1999). Inhibitory synaptic transmission is mediated by the action of γ-aminobutyric acid (GABA) on GABAergic receptors (Ramakers et al., 1990; Baltz et al., 2010). GABAergic signaling is crucial in the development of cortical network activity (Moody & Bosma, 2005; Ben-Ari et al., 2007) because the shift of GABAergic signaling from depolarizing to

hyperpolarizing represents cortical network maturation (Rivera et al., 2005; Wang & Kriegstein, 2011). The developmental GABA shift and its alterations in network activity have also been shown to occur in dissociated cortical cultures (Soriano et al., 2008; Baltz et al., 2010). However, how excitatory, and inhibitory synaptic transmissions affect the initiation, propagation, and termination of spontaneous network bursts is not yet well understood.

Considering that burst dynamics are an essential feature in the functional maturation of cortical networks in the late embryonic and early postnatal stages, both *in vivo* and *in vitro,* and that cellular and synaptic mechanisms modulating this activity are not well understood, better characterization of the synaptic mechanisms influencing the networks is essential. The effects of molecular- and cellular-level variables on network-wide activity during functional maturation stages are difficult to control and record simultaneously in a live postnatal animal *in vivo* (Yang et al., 2016). In contrast, *in vitro* networks are easier to control, and a variety of pharmacological conditions can thus be simultaneously tested using microelectrode arrays (MEAs). MEAs allow the simultaneous extracellular recordings of several neurons in the long-term and the analysis of network-wide activity which consists of the organized activity of neurons in the cell culture. Neuronal cultures provide a biological model system that can be used to study the effects of receptor mechanisms on network dynamics *in vitro*, suggesting how these receptors affect the dynamics of cortical circuits. In addition, the development of data-driven *in silico* models is very important because they can be used to design and test new biological hypotheses for *in vitro* and *in vivo* experiments and to increase the reproducibility of studies (Manninen et al., 2018).

Because animal models only partially mimic the underlying pathogenic processes, human models of neurological and psychiatric diseases will also be needed in the future. Human models have been developed for neuronal research, such as the SH-SY5Y neuroblastoma cell line isolated from the bone marrow of a four-year-old female patient (Biedler et al., 1973) and primary cell cultures isolated from the postmortem brain tissue of an adult neurological patient (Verwer et al., 2002). The SH-SY5Y neuroblastoma cell line has been widely used to model the structure and function of the human neuronal network in healthy and pathological conditions (Biedler et al., 1973). These cells retain their ability to differentiate, leading to the proliferation of these cells if they are not differentiated (Kuramoto et al., 1981). Differentiated SH-SY5Y cells have been used as human cell models in studies on Parkinson's and Alzheimer's diseases, amyotrophic lateral sclerosis, ischemia, and

neurotoxicity (Agholme et al., 2010; Kovalevich & Langford, 2013; Krishna et al., 2014).

This thesis focuses on studying how synaptic mechanisms underlie the functionality of rodent and human neuronal networks *in vitro* and *in silico*. In **Publications I** and **II**, I describe in detail the role of excitatory and inhibitory synaptic transmissions and their mediating receptors (AMPA, NMDA, and $GABA_A$) in burst activity in networks extracted from postnatal rat prefrontal cortex. I study the role of synaptic receptors in network activity by recording network-wide burst data (i.e., multiunit spike data) with MEAs under pharmacological conditions using various synaptic receptor antagonists alone and in combination. I alter the functionality of synaptic ionotropic excitatory glutamatergic and inhibitory GABAergic receptors by specifically antagonizing receptors one at a time. I present and discuss the effects of these receptors on the initiation, propagation, and termination of NBs. In **Publication II** and **III**, I analyze several features of network activity under a variety of pharmacological conditions, including measures to support the construction, fitting, and validation of data-driven network models *in silico*. In **Publications IV** and **V**, I develop neuronal-like networks from human neuroblastoma cells by morphologically differentiating them towards neuronal phenotypes and network structures *in vitro*. In **Publication IV**, I evaluate the effects of 17-β-estradiol (E_2), 3β-hydroxy-5-cholestene, i.e., cholesterol (CHOL), brain-derived neurotrophic factor (BDNF) and retinoic acid (RA) on the level of cell differentiation by determining the proliferation rate and synapse and network formation. In **Publication V**, I examine how cell culture coatings influence the optimal adhesion and morphology of human neuroblastoma cells and, consequently, the formation of the network structure of differentiated cells.

1.2 Objectives of the thesis

This thesis focuses on understanding the functional maturation of mammalian neuronal networks *in vitro*, emphasizing the role of synaptic transmission in the dynamics of network burst activity in postnatal rat cortical cultures. The thesis also reinforces the utilization of experimental results in data-driven computational modeling, which has the potential to contribute to the testing of new neurobiological hypotheses.

Specific research questions in this thesis address neuronal morphology involving neurite outgrowth, synapse and network formation, synaptic transmission, and

spontaneous network activity in cell cultures *in vitro*. The questions are studied primarily in postnatal rat cortical cultures, and some of the studies are conducted on human neuroblastoma cell cultures. Spontaneous activity recorded from rat cortical cultures under the modulation of synaptic receptor pharmacology is quantitatively analyzed to facilitate the computational modeling of network activity. The following methods are used in this work: primary and secondary cell culturing, immunocytochemistry, electrophysiology (MEA recordings), pharmacology, image analysis, and multiunit spike analysis. The combination of these techniques supported answering biological questions *in vitro* and helped to develop data-driven modeling *in silico*.

The specific aims of this thesis are threefold:

1) To characterize the effects of synaptic ionotropic excitatory and inhibitory receptors and neurotransmitters that bind to these receptors on spontaneous network activity in postnatal rat cortical cultures *in vitro* (**Publications I**, **II**).

    a) To examine the role of excitatory glutamatergic AMPA and NMDA and inhibitory GABAergic $GABA_A$ receptors in the initiation, propagation, and termination of NBs.

    b) To study the role of $GABA_A$ receptors in shaping AMPA and NMDA receptor-mediated network activity.

2) To analyze experimental multiunit time-series data recorded from rat cortical networks with MEAs under synaptic receptor antagonists *in vitro* and to retrieve relevant measures from the obtained data sets for the training and validation of *in silico* network models (**Publication III**).

3) To assess the degree of morphological differentiation of human neuroblastoma cells into neuronal phenotypes by quantifying proliferation, neurite outgrowth, synaptogenesis, and network formation with potential differentiation inducers and coatings in cell cultures *in vitro* (**Publications IV**, **V**).

1.3 Outline of the thesis

The thesis is organized as follows. **Chapter 2** provides an overview of the literature that forms the basis for understanding the experiments performed in this thesis and evaluating their value. The thesis focuses on the dependence of neuronal network activity on synaptic transmission in postnatal rat cortical cultures *in vitro* and in neuronal networks *in silico*. The first section of the literature review provides a brief overview of neocortical development *in vivo* and in slices *in vitro*. The second, third, and fourth sections focus on describing functional network maturation in dissociated cultures *in vitro*, spontaneous activity in cortical networks *in vitro*, and the role of ionotropic receptors in network activity. The fifth section describes the origin and nature of human neuroblastoma cells and the previously used differentiation protocols for them. **Chapter 3** presents the materials and methods used in the thesis. **Chapter 4** summarizes the main results of the thesis. **Chapter 5** summarizes the results, discusses the results in relation to the findings by other researchers obtained both *in vitro* and *in silico*, addresses the relevance and reliability of the results, and examines the theoretical and practical implications of the study. **Chapter 6** concludes the results, presents how the aims were achieved and describes the importance of the thesis research.

2 REVIEW OF THE LITERATURE

This chapter provides a review of the literature related to the topics covered in **Publications I – V**. **Section 2.1** provides a summary of spontaneous neural activity observed in mammals during neocortical development. This section presents activities observed in slices *in vitro* and in animals *in vivo* at both the embryonic and postnatal stages. **Section 2.2** describes the functional maturation of dissociated cortical networks *in vitro*. The description includes the following four mechanisms critical for maturation: dendritic and axonal growth, synapse development, formation of synaptic transmission, and ultimately formation of spontaneous network activity. **Section 2.3** presents in more detail the maturation of spontaneous activity in dissociated cortical networks *in vitro* and the factors influencing various aspects of spontaneous network activity. **Section 2.4** describes the background regarding the role of excitatory and inhibitory receptors in network activity. **Section 2.5** provides a summary of the origin and differentiation of human neuroblastoma cells *in vitro*.

2.1 Spontaneous activity during neocortical development

Development of prefrontal cortex during the embryonic and postnatal stages is an important period because abnormalities in the functional maturation of cortical circuits can lead to neurodevelopmental disorders, including intellectual disabilities (Goldman-Rakic, 1994; Rubenstein, 2011). The following paragraphs give a brief description of the neocortical development associated with cortical network formation and spontaneous network activity observed in rodent cortical slices *in vitro* and in the cortices *in vivo* in the early embryonic and postnatal stages.

The cerebral cortex, including the prefrontal cortex, consists of six distinct layers, the first forming the inner layer and the last the outer layer (Molnar & Clowry, 2012). Cortical neurons are important for the maturation of cortical layers as they tune early activity in local circuits and form the basis for horizontal layers and cortical columns by acting as amplifiers and hubs (Kanold & Luhmann, 2010; Minlebaev et al., 2011). Cortical neurons also organize thalamocortical circuits by integrating spontaneous

and sensory-driven activity (Thivierge, 2009; Ben-Ari & Spitzer, 2010; Kanold & Luhmann, 2010; Kirkby et al., 2013). Spontaneous activity synchronizes neurons, affecting developmental processes during corticogenesis, including neurogenesis, migration, programmed cell death, cell differentiation, formation of local and long-range axonal connections, synaptic plasticity, and myelination (Figure 1) (Demerens et al., 1996; Chen & Ghosh, 2005; Bonetti & Surace, 2010; Aronoff et al., 2010; Golbs et al., 2011; Mao et al., 2011; Yamamoto & Lopez-Bendito, 2012; Bando et al., 2016).

Already in the embryonic stages, cortical neurons express voltage-dependent channels that are responsible for the bioelectrical activity of neurons. Thereafter, spontaneous activity is dominated by electrical synaptic transmission, resulting in highly synchronized activity in local networks. Later in the postnatal stages, patterns of activity become more complex, recruit large networks, and propagate to several areas of cerebral cortex. The transition from local activity to large-scale network activity involves a gradual shift from electrical to chemical synaptic transmission, where chloride–gated channels activated by GABA, glycine, and taurine have an initial excitatory effect (Linne et al., 1996; Kilb et al., 2002; Sun et al., 2010).

The development of spontaneous activity during corticogenesis begins in the early embryonic stage. Initially, spontaneous activity is scarce and asynchronous because the cortical neurons are not yet in contact with each other (Figure 1(1)). however, neurons reveal long calcium transients that are affected by GABA- and glutamate-activated receptors. From embryonic day 15 (E15) until E18 Cajal-Retzius neurons (orange) and subplate neurons (purple) begin to fire APs faster and at a higher frequency than cortical plate neurons (black) (Figure 1 (1)). From E19 until postnatal day 0 (P0) electrically and chemically coupled neurons produce either local synchronized activity or propagating activity waves (Figure 1(2)). From P1 to P3 the firing is accelerated, and local networks begin to display synchronized bursts (periods of correlated APs of cortical neurons, separated by longer silent periods) (Figure 1 (3)). After P4, the activity again becomes sparse and asynchronous (Figure 1 (4)) (Molnar et al., 2020).

Spontaneous activity is known to change in the early stages of development *in vivo* and in slices *in vitro*. Activity can be detected in the neocortex at the single cell and network levels surprisingly early. The first correlated slow calcium transients with low-frequency (<1 min^{-1}) activity between neurons have been observed in embryonic rodent cortex slices as early as E16. Neurons appear to be sensitive to voltage-gated sodium channels and rely on voltage-gated calcium channels (Corlew et al., 2004). Calcium transients have been shown to be independent of electrical

activity, glutamate, and GABA receptors (Owens et al., 2000). Calcium waves have been shown to be mediated by connexin hemi-channels and purinoreceptors (Weissman et al., 2004). Spontaneous calcium transients are thought to propagate by proliferating radial glial cells *in vivo* (Owens et al., 2000; Weissman et al., 2004). In addition, some neurons have been shown to display high-frequency APs and glutamatergic and GABAergic synaptic inputs already at E16 (Kilb et al., 2011).

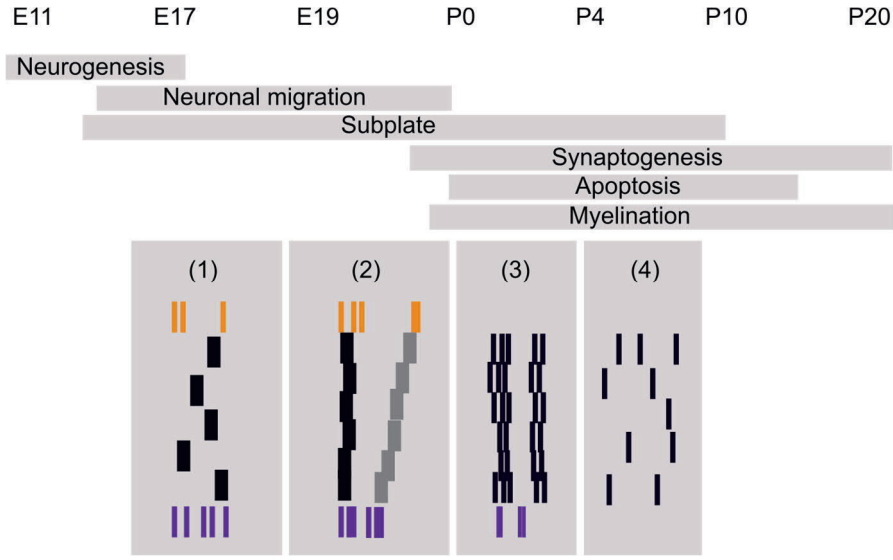

Figure 1. Development of spontaneous activity during corticogenesis *in vivo*. Rodent cortex development and changes in spontaneous activity on embryonic (E) and postnatal (P) days. (1) Cajal-Retzius (orange) and subplate neurons (purple) display asynchronous activity. (2) Neurons connected by gap junctions produce either local synchronized activity or propagating activity waves. (3) Firing speeds up and local networks indicate synchronized bursts. Early born Cajal-Retzius neurons begin to disappear at this stage. (4) Activity becomes sparse and asynchronous at P4. Figure modified from Molnar et al. (2020).

Spontaneous calcium transients have been observed in the later stage of development (P0). These transients occur at low frequency (<0.5 min^{-1}) and do not correlate with each other, but reveal an underlying network of connected neurons (Schwartz et al., 1998). During these spontaneous calcium transients, the correlation of cortical neurons is eliminated in the presence of tetdrotoxin and inhibition of α-amino-3-hydroxy-5-methyl-4-iso-xazolepropionic acid (AMPA), *N*-methyl-D-aspartate (NMDA) or γ-aminobutyric acid type A ($GABA_A$) receptors, indicating neurons' dependence on synaptic transmission (Schwartz et al., 1998; Aguilo et al.,

1999). Cortical early network oscillations (cENOs) have been found in rat cortical slices at P3. cENOs occur once a minute and propagate at a speed of 2 mm/s (Garaschuk et al., 2000). AMPA and NMDA receptor antagonists inhibit cENOs. It has been found that autonomously active layer 3 neurons trigger cENOs in slice preparation from P1 until P6 (Namiki et al., 2013). Spontaneous calcium waves resembling cENOs *in vitro* have also been observed *in vivo* in non-anesthetized rodents (Adelsberger et al., 2005). The cENOS are followed by cortical giant depolarizing potentials (cGDPs) that are shown to appear in somatosensory slices in P4-P5. cGDPs differ from cENO in that they have a higher frequency (about 8 min^{-1}) and faster kinetics (Allene et al., 2008).

The properties of spontaneous activity (see **Section 2.1**) have been studied in both cortical slices *in vitro* and in living animals *in vivo*, but also in dissociated cortical cultures *in vitro* (see Section 2.3). The advantage of dissociated cell cultures is that their structural network formation can be accurately manipulated by various microfabrication techniques (Wilson et al., 2007). In addition, biochemical interactions between synapses of cortical networks *in vitro* can also be manipulated by pharmacological or optogenetic means while still measuring electrophysiological signals from neurons (Barral and Reyes, 2016; Sukenik et al., 2021). Molecular-level phenomena, such as the role of receptors and neurotransmitters mediating synaptic transmission in the dynamics of spontaneous network activity, are more challenging to study systematically in a young animal *in vivo* than in dissociated cortical cultures *in vitro*.

In comparison to brain slices, *in vitro* cell cultures also pose some advantages. During the preparation of acute brain slices, dendrites and axons are partially excised and broken. This can result in different types of activity and functional maturation of networks in brain slices compared to networks present in dissociated cell cultures. Moreover, it is worth mentioning that cortical tissue explants excised at a very early stage of development and seeded in a cell culture dish form an organotypic co-culture that has been shown to maintain appropriate neuronal outgrowth to study high cytoarchitectural details (Baker and Van Pelt, 1997; Corner et al., 2008).

Nevertheless, extraction of cells from the cerebral cortex and their mechanical and chemical dissociation interferes also with tissue architecture and synaptic connections, leading to neuronal self-assembly and re-establishment of synaptic connections and network formation in cultures *in vitro*. These *in vitro* networks need to be allowed to functionally mature before their mature spontaneous activity can be recorded and studied. It has been shown that the functional maturation process of postnatal cortical cells takes about three weeks *in vitro* (Kamioka et al., 1996; Marom

& Shahaf, 2002; Harrill et al., 2015). The following **Sections 2.2**, **2.3**, and **2.4** briefly describe the stages of functional maturation of cortical networks, including neurite outgrowth and branching of dendrites and axons, synapse formation, synaptic transmission, and network formation, and ultimately the generation of network activity in dissociated networks *in vitro*.

2.2 Functional maturation of cortical networks *in vitro*

Cortical cultures derived from dissociated neocortical tissue provide an excellent model system for evaluating the relationships between spontaneous network and synaptic activities. The cultures allow the study of neuronal interactions in a neuronal population of hundreds of thousands of cells. Together with standardized MEAs, network activity can be recorded in detail (Egert et al., 2002). Dissociated neocortical culture includes almost all cell types present in the brain, including neurons, glial cells, and their precursors, but excluding blood cells. Most neurons are excitatory glutamatergic cells, 11-25% inhibitory GABAergic and 2-3% acetylcholinergic (de Lima et al., 1997; Marom & Shahaf, 2002; Kato-Negishi et al., 2004; Gullo et al., 2010).

Cultures prepared from the cortex of rat at postnatal day 0 (P0) and cultured for three weeks *in vitro* have been shown to undergo many stages of functional maturation, including GABAergic transition from depolarization to hyperpolarization (Baltz et al., 2010), synaptogenesis (Harrill et al., 2015), the size of dendritic field no longer increase (Okujeni & Egert, 2019b), and network formation, synaptic transmission, and network activity have reached a so-called mature stage (Kamioka et al., 1996; Lin et al., 2002; Marom & Shahaf, 2002; Moutaux et al., 2018). On the other hand, it has also been shown that physiological changes persist after the third week *in vitro*. Network burst patterns increase significantly in week 3 and decrease in week 4 *in vitro*. At week 4, bursts develop into short events that begin rapidly (van Pelt et al., 2004). Functional maturation of cells extracted from the postnatal cortex, dissociated, and plated on a culture dish or MEA plate is an essential process for the development and formation of network activity *in vitro*. In this section, I provide a brief overview of the functional maturation and factors influencing the degree of maturation.

The functional maturation of networks is a complex process in which network structure and synapses are formed in parallel with the development of activity *in vitro* (van Huizen et al., 1985; Muramoto et al., 1993). First, cortical neurons extracted

from tissue, dissociated, and plated on culture dishes continue to specialize in a variety of cell types already defined in the cerebral cortex (Kriegstein & Dichter, 1983). Second, neurites gradually grow into dendrites and axons (de Lima et al., 1997; Smith-Swintosky et al., 2005). Third, branching of the dendrites increases and synapses and synaptic connections start to form (Ichikawa et al., 1993). Fourth, neurons initiate mutual communication through synapses using action potentials (APs), i.e., an activation-dependent mechanism, eventually forming a neuronal network (van Pelt et al., 2005). Finally, the formation of active synapses and synaptic connections is followed by synaptic transmission and spontaneous network-wide burst activity (Marom & Shahaf, 2002; Wagenaar et al., 2006).

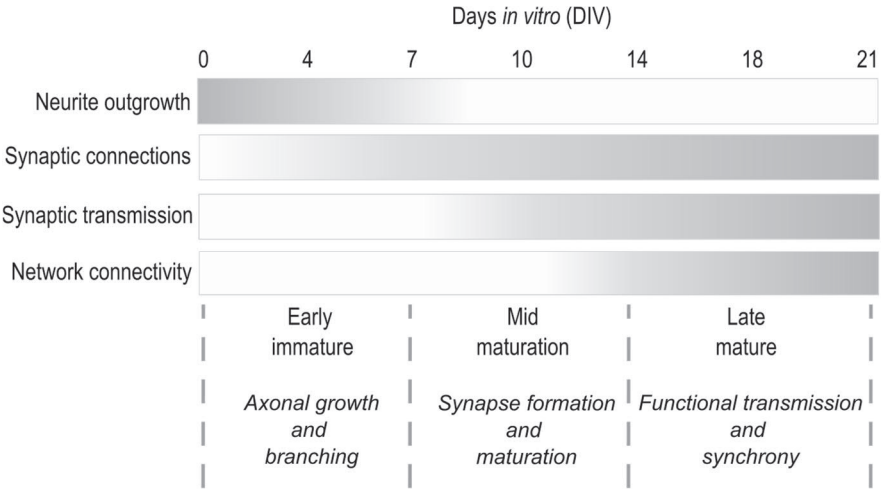

Figure 2. Maturational stages of cortical network formation *in vitro*. In the early stage (0-7 DIV), neurites start their outgrowth and synapses form connections to each other. During the mid-maturation stage (7-14 DIV), synaptic transmission starts progressively first with functional excitatory connections and later with inhibitory connections. In the late stage (14-21 DIV), networks are functional with network connectivity and spontaneous and synchronized network activity. Figure modified from (Moutaux et al., 2018).

Recently, a three-step process for functional maturation was defined, during which networks are formed and matured (Figure 2). The first stage is called the early immature stage. The immature stage begins on the first day after plating *in vitro* and continues until 7 DIV. In the early immature stage, growth and branching of cortical axons and dendrites and early formation of non-functional synapses occur. The next stage is called the middle maturation stage, which lasts from 8 DIV until 14 DIV, in which axonal branching increases and the synapses become functional. The final

stage, i.e., the late mature stage, lasts from 15 DIV to 21 DIV. During the late stage, the network begins to be fully functional and synaptic transmission and synchronized activity of neurons has reached an optimal stage (Moutaux et al., 2018).

The early immature stage begins with the cortical cells growing neurites independently. The morphological changes in neurite outgrowth have been divided into five stages (Craig & Banker, 1994). Immediately after plating, neurite outgrowth begins in growth cones that are at the tip of neurites. They recognize molecular markers from the environment and spread their filopodia. In the second stage, which occurs from 0.5 to 1.5 DIV, neurons form several small neurites, showing typical variations in growth and withdrawal. In the third stage, which occurs from 1.5 to 4 DIV, is called the polarity event, in which one of these neurites grows rapidly to become an axon. In the fourth stage, the morphological development of the remaining short neurites grows into dendrites from 4 to 7 DIV. In the fifth stage, functional polarization of axons and dendrites occurs, including dendritic spine formation (Craig & Banker, 1994). When the growth cone encounters the desired target, it begins to form a synapse, if necessary. Using these mechanisms, neurons develop axonal and dendritic arborization, which is typical of their neuronal type, and form a strongly interconnected cellular network through synapses. In particular, the complexity of dendritic trees determines how many axonal connections and branched dendrites a neuron can have during the first week *in vitro* (de Lima et al., 1997).

Synaptogenesis, i.e., the establishment of contacts between the neurons that facilitate fast neurotransmission, begins simultaneously with the growth of dendrites (Harrill et al., 2015; Ichikawa et al., 1993). In cultures isolated from embryos, synaptic terminals have been observed as early as 3 DIV (de Lima et al., 1997). One-week-old cultures already have many synapses, but the morphology of neurons is still immature (Ichikawa et al., 1993). In two-week-old embryonic cultures, the density and number of synapses have been observed to increase 2–5-fold per neuron (Ichikawa et al., 1993; de Lima et al., 1997; Brewer et al., 2009; Harrill et al., 2015). Harrill et al. (2015) found a significant increase in the number of synapses per soma and per length of dendrites between 6–15 DIV. This time frame also corresponds to an increase in spontaneous synaptic activity in cortical cultures *in vitro* (Wagenaar et al., 2006) and to a rapid increase in the number of cortical synapses in P4-P5 animals *in vivo* (Micheva & Beaulieu, 1996). In three-week-old cultures, the size of the synaptic contact area, the number of synapses per neuron, and the number of synaptic vesicles were found to increase further (Ichikawa et al., 1993). Later, as functional maturation of the network progresses, the number of synapses generally

decreases from the fourth week to the sixth week of maturation due to pruning of dendritic spines (van Huizen et al., 1985).

The role of synapse activity in changes in network structure has also been studied by pharmacological manipulations (van Huizen et al., 1985; van Huizen et al., 1987; Ramakers et al., 1990; Ramakers et al., 1991). Inhibition of the electrical activity by tetrodotoxin has been shown to prevent network maturation, increase neurite outgrowth and branching, and terminate synaptic pruning at week four *in vitro* (van Huizen et al., 1985). Chronic blockade of fast GABAergic synapses with picrotoxin (PTX) accelerated the maturation of neuronal networks (van Huizen et al., 1987). Decreased network activity was shown to increase neurite outgrowth and inhibit normal synapse elimination (van Huizen et al., 1987). In summary, network maturation requires spontaneous, possibly synchronous, electrical activity, and if electrical activity is inhibited, network growth and branching increase.

It should be noted that the development of synapses may be slightly faster in postnatal cultures than in embryonic cultures. There are also other factors such as cell density (Wagenaar et al., 2006), the ratio of excitatory-inhibitory neurons or receptors (Lin et al., 2002; Kato-Negishi et al., 2004), the age of donor animal (Luhmann et al., 2016), the composition of culture medium (Brewer et al., 2008), and the network structure (Okujeni et al., 2017), which influence the rate of synapse development and thereby the generation of activity. In addition, the number of synapses in cultures is limited by cell apoptosis (Ichikawa et al., 1993) and activity-dependent synapse pruning (van Huizen et al., 1985; van Pelt et al., 2005; Tetzlaff et al., 2010).

2.3 Network burst activity in cortical cultures *in vitro*

Cortical networks, co-cultured with glial cells, represent a neurobiological model in which universal mechanisms that control neuronal survival and neuronal network formation, and its spontaneous activity can be studied. The two-dimensional structure of cultured neuronal networks reveals properties of synaptic transmission and spontaneous activity of cells that can be experimentally studied with MEA recordings for long periods of time. In such models, unlike other experimental models such as acute slices *in vitro*, neurons self-organize during the functional maturation process, creating networks with complex spatio-temporal patterns of activity (Raichman & Ben-Jacob, 2008). Cortical networks extracted and cultured from the postnatal cortex develop spontaneous activity which has been described as

mature after three weeks *in vitro* (Kamioka et al., 1996; Marom & Shahaf, 2002). Relatively stable synchronized network-wide burst activity has been shown to occur in these networks (Wagenaar et al., 2006). The following is a summary of the functional maturation of spontaneous activity up to three weeks *in vitro*.

Spontaneous activity of cells extracted from rat neocortex develops as neuronal network matures. The increase in the number of synapses is followed by an increase in the frequency of APs and the synchronous activity of the network depending on the maturation stage and the density of the network (Muramoto et al., 1993; Wagenaar et al., 2006). Dense cultures fire APs and show intracellular calcium transients at irregular intervals as early as 3–4 DIV immediately after dissociated neurons have grown neurites and formed interconnected circuits after plating (Kamioka et al., 1996; Nakanishi & Kukita, 1998; Marom & Shahaf, 2002; Wagenaar et al., 2006). The first small bursts have been observed in dense cultures at 4–6 DIV and network-wide synchronized bursts at 5–7 DIV (Wagenaar et al., 2006). As dendritic branching and the number of synapses increase, synapses begin to transmit information through their excitatory connections, allowing neurons to self-organize into a network structure that generates spontaneous synchronized network activity (Harrill et al., 2015; Moutaux et al., 2018).

In the second week *in vitro*, axonal branching and activity-dependent synapse formation begin, resulting in an increase in the firing rate of neurons (van Pelt et al., 2005; Wagenaar et al., 2006; Harrill et al., 2015). Inhibitory connections also develop, and they gradually shift from depolarizing to hyperpolarizing mode (Baltz et al., 2010). Previous studies have shown that neurons self-organize, creating networks with synchronous regular burst activity during the second week of maturation, followed by richer synchronized activity with complex spatio-temporal patterns in the third week *in vitro* (Kamioka et al., 1996; van Pelt et al., 2004; Wagenaar et al., 2006; Chiappalone et al., 2006; Gandolfo et al., 2010). Finally, cortical networks mature and functionally stabilize, facilitating the passage of synaptic transmission and spontaneous synchronized activity across the network at three weeks *in vitro* (Kamioka et al., 1996; Marom & Shahaf, 2002; Moutaux et al., 2018; Harrill et al., 2015). The frequency (0.01–0.5 Hz) and propagation speed (5–100 mm s^{-1}) of synchronous activity have been shown to increase as well as the burst patterns to change as the network matures (Maeda et al., 1995; Kamioka et al., 1996; Marom & Shahaf, 2002; Wagenaar et al., 2006). Subsequently, as functional maturation of the network progresses, the number of synapses has been shown to decline via pruning between 5 and 6 weeks *in vitro* (van Huizen et al., 1985; van Pelt et al., 2005). During

this time, network activity is characterized by complex non-periodic, synchronized, and clustered activity.

In summary, many factors have been shown to affect maturation stages and spontaneous activity patterns. In particular, cell plating density has been shown to have a profound effect on network maturation. The firing rate of APs has also been shown to scale linearly with density and network burst behavior (Wagenaar et al., 2006). In addition, the preparation batch appears to have a slight effect on the maturation rate of the cultures and the type of network burst patterns (personal communication). The following **Section 2.4** below summarizes the connectivity and synaptic coupling of neocortical networks as well as what is known about the role of ionotropic receptors in the activity of the cortical networks.

2.4 Excitatory and inhibitory synaptic transmissions in cortical network activity *in vitro*

Next, I summarize the main findings on synaptic coupling and the effects of excitatory and inhibitory synaptic transmission on spontaneous network activity in neocortical networks *in vitro*. It has previously been shown by studying cortical connectivity using a two-electrode whole cell recording technique in *in vitro* cultures, that synaptic potentials begin to appear within two days of plating (Jones & Baughman, 1991). In mature networks, it has been reported that in 40% of randomly selected neuron pairs after evoked APs in one neuron, it produced an excitatory postsynaptic potential in another neuron with a synaptic delay of 2 msec (Nakanishi & Kukita, 1998). Others have confirmed that each mature cultured neuron is monosynaptically coupled to 10–30% of other neurons in culture (Jimbo et al., 2000; Marom & Shahaf, 2002). The stability of spontaneously formed synaptic connections has also been studied by estimating the number of times a neuron pair is active over a period. The study confirmed that 70% of neuron pairs remained unchanged even after five hours – i.e., stimulated AP induced another AP in second neuron with an exact time delay (Shahaf & Marom, 2001). In addition, bioelectrical and dye coupling experiments have confirmed that neurons in cell culture are not connected through gap junctions (Nakanishi & Kukita, 1998). Murphy et al. (1993) in their early work also ruled out the direct gap junction -based coupling between neurons and astrocytes. On the other hand, cultured astrocytes have been shown to be coupled to each other by gap junctions (Cornell-Bell et al., 1990). Astrocytes have also been shown to respond to synchronous neuronal activity by increasing their calcium levels

(Cornell-Bell et al., 1990; Bazargani & Attwell, 2016). This astrocytic calcium response has been shown to be mediated by the release of neurotransmitters, spilled over from synapses of the nearby neurons (Murphy et al., 1993). Recent work has also shown that astrocytes can directly modulate the function of synapses in brain slices, obtained from specific brain areas (Bazargani & Attwell, 2016).

In three-week-old cortical cultures, network bursts have been shown to be driven by excitatory synaptic transmission (Robinson et al., 1993; Jimbo et al., 2000), which is primarily mediated with glutamate at two types of glutamatergic ionotropic AMPA and NMDA receptors (Hollmann & Heinemann, 1994; Dingledine et al., 1999). Furthermore, it has been shown that the depolarization of network bursts is reversibly inhibited either with 100 μM NMDA receptor antagonist 2-amino-5-phosphovaleric acid or 2 mM Mg^{2+}, which induces hyperpolarization in cortical cultures (Robinson et al., 1993). This inhibition indicates that the NMDA receptor mediated component of the synaptic current is essential for network burst activity. Spontaneous network bursts have also been shown to be inhibited by the 30 μM AMPA receptor antagonist 6-cyano-7-nitroquinoxaline-2,3-dione, implying that synaptic currents also have a significant AMPA component (Robinson et al., 1993). Electrical stimulation has also been shown to induce responses that consist of early and late stages, which occur when separate synaptic pathways are activated (Jimbo et al., 2000; Marom & Shahaf, 2002; Wagenaar, Pine, & Potter, 2004). The early-stage component contains postsynaptic APs that appear 5-50 ms after stimulation of the cells (Wagenaar et al., 2004) and the late-stage response contains NMDA receptor mediated activity that lasts about 160 msec (Jimbo et al., 2000).

In neocortical networks, GABA is known to mediate inhibitory synaptic transmission via $GABA_A$ receptors (Ramakers et al., 1990; Baltz et al., 2010). GABAergic signaling is a very essential part of developing spontaneous network activity in neocortex (Moody & Bosma, 2005; Ben-Ari et al., 2007). Depolarizing GABAergic signaling is involved in the early functional maturation of cortical networks (Wang & Kriegstein, 2011). The transition of developmental GABA from depolarizing to hyperpolarizing signaling represents maturation of the cortical network. This change stops GABA receptor mediated developing network activity and initiates mature GABAergic activity (Rivera et al., 2005; Ben-Ari et al., 2007). Developmental changes in network activity and GABA shift have been shown to occur in dissociated three-week-old cortical cultures *in vitro* (Soriano et al., 2008; Baltz et al., 2010). Previous studies have shown that late phase is significantly increased as a result of inhibition of $GABA_A$ receptors, indicating that late phase

duration is regulated at least indirectly by inhibiting synapses in cortical networks *in vitro* (Jimbo et al., 2000; Weihberger et al., 2013; Baltz & Voigt, 2015).

Prior to the initiation of this thesis work, it was not known how the glutamatergic AMPA, and NMDA receptors affect the initiation, propagation, and termination of network bursts *in vitro*. It was also not known how these excitatory receptors interact with $GABA_A$ receptors to initiate dynamic changes in network activity. Moreover, the interactions of these three-receptor type had not been previously studied using a data-driven approach to reproduce network dynamics *in silico*.

2.5 Differentiation of human neuroblastoma cells *in vitro*

Human SH-SY5Y neuroblastoma cell line, a malignant tumor of the sympathetic nervous system, has been isolated from the bone marrow of a four-year-old female patient (Biedler et al., 1973; Duckett & Koop, 1977). Neuroblastoma cells retain their ability to differentiate i.e., they proliferate uncontrollably (Kuramoto et al., 1981). Due to their ability to proliferate and easy availability, the use of these human cells has increased significantly in recent decades. Since it was established, the cell line has been extensively used in many studies.

Human neuronal network models have been used to study human-related neuropathological research questions that cannot be studied in living humans or animals. By developing the differentiation of the human neuroblastoma cell line into neuron-like phenotypes, the future development of cancer therapies can be further promoted. In addition, a differentiated human cancer cell line can also be used as a basis for the development of mathematical models in which some of the information that cannot be assessed in human comes from rodent neuronal networks. However, a detailed structural and functional evaluation in which neuroblastoma cells have been differentiated into neuronal phenotypes has not been performed. It is of great interest to understand the degree of morphological differentiation of human neuroblastoma cells into neuronal phenotypes. The following is a brief description of the protocols previously used to differentiate human neuroblastoma cell lines towards neuronal-like cells and networks.

In the past, human SH-SY5Y neuroblastoma cells have been differentiated with retinoic acid (RA), because RA has been shown to increase the expression of neuronal markers and the expression of the neuronal phenotypes (Pahlman et al., 1984; Preis et al., 1988; Toselli et al., 1996; Cheung et al., 2009). 12-*O*-tetradecanoyl phorbol 13-acetate (TPA) has also been widely used to differentiate SH-SY5Y cells

alone or in combination with RA. TPA has been shown to increase noradrenaline levels in differentiated cells (Pahlman et al., 1984). TPA in combination with RA has been shown to differentiate SH-SY5Y cells towards dopaminergic neurons (Presgraves et al., 2004). In addition, BDNF has been used with RA and has been shown to lead to a homogeneous neuronal population with neuronal markers and reduced proliferation (Encinas et al., 2000). It has been arguably shown that the combination of BDNF-RA differentiates SH-SY5Y cells towards a cholinergic phenotype (Goldie et al., 2014) but also towards dopaminergic neurons (Mastroeni et al., 2009).

The human neuroblastoma cell line has previously been used as a model in Parkinson's disease due to its catecholaminergic neuronal properties after differentiation. In addition, neuroblastoma cells have been used as research models in Alzheimer's disease, amyotrophic lateral sclerosis, ischemia, and neurotoxicity (Agholme et al., 2010; Kovalevich & Langford, 2013; Krishna et al., 2014). *In vitro* human neuronal network models are increasingly needed to understand their functionality and to support development of therapies.

3 MATERIALS AND METHODS

This chapter presents the materials and methods used in **Publication I - V**. **Section 3.1** presents the preparation and maintenance of rat cortical cell cultures, handling protocols of microelectrode array (MEA) plates, and maturation of cortical cell networks. **Section 3.2** describes methods for electrophysiological MEA recordings and protocols for pharmacological treatments of cells. **Section 3.3** discusses the data analysis of the recordings in detail. **Section 3.4** presents the preparation and maintenance of human neuroblastoma cell cultures as well as the differentiation protocols of neuroblastoma cells. **Section 3.5** provides a summary of immunocytochemical techniques and analysis of obtained images.

3.1 Rat cortical cultures

3.1.1 Preparation of cell cultures from prefrontal cortex

Microelectrode arrays (MEAs, Multi-Channel Systems Ltd. (MCS), Reutlingen, Germany) and coverslips (CSs; Ø 19/12 mm, Plano, Wetzlar, Germany/Carl Roth GmbH, Karlsruhe, Germany) were prepared for cell culture experiments. The MEAs were rinsed with soap, cleaned overnight with deionized (DI) water on a custom-made agitator, sterilized for one hour in boiling DI water (180°C), and dried for two hours. MEAs were hydrophilized in a humidified oxygen plasma device (70 W, 0.15 mbar, 4 min). CSs were cleaned by ultra-sonication in acetone bath for 15 minutes, rinsed three times with DI water, and autoclaved in DI water at 121°C for 60 min.

MEAs and CSs were coated with 0.1 - 0.2% polyethylene imine (PEI, Sigma-Aldrich, Steinheim, Germany), 300 µl per MEA, 200 µl per Ø 19 mm CSs, and 150 µl per Ø 12 mm CSs. The solutions were pipetted in a center of the MEA or CS. MEAs and CSs were incubated for two hours with the PEI, then coating was removed by pipetting, and the substrates were rinsed three times with DI water. Substrates were led to dry overnight and sterilized with shortwave ultraviolet

radiation lamp (2 min, 254 nm, model XX-15S, UVP Inc., Upland, CA, USA). Substrates were used for culture seeding immediately or within the next days.

Animal handling and tissue extraction were performed according to the guidelines approved by the animal ethics committee of the University of Freiburg. Postnatal (P0) Wistar rat pups of either sex were decapitated without anesthesia within 24 hours after the birth (Figure 3A). The scalp was removed from a forehead until a neck with a tweezer in a clean and sterile bench conditions (Figure 3B and 3C). The head was transferred to a dish filled with cool phosphate-buffered saline solution (PBS; all reagents from Gibco, Invitrogen, Karlsruhe, Germany, unless otherwise stated). The skull plates were cut and removed from both sides. The brain was removed and transferred to a new dish with cool PBS. The dura and the pia maters of the brain were removed with tweezers. Small sections from both hemispheres of the prefrontal neocortex (yellow area in Figure 4) were cut with a scalpel and transferred to a tube with PBS.

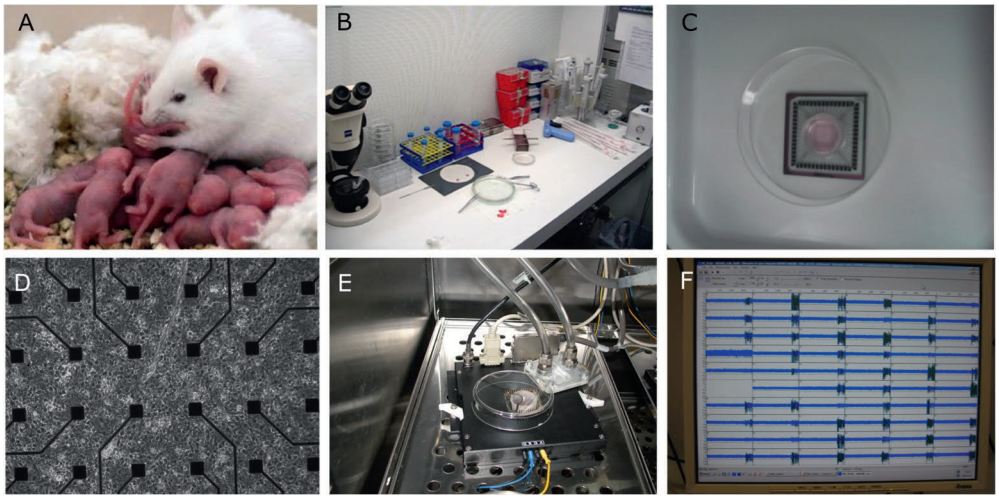

Figure 3. Procedure for preparing rat cortical cultures for MEA recordings. A) Postnatal (P0) Wistar rat pups of either sex were decapitated within 24 hours after the birth. B, C) Forebrains were removed, and cultures prepared in a clean and sterile bench conditions on coated MEA plates. D) Neurons and glial cells were grown and maintained on top of the MEA electrodes until 3 weeks *in vitro*. E) MEA recordings were performed inside a dry incubator at 37ºC, and 5% CO_2, and the recorded signals were amplified using MEA 1060-Inv-BC System amplifier. F) Activity recordings of the network-wide bursts were observed online with the computer program of Multi-Channels System to verify the quality and level of maturation of the cultures.

The cortical cells were extracted from the prefrontal cortex of both hemispheres (Figure 4). The tissue was mechanically chopped with the scalpel in a tube. The cells were enzymatically dissociated by adding 0.05% Trypsin solution and incubated on a shaker at 37ºC for 15 min. Trypsinization was stopped by adding 20% horse serum (HS) into the tube. The tube was gently turned three times and the solution was incubated again for 5 min for allowing settlement. The deoxyribonuclease (DNase, type IV 50 µg/ml, Sigma-Aldrich, Steinheim, Germany) was added to degrade DNase around the cells and incubated for 5 min for allowing a pellet fraction to form. Supernatant was discarded with a pipette. Warm PBS solution (37ºC) was added, and the cells were gentle triturated with serological pipette (volume of 10 ml; Becton Dickinson, Franklin Lakes, NJ, USA). Solution could settle for 5 min after the supernatant was transferred to a new tube. The remained solution was centrifuged for 5 min with 2000 rcf (Rotofix 32A, Hettich, Tuttlingen, Germany) and the supernatant was discarded. The pellet was triturated into minimum essential medium (MEM, supplemented with 5% heat-inactivated HS, 20 µM glucose, 0.5 mM L-glutamine (L-gln), and 1% gentamicine, 1ml MEM/rat). This procedure was for the first time described by Shahaf & Marom (2001).

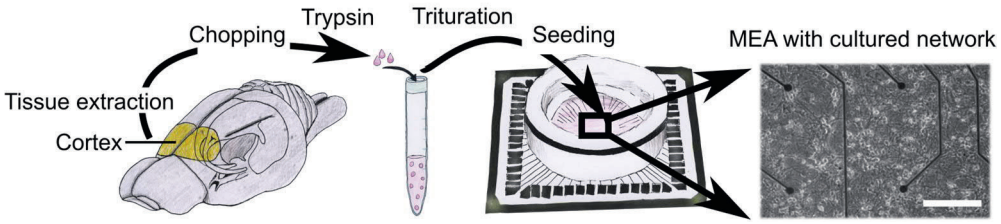

Figure 4. Tissue and cell extraction from the prefrontal cortex of a rat. Sections from both hemispheres from prefrontal cortex of postnatal rats were extracted (yellow area). Tissue was transferred to a tube, mechanically chopped, trypsinized, and triturated. After determining the final cell count, the cells were seeded on the PEI-coated MEA plate covered with a lid. A cortical cell culture at 21 DIV on a MEA plate (scale bar 250 µm).

Cell counts were determined with an automated cell counter (CAS TT, Schärfe Systems GmbH, Reutlingen, Germany). Cells were seeded at densities of 2,000 cells/mm^2 onto 0.2% PEI-coated MEAs or CSs by pipetting. The cells were allowed to settle for 30-60 min in 5% CO_2 humidified incubator (Thermo Fisher Scientific,

Germany) at 37°C before adding 2 ml MEM. One third of the medium was changed twice a week and recordings were done between 18-27 DIV.

3.1.2 Maintenance of cells and maturation of networks

Cells were cultured and maintained in MEM supplemented with 5% heat inactivated HS, 20 mM glucose (Sigma-Aldrich, Steinheim, Germany), 1% gentamycine, and 0.5 mM L-gln in 5% CO^2 humidified incubator at 37°C. Two-thirds of the medium was changed at 1 and 5 DIV (MEM including 1 mM L-gln)) and from 9 DIV onwards one third of the medium was changed twice a week (MEM including 0.5 mM L-gln).

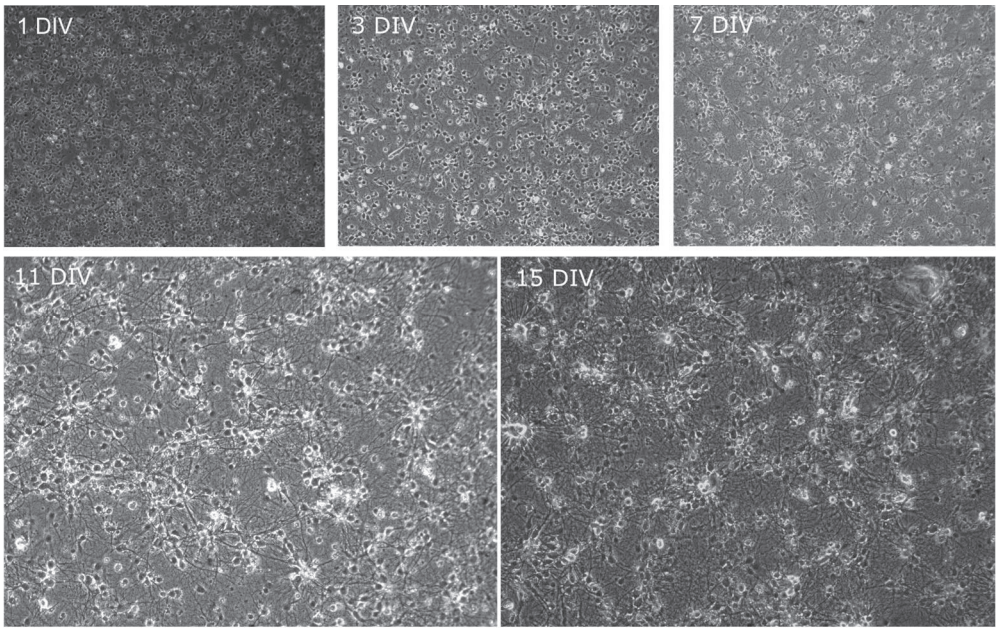

Figure 5. Formation of rat cortical network from day 1 until day 15 *in vitro*. Neurons are evenly adhered on the cover slips at 1 DIV. Formation of neurites is in progress at 3 DIV. First contacts between the neurons are formed at 7 DIV. Cortical neurons have network formation at 11 DIV. Synapses and neuronal network have matured at 15 DIV.

Preliminary experiments were performed on cortical cells plated on coverslips to determine the maturation of cortical networks (Figure 5) and the impact of cell density on final network formation (Figure 6), before starting the actual recordings on MEA plates at 3 weeks *in vitro*. In Figure 5, neurons attach widespread and

homogenously on the substrates at 1 DIV, neurons start sprouting neurites and develop synapses at 3 DIV, synaptic connectivity develops at 7 DIV, and subsequently uncorrelated spikes can be recorded. At 11 DIV, the network structure has developed, and stereotypical network bursts (NBs) can be recorded until the end of the lifetime of the culture. During the third week *in vitro* excitatory and inhibitory synapses, neuron-neuron contacts, dendrites, and network structure have developed. Compared to previous weeks NBs are more stable and burst frequency (BF) has increased.

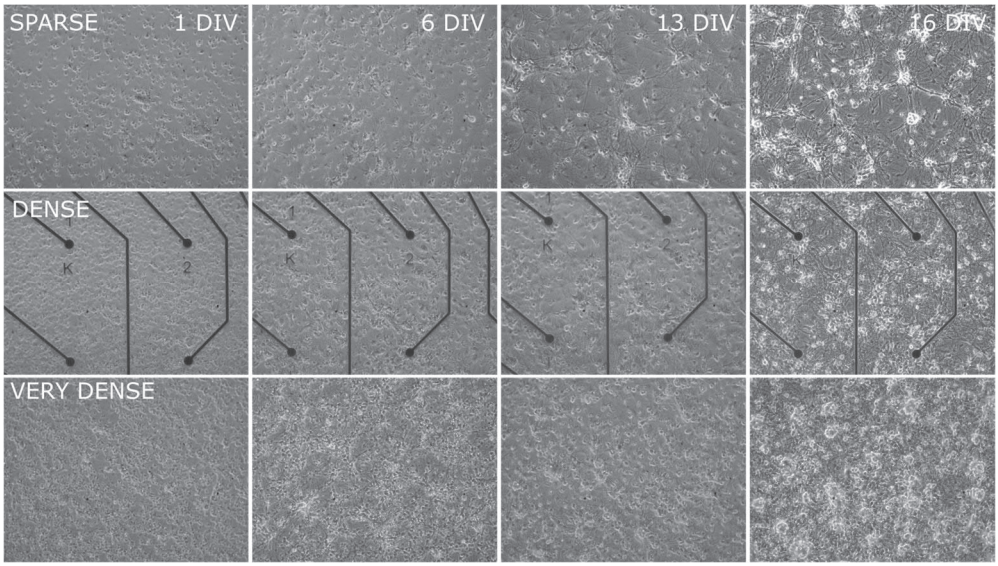

Figure 6. Growth of cortical networks at different cell densities. Growth of cells at different densities on coverslips and a MEA plate (sparse, dense, and very dense) on 0.2% PEI coating at 1, 6, 13 and 16 DIV. Seeding densities influence cell clustering, because cells prefer to grow near to each other. Neuronal adhesion and network formation are optimal in dense cell cultures on PEI-coated MEA plates (middle row).

The cell adhesion, growth, maturation, and network formation were observed at different cell densities including sparse, dense, and very dense at 1, 6, 13, and 16 DIV. Dissociated rat primary cells successfully adhered on PEI-coated coverslips and MEA plates at 1 DIV (Figure 6). Seeding density influenced on the network maturation. Very dense and dense cultures promoted network formation of dissociated rat neocortical already at 6 DIV, whereas sparse seeding density supported the network formation as late as 13 DIV (Figure 6). In sparse cultures, neurons formed small clusters and bundles between the clusters due to low cell

density at 16 DIV (Figure 6). Clusters were not seen in dense cultures at 16 DIV. Dense rat neocortical cultures were grown on 0.2% PEI-coated MEA plates for all the MEA recordings done between 18-27 DIV.

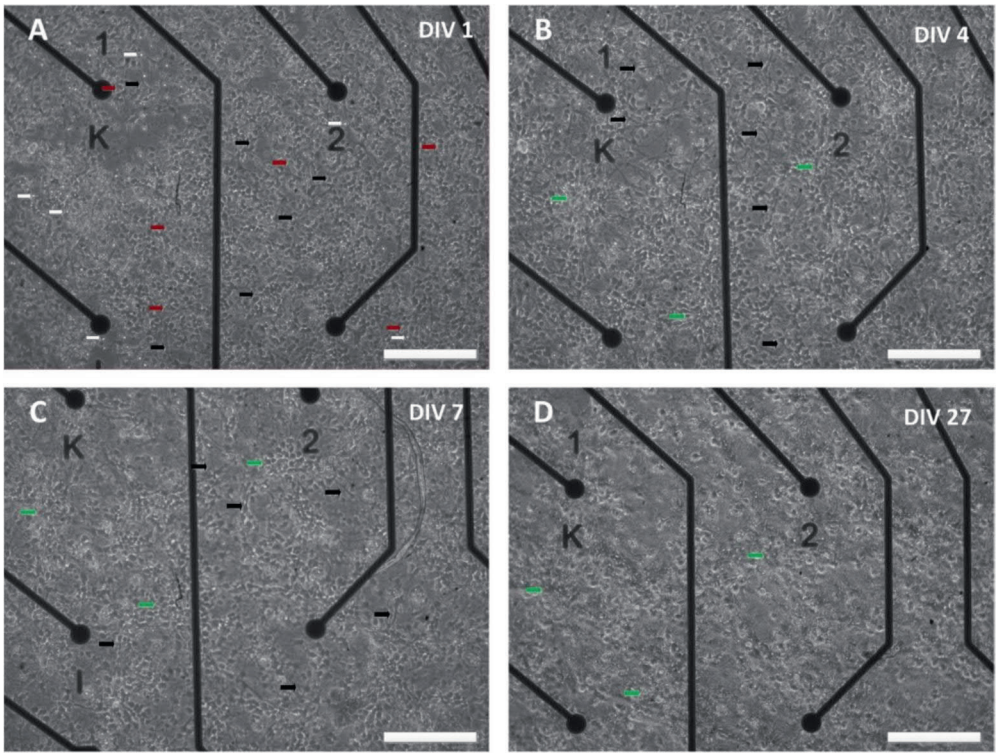

Figure 7. Cortical cell attachment and network development. A) Cells were well attached on the PEI-coated MEA plate at 1 DIV. Most of the cells are healthy (red marker), but also some apoptotic cells can be seen (white marker). Healthy neurons grow neurites already after 1 DIV (black marker). B) The growth of neuritis has greatly increased (black markers) at 4 DIV. Clusters of neurons may also exist (green markers) due to incomplete dissociation. C) Neurons in a network start the maturation process around 7 DIV. The cell density decreases, and unnecessary connections are eliminated by pruning process, and the first evidence of network activity can be seen in MEA recordings at 7 DIV. D) This example culture was recorded at 27 DIV. The network expresses network wide bursting (NB) which can be recorded with MEA technique (scale bar 250 µM).

The MEA plate with cell culture was covered with polytetrafluoroethylene (i.e., Teflon) membrane lids (ALA Scientific, Westbury, NY, USA). Lids were used to prevent the changes in pH and osmolality through evaporation of MEM at 37ºC (Potter & DeMarse, 2001). The condition and status of the cells and the network

morphology were also observed on MEA plate with a microscope (Axiovert 40; Carl Zeiss, Oberkochen, Germany) and images were taken with digital camera (Nikon Coolprix 4500, Düsseldorf, Germany) at 1, 4, 7 DIV and at the recording date 18-27 DIV (Figure 7).

3.2 Electrophysiology and pharmacology

3.2.1 Microelectrode array recordings

The extracellular network activity recordings were performed from cultures grown on standard MEAs (MSC, Reutlingen, Germany) with 60 titanium nitride electrodes (Ø 30 μM)) including one internal reference electrode. Electrodes were placed either in square (8 x 8 grid layout with 200 μM distance from each other) or rectangular pattern (6 x 10 electrode grid with 500 μM distance from each other). The square and rectangular grids were covering of area of 1.96 mm^2 and 11.25 mm^2, respectively. Recordings were made inside a dry incubator (Binder, Tuttlingen, Germany) at 37°C and 5% CO_2, and the recorded signals were amplified using MEA 1060-Inv-BC System amplifier (MSC; gain 1,100x, bandwidth 20-8,500 Hz). The amplifier was water-cooled to prevent overheating of the culture.

Raw data from each electrode was sampled at 25 kHz with an input voltage range of ± 819 mV and digitally high pass filtered with a 2nd order Butterworth at 200 Hz cut-off frequency. The data was acquired using personal computer equipped with a data acquisition card (MC_Card, MCS) and MC_Rack acquisition software (MCS, versions 3.3-4.5). The spikes were detected with a threshold of 5 times the standard deviation (SD) from the mean noise baseline. The times when the signals crossed this voltage threshold were detected as spike times from each electrode and were stored to hard disk for further analysis. Data was imported to MATLAB (versions 2009b-2018b, Mathworks Inc., MA, USA) using MCStreamSupport. The spike time data and electrode indices were preliminary analyzed with MATLAB using the MEA-tools (Egert et al., 2002) and the FIND toolboxes (Meier et al., 2008). The network burst detection and further advanced data analysis, including the calculation of statistical measures and the preparation of results and image illustrations, were completed with self-written MATLAB scripts and functions. Figures were prepared with free and open-source software Inkscape version 0.91 (Inkscape).

3.2.2 Synaptic receptor antagonists

Pharmacological receptor antagonists were used for studying the contribution of excitatory and inhibitory synaptic receptors and their neurotransmitters to network activity dynamics. Activity was recorded with the electrophysiological MEA technique from rat cortical cultures matured until 3 weeks *in vitro*. The ionotropic glutamatergic α-amino-3-hydroxy-5-methyl-4-isoxazolepropionic acid (AMPA) receptors were antagonized with a competitive antagonist 2,3-dioxo-6-nitro-1,2,3,4 tetrahydrobenzo-[*f*]quinoxaline-7-sulfonamide (NBQX). The ionotropic glutamatergic *N*-methyl-D-aspartate (NMDA) receptors were antagonized with a competitive antagonist of the glutamate site of the NMDA receptors D-(-)-2-amino-5-phosphonopentanoic acid (D-AP5). The ionotropic GABAergic $GABA_A$ receptors were blocked with a non-competitive antagonist picrotoxin (PTX). All drugs were directly applied with a pipette into the culture medium inside the dry incubator. All pharmacological chemicals were purchased from Sigma-Aldrich, Steinheim, Germany.

Changes in the cortical network activity were studied by both acute and gradual applications of each ionotropic AMPA, NMDA, or $GABA_A$ receptor antagonists. In the case of acute applications, higher concentrations of the antagonists were applied to antagonize all receptors, which enabled studying the immediate effect of the complete antagonism of each receptor type to network activity dynamics and ultimately to synaptic transmission (protocol id 1, 2, 6, and 7 in Table 1). In the case of gradual applications, increasing concentrations of the antagonist were applied to the medium to allow neurons to adapt to the reduced receptor functioning in a relatively short time window (one hour) in contrast to other studies that have addressed homeostatic mechanisms over a longer period (24-hour adaptation) (Corner et al., 2008). Gradual application enabled studying the dependence of the concentration of the synaptic receptor antagonists to network dynamics in the short term (protocol id 3, 4, 5, 6, and 7 in Table 1).

The AMPA receptors were acutely antagonized with 10 μM or 30 μM NBQX. The concentration of 10 μM of NBQX has been shown to completely antagonize AMPA receptors (Parsons et al., 1994). The NMDA receptors were acutely antagonized with D-AP5 that was applied at concentrations of 10 μM or 30 μM. Previous literature has shown that 10 μM of D-AP5 blocks 95% of the NMDA receptors and 30 μM blocks 100% (Benveniste & Mayer, 1991). $GABA_A$ receptors were acutely and completely antagonized with 10 μM PTX (Krishek et al., 1996). In the case of gradual application of the AMPA receptor antagonist, an increasing

amount of NBQX was applied to first partially (0.1 μM and 1 μM) and then completely antagonize the AMPA receptors (10 μM). For the gradual application of the NMDA receptor antagonist, the selected amount of D-AP5 (0.1 μM, 1 μM, and 10 μM) was applied to gradually reduce the functioning of the NMDA receptors.

Table 1. Pharmacological protocols used for MEA recordings. Recordings of cortical cultures, including abbreviated name of the receptor antagonists, their used concentrations, antagonized and functional receptor types as well as the Roman number of the publication that the specified protocol was used.

Protocol id	Antagonist	Concentration	Antagonized receptor types	Functional receptor types	Publication
Acute application					
1	CTRL NBQX PTX	- 10 μM 10 μM	None AMPA $GABA_A$	All NMDA, $GABA_A$ NMDA	I, II, III
2	CTRL D-AP5 PTX	- 10 μM 10 μM	None NMDA $GABA_A$	All AMPA, $GABA_A$ AMPA	I, II, III
Gradual application					
3	CTRL NBQX	- 0.1, 1, 10 μM	None AMPA	All NMDA, $GABA_A$	I
4	CTRL D-AP5	- 0.1, 1, 10 μM	None NMDA	All AMPA, $GABA_A$	I
5	CTRL PTX	- 0.1, 0.2, 0.3, 1, 2, 3 μM	None $GABA_A$	All AMPA, NMDA	I (suppl. mat.)
Acute and gradual application					
6	CTRL NBQX PTX	- 30 μM 0.1, 1, 10, 40 μM	None AMPA $GABA_A$	All NMDA, $GABA_A$ NMDA	I (suppl. mat.)
7	CTRL NBQX PTX	- 30μM 0.1, 1, 10, 40 μM	None NMDA $GABA_A$	All AMPA, $GABA_A$ AMPA	I (suppl. mat.)

For pure gradual disinhibition the selected amount of PTX (0.1 μM, 0.2 μM, 0.3 μM, 1 μM, 2 μM, 3 μM) was applied to partially block the $GABA_A$ receptor mediated ionotropic GABAergic transmission. In the case of gradual disinhibition after the acute application of excitatory receptor antagonist (AMPA or NMDA receptor complete antagonism), an increasing amount of PTX was gradually applied to first partially (0.1 μM, 1 μM) and then completely antagonize the $GABA_A$ receptor mediated transmission (10 μM, 40 μM).

Each combined pharmacological and MEA recording experiment consisted of the following steps: (1) minimum 25 minute- or maximum 60 minute-long control (CTRL) MEA recording, (2) application of the first receptor antagonist, (3) MEA recording for 25/60 minutes, (4) application of the second antagonist, (5) MEA recording for 25/60 minutes, (6) application of the third antagonist, and (7) MEA recording for 25/60 minutes and so forth depending of the amount of antagonists used for each protocol (Table 1). For each recording, the first 10 minutes were not analyzed to avoid transition phases. The remaining 15 to 50 minutes were analyzed (Figure 8).

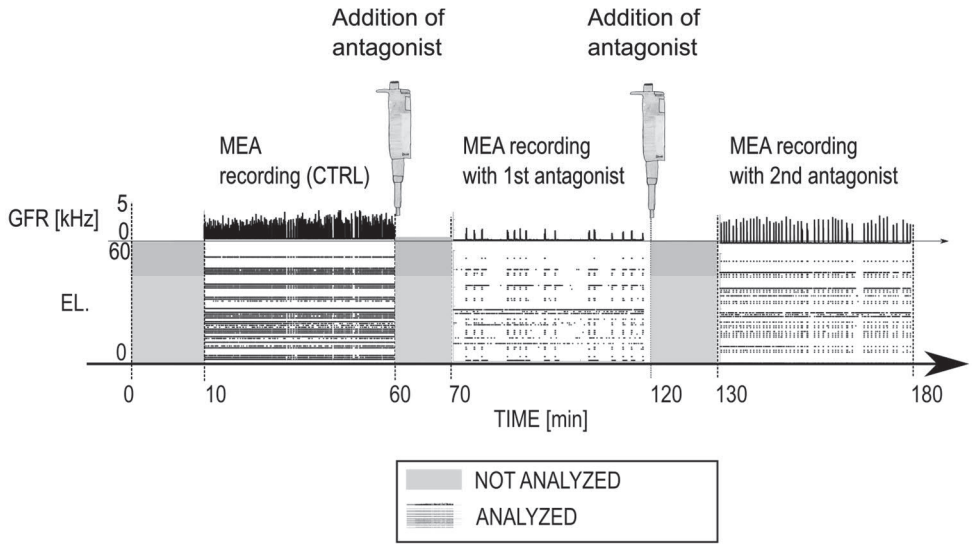

Figure 8. MEA recording protocol with pharmacology. Timeline of a total of 180 minutes shows an example recording protocol with a CTRL, an acute addition of first excitatory and second inhibitory receptor antagonist. The first ten minutes of the recording were not analyzed (gray period) and the rest 50 minutes of the recording were analyzed (spike time raster plots). GFR denotes the global firing rate [kHz] and EL the electrode numbers.

3.3 Data analysis of recordings

3.3.1 Preprocessing of data, burst detection, global firing rate and burst frequency

Data was imported to MATLAB (versions 2009b-2018b, Mathworks Inc., MA, USA) using MCStreamSupport (MCS). The initial 10 minutes of the recording after the application of an antagonist were not analyzed to avoid transient phases. The following 15 minutes or 50 minutes, depending on the recording protocol, were then analyzed (Figure 8). Electrodes with firing rates (FR) lower than 9% of the average FR on electrodes with spike activity were excluded. Spontaneous network bursts (NBs) were detected with the algorithm that include the following four criteria: (1-2) the onset and offset time of the NB were defined as the first interspike interval (ISI) smaller than 100 ms and the first ISI bigger than 100 ms respectively, (3) a minimum of 10 spikes must be recorded per NB, and (4) a minimum of 10 electrodes must be active during the NB in **Publications I, II** and **III**. All data was manually inspected to verify that the bursts were correctly identified. The burst detection method was chosen because it was found to be adequate at an early stage of the work, and the same methods was used systematically throughout the study. Different burst detection methods have been developed and their effectiveness has been recently compared (e.g., Chiappalone et al., 2005; Cotterill et al., 2016).

The relative global firing rate (GFR, [Hz]) and BF [NB/min]) were computed for each recording in **Publications I** and **II**. These were displayed either by the box plot representation of pooled rates or by separate graph representations of the rates in the acute application of the antagonists (see Table 1, protocol ids 1 and 2) or in the gradual application of the antagonists (see Table 1, protocol ids 3, 4, 5, 6 and 7) respectively. To compute the relative GFR, the number of all spikes was divided by the duration of the recording period in seconds. To compute the BF, the number of NBs was divided by the duration of the recording period in minutes. The values were normalized to CTRL condition by dividing the value with the CTRL value. Statistical analysis was performed for pool rates using Wilcoxon rank sum test. Differences were significant when $p < 0.05$, $p < 0.01$, or $p < 0.001$, different significances are indicated with *, **, ***, respectively.

3.3.2 Characterization of network burst measures

In this thesis, a rich set of multi-unit spike data was recorded with MEAs in order to systematically analyze network activity dynamics and synaptic transmission in rodent neocortical cultures. The importance of the systematic analysis of data is emphasized throughout this thesis to enable efficient comparison of data obtained under different pharmacological condition from multiple *in vitro* networks and, further, to support the validation of computational models *in silico*. Particularly, the network burst measures, and their characterization were developed to quantitatively characterize the various aspects of spontaneous network burst activity to support the development of computational models.

To analyze the characteristic burst measures, network burst (NB) rate profiles [Hz] were created for each NB. The NB rate profiles were calculated by smoothing the spike counts in the bins via convolution with a Gaussian kernel. The NB measures were calculated from the NB rate profiles. The maximal firing rate (MFR [Hz]) was defined as the peak of the profile, the rising phase (RP [s]) as the time between the time point when the FR reaches $1/16^{th}$ of the MFR and the point when the FR reaches the MFR, instead the falling phase (FP [s]) was determined to start from the time point of MFR and to end when FR decreases back to $1/16^{th}$ of the MFR, and the burst length (BL [s]) was the sum of RP and FP (Figure 9). Finally, the burst size (BS [# spikes/NB]) and the electrode recruitment count (eRC) were calculated as the number of spikes per each NB and the number of active electrodes during the NB, respectively. BS and eRC were defined from the start time point until the end time point of the detected NBs. The BL, RP, and FP were computed similar as (Gritsun et al., 2010). The method reduces the variability and possible oscillating tails of NBs and provides a systematic measure for comparing NB rate profiles under different pharmacology, which is especially important for data-driven computational modelling and model fitting. The MFR and BS were additionally divided by the number of active electrodes to have MFR and BS per electrode.

In **Publication II**, the SD and mean of median of each NB measure (except for eRC) were computed for applications (Table 1 protocol ids 1, 2, 3, and 4). SDs were divided by the mean values to calculate the coefficient of variation and finally, the mean of medians were normalized w.r.t control (CTRL). Coefficient of variations of all NB measures were displayed as bars with error bars in the **Publication II**. Wilcoxon rank sum test and p-values were computed for all burst measures in each condition and in each culture. If the tests showed a similar result for each culture, the significance was displayed as ***($p < 0.001$), **($p < 0.01$), *($p < 0.05$). Burst

measures were not normalized w.r.t CTRL and were displayed as a box plot representation of the pooled measures for applications of gradual disinhibition (Table 1 protocol ids 5, 6, and 7). Wilcoxon rank sum test and p-values were computed for all pooled burst measures between CTRL and each condition. Differences were significant when $p < 0.001$. These burst measures can be further used to efficiently fit computational network models (see **Publication III)**.

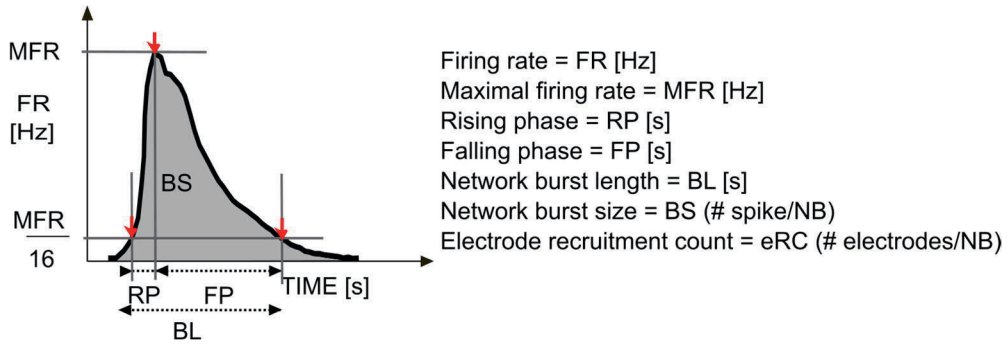

Figure 9. Characterization of network burst measures. Maximal firing rate (MFR [Hz]) is the maximal peak of the network burst firing rate profile, rising phase (RP [s]) is the length of time between the time points when the firing rate (FR) of network burst profile reaches the $1/16^{th}$ of the MFR and MFR, falling phase (FP [s]) starts at the time point of MFR and ends to the time point when FR decreases the $1/16^{th}$ of MFR, burst length (BL [s]) is the sum of RP and FP. Burst size (BS # spikes /NB) is the number of spikes per network burst (NB) and eRC is the number of active electrodes per NB.

3.3.3 Interspike and interburst intervals

The distributions of ISI [s] within NB (i.e., the time difference between the consecutive spikes during NBs) were computed for each condition and for each culture in **Publication II**. The histograms were calculated using the following values for the edges of the bins: 10^i, where i is in {-10, -9.8, ..., 6}. The mean of ISI distributions from all cultures of the same condition were computed and the values of i were plotted on the x-axis with a logarithmic scale (log (TIME[s]). Significance analysis was performed for all ISIs between each condition in the same culture using Wilcoxon rank sum test. If the tests showed a similar result for every culture when the same conditions were compared, the differences were considered significant and were displayed as ***($p < 0.001$), **($p < 0.01$), *($p < 0.05$).

The distributions of interburst intervals (IBI [s]) (i.e., the time difference between the last spike of NB and the first spike of NB+1) were calculated for each condition

and for each culture in **Publication II**. The IBI data matrices were smoothed using the Gaussian window method (matlab function smooth) with an integer scalar of 5 for the size of the window and a scalar of 0.65 for SD of the Gaussian window. Then the histograms were created using the following values for the edges of the bins: 10^i, where i is in {0, 0.05, ..., 5}. The mean of IBI distributions from all cultures of the same condition were computed and the values of i were plotted on the x-axis with a logarithmic scale. Significance analysis was performed for all IBIs between each condition in the same culture using Wilcoxon rank sum test. If the tests showed a similar result for every culture when the same conditions were compared, the differences were considered significant and were displayed as ***($p < 0.001$), **($p < 0.01$), *($p < 0.05$).

3.3.4 Network recruitment

Network recruitment was computed as cumulative number of active electrodes recruited at the onset of a NB for each condition and culture, relative to the CTRL condition in **Publication II**.

The first spike times from each active electrode were used to compute time vectors for each NB. The duration of NBs or period of 0.5 seconds was discretized using 0.0001s time step. The number of active electrodes until each time step were counted, which were stored into the time vector. Finally, all time vectors of each NB from the same culture and condition were pooled and the mean value of active electrodes was computed for each time step by averaging over all NBs. The results illustrate the time spent to recruit the network at the beginning of the NB. i.e., recruitment time (RT).

3.3.5 Similarity analysis of spatio-temporal patterns

Previous literature has shown that NB has a unique structure, which is defined as "momentary spatio-temporal pattern in which neurons at different locations fire spike-trains at different delays relative to each other" (Raichman & Ben-Jacob, 2008). Therefore, the unique structure is referred in this thesis as "spatio-temporal patterns". To analyze the contribution of synaptic excitatory and inhibitory receptors on spatio-temporal patterns of network activity, the NBs were characterized by the first spike time relative to the burst onset from each electrode, i.e., the rank order of the first spike from each electrode within the NB in **Publication II**. Pairwise-spike-

time-difference matrices for the first spike times of each pair of electrodes within each NB were computed. The similarities between NBs were computed as the correlation coefficient (CC) between their pairwise-spike-time-difference matrices with the matlab function "corrcoef". CSs that are close to one indicate similar spatio-temporal patterns between the NBs, CCs close to zero indicate no correlation, and CCs close to minus one indicates anticorrelated spatio-temporal patterns. To compare the results of multiple cultures, the distributions of CCs in each condition and in each culture from the CC matrices were computed. Statistical analysis was performed for all CCs between each condition in the same culture using Wilcoxon rank sum test and p-values. If the tests showed a similar result for every culture when the same conditions were compared, the differences were considered significant and was displayed as ***($p < 0.001$), **($p < 0.01$), *($p < 0.05$).

3.3.6 Burst measures for data-driven models

The constructed spiking neuronal network model used the generic Izhkevich-model formalism for modeling the neurons and a conventional synapse model (see detail in **Publication III**). Models were fitted to represent BL and BS of all acute experimental conditions, including the CTRL, AMPA receptor blocked, NMDA receptor blocked, AMPA and $GABA_A$ receptor blocked or NMDA and $GABA_A$ receptor blocked conditions.

Features extracted from experimental data: The 50 minutes long recordings contained between 4 and 722 NBs, depending on culture and experimental condition. Individual bursts were detected using a standard NB detection method (see **Section 3.3.1**). The ISI between the successive spikes in a recording were computed: beginning of a burst corresponds to the first pair with ISI > 100ms, ending of a burst corresponds to the last pair satisfying this condition. The bursts that spread over at least 10 electrodes and contained at least 10 spikes were analyzed. In total, 4913 bursts from the CTRL condition of 13 cultures, between 155 and 722 bursts per culture were extracted. The experiments with NMDA receptor blocking resulted in 1368 NBs, between 34 and 704 bursts per culture, and the experiments with additional disinhibition gave 1342 bursts, 75-305 per culture. The blocking of AMPA receptor reduced the number of bursts since AMPA receptors were largely involved in burst initiation. In AMPA receptor blocked networks 120 bursts from 7 cultures, 4-34 per culture were recorded. Disinhibition of these cultures increased the number of bursts to 500, 20-132 per culture.

In **Publication III**, the burst profiles i.e., the instantaneous population spike rates were computed. I described the structure of bursts using two measures: 1) the BS which is the number of spikes within a NB normalized to the number of active electrodes, 2) the BL, the time while burst profile exceeds a threshold value (set to $1/16^{th}$ of the burst profile maximum, like (Gritsun et al., 2010). The definition of BL reduced the significant trial-to-trial variability in burst profiles by reducing the contribution of burst tails. The distribution, means, medians, and percentiles (25^{th} and 75^{th}) for these two measures were evaluated across cultures and experimental conditions. The results obtained from different experimental conditions were compared using Wilcoxon rank sum test ($p = 0.01$). To use this data for model fitting, all the results for the same experimental condition together were pooled (i.e., all the bursts from all cultures) which gave five datasets for the five experimental conditions. The 70% of each set was used for fitting the computational model. The remaining 30% was used as a test data for objective evaluation of the goodness of fitting.

3.4 Human neuroblastoma cell cultures

3.4.1 Coating of substrates

The effects of surface coatings on the morphology of differentiating and undifferentiating human SH-SY5Y neuroblastoma cells (CRL-2266, ATCC, Manassas, VA, USA) were studied on substrates such as MEAs and CSs. These evaluation studies on cell culture coating agents promote the use of human *in vitro* cell model system, such as the SH-SY5Y neuroblastoma cell line, in future research of neurodegenerative diseases. Human cell culture systems will be an important next step to assess the functionality of networks using MEAs.

In **Publication V,** coatings were tested to obtain proper cell attachment and neuronal cell type morphology of neuroblastoma cells. Substrates were either uncoated for CTRL use or coated with 0.1% PEI (Sigma-Aldrich, St. Louis, MO, USA), 0.002% laminin (LAM, L2020 mouse, Sigma-Aldrich, St. Louis, MO, USA) or with 0.1% PEI with 0.002% LAM. All coatings were diluted in sterile DI water. MEAs and CVs were incubated overnight with PEI coating at 4 ° C, the coating was removed by pipetting, and the substrates were rinsed three times with DI water.

LAM was added and incubated for one hour at room temperature and then removed with a pipette. The substrates were used immediately.

3.4.2 Maintenance and differentiation of cells and networks

Human SH-SY5Y neuroblastoma cells were differentiated in **Publications IV** and **V**. The maintenance and differentiation of human cells are described as follows. SH-SY5Y neuroblastoma cells (CRL-2266; American Type Culture Collection, Manassas, VA, USA) were plated at passage of 29-30 with density of 5000 cells/cm^2 in 48-well cultures dishes, CS, or MEA plate. Cells were cultured and maintained in 1:1 nutrient mixture F-12K Kaighn's modification and MEM supplemented with 10% fetal bovine serum, 2 mM/L L-gln, 1% antibiotic-antimycotic mixture, and 1% non-essential amino acids in a 5% CO_2-humidified incubator 37ºC (all reagents used to maintain SH-SY5Y cells, Gibco, Invitrogen, Carlsbad, CA, USA, unless otherwise stated).

In **Publication V**, cell differentiation was induced with 10 μM/L all-*trans* retinoid acid (RA, Sigma-Aldrich, St Louis, MO, USA), 10 μg/mL 3β-hydroxy-5-cholestene i.e., cholesterol (CHOL), or a combination thereof at 10 μM/L RA and 10 μm/mL CHOL (RC). In **Publication IV**, cell differentiation was further studied with the following differentiation agents; 1 nM 17-β-estradiol (E_2), 50 ng/mL BDNF and combinations thereof RA and BDNF (RB), RA and E_2 (RE), RA, CHOL, and BDNF (RCB), as well as RA, CHOL, E_2, and BDNF (RCBE). All differentiation agents were from Sigma-Aldrich, St. Louis, MO, USA, unless otherwise noted.

Stock solutions of differentiation substances were diluted in 96% ethanol. CTRL cells were also treated with < 0.1% ethanol. Differentiation substances were applied simultaneously during medium exchange on days 1, 3 and 7 *in vitro*. Cell growth, condition, and morphology were observed with a microscope (Olympus CK40) and images were taken with a DP10 microscope digital camera system (Olympus, Tokyo, Japan) on days 1, 3, 7, and 10 *in vitro*.

3.5 Immunocytochemistry and image analysis of human cultures

3.5.1 Nuclei staining and cell number quantification

In **Publications IV** and **V**, the effects of coatings and differentiating agents on the number of human neuroblastoma cells were determined by staining cell nuclei with 10μg/mL Hoechst 33258 (Sigma-Aldrich) for 5 minutes on day 10. After staining, cultures were washed five times with PBS and then were mounted. Nuclei fluorescence was visualized with a Nikon DS Camera Control Unit DS L-1.

Images were analyzed with CellC analysis software in both coating and differentiation studies (Selinummi et al., 2005). The software corrects the background of the image for auto-fluorescence by fitting a two-dimensional quadratic polynomial to the image and subtracting the fitted polynomial surface from the original image. The algorithm then separates the nuclei pixels from the background pixels with a global threshold and produces a binary image with white nuclei on a black background. In addition, it separates clustered nuclei from each other in a marker-controlled watershed segmentation based on the intensity of the nuclei. The software removes objects, such as staining residues, by removing artefacts smaller than 1/10 of the average size of all objects. The images were organized with Microsoft Visio 2010. The obtained nuclei count, and statistics were analyzed and plotted in MATLAB (version 2013b, The Mathworks Inc., MA, USA).

3.5.2 Assessment of neurogenesis and synaptic exo- and endocytosis

In **Publication IV**, to evaluate differentiation-induced neurogenesis in human neuroblastoma cultures, cells were stained with neurofilament 68kD (NF-68) immunostaining on day 10. NF-68 stains potential neurofilaments induced by differentiation treatment. Cell nuclei were further stained with Hoechst to count cells. Cells were first fixed for 20 min with 4% paraformaldehyde (Sigma-Aldrich) diluted in PBS, washed three times with PBS and permeabilized in 0.5% Triton X-100 (J.T.Baker, Phillipsburg, NJ, USA) for 15 min. After washing with PBS, nonspecific antibody binding sites were blocked with 10% bovine serum albumin (BSA, Gibco) in PBS for 30 min to reduce the background. The cells were then incubated with primary antibody mouse monoclonal anti-NF-68 1:100 (Sigma-

Aldrich) for 1 hour at room temperature, rinsed three times with PBS, and then incubated with secondary antibody FITC- conjugated goat anti-mouse IgG 1:100 (Sigma-Aldrich) for 30 min at room temperature. Neurofilament fluorescence was visualized with Nikon Eclipse TS100 microscope equipped with Nikon DS Camera Control Unit DS L-1 and images were processed with Adobe Photoshop Elements 12. Ink and organized with Microsoft Visio 2010.

SH-SY5Y cells were treated up to 10 DIV with ethanol (CTRL), CHOL, E_2, BDNF, RA or combinations thereof such as RA with E_2, RA with BDNF, RA with CHOL, RA with CHOL and BDNF, RA with CHOL, BDNF, and E_2. The neurites were traced from phase contrast images using ImageJ software (version 1.48) (National Institute of Mental Health, Bethesda, Maryland, USA) (Schneider et al., 2012) and NeuronGrowth plugin (Fanti et al., 2008), captured from each treatment group on day 7 and day 10. The NeuronGrowth automatically calculates the length of traced neurites in pixels and exports the data directly to Excel2010. Data on neurite length and statistics were analyzed and plotted in MATLAB (version 2013b).

The intensity of total fluorescence (NF-68) of neurofilaments and the intensity of total background fluorescence were measured for each image with ImageJ software. The corrected total neurofilament fluorescence (CTNF) was calculated from the data in Excel 2010 (Microsoft, WA, USA) by the previously used method (Gavet & Pines, 2010; Burgess et al., 2010) as follows: The fluorescence of the neurofilaments of interest was selected with a selection tool. The region of interest, integrated density, and mean gray value were calculated for selected regions with ImageJ software. The area next to the selected neurofilament was selected as the background value. The CTNF was calculated using the following equation CTNF = integrated density – (area of selected neurofilaments x mean fluorescence of background readings).

Neuroblastoma cells were stained with AM1-43 styryl dye to detect synaptic exo/endocytosis after cell differentiation. AM1-43 is a fixable nerve terminal probe. It cannot pass through the membranes. However, when cells are depolarized with a high potassium Tyrode solution, the styryl dye adheres to the vesicles under exocytosis, if the cells repeatedly depolarized, then the dye exits from the vesicle due to endocytosis.

In the first experiment, cells were incubated for 1 min with 4 μmol/L AM1-43 (Biotium, Hayward, CA, USA) in depolarizing Tyrode's solution containing 80 mmol/L potassium (K^+) for live staining of recyclable synaptic vesicles, after which the cells were washed several times with SCAS quench solution (Biotium) at room temperature to reduce background fluorescence. Depolarization-dependent staining

has been also described by (Pyle et al., 1999) and (Croft et al., 2005). After depolarization, images were taken as above, and cultures were continuously monitored under a microscope. In a second experiment, cells were incubated for 1 min with 4 μmol/L AM1-43 with low potassium Tyrode's solution, after which the cells were washed with SCAS at room temperature and fixed for 20 min with 4% paraformaldehyde (Gibco), permeabilized in 0.01% Triton X-100 (J.T. Baker) for 12 minutes and washed three times for 1 minute in cold PBS. AM1-43 fluorescence was visualized as in NF-68 immunostaining.

Images were analyzed with ImageJ analysis software using the following steps specifically designed for this study: Image background was reduced by setting a rolling ball radius to 50 pixels after the image was sharpened and then the maximum fluorescence puncta were found with noise tolerance of 20 and with the point selection style. This procedure was evaluated by visual inspection and was found to be the best to find the correct number of AM1-43 puncta in the fluorescence images. The number of fluorescence puncta per image was divided by the median number of nuclei. The fluorescence scores per median nuclei number and statistics were analyzed and plotted in MATLAB (version 2013b). Statistical analysis was performed using one-way ANOVA in MATLAB (version 2013b). Differences were considered significant when $p < 0.01$ or $p < 0.05$, different significances are indicated with ** or *, respectively in **Publication IV**.

4 SUMMARY OF RESULTS

This thesis focuses on the study of the functionality and synaptic properties of the rodent cortical networks and differentiated human neuronal networks *in vitro*. The main aim of the thesis was to understand how synaptic excitatory and inhibitory receptors alter network burst activity in rodent cortical cultures *in vitro* as well as in computational models *in silico*. **Publications I** and **II** describe the dependence of synaptic transmission on spontaneous network activity in postnatal rat cortical cultures *in vitro*. The relationship between synapses and network activity was studied by recording network-wide burst data – i.e., multi-unit spike data – with MEA recordings under a variety of pharmacological conditions. The functionality of synaptic ionotropic excitatory glutamatergic and inhibitory GABAergic receptors was altered by specifically antagonizing receptors one at a time.

In **Publication III**, a systematic data analysis procedure was developed for different types of network burst data sets that were recorded under each pharmacological receptor antagonist. The procedure was used to quantify several measures that described the dynamics of the data sets. Subsequently, these measures were used in a data-driven computational model generation approach in which spontaneous neuronal activity with cellular, synapse and network mechanisms were modeled and studied (**Publication III**). This new approach combined spiking neuronal network models *in silico* with network burst data in which synaptic receptor functioning was altered *in vitro*. The resulting models helped to interpret the recorded data and allowed further computational analysis of cellular, synaptic and network mechanisms underlying spontaneous cortical activity.

Publications IV and **V** extend studies of rodent cortical networks to facilitate understanding of network functionality and synaptic properties in human cells that were morphologically differentiated towards neuronal cells and networks. In these two **Publications IV** and **V**, the effects of differentiation and coating agents on network and synapse formation in human neuroblastoma cells *in vitro* were addressed.

Section 4.1 presents the effects of excitatory AMPA and NMDA as well as inhibitory $GABA_A$ receptors on the initiation, propagation, and termination of network-wide bursts in rat cortical networks *in vitro* (**Publications I** and **II**). **Section**

4.2 extends the use of experimental data from **Publications I** and **II** to specific measures and data analysis procedure that supported the fitting and validation of computational spiking network models (**Publication III**). In addition, **Section 4.2** provides a brief overview of how well the data-driven spiking network models reproduced the network burst profiles recorded from rat cortical networks. **Section 4.3** describes the induced level of differentiation of human neuroblastoma cells by determining the arrest of cell division, the number of neurites and synaptic vesicles, and the level of network formation (**Publication IV**). Finally, it summarizes the effect of surface coatings on the adhesion and network morphology of differentiated and undifferentiated human neuroblastoma cells (**Publication V**).

4.1 Synaptic receptors and spontaneous activity dynamics in postnatal rat cortical networks

Publications I and **II** studied the effects of excitatory AMPA and NMDA on spontaneous network burst dynamics and the effects of inhibitory $GABA_A$ receptors on predominantly AMPA or NMDA receptor-mediated network activity. In these two publications, neuronal network activity was recorded as multi-unit spike data using the MEA technique under pharmacological conditions. The role of each synaptic ionotropic receptor in network activity was examined by acute and gradual applications of receptor antagonists. In **Publications I** and **II**, control (CTRL) networks were probed by acute application of either AMPA (NBQX) or NMDA receptor (D-AP5) antagonist and then by acute application of the $GABA_A$ receptor (PTX) antagonist i.e., disinhibition. In **Publication II**, in addition to acute application, increasing concentrations of AMPA, NMDA or $GABA_A$ receptor antagonists were gradually applied for allowing neurons to adapt to the reduced functioning of each specific receptor type and to study the gradual effects of receptor blockade on network burst dynamics.

Data analysis for **Publications I** and **II** focused on showing the main effects of acute addition of synaptic receptor antagonists on neuronal network activity, including global firing rate (GFR [kHz]) and burst frequency (BF [NB/min]) throughout the recording period (Figure 10 and 11) as well as the firing rate (FR) in NB profiles [Hz] (Figure 12). The aim of **Publication II** was to understand in more detail how synaptic receptors affect spatio-temporal activity propagation patterns spreading across the network. Data analysis consisted of several computable measures such as burst length (BL [s]), falling phase (FP [s]), rising phase (RP [s]),

maximal firing rate (MFR [Hz]), burst size (BS [#spikes/NB]), electrode recruitment count (eRC [# electrodes])), interspike interval (ISI [s]), interburst interval (IBI [s]), recruitment time (RT), and similarity measure (SM) (see **Materials and Methods** for more information). These measures allow a detailed study of the spatio-temporal role of synaptic receptors in network burst dynamics, as presented in **Publication II**, and are quantified, compared, and summarized in Table 3. Two of these measures BL and BS were selected for use in data-driven model development by combining *in silico* network model and *in vitro* data in **Publication III** (**Section 4.2**).

4.1.1 Effects of excitatory receptors on cortical network bursts

The results of the role of excitatory receptors in rat cortical activity showed that the dynamics of network bursts depend on both excitatory AMPA and NMDA receptors. **Publications I** and **II** confirmed that NBs are generated regardless of whether excitatory AMPA or NMDA receptors are antagonized. The GFR and BF decreased under both conditions compared to the CTRL group (Figure 10). The GFR decreased more in networks in which NMDA receptors were antagonized – i.e., in AMPA receptor-mediated activity– than in those in which AMPA receptors were antagonized –i.e., NMDA receptor-mediated activity (Figure 10B). In contrast, BF decreased more in networks in which AMPA receptors were antagonized than in those in which NMDA receptors were antagonized (Figure 10C). These and subsequent results indicate that AMPA receptors promoted the network burst initiation, whereas NMDA receptors contributed to the maintenance of NBs.

To further analyze the differences in network bursts, the network burst rate profiles [Hz] were calculated by smoothing the spike counts in the bins via convolution with a Gaussian kernel for each network burst in **Publication I** (Figure 12), from which the network burst measures such as BL, BS, FP, RP, MFR, and eRC were computed in **Publication II** (Tables 2 and 3). When NMDA receptors were blocked, the burst profiles were shorter and had fewer spikes than the CTRL profiles (Figure 12B). This was also reflected in a decrease in burst measures such as BL and BS, likely due to lower excitation (Tables 2 and 3). Network burst profiles with impaired AMPA receptors were longer and contained more spikes than the CTRL profiles (Figure 12F). **Publication II** showed an increase in burst measures in AMPA receptor blocked networks, including BL and BS (Tables 2 and 3). These results confirmed that AMPA receptors contributed to the early phase of burst profiles and NMDA receptors to the late phase.

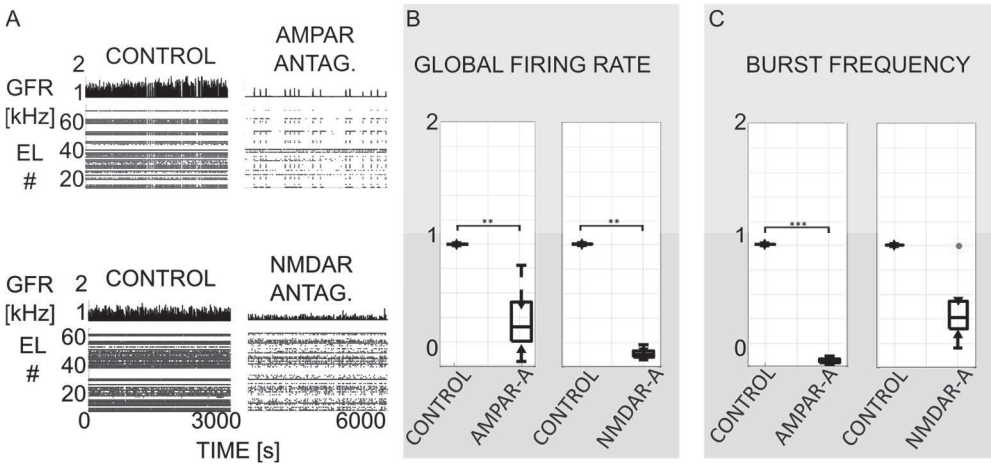

Figure 10. Firing rate and burst frequency in excitatory receptor blocked networks. A) Raster plots of spikes recorded with 59 electrodes for 3000 seconds show how glutamatergic AMPA and NMDA receptor antagonists altered network activity compared to control conditions. B) The global firing rate (GFR [kHz]) decreased less with the AMPA receptor antagonist (left subpanel) than with the NMDA receptor antagonist (right subpanel) compared to the control activity. C) Burst frequency (BF [NB/min]) decreased more with the AMPA receptor antagonist (left subpanel) than with the NMDA receptor antagonist (right subpanel) compared to the control. The results show that AMPA receptors promote burst initiation and NMDA receptors maintain network bursts.

4.1.2 Effects of inhibitory receptors on excitatory receptor-mediated network bursts

Next, the effects of $GABA_A$ receptors on AMPA and NMDA receptor-mediated network activities were addressed (**Publications I and II**). To study the influence of GABAergic signaling on NMDA or AMPA receptor-mediated network dynamics, each excitatory receptor was first antagonized in different networks, followed by $GABA_A$ receptor antagonism –i.e., disinhibition. The results showed that disinhibition significantly increased the GFR in networks in which NMDA receptors were antagonized –i.e., AMPA receptor-mediated activity– but not in networks in which AMPA receptors were antagonized –i.e., NMDA receptor-mediated activity (Figure 11B and Table 3). These results indicate that $GABA_A$ receptors strongly inhibited AMPA receptor-mediated firing, suggesting that there is a tighter coupling between fast AMPA and $GABA_A$ receptors than between slow NMDA and fast $GABA_A$ receptors.

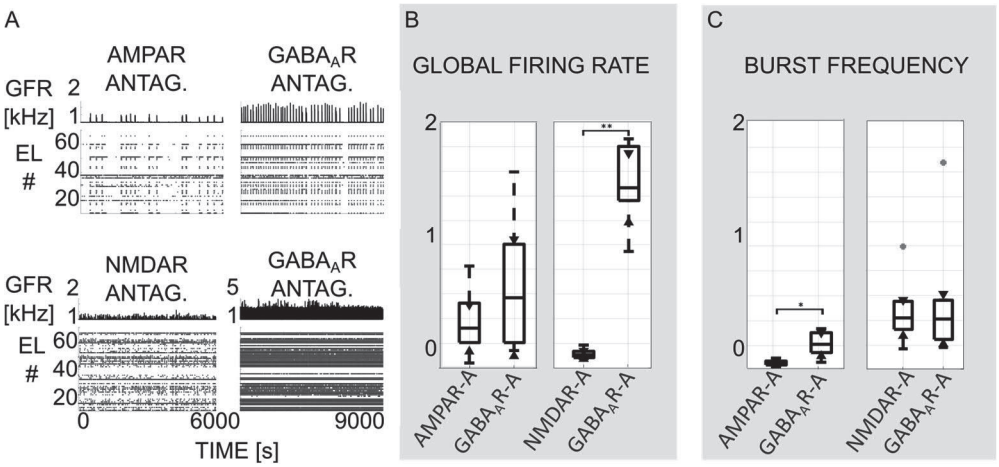

Figure 11. Firing rate and burst frequency in disinhibited networks. A) Raster plots of spikes recorded with 59 electrodes for 3000 seconds show how disinhibition altered network activity in NMDA and AMPA receptor-mediated networks compared to with inhibition. B) The global firing rate (GFR [kHz]) increased more in NMDA receptor antagonized and disinhibited networks (right subpanel) than in AMPA receptor antagonized and disinhibited networks (left panel) compared to the activity before disinhibition. C) Network burst (NB) frequency (BF [NB/min]) increased slightly more in AMPA receptor antagonized and disinhibited networks (left subpanel) than in NMDA receptor antagonized and disinhibited networks (right panel). The change in GFR indicate that $GABA_A$ receptors inhibited AMPA receptor-mediated firing more strongly than NMDA receptor-mediated firing.

The role of $GABA_A$ receptor-mediated inhibition in network activity was further examined by comparing disinhibited and CTRL burst profiles and burst measures calculated from their burst profiles (Figure 12A, C, E, and G). In addition, disinhibited and pre-state profiles when either AMPA or NMDA receptors were antagonized were compared (Figure 12B, C, F, and G). Disinhibition increased the RP and FP of both AMPA, and NMDA receptor-mediated network burst profiles when compared to CTRL conditions (Figure 12A, C, D, E, G, and H). Increases in RP and FP suggest that disinhibition caused a fast increase in activity and its maintenance in both AMPA and NMDA receptor mediated bursts when compared to baseline burst profiles. In addition, the MFR and BS of the burst profiles increased due to disinhibition in AMPA receptor-mediated burst profiles when compared to CTRL profiles (Figure 12A, C, D, Tables 2 and 3). In contrast, the BL of the burst profiles increased due to disinhibition in NMDA receptor-mediated networks compared to CTRL condition (Figure 12E, G, H, Tables 2 and 3). Comparing the

effect of disinhibition with the previous AMPA receptor-mediated state where $GABA_A$ receptors were still active BL, FP, and MFR increased (Figure 12B, C, D, Table 2, and 3). These results support my previous observation that $GABA_A$ receptors strongly inhibit AMPA receptor-mediated network burst activity. In contrast, disinhibition shortened the late phase of NMDA receptor-mediated profiles when compared to the preceding condition when inhibition was still active (Figure 12F, G, and H). This was also shown by decreased BL, FP, and BS (Tables 2 and 3), indicating that $GABA_A$ receptors played a role in attenuation of the late phase of NMDA receptor-mediated burst profiles.

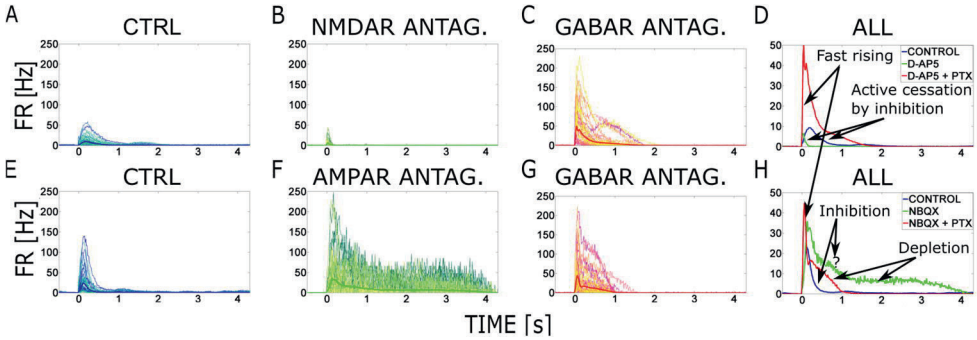

Figure 12. Burst rate profiles with an altered synaptic receptor functioning. A-D) NB profiles (FR within NBs [Hz]) were shorter and contained fewer spikes with blocked NMDA receptors (B) compared to CTRL profiles (A), disinhibition enhanced the early and late phases of NB profiles (C) in comparison to CTRL (D). E-H) NB profiles with attenuated AMPA receptors were longer and contained more spikes (F) than CTRL profiles (E), whereas disinhibition enhanced the late phase of NB profiles (G) in comparison to CTRL condition (H). NB profiles were actively terminated when both AMPA and $GABA_A$ receptors were functioning (A, B, and E). Disinhibition gave rise to a fast increase in NB profile activity (D, H, red). NB profiles terminated in depletion when AMPA receptors were blocked indicating that AMPA receptors were essential for active cessation of bursts (F and G).

The network burst profiles terminated with active cessation when both AMPA and $GABA_A$ receptors were functioning (Figure 12A, B, and E). In contrast, networks lacking functional AMPA receptors appeared to further prolong the late phase of network bursts, indicating that the profiles most likely ended in depletion of neurotransmitters (Figure 12F, and G). Presumably, $GABA_A$ receptors were unable to terminate burst profiles without AMPA receptors (Figure 12F). Therefore, AMPA receptors also appeared to play a crucial role in the cessation of NBs. These results suggest that possibly AMPA and $GABA_A$ receptors interact together to terminate

network bursts. NMDA receptor-mediated network bursts were shorter after disinhibition compared to with inhibition, indicating that $GABA_A$ receptors without AMPA receptors further slowed the late phase of network activity in NMDA receptor-mediated networks (Figure 12G). This result suggests that without $GABA_A$ receptor-mediated inhibition, network burst activity ceased more rapidly and thus neurons were faster ready for the next burst in NMDA receptor-mediated networks compared to NMDA and $GABA_A$ receptor mediated networks.

Finally, disinhibition also accelerated the rise of burst profiles (Figure 12C, D, G, and H), implying that $GABA_A$ receptors attenuated both the early and late phases of network activity. This will be discussed in more detail in the following paragraphs, which summarize how the ISIs, RT, and SM of spatio-temporal activity propagation patterns changed as a result of disinhibition in AMPA and NMDA receptor-mediated networks.

4.1.3 Temporal propagation of network bursts

The roles of excitatory AMPA and NMDA and inhibitory $GABA_A$ receptors in the temporal propagation of network activity were further examined (**Publication II**). The effects of receptors on the temporal onset of spikes were studied by analyzing the distributions of ISIs recorded throughout the NBs and the RT used for the activity to propagate across all active electrodes at the beginning of the NBs. The RT was calculated as the time elapsed from the first recorded spike time from the first active electrode to the first spike time from the last active electrode at the beginning of each network burst. Results showed that ISIs did not change in AMPA receptor-mediated network activity (NMDA receptors blocked), but prolonged in NMDA receptor-mediated activity (AMPA receptor blocked) (Tables 2 and 3). The time required for the network to recruit active electrodes (RT) at the onset of bursts was shortened in AMPA receptor-mediated activity and prolonged in NMDA receptor-mediated activity (Table 3). These results suggested that the presence of AMPA receptors accelerated the activity propagation, whereas either NMDA receptors or their interaction with GABAergic signaling potentially slowed the course of activity in the network. I conclude that network dynamics of neuronal activity, such as FR and network RT, were prominently slowed in the absence of fast AMPA receptors – i.e., AMPA receptors were needed for fast activity propagation.

To understand how $GABA_A$ receptor-mediated inhibition interacts with AMPA and NMDA receptor-mediated temporal activity propagation, I studied the changes

in ISIs, and RTs caused by disinhibition. ISIs indicate how fast and sensitively the cells fire on average in these networks. RTs describe well how fast the activation spreads across the neuronal network. Disinhibition significantly shortened the ISIs of AMPA receptor-mediated bursts compared to CTRL condition (Table 3). $GABA_A$ receptors also inhibited the NMDA receptor mediated ISIs. In particular, the shortening of NMDA receptor-mediated ISIs was not as profound as in AMPA receptor-mediated network activity, highlighting the interaction between fast AMPA and $GABA_A$ receptors. The RT decreased in all cultures by disinhibition (Table 3), indicating that $GABA_A$ receptors slowed down the activity propagation of both AMPA and NMDA receptor-mediated activity.

4.1.4 Spatial propagation of network bursts

The spatial spread of activity was examined by determining the number of electrodes involved and analyzing the similarity of the spatio-temporal propagation patterns of the NBs. The similarity measure (SM) was calculated by selecting the first spike time from each electrode as soon as the burst was generated and comparing the similarity of the spatio-temporal activity patterns to each other (for more details see **Materials and Methods**). SM indicates whether the activation propagates along the same or different pathways over the network in AMPA and NMDA receptor blocked cultures and after the disinhibition of AMPA or NMDA receptor-mediated activities. These results show that blockade of NMDA receptors significantly reduced the eRC of electrodes involved in network-wide activity. eRC was not reduced in networks where AMPA receptors were blocked (Tables 2 and 3), suggesting that NMDA receptors may play a spatial role in maintaining the network activity. Disinhibition increased eRC in NMDA receptor blocked networks, but not in AMPA receptor blocked networks.

Table 2. Network activity measures used to train and validate *in silico* models. Measures computed from two types of recordings, CTRL networks from group 1 (CTRL1, n=7) with an acute application of AMPA receptor antagonist (NBQX) and subsequently $GABA_A$ receptor antagonist (NBQX+PTX), and CTRL networks from group 2 (CTRL2, n=6) with an acute application of NMDA (DAP5) and $GABA_A$ receptor antagonists (DAP5+PTX). Quantified measures were used to train and validate the computational models during the data-driven optimization in Publication III.

Condition/ Measures	CTRL1 (n = 7)	CTRL2 (n = 6)	NBQX (n = 7)	DAP5 (n = 6)	NBQX+ PTX (n = 7)	DAP5+ PTX (n = 6)
Mean NB length [s]	0.64 ± 0.64	0.75 ± 0.51	3.46 ± 2.19	0.17 ± 0.18	0.93 ± 0.61	0.39 ± 0.35
Median IBI [s]	7.71 ± 8.98	6.42 ± 7.34	72.85 ± 237.91	5.84 ± 24.12	14.87 ± 63.70	5.51 ± 14.84
Mean NB size (spikes)	248.61 ± 255.73	272.39 ± 191.97	1088.37 ± 1282.20	48.03 ± 25.54	427.32 ± 392.09	656.89 ± 583.69
Mean NB size per el. (# spikes)	7.93 ± 5.49	8.12 ± 3.92	33.04 ± 28.19	2.16 ± 0.76	13.72 ± 8.39	15.88 ± 10.36
Mean no. of el. (# el.)	25.83 ± 10.37	31.24 ± 11.04	29.23 ± 8.85	21.67 ± 6.49	29.20 ± 8.15	30.09 ± 11.29
Mean MFR [Hz]	1.39 ± 1.06	1.44 ± 0.93	1.54 ± 1.04	0.73 ± 0.35	1.49 ± 1.00	4.43 ± 2.86
Mean MFR per el. [Hz]	0.05 ± 0.02	0.05 ± 0.03	0.05 ± 0.02	0.03 ± 0.01	0.05 ± 0.02	0.11 ± 0.04
Mean falling phase [s]	0.51 ± 0.65	0.60 ± 0.49	3.33 ± 2.17	0.10 ± 0.15	0.75 ± 0.58	0.32 ± 0.37
Mean rising phase [s]	0.13 ± 0.11	0.14 ± 0.14	0.13 ± 0.09	0.72 ± 0.06	0.18 ±	0.07

In AMPA receptor antagonized networks, the SM was shown to increase –i.e., spatio-temporal activation patterns correlated more with each other in AMPA receptor blocked networks than in the CTRL networks (Table 3). NMDA receptor blockade did not alter the SM between activity propagation patterns, indicating that

AMPA receptors promoted the diversity and that NMDA receptors the similarity of the spatio-temporal patterns (Table 3). The similarity of these patterns may have increased in AMPA receptor antagonized networks, as NBs have more frequently originated from the same burst initiation zone and were therefore more likely to use the same pathway to propagate over the network. If this is the case then AMPA receptors played an important role not only in accelerating the activity propagation but also in more heterogeneously determining the burst initiation zones, see **Discussion** for more information. Disinhibition significantly increased the SM between the spatio-temporal patterns of NMDA receptor-mediated networks in four out of seven cultures (rest of the cultures contained too few NBs to compute statistical significance) (Table 3). However, the role of $GABA_A$ receptors in spatio-temporal activity propagation patterns needs to be further examined to be certain that both AMPA and $GABA_A$ receptors increase diversity of spatio-temporal activity patterns.

Finally, it was further studied whether the gradual administration of excitatory receptor antagonists affected the network burst dynamics in a different way than their acute administration. Table 3 shows that depending on whether the AMPA receptor antagonist was administered acutely or gradually, the GFR decreased or increased and the IBIs in turn decreased or increased, respectively. It was expected that as the number of fast excitatory receptors decreased after acute administration of the AMPA receptor antagonist, the GFR would also decrease, and IBIs would prolong due to reduced excitation. Exceptionally, the gradual decrease in AMPA receptors resulted in superbursts described in **Publication II**. Superbursts increased the GFR and shortened the IBIs. The increased GFR can be explained by changes in the excitation-inhibition balance that may increase the overall excitation ratio. Network sub-bursts inside the superbursts showed increase in the SM between spatio-temporal propagation patterns, which may be due to slowed network dynamics and bursts originating from the same location unlike before the gradual blockade of AMPA receptors. Possible mechanisms for the generation of superbursts are described in more detail in **Discussion**. Acute and gradual administration of NMDA receptor antagonists produced consistent results, suggesting that a reduction in NMDA receptor activity is less sensitive to changes in network activity than a decrease in AMPA receptor activity.

Table 3. Summary of data analysis of activity dependence on synaptic receptors. Data is presented in **Publication II** to understand how cortical network activity depends on synaptic receptors. Part of this data was used to develop the computational model presented in **Publication III**. The first column 'treatment' defines the antagonized receptor type (AMPA, NMDA or $GABA_A$) and the method by which the pharmacology is administered (acute or gradual). The second column presents the results of data analysis methods computed either throughout the recording period such as GFR, BF and IBI or within the NBs such as ISIs (purple). The third column introduces network burst measures that were extracted from burst profiles, including BL, FP, RP, MFR and BS (blue). Yellow depicts the eRC. The fourth column contains the RT and the SM for the spatio-temporal propagation patterns. The arrows indicate whether the measure in question increased or decreased compared to the state before the synaptic receptor was antagonized. Asterisks indicate how statistically significant the observed change was. Three asterisks indicate $p < 0.001$, two indicate $p < 0.01$, and one indicates $p < 0.05$. A hyphen means that there is no valid data or no change in the value.

Treatment		Network activity				Network burst measures						Patterns	
Data-analysis method		GFR	BF	IBI	ISI	BL	FP	BS	RP	MFR	eRC	RT	SM
AMPA	Gradual n=2	↗	-	↘ ***	↗ ***	↗ ***	↗ ***	↗ ***	↗ ***	↘ ***	↘ ***	↗	↗ ***
	Acute n=7	↘ **	↘ ***	↗ ***	↗ ***	↗ ***	↗ ***	↗ ***	-	-	-	↗	↗
(AMPA+) $GABA_A$	Acute n = 7 vs.AMPA	-	↗ *	-	↘ ***	↘ ***	↘ ***	↘ *	-	-	-	↘	-
NMDA	Gradual n=2	↘	↘	↗ ***	↘ ***	↘ ***	↘ ***	↘ ***	↘ ***	-	↘ ***	↘	-
	Acute n=6	↘ **	↘	↗ ***	-	↘ **	↘ **	↘ **	↘ *	-	↘ *	↘	-
(NMDA+) $GABA_A$	Acute n = 6 vs.NMDA	↗ **	-	-	↘ ***	↗ **	↗ **	↗ **	-	↗ **	↗ *	-	↗
$GABA_A$	Gradual n=1	↗	↗	↘ ***	↘ ***	↗ ***	↗ ***	↗ ***	↗ ***	↗ ***	↗ ***	↘	↗ ***

(AMPA+) $GABA_A$	Acute n = 7 vs. CTRL	↘	↘ ***	↗ ***	↘ ** *	↗ **	↗ *	↗ *	-	-	-	↘	-
(NMDA +) $GABA_A$	Acute n=6 vs.CTRL	↗	↘	↗ ***	↘ ** *	-	-	↗ *	-	↗ *	↗	↘	↘

4.2 Evaluation of microelectrode array data for computational modeling

In **Section 4.2**, I present how experimental MEA data, recorded from cortical networks as burst activity *in vitro* and described in **Section 4.1**, is prepared for optimal data-driven spiking network model construction. I justify the selection of measures described in **Section 4.1** to maximally support the construction of the spiking network models. Next, I describe the data-analysis workflow that was used to systematize the computational data-driven modeling approach *in silico*, the use of measures in the model-building process, and briefly the process of fitting the computational models. Finally, I also summarize the results of the data-driven modeling and show how the model succeeded in reproducing network activity under synaptic excitatory and inhibitory receptor antagonists (**Publication III**).

4.2.1 Data-analysis workflow and data-driven network modeling approach

A data analysis workflow was developed for *in vitro* MEA data to support the building of data-driven spiking network modeling approach *in silico* (Figure 13). The development of such data-analysis workflows and data-driven models is important because they can be used in the future to design and test new biological hypotheses *in vitro* and *in vivo* experiments. Well-designed data-analysis workflows support the integration and storage of metadata, recorded raw rata, and simulated data into database infrastructures to ensure efficient data management and reproducibility of previous studies.

The computational data-driven model presented in **Publication III** is the first to combine the analysis of MEA data from several different pharmacological protocols with network models to create an optimal fitting approach (Figure 13). The model

incorporates the necessary synaptic, point-neuron, and network mechanisms to simulate the dynamics of network activities like those recorded under different pharmacological conditions from *in vitro* networks in **Publication II**. The selected computational model composed of a phenomenological spiking point-neuron (Izhikevich, 2003) and synapse models (Wang, 1999; Tsodyks et al., 2000; Compte et al., 2000) with a random connectivity between neurons to describe the network (for more details see **Publication III**). This choice was made for computational reasons in order to perform computationally heavy estimations of the model parameter values. Estimates were computed using the datasets that were recorded and for the first time presented in **Publication I** and further analyzed in **Publications II** and **III** (see also **Section 4.1**).

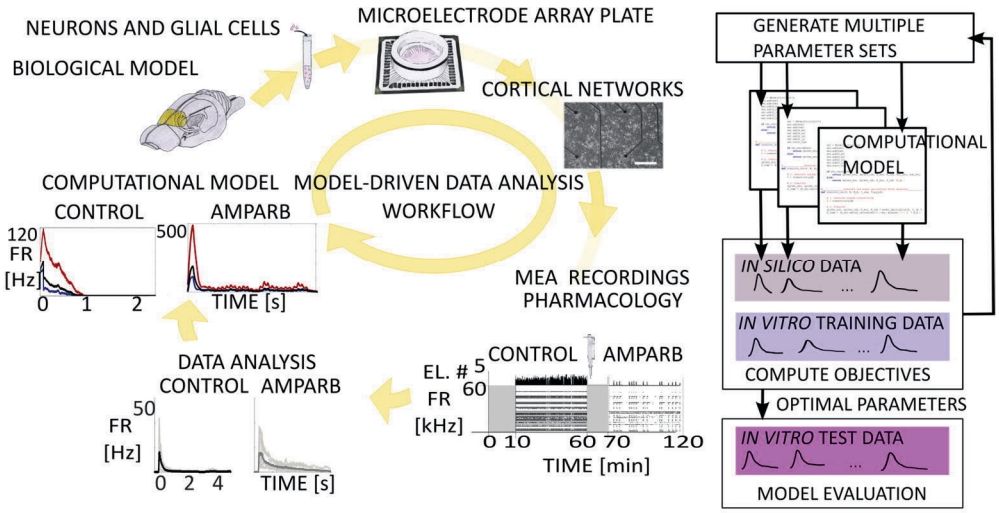

Figure 13. A model-driven data analysis workflow and modeling approach. Burst measures were calculated from the network burst data that was recorded with MEAs under pharmacology from rat cortical networks. A data analysis procedure supported the data-driven computational model design, fitting, and validation. In the computational spiking network model approach the cellular and synaptic model parameters were fitted. In each iteration of the fitting algorithm a number of copies of the model were generated with different model parameters. Models were simulated, NBs detected, and quantitative measures such as distributions of BL and BS were computed. Comparison between *in silico* and *in vitro* test data allowed selection of the best models. Approach enables to examine the effects of cellular and synaptic mechanisms on cortical network activity *in silico* (**Publication III**). The figure component of the computational modeling on the left is provided as a courtesy of Jugoslava Aćimović.

In **Publication III**, a new model fitting approach was constructed based on multi-objective genetic algorithms with spiking network model (Bahl et al., 2012). Experimental data from five different pharmacological conditions, including CTRL

activity, AMPA and NMDA receptor antagonized activities and $GABA_A$ receptors antagonized AMPA, and NMDA receptor-mediated activities (protocol ids 1 and 2 in Table 1) were analyzed. Selected network burst measures were integrated into the model by formulating model fitting objectives (Figures 14 and 15). Data-derived objectives were used to compare burst measures extracted from *in vitro* and *in silico* data to allow quantitative comparison of simulated and experimental data. This approach enables the selection of optimized model parameter values to fine-tune the model to appropriate bursting dynamics of the network. A summary of how well the computational model reproduced the result of analyzed data recorded from rat cortical networks *in vitro* is presented later in this section (Figure 16).

4.2.2 Quantification of network burst measures for computational modeling

The MEA data recorded from rodent cortical networks *in vitro* were first categorized to support data-driven computational modeling of network burst activity. Several measures representative of network burst activity were then quantified (see **Publication III** for details of methods). A workflow describing how the data was handled and analyzed to maximally support the fitting of the computational model is shown in Figure 13. The same procedure was also used in **Publication III**. Table 2 summarizes several NB measures of the multi-unit spike data in the five different pharmacological conditions of the cultures. The distributions, means, and variances of BS and BL were used for the model fitting protocols in **Publication III** (Figures 14 and 15).

Measures in Table 2 quantitatively present that in the CTRL activity the mean network BL was ~700 ms, consisted of an average of ~260 spikes and occurred at an average interval of ~7 seconds. The RPs and FPs of the network bursts lasted on average ~ 135 ms and ~555 ms, respectively, and the MFR reached ~1.41 Hz in CTRL condition. Finally, on average ~ 29 of 59 electrodes were active in CTRL cultures. When AMPA receptors were antagonized, the mean BL increased to ~3.46 s, consisted of more than 1000 spikes and occurred at an average interval of ~73 s. Disinhibition reduced BL back to ~930 ms, BS to ~427 spikes, and IBIs to ~15 s in AMPA receptor antagonized networks. In contrast, when NMDA receptors were antagonized, the BL decreased to ~170 ms, consisted of an average ~ 48 spikes and occurred every ~6 seconds. Disinhibition increased BL to ~390 ms, BS to ~657 spikes, and IBIs to ~ 5.51 s in AMPA receptor antagonized networks (Table 2). Data curation helped to organize and integrate data from different experiments and

pharmacological protocols. Proper data curation and well-quantified measures greatly supported the data-driven model fitting and validation procedures for modeling of network activity as shown in **Publication III.**

The model construction and fitting process required carefully selected measures (Figures 14, 15, and Table 2) that were calculated from the network burst data (Figure 12). The aim was to select the measures that best describe the recorded network bursts under different pharmacological conditions and that could be used to optimize the parameter values for model validation. The computational study focused on modeling the effects of synaptic receptors and their modulations during the bursts, so the analysis of other cellular and network mechanisms was omitted.

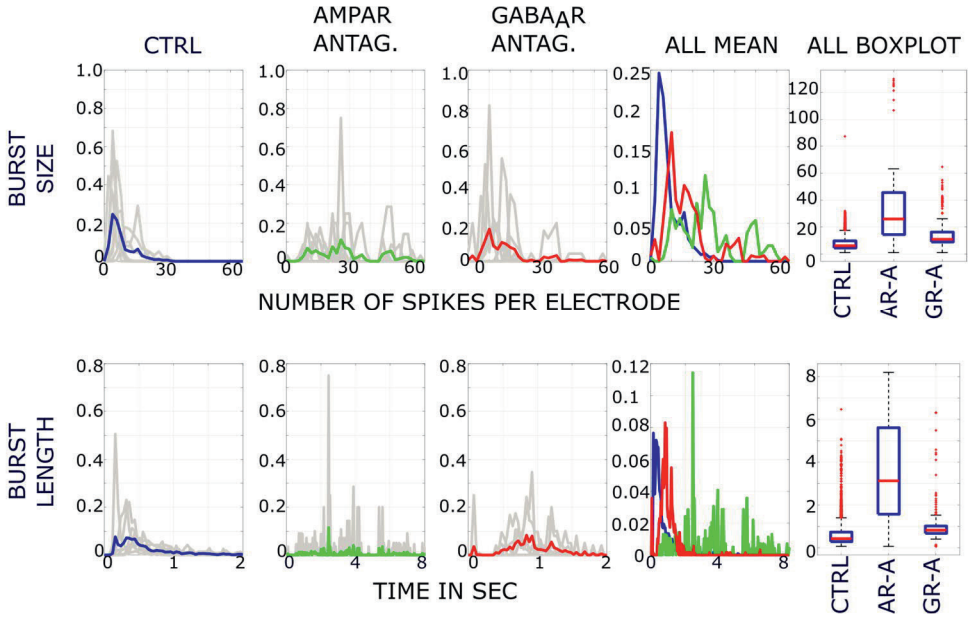

Figure 14. Analysis of MEA data in AMPA & $GABA_A$ receptor blocked networks. This analysis was performed for model fitting. Average distributions of burst measures over all cultures (n= 7); BS and BL in CTRL (blue), AMPA receptor antagonized (AR-A, green) and AMPA with $GABA_A$ receptor antagonized (GR-A, red) conditions were computed to support the fitting of spiking network model. Distributions of individual cultures are shown with grey lines. Mean values (red line in the boxplots), SDs (mean+/- std, blue box) and quantiles (whiskers) for BS and BL. Distributions of BS and BL increased in AMPA receptor antagonized networks in comparison to CTRL and decreased in disinhibited networks compared to previous condition. Measures computed here were used as training and validation data in the optimization process of the computational model.

In **Publications I** and **II**, the experimental results showed that the network burst profiles changed significantly in each of the five conditions (Figure 12). Therefore, these changes were quantified by calculating the average burst measures from the burst profiles (Tables 2 and 3). Several burst measures, such as BL, FP, RP, MFR, BS, and eRC, were considered for use in model optimization. However, the number of burst measures had to be minimized to avoid an excessive increase in the number of fitting objectives as they overload the model simulation. The intention was to avoid the selection of highly correlated network burst measures, so the cross-correlation between them was calculated.

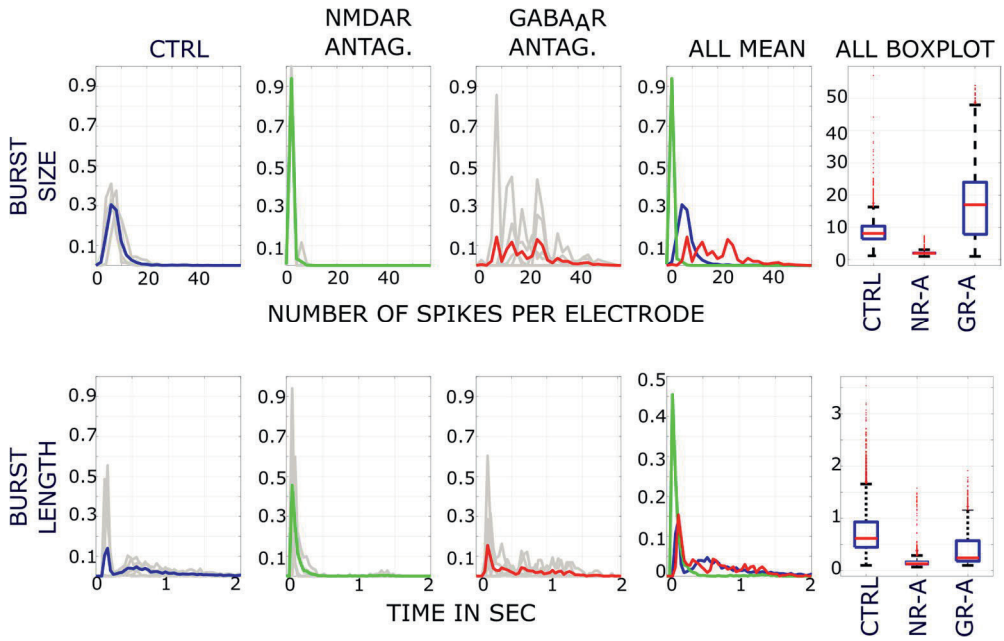

Figure 15. Analysis of MEA data in NMDA & GABA$_A$ receptor blocked networks. This analysis was performed for model fitting. Distributions and boxplots of BS and BL in CTRL (blue), NMDA receptor antagonized (AR-A, green) and NMDA receptor with GABA$_A$ receptor antagonized (GR-A, red) conditions were computed to support the fitting of network models. Distributions of individual cultures is shown with grey lines. Mean values (red line in the boxplots), SDs (mean+/- std, blue box) and quantiles (whiskers) for BS and BL. Distributions of BS and BL decreased in NMDA receptor antagonized networks in comparison to CTRL and increased in disinhibited networks compared to previous condition. Measures computed here are used as training and validation data in the optimization process of the computational model.

Two burst measures, the BS and BL, that best described the observed differences in burst profiles between different pharmacological conditions but did not correlate too much with each other were selected for data analysis to train and validate the model. Both burst measures BL and BS for each experimental condition were combined from different cultures to obtain five datasets for the five experimental conditions. The distributions, means, and percentiles (25^{th} and 75^{th}) of BL and BS under each pharmacological condition were analyzed from the experimental data (Table 2, Figure 14, Figure 15). 70% of each data set was used to train the computational model in the model fitting process (Figure 13). 30% of each experimental data set was used to assess the goodness of fitting. Data-derived objectives were used to compare burst measures extracted from *in vitro* and *in silico* data to allow a quantitative comparison of the simulated and experimental data in **Publication III** (Figure 16).

4.2.3 Reproduction of network bursts using computational modeling

The aim of the data-driven modeling approach in **Publication III** was to reproduce experimentally recorded data, particularly the measures of network BL and BS. The model selection was based on two objectives, the distances between the BL and the distances between the BS distributions of the *in silico* and *in vitro* measurements. The distances were expressed as model fitting error (Figure 16) (more details in **Publication III**). In short, the results show that the model was successfully fitted to the recorded *in vitro* data, to the distributions of BL under all conditions, and to the distributions of BS under all conditions except in NMDA and $GABA_A$ receptor blocked networks (Figure 16).

As presented in **Publication III**, the modeling results obtained highlight the importance of the modeled mechanisms, which were considered crucial in reproducing the experimental results. The approach presented in **Publication III** was able to reproduce most of the experimental conditions and changes in network burst structures after blocking the synaptic receptors, as in experimental **Publications I** and **II.** The fitting of the BS distribution of NBs in modeled spiking neuronal networks in which NMDA and $GABA_A$ receptors were antagonized failed more often than the fitting of other conditions (Figure 16, **Publication III**). This indicates that the chosen spiking neuronal network model may not include sufficiently broad dynamics, particularly in a condition where only AMPA receptors are active. In summary, the modeling results of **Publication III** confirm what is seen

in the experimental data, i.e., that the interplay between synaptic excitatory and inhibitory receptors results in the observed changes in activity. Additional data for future modeling can also be obtained from **Publication II** and **Table 2**.

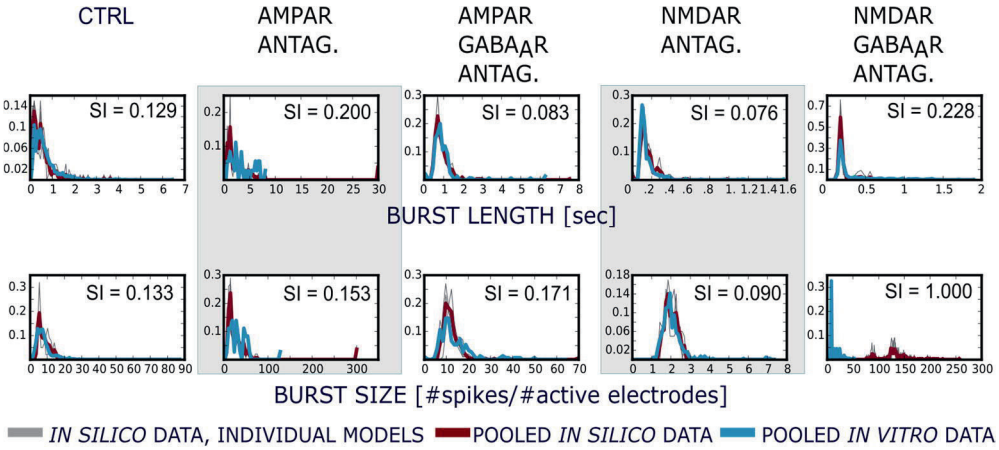

Figure 16. Convergence of the results of the data-driven network models. Distributions of BL and BS for experimental data (blue) and simulations of optimal models (red). This model approach used a fitting protocol in which a separate neuronal network model was constructed for each of the five experimental conditions, CTRL, AMPA receptor blocked, AMPA and $GABA_A$ receptor blocked, NMDA receptor blocked and NMDA and $GABA_A$ receptor blocked. Each column shows model fitting precision for the selected burst measures which are distributions of BL and BS in each pharmacological condition. The blue lines show the distributions computed from experimental *in vitro* data obtained by pooling all available cultures and the red lines represent the pooled simulated *in silico* results obtained from repetitions of the model fitting. The similarity between the experimental and simulated data is quantified by fitting errors. If the value is less than 0.2 it indicates that model fitting succeeded. Fitting succeeded for almost all conditions except for NMDA and $GABA_A$ blocked condition. For details of the statistical analysis see **Publication III**. The figure is provided as a courtesy of Jugoslava Aćimović.

4.3 Differentiation of human neuroblastoma cells

Section 4.3 summarizes how external substances affected the level of neuronal differentiation of human neuroblastoma cells and how the adhesion of these cells and differentiated network formation and morphology depends on the coating agents. The aim was to expand the understanding of network functionality and synaptic properties from rodent networks to morphologically differentiated human neuroblastoma cells and networks. In **Publication IV** the effects of E_2, CHOL, and BDNF alone and in combination with RA were studied for neurite outgrowth,

synaptic vesicle recycling, and arrest of cell population growth in human neuroblastoma cells *in vitro*. In **Publication V**, the effects of coating agents were examined to differentiated and non-differentiated human neuroblastoma cell adhesion and network morphology.

4.3.1 Morphological characterization of differentiated cells, synapses, and networks

Human neuroblastoma cells retain their ability to differentiate under culture conditions. The RA is the most common substance known to induce these cells into neuron-like phenotypes. However, RA has not been shown to lead to terminal differentiation, so other substances must be examined to increase the level of differentiation. The aim of the **Publication IV** was to find a functional combination of substances for effective induction of differentiation in human cells. The level of the induced neuronal differentiation was characterized by immunocytochemical technique by staining synaptic vesicles, neurofilaments, and nuclei that were automatically traced and analyzed with image analysis software (see more details in **Materials and Methods**).

The effects of estradiol (E_2) to induce the higher level of differentiation was evaluated. In **Publication IV,** E_2 was shown to increase neurite sprouting and synaptic vesicle recycling. E_2, when used in combination with RA (RE), increased neurite length, synaptic vesicle recycling and inhibited cell population growth. However, some of the RE treated cells had unwanted thin neurites without profuse branching. E_2 provides interesting results in terms of functional differentiation because of its ability to increase synaptic vesicle recycling in human neuroblastoma cell cultures.

Cholesterol (CHOL) was known to play an important role in the development of active synapses. Therefore, the effect of CHOL to increase the degree of differentiation of human neuroblastoma cells was examined. Results showed that CHOL increased neurite outgrowth and when used in combination with RA, it increased the number of synaptic vesicles in a supra-additive manner. In addition, CHOL supported RA-induced neurofilament growth and arrest of cell population growth. CHOL combined with RA showed good results in differentiation due to its ability to produce increased synaptic vesicle recycling. Combining RA with CHOL has an advantage over conventional RA treatment because it supported the differentiation of human neuroblastoma cells into neuronal phenotypes.

The effect of brain-derived neurotrophic factor (BDNF) on human neuronal differentiation was also studied. BDNF was known to support the neuronal survival and stimulate the growth and differentiation of new neurons and synapses. BDNF works as a ligand for the tropomyosin-related kinase B (TrkB) receptor. TrkB receptors are not existing in naïve neuroblastoma cells. RA, in turn, induces TrkB expression and responsiveness to BDNF. Presumably, BDNF when used alone showed no outgrowth of neurites or increased synaptic vesicle recycling in human neuroblastoma cells (**Publication IV**), but when combined with RA (RB) it supported the branching of long neurites, complete network formation and synaptic vesicle recycling, but did not arrest cell population growth. This may be due to the tendency of BDNF to support neuronal survival (more on this in the **Discussion**).

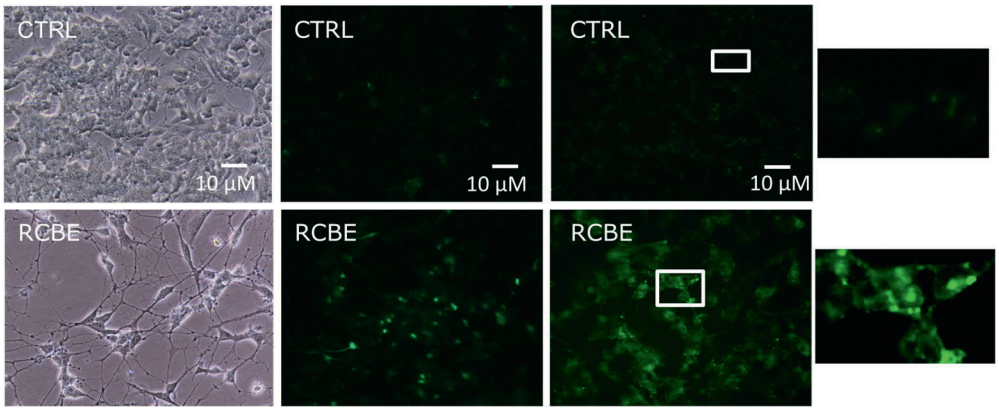

Figure 17. Differentiation of human neuroblastoma cell networks. Human cells were differentiated with RA, CHOL, E_2, and BDNF (RCBE) until 10 DIV. Top row shows the CTRL culture without external differentiation substances and bottom row RCBE differentiation in human neuroblastoma cells. Second column illustrates the staining of neurofilaments-68 and third column synaptic vesicle recycling. RCBE induces network and synapse formation.

Ultimately, the level of differentiation was determined by combining all the above substances, including RA, CHOL, E_2, and BDNF (RCBE). RCBE combination treatment showed neurite outgrowth, branching of neurites, neuron-neuron interactions, synaptic vesicle recycling and cell network structure (Figure 17). RCBE showed results of functional differentiation with the ability to produce functional synaptic vesicle recycling and network formation. RCBE has potential advantages over traditional treatments. However, the efficacy of BDNF in arresting the population growth rate of human neuroblastoma cells should be further research to ensure its ability to differentiate. The network activity of differentiated human

neuroblastoma cells was recorded with MEA technique, but preliminary tests with high potassium levels proved negative. The emergence of network-wide activity in differentiated human neuroblastoma cell cultures requires further studies (see **Discussion**).

4.3.2 Cell adhesion and network formation with surface coatings

The connectivity and structure of cell networks are known to affect neuronal activity patterns. To study the electrophysiological properties of network activity in a standardized manner with MEA technique from multiple cultures for long periods of time, it is essential that cells adhere, grow, and mature healthy and evenly on recording plates. The silicon nitride surface properties of the MEA plate are hydrophilic and negatively charged, resulting in uneven distribution and adhesion if the MEA plate is not handled properly, including cleaning, rinsing, sterilizing, drying, hydrophilizing and coating. Therefore, it is essential to verify and find an optimal coating that promotes cell adhesion, viability, neurite outgrowth, and network formation of cells. The aim was to optimize homogenous cell adhesion, neurite sprouting, and network formation of human neuroblastoma cells (induced by differentiation). The effects of coatings on the adhesion and morphology of undifferentiated cells and network formation of differentiated human cells were studied. In addition, the cell adhesion, growth, and network formation of dissociated rat neocortical cells were demonstrated on coated cover slips and MEA plates over two weeks *in vitro* (see **Materials and Methods** section).

In **Publication V**, morphological and immunocytochemical analysis of cell nuclei were performed to study the effects of coatings such as LAM and PEI on undifferentiated and differentiated human neuroblastoma cells and networks. Adhesion of undifferentiated cells, cluster formation, and the shape and number of cell nuclei, as well as adhesion of differentiated cells, neurite outgrowth, network formation, and number of cell nuclei were assessed. Result showed that undifferentiated cells adhered optimally to the LAM coating (Figure 18). LAM allowed homogenous and widespread attachment of cells and the formation of a compact and round nuclei of undifferentiated cells (Figure 18). Cells attached poorly and were unevenly distributed on PEI-coated substrates (Figure 18). LAM used in combination with PEI (PEI + LAM) slightly increased the adhesion rate at 1 DIV (Figure 18). However, cell clusters were formed with PEI and PEI + LAM coatings beginning at 3 DIV. The radii of the clusters increased over time and were larger in

size on LAM + PEI coatings compared to PEI coatings. The number of nuclei was decreased on PEI coating in comparison to CTRL and LAM surfaces, which may be due to clustering.

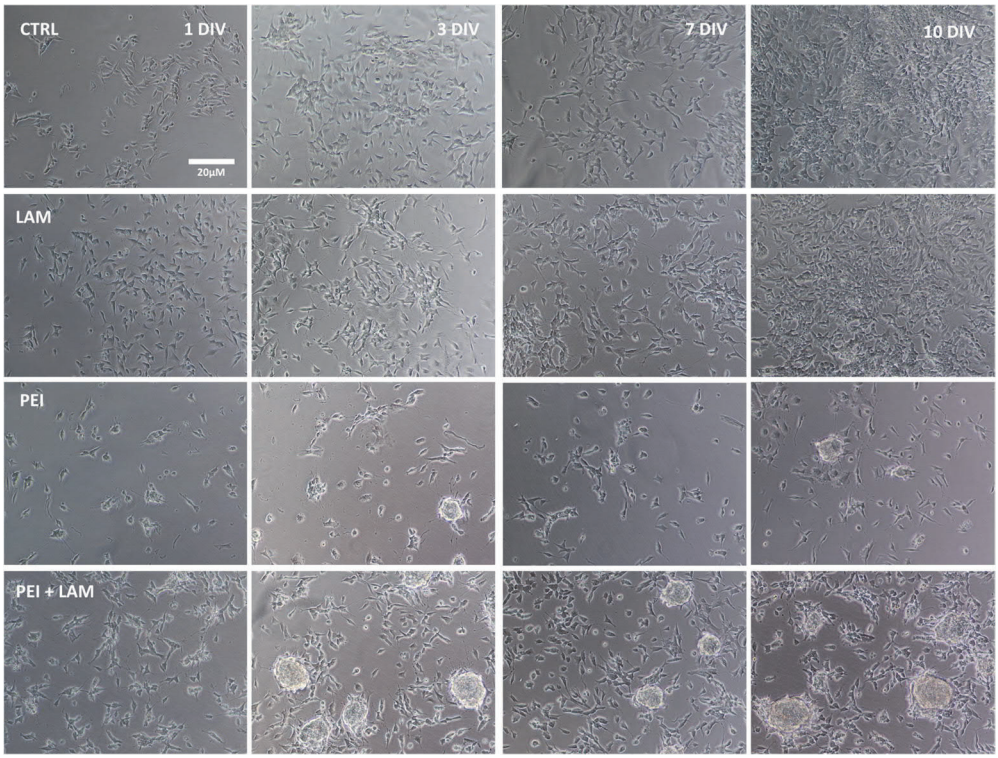

Figure 18. Morphology of human neuroblastoma cells with different coatings. Cell adhesion was optimal on CTRL and LAM surfaces. Over time, cells with PEI alone or in combination with the LAM coating attach unevenly and form clusters compared to cells on CTRL or LAM surfaces.

The effects of coatings on both undifferentiated and differentiated cells were studied because differentiation substances and coatings may interact or have supra-additive effects with each other. When studying the effects of coatings on differentiated cell nuclei counts, it had to be considered that both successful differentiation and poor adhesion could reduce the number of nuclei and thus affect the measurement of the growth rate of the cell population. The number of differentiated nuclei was compared with each other and not with the number of undifferentiated nuclei (Figure 19).

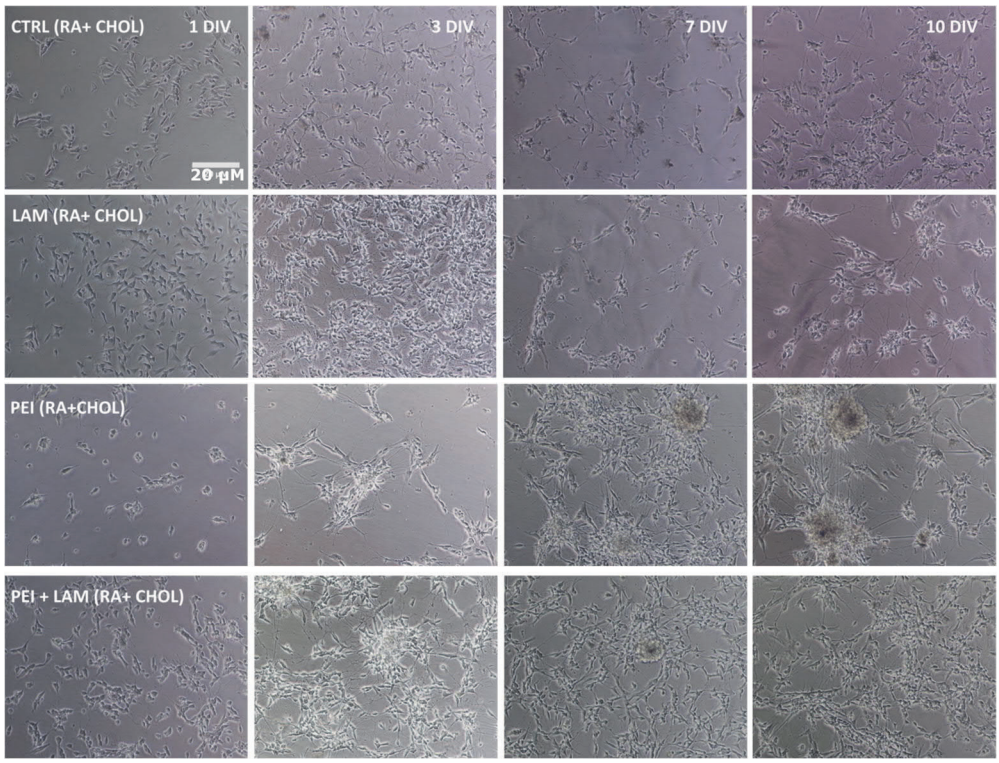

Figure 19. Effects of coatings on network formation in differentiated human cells. Cells were differentiated with RA and CHOL. Neuronal adhesion and network formation were optimal on CTRL and LAM coatings. Neuronal adhesion was low on the PEI surfaces. After seeding, clusters of cells formed, and straight bundles of neurites grew between the clusters on PEI and PEI together with LAM surfaces. Based on these studies LAM alone was the optimal coating agent for differentiated human neuroblastoma cells.

The results showed that the adhesion of the differentiated cells was poor on PEI coatings and optimal on LAM and PEI+LAM -coated surfaces at 1 DIV (Figure 19). At 3 DIV, cells begin to cluster on PEI and PEI+LAM -coated surfaces. LAM supported the formation of the shape of oval nuclei, extensive neurite outgrowth, and branching, and the complete network structure of differentiated human cells at 10 DIV (Figure 19). PEI promoted direct bundles of neurites between clusters. The number of differentiated cell nuclei was low on PEI and PEI+LAM surfaces. PEI decreased the number of nuclei with and without differentiation. LAM was shown to be a suitable coating for undifferentiated cells because it allowed widespread adhesion and therefore also proper network formation for differentiated human cells (Figure 18, 19, and Table 4).

Table 4. Human neuroblastoma cell adhesion and network formation on coatings

Coating	Cell adhesion	Form of nucleus	Cluster formation	Count of nuclei	Suitability
CTRL	++	compact, roundish	--	++	n/a
LAM	++	compact, roundish	--	++	++
PEI	-	tapered	+	-	--
PEI + LAM	+	tapered	++	-	-
Coating with differentiation	**Cell adhesion**	**Neurite outgrowth**	**Network formation**	**Count of nuclei**	**Suitability**
CTRL (RA+CHOL)	++	++	++	++	n/a
LAM (RA+CHOL)	++	++	++	++	++
PEI (RA+CHOL)	-	-	-	-	--
LAM+PEI (RA+CHOL)	+	+	-	-	-

--none; -minimal; +moderate; ++maximal; n/a not applicable

5 DISCUSSION

This thesis presents results on synaptic properties and neuronal network function in rodent and human cells using *in vitro* cell cultures, immunocytochemistry, microelectrode array (MEA) recordings, advanced data and image analysis, and *in silico* modeling techniques. Emphasis is on the functional maturation of rodent and human networks, as well as on synaptic transmission and spontaneous activity in rodent networks. The maturation and function of the network and the role of synaptic properties in them are investigated in three approaches: the first part examines the role of excitatory and inhibitory synaptic transmission and their mediator receptors in network-wide activity using MEA technique combined with pharmacology in postnatal rat cortical networks *in vitro*; the second part presents a data analysis workflow protocol that provides statistical measures of MEA activity to support the fitting and validation of computational data-driven neuronal network models; and a third evaluates synaptic properties and network formation in differentiating human neuroblastoma cell cultures. This chapter discusses the main findings and compares them to previous related research.

The discussion is organized as follows. In **Sections 5.1** to **5.4**, I discuss the state of the art of the synaptic and cellular mechanisms underlying the initiation, propagation, and termination of network-wide bursts in dissociated cortical cell cultures *in vitro* and *in silico*. I also discuss in detail how the results presented in this thesis change our understanding of the role of excitatory and inhibitory synaptic receptors in network-wide activity and dynamics. In **Section 5.5**, I discuss how molecules identified as essential for synapse development, such as E_2, CHOL, and BDNF, influence the differentiation of human cells into neuronal phenotypes and networks. In all sections, I discuss how the key findings of my research in **Publications I–V** are reflected in the results presented by others.

5.1 Initiation of network bursts

The spontaneous synchronized activity of neurons in dissociated cortical cultures – i.e. repetitive NBs – is a hallmark of the functional maturation of networks extracted from the prefrontal cortex in the embryonic and postnatal stages (Blankenship & Feller, 2010; Egorov & Draguhn, 2013; Luhmann et al., 2016). Maturation of the functional network is a complex process in which the structure and synapses of the network are formed in parallel with the development of the activity (Harrill et al., 2015; Matsumoto, N. et al., 2016). Cortical networks independently mature and functionally stabilize by producing synaptic transmission and spontaneously synchronized activity across the network at three weeks *in vitro* (Wagenaar et al., 2006; Baltz et al., 2010). Networks are spontaneously active without input, which means that NBs are generated due to the intrinsic properties of the cells and the network they form (Marom & Shahaf, 2002). Although there are many theoretical and experimental studies on the mechanisms that explain the initiation of NBs, the conclusions are controversial (Brunel & Wang, 2003; Giugliano et al., 2004; Eytan & Marom, 2006; Shein et al., 2008; Gritsun et al., 2010; Yarom & Hounsgaard, 2011; Suresh et al., 2016; Lonardoni et al., 2017; Okujeni & Egert, 2019b). In essence, most studies have addressed only one or a few factors that influence the dynamics of NBs in cortical networks *in vitro* or *in silico*. In this thesis, I examined the role of both excitatory and inhibitory receptors in burst dynamics *in vitro* and in data-driven models *in silico*.

In **Publications I** and **II**, when studying the effects of synaptic ionotropic AMPA, NMDA, and $GABA_A$ receptors on NB dynamics, I found that AMPA receptors play a key role in the initiation of spontaneous NBs. This finding is supported by the fact that the inhibition of AMPA receptors significantly reduced the number of NBs, whereas the inhibition of NMDA or $GABA_A$ receptors did not significantly affect the number of NBs. In addition, I showed that AMPA receptors contribute to the early phase of NBs by rapidly recruiting neurons to participate in network activity. The results of this thesis are consistent with previous studies, showing that synaptic currents have a significant AMPA component responsible for initiating cortical network activity (Robinson et al., 1993; Jimbo et al., 2000; Fong et al., 2015). Some recent studies on hippocampal cultures indicate that NBs do not occur after blockade of AMPA receptors (Suresh et al., 2016; Lonardoni et al., 2017), while others show that blockade of AMPA receptors retains NBs in rat cortical networks (Ramakers et al., 1993; Martinoia et al., 2005; Fong et al., 2015). The latter results are consistent with the result of **Publications I** and **II** of this thesis. These

conflicting results may be due to many factors, such as the varying numbers of receptors in cortical and hippocampal tissues, or the age of the donor animal (embryo vs. postnatal). The age of the donor animal has been shown to affect synaptic properties, such as the maturation and strength of the AMPA and NMDA receptors (Lin et al., 2002).

It has been suggested that spontaneous NB activity could begin in slices of the neocortex due to an imbalance in excitation and inhibition (Brunel & Wang, 2003). The excitation-inhibition balance has been shown to be impaired during epileptic seizures in animals *in vivo*, suggesting that a basic feature of healthy brain function would be the balanced activity of excitation and inhibition, resulting in activity without NBs (Dehghani et al., 2016). Nevertheless, rodent cerebral cortices are known to exhibit NBs to prime the cells for incoming sensory input in the embryonic and postnatal stages (Molnar et al., 2020). **Publication II** showed that there were fewer NBs in network activity after the acute blockade of AMPA receptors – i.e., when excitation decreased compared to inhibition – and the NBs were substantially longer compared to the control NBs. After the gradual blockade of AMPA receptors, so-called superbursts occurred. These results are consistent with studies in which the excitation-inhibition balance was manipulated by increasing the number of interneurons (Chen, X. & Dzakpasu, 2010) or decreasing the number of AMPA receptors (Fong et al., 2015). In both studies, superbursts or long NBs were recorded after the inhibition increased relative to the excitation. All these studies support the hypothesis that an increase in inhibitory drive relative to excitatory drive would cause long superbursts or the epileptic type of NBs. However, these studies do not directly explain which factors initiate the NBs.

Theoretical studies have suggested that pacemaker neurons play a role in NB initiation (Shein et al., 2008; Gritsun et al., 2010). In fact, pacemaker neurons have been found in cultures prepared from spinal cord neurons and in slices of the primary visual cortex *in vitro* (Latham et al., 2000; Latham et al., 2000; Le Bon-Jego & Yuste, 2007). In the studies of this thesis, activity between NBs appeared to be very low, so there were no continuously firing neurons that could act as pacemakers before the onset of NBs. To the best of my knowledge, my observation is consistent with other studies in which no pacemaker or intrinsically active neurons have been found in cortical cultures (Maeda et al., 1995; Marom & Shahaf, 2002). In contrast, in postnatal cortical cultures an increase in spiking activity was recently observed in NB initiation zones before the onset of an individual NB due to the integration and amplification of activity (Okujeni & Egert, 2019a). Okujeni and Egert (2019a) also oppose the dominant role of intrinsically active pacemaker neurons in initiating NBs

but acknowledge that such critical neurons may have been overlooked due to the low sampling rate of the neuronal activity. Using single-cell resolutions of high-density MEA recordings, Lonardoni et al., (2017) have also observed that NBs begin in highly correlated local neuron ensembles with amplified activity in embryonic hippocampal cultures. Finally, my observation of the role of AMPA receptors as NB initiators is indirectly supported by Okujeni et al., (2017) showing that NB initiation zones are typically located at the transition point between hot and cold zones. It can be assumed that there are potentially more synapses at these transition points or group of neurons, and thus AMPA receptors are more likely to be located at these sites as well. From cellular level patch clamp studies, it is known that AMPA receptors are important for cell depolarization – i.e., an increase in activity – which would explain the amplification of activity in these cell groups.

It has also been reported that a persistent sodium current I_{NaP} is associated with the intrinsic pacing of neurons, thus contributing to the induction of intrinsic firing and the initiation of spontaneous NBs in the spinal cord as well as cortical and hippocampal cultures (Darbon et al., 2004; van Drongelen et al., 2006; Suresh et al., 2016). I_{NaP} has been shown to drive depolarizing subthreshold potentials and to maintain rhythmic bursting in cerebellar granule cells (D'Angelo et al., 1998). On the other hand, subthreshold oscillations in cortical neurons are clearer and more regular than those observed in granule cells (Gutfreund et al., 1995), and thus may be caused also by other factors. In spinal cord cultures, the generation of NBs has been shown to be associated with both I_{NaP}-dependent intrinsic activity and repetitive excitation via glutamatergic synaptic circuits (Czarnecki et al., 2008). The interpretation of these studies is challenging because the role of I_{NaP} has been examined by blocking the Na_P channel with Riluzole, which also reduces glutamate release and thus interferes with AMPA and NMDA receptor functions (Martin et al., 1993). In this thesis, I did not study the role of I_{NaP} in the generation of bursts. Nevertheless, I hypothesize that I_{NaP} might have a potential synergistic role with AMPA receptors, in which case both could be necessary for the initiation of NBs in the correlated neuron ensembles found in the initiation zones. The involvement of I_{NaP} alone and in interaction with the glutamatergic synaptic circuit in the generation of NBs in cortical cell cultures should be further studied.

It has also been described in the literature that NBs could be triggered when background noise due to the stochastic nature of ion channel openings reaches a certain threshold (Giugliano et al., 2004; Eytan & Marom, 2006). Stochasticity, which occurs naturally in ion channel functions, has been shown to be important in regulating the membrane voltage at the firing threshold of AP (Linne et al., 1996).

The potential role of stochasticity in single neuron dynamics has been further examined in a computational neuron model that incorporates stochasticity in the ion channel function (Saarinen et al., 2008). In this thesis, I did not examine the role of stochasticity in the initiation of NBs, but I hypothesize that Na_P channels would contain inherent stochasticity different from synaptic receptors. In fact, in small cerebellar granule cells, it has been shown that by blocking glutamatergic and GABAergic receptors, irregularities in neuronal firing are due to intrinsic mechanisms and not due to synaptic mechanisms (D'Angelo et al., 2001).

In the constructed data-driven network model of **Publication III**, a Gaussian noise was included in all *in silico* neurons. The noise affected the subthreshold dynamics but did not cause APs. This process describes the stochasticity observed when recording ion channels *in vitro* (Linne et al., 1996). In addition to this, a few neurons were randomly injected with a small external stimulus in the form of a pulse current, thus triggering a burst. The synaptic current of the model also included inputs from glutamatergic and GABAergic receptors. Other computational studies that have simulated the network activity of dissociated cultures have used a few slightly different ways to induce network bursting *in silico*, including pacemaker neurons, Poisson noise input to each neuron, intrinsically generated random spiking, and spontaneous synaptic activity (Latham et al., 2000; Gritsun et al., 2010; French & Gruenstein, 2006; Baltz et al., 2011; Yamamoto et al., 2016; Lonardoni et al., 2017).

The results obtained here, along with those of other laboratories, suggest that glutamatergic AMPA receptors, together with ion channel currents such as I_{NaP}, are involved in increased firing activity, activity integration, and amplification, as seen in highly correlated neuron ensembles in burst initiation zones. It is likely that the dynamics of voltage-dependent Na_P channels incorporate stochasticity and inherent pacing, and that the channels thus could act as a neuronal pacemaker. In addition, changes in the excitation-inhibition balance, including possible local changes in the amount of different ion types, may affect the exhibition and forms of NBs. In the next sections, the role of synaptic receptors in the propagation and termination of NBs is discussed.

5.2 Propagation of network bursts

Spontaneous NBs of cultured cortical networks have been shown to maintain spatio-temporal activity propagation patterns with a unique structure in which neurons fire a spike-train with different delays relative to each other (Volman et al., 2005;

Raichman & Ben-Jacob, 2008). However, the detailed properties of these patterns are not yet understood. For example, it is not known how excitatory and inhibitory synaptic receptors affect the rate of activity propagation and the similarity of spatio-temporal patterns. In this thesis, the dependence of the speed and the structural similarity of spatio-temporal propagation patterns on synaptic AMPA, NMDA, and $GABA_A$ receptors were examined.

In **Publication II**, I focused on analyzing how quickly the neurons are recruited to network-wide activity (i.e., the time it takes for the activity to pass through the network) under the influence of excitatory and inhibitory receptor antagonists. I found that when AMPA receptors were blocked, neurons were recruited more slowly than in control networks, whereas blockades of the NMDA and $GABA_A$ receptors accelerated neuronal recruitment – i.e., the propagation of network activity. The slowing effect of the $GABA_A$ receptors on activity propagation is supported by a calcium imaging study that determined the average velocity of propagation in control and disinhibited cultures (Orlandi et al., 2013). To the best of my knowledge, **Publication II** is the first report to show that, when compared to control networks, the propagation of activity accelerates when NMDA receptors are blocked and slows down when AMPA receptors are blocked. The temporal dynamics of network activity propagation observed in **Publication II** can be partly explained by the fact that AMPA receptors are known to have fast channel kinetics and NMDA receptors slow channel kinetics (Ozawa et al., 1998; Kleppe & Robinson, 1999; Li & Gulledge, 2021).

Publication II showed that AMPA receptors increased the diversity of spatio-temporal patterns when the NB structures were compared with each other. In other words, it was found that the blockade of AMPA receptors caused slowly propagating NBs with a similar structure when compared to each other, in contrast to networks in which AMPA receptors were also active. In addition, it was observed that when AMPA receptors were gradually blocked, NBs originated from fewer locations than in control networks and mostly at the culture boundary (unpublished data). Combining these results on the role of AMPA receptors as NB initiators and enhancers of NB structural diversity, I suggest that AMPA receptors increase NB initiation zones in cortical cultures. This conclusion is consistent with a study showing that the number of NB initiation zones decreases when protein kinase C is inhibited (Okujeni et al., 2017). Protein kinase C is known to enhance the conductivity of AMPA receptors (Jenkins et al., 2012). It was also recently shown that the number of different spatio-temporal patterns decreased when neural stem cells with more NMDA than AMPA receptors were added to the culture (Moriya et

al., 2021). This result is in agreement with my conclusion that AMPA receptors increase the diversity of the spatio-temporal patterns of NBs.

Lonardoni et al. (2017) have shown that similar NB structures start from the same cell culture location. Thus, they concluded that the initiation zone determines the propagation path of NBs (Lonardoni et al., 2017). In addition, other studies have reported that NBs originate from zones located at the boundaries of the culture or in the middle of the culture at the transition sites of high and low activity (Orlandi et al., 2013; Okujeni & Egert, 2019a). Boundary regions and transition sites have been discussed as creating an anisotropic connection to neurons to increase the recurrent network connectivity, which would better amplify local activity to maintain adequate input levels for neuronal survival (Van Ooyen et al., 1995; Okujeni & Egert, 2019b). Clusters have also been shown to promote spontaneous activities and recurrent connectivity (Kaiser & Hilgetag, 2010). It is likely that there are more synapses in cell clusters and thus more AMPA receptors, which could facilitate the initiation of NBs at several sites, including the center of cultures. The location of AMPA receptors in the clusters would also explain why NBs started at several sites when AMPA receptors were fully active and only in a few sites when the AMPA receptors were gradually blocked.

In **Publication II**, I demonstrated that AMPA receptors accelerate the onset of network activity, NMDA and $GABA_A$ receptors slow the propagation of activity, and AMPA and $GABA_A$ receptors enrich the propagation of activity in cortical cultures *in vitro*. In **Publication III**, the propagation of activity was modeled in the form of NB profiles under different synaptic receptor antagonists. For the first time ever, a data-driven model of spiking neuronal networks was used to reproduce the AMPA receptor-mediated fast recruitment of neurons to NB activity and the propagation of slow activity mediated by NMDA and $GABA_A$ receptors. The computational model was not a fully detailed spatio-temporal model because the fitting and validation of 2D estimates would become computationally too complex and resource consuming. In previous studies, the propagation of NB activity has been modeled *in silico* (Lonardoni et al., 2017; Orlandi et al., 2013). Lonardoni et al. (2017) simulated NBs based on the center of activity trajectory (CAT) analysis developed by Chao et al. (2008). They clustered spatio-temporal patterns into classes by CAT analysis and evaluated the model by comparing the simulated and experimental data under different pharmacological conditions of synaptic receptor antagonists in the same way as in **Publication III**, but with the difference that they did not fit and validate their model based on the experimental data (Lonardoni et al., 2017). Orlandi et al. (2013) modeled the propagation of NB activity through

avalanches. They experimentally studied the role of inhibition in activity propagation, but they also did not use the data to fit and validate the model as in **Publication III** (Orlandi et al., 2013).

Even though the cortical networks studied in this thesis have lost their original neuronal connectivity and architecture during culture preparation process, the studies presented in **Publications I–III** provide important insights into how AMPA, $GABA_A$, and NMDA receptors may contribute to network burst initiation, propagation, and information transmission in the developing neocortex. Combining experimental *in vitro* data, carefully selected statistical measures of this data, and computational modeling can give useful insights into the dynamics of the cell culture systems and guide future *in vitro* studies.

5.3 Termination of network bursts

Synchronized NBs have been shown to actively cease due to $GABA_A$ receptor-mediated hyperpolarization or GABA shunting activity in three-week-old cultures *in vitro* (Baltz et al., 2010). It has also been reported that when $GABA_A$ receptors are blocked, the late phase of NBs begins to oscillate, leading to longer NBs rather than the active cessation of NBs (Baltz et al., 2010; Weihberger et al., 2013). $GABA_A$ receptors play a clear role in the cessation of NBs, but the termination of NBs is also likely to be influenced by glutamatergic drive. In this thesis, the effects of all three AMPA, NMDA, and $GABA_A$ receptors on NB termination were for the first time studied both individually and together.

Publications I and **II** showed that the NB profiles ended in active cessation when AMPA and $GABA_A$ receptors were active. In contrast, networks lacking functional AMPA receptors had oscillating late phases and the NBs were longer than in the control networks. In addition, when AMPA receptors were gradually blocked, superbursts arose. From these results, it can be concluded that $GABA_A$ receptors were unable to terminate NB profiles without AMPA receptors – i.e., AMPA receptors also appeared to play a crucial role in terminating NBs. In fact, when AMPA receptors were blocked, NBs were significantly prolonged, and when $GABA_A$ receptors were further blocked in these same networks, NB lengths were in turn shortened compared to before the disinhibition. This finding suggests that $GABA_A$ receptors without AMPA receptors further slowed and attenuated the late phase of network activity in NMDA receptor mediated NBs and did not actively

terminate these NBs. The results in **Publications I** and **II** suggest that AMPA and $GABA_A$ receptors interact to terminate the NBs.

The role of NMDA receptors in the termination of NBs must also be considered. **Publication II** showed that NMDA receptors contribute to the maintenance of NBs – i.e., they played a significant role in the length of NBs in the late phase. NBs in which AMPA or AMPA and $GABA_A$ receptors were blocked showed late-phase oscillating activity in **Publication II**, similarly as described by Weihberger et al. (2013) and Baltz & Voigt (2015) in their studies in which only $GABA_A$ receptors were blocked. These studies propose that the oscillations are due to the depletion of neurotransmitters (Weihberger et al., 2013; Baltz & Voigt, 2015). They also indicate that short-term synaptic depression (STD) limits the length of NBs combined with GABAergic inhibition (Weihberger et al., 2013). In **Publication II**, I showed that in networks where NMDA and $GABA_A$ receptors were blocked, the early phase of NBs was enhanced, but the late phase did not oscillate. These results indicate that when NMDA receptors are active, both AMPA and $GABA_A$ receptors are required for active NB termination, but not in networks where NMDA receptors are blocked. In **Publication III**, an *in-silico* model was able to reproduce all other pharmacological conditions except when the NMDA and $GABA_A$ receptors where blocked. In summary, oscillating activity requires NMDA receptor-mediated activity and the blockade of either AMPA or $GABA_A$ receptors. It can be concluded that NMDA receptor-mediated activity also significantly affects STD. When NMDA receptor-mediated NBs were disinhibited, the NBs ceased more rapidly and thus the neurons were earlier ready for the next NB compared to the state before disinhibition. This result indicates that $GABA_A$ receptors slow down the use of NMDA receptor-mediated synaptic resources. In control networks, in the presence of AMPA receptors, $GABA_A$ receptors facilitate the efficient use of synaptic resources and vesicle replenishment.

Previous studies have shown that STD modulates synaptic transmission properties depending on the temporal structure of sequences of presynaptic APs (Tsodyks & Markram, 1997). These results are in line with my observation that NMDA receptors have a crucial contribution to STD. In addition, depletion of neurotransmitters from readily releasable vesicles during a spontaneous NB has been shown to empty pools until firing ceases (Xu & Wu, 2005) and subsequent vesicle replenishment increases resource availability but also prolongs the time between the bursts (Kavalali, 2007). It has been shown that STD is more likely to affect the distribution of burst intervals –i.e., the exponential recovery time of synapses after saturation produced by a NB (Opitz et al., 2002). Indeed, in **Publication II**, I

showed that the distance between NBs was first significantly increased when AMPA receptors were blocked, but then was shortened when $GABA_A$ receptors were blocked in NMDA receptor-mediated NBs. The shortening of the time distance between NBs may be due to accelerated STD and subsequent vesicle replenishment compared to possible slower STD and vesicle replenishment in the presence of $GABA_A$ receptors.

Weihberger et al. (2013) have presented two analytical models for modulating NB length and delay based on the duration of pre-stimulus inactivity during bursting. They concluded that long NBs reduced resource availability and thus slowed down the recovery process and that the time constant of the process in their analytical model was activity-dependent and determined by previous activation history. The conclusions drawn from their model are consistent with the experimental results in **Publication II**, which show that long NMDA-mediated NBs have longer IBIs and, when disinhibited, NBs and IBIs become shorter. Similar models have also been presented in other studies to characterize the recovery process that determines resource availability after NB activity (Toib et al., 1998; Marom, 2009). The results presented in this thesis suggest that the interaction between NMDA receptor-mediated excitatory drive and the restorative drive mediates the overall balance between periods of activity and inactivity. However, this conclusion needs to be confirmed e.g., in a study comparing NB responses to current stimulation in networks where AMPA, NMDA, AMPA and $GABA_A$ or NMDA and $GABA_A$ receptors are blocked.

5.4 Superbursts

The gradual decrease in AMPA receptors resulted in NMDA and $GABA_A$ receptor-mediated superbursts consisting of dozens of slow bursts with highly repetitive activity patterns, as described in **Publication II**. The NBs in the superbursts followed a very similar pattern of spatio-temporal activity to each other. The similarity may be due to the slowed dynamics of the network, because when cells are very active for long periods of time such as in networks that are gradually blocked by AMPA receptors, it is more likely that the network burst starts at the same location as before. In this case, the cells that initiated the first NB, have had time to repolarize themselves, unlike those cells that were still newly active. In **Publications I** and **II**, I showed that the role of NMDA receptors in the network function is to contribute to the maintenance of slowly prolonged bursts with more spikes than

control bursts. In addition, I showed that the propagation of NMDA and $GABA_A$ receptor-mediated network activity slowed down, but NBs propagated evenly across the culture. Fong et al. (2015) support my findings by showing that after NMDA receptor blockade, the NB duration was significantly shortened, whereas after AMPA receptor blockade, the NB duration was clearly prolonged. In addition, networks activated by current stimulation show slower late phase of NBs which are driven by NMDA receptors (Jimbo et al., 2000). However, it has not been previously shown that sub-bursts of superbursts propagate more slowly than NBs in control networks or that sub-bursts would share similar structure as shown in **Publication II**.

When AMPA receptors are gradually blocked, it is possible that some active AMPA receptors that further activate the inhibitory receptors increase the overall inhibition-excitation ratio. This would disturb the inhibition-excitation balance, causing superbursts, as discussed earlier in **Section 5.1**. Several other cellular mechanisms and phenomena may also affect the observed superburst dynamics *in vitro*, including synaptic scaling (Fong et al., 2015), AMPA and NMDA receptor trafficking (Sheng & Lee, 2001; Carroll & Zukin, 2002), extrasynaptic receptors (Parri et al., 2001), astrocytes and their capacity to control the composition of extracellular ions and neurotransmitters (Bazargani & Attwell, 2016), as well as dendritic properties and NMDA spikes (Palmer et al., 2014). It has also recently been shown in slices obtained from somatosensory and anterior cingulate cortices that there is a tightly controlled interaction between NMDA receptors and glutamate uptake which may affect network hypersensitivity-related diseases differently in different brain regions (Romanos et al., 2019). The interaction is based on the regulation of extracellular glutamate by glutamate transporters, which can be in both neurons and astrocytes. Such a putative interaction between synaptic receptors and glutamate transporters in cell cultures requires further studies.

In **Publication II**, it was found that NMDA receptors also play an important spatial role in network activity in addition to the temporal maintenance of bursts, because when blocked, the number of active electrodes was significantly reduced. This may be due to Ca^{2+} mediated by NMDA receptors or the association of NMDA receptors with astrocytic mechanisms and activity. There are also indications that bursts act as a crucial factor in synaptogenesis, accelerating functional development in postnatal cultures (van Huizen et al., 1987). The role of NMDA receptors in NBs has been known to mediate activity-dependent plasticity and ensure a stable level of background activity for homeostatic growth mechanisms (Ramakers et al., 1993).

Therefore, it can be concluded that slow NMDA receptor-mediated activity plays a significant role in the development and spontaneous bursting activity of cortical cells. In summary, the results of **Publication II** on the role of NMDA receptors show for the first time that when there is sufficient depolarization in the network to initiate NBs, NMDA receptors maintain NBs throughout the network. NMDA receptors alone seem unable to initiate or cease NBs. Instead, they promote with $GABA_A$ receptors the slow propagation of bursts across the network. To fully understand the role of superbursts in cell culture networks, we need additional *in vitro* and *in silico* studies on the putative roles of different synaptic and cellular mechanisms in network activity.

5.5 Human neuroblastoma cell differentiation towards neuronal phenotype and network formation

Human neural networks have been studied less than the rodent ones. The goal of **Publication IV** was to contribute to this lack of knowledge by using human neuroblastoma cells that can be easily obtained and cultured using a specific SH-SY5Y cell line. The specific aim of the study was to find a functional combination of substances that effectively induced human cell differentiation towards neuron-like phenotype and neuronal networks. The effects of the substances – such as RA, E_2, CHOL, and BDNF – and their interactions were studied by the immunocytochemical technique by staining neuronal markers, such as synaptic vesicles and neurofilaments. In addition, the arrest of substance-induced cell population growth was defined by counting the number of stained nuclei. These substances were selected for the study because of their high potential to differentiate cells towards the neuronal phenotype. RA is known to be a successful neuronal differentiation agent for human neuroblastoma cells (Pahlman et al., 1984). The effects of the other studied substances on differentiating human cells are less known. The role of E_2 and some of the combinations of these substances in inducing differentiation were not studied in human SH-SY5Y neuroblastoma cells before **Publication IV**.

It was of interest to study the effects of E_2 on the differentiation of human neuroblastoma cells because the positive impacts of E_2 were evident in primary cell cultures. Previous studies showed that E_2 increased the number of dendritic spines and excitatory synapses, altered the synaptic physiology of neurons, increased synaptogenesis and synaptic plasticity, and enhanced NMDA receptor expression

and activity as well as long-term potentiation (McEwen et al., 1990; Smith & McMahon, 2005; Wong & Moss, 1992; Liu et al., 2008; Babayan & Kramar, 2013). The impacts of E_2 on the differentiation of human neuroblastoma cells were not known. The results in **Publication IV** showed for the first time that E_2 increased the neurite outgrowth and synaptic vesicle recycling when used alone or in combination with RA (RE) in human neuroblastoma cells. Consistent with these results, estrogen treatment was shown to increase the expression of synapse-related proteins in human neuroblastoma cells (Chamniansawat & Chongthammakun, 2009). These results are important because they show for the first time that E_2 alone can significantly increase the number of synaptic vesicles and thus affect the differentiation of human neuroblastoma cells. Recently, E_2 research has reached a new level. Interesting new studies have been published showing that E_2 has plasticity-promoting, neuromodulatory, and epigenetic effects on memory and learning formation (Sengupta et al., 2019; Taxier et al., 2020; Hokenson et al., 2021). In addition, enhanced estrogen signaling was recently shown to induce the expression of nerve growth factor receptor-mediated neuronal differentiation in mice neuroblastoma cells (Dzieran et al., 2018). The results of this thesis and others encourage further research the E_2 as a differentiation agent for human cells and a potential treatment for cancer.

Cholesterol (CHOL) is known to be ubiquitous in the central nervous system, membrane structures, and synapse development. In addition, it affects synaptic transmission both presynaptically and postsynaptically (Mauch et al., 2001; Pfrieger, 2003; Renner et al., 2009; Korinek et al., 2020). On the other hand, the role of CHOL in cognition has been the subject of highly controversial research (Schreurs, 2010). In **Publication IV**, I showed that when used alone, CHOL increased neurite outgrowth, and when it was used in combination with RA, it increased the number of synaptic vesicles in a supra-additive manner. In addition, CHOL supported RA-induced neurofilament growth and the arrest of cell population growth. I also showed that synaptic vesicle recycling was significantly enhanced in all combination treatments using CHOL (RC, RCB, and RCBE). The results highlighted the essential role of CHOL in the differentiation of cells and indicated its potential therapeutic role in the treatment of human neuroblastoma. These results are important because they show that CHOL supported RA-induced neuronal differentiation, consistent with three other publications, all of which show a role for CHOL in increasing neuronal differentiation in human SH-SY5Y neuroblastoma cells (Sarkanen et al., 2007; Agholme et al., 2010; Xicoy et al., 2020). In addition, Xicoy et al. (2020) found no protective effect with CHOL -lowering drugs (i.e., statins) when SH-SY5Y cells

were treated with neurotoxin-6-hydroxydopamine (6-OHDA), whereas CHOL doses protected SH-SY5Y cells from 6-OHDA toxicity. More recently, simvastatin, a CHOL-lowering drug has been shown to impair hippocampal synaptic plasticity and cognitive function in mice (Guo et al., 2021), indirectly suggesting a role for CHOL in memory formation. The results obtained here, along with those of other laboratories, encourage further research into the role of CHOL in the pathogenesis of cancer and as a therapeutic agent.

The BDNF-mediated function is known to require the TrkB receptor, which is lacking in naive neuroblastoma cells, but the TrkB receptor could be induced by RA (Encinas et al., 2000). Studies of neuronal differentiation induced by BDNF have been shown to be controversial. Some studies showed that sequential treatment with RA-BDNF induced differentiated neuron-like cells and increased the expression of synaptic genes and acetylcholine activity compared to cells treated alone with RA (Goldie et al., 2014; Low et al., 2015). On the other hand, BDNF has been shown to provide little benefit for RA-induced differentiation, to increase metastasis and angiogenesis, and to protect against chemotherapy (Matsumoto et al.,1995; Jaboin et al., 2002; Nakamura et al., 2006; Cernaianu et al., 2008). In **Publication IV**, as expected, BDNF when used alone showed no outgrowth of neurites or increased synaptic vesicle recycling in human neuroblastoma cells, but when combined with RA (RB), BDNF supported the RA-induced branching of long neurites, complete network formation, and synaptic vesicle recycling, but it did not arrest cell population growth. I did not observe the inhibition of cell proliferation by the sequential treatment of RA (10μm) and BDNF (50 ng/ml), unlike (Encinas et al., 2000), who did with RA (10μm) and BDNF (10ng/ml). The difference between the results might be explained by the BDNF concentration used. A BDNF concentration of 10 ng/ml has been shown to cause significant inhibition in cell population growth, but concentrations of 50 or 100 ng/ml were not shown to cause the inhibition of proliferation (Cernaianu et al., 2008). In addition, the cell line used may also affect the differentiation properties of BDNF. It has been presented that SH-SY5Y-A cells (American Type Culture Collection; used in **Publication IV**) differentiated these cells already in the presence of RA, whereas RA-treated SH-SY5Y-E cells (European Collection of Cell Cultures) required additional BDNF treatment for full differentiation. This is due to the defects in several signaling pathways in SH-SY5Y-E cells. In conclusion, the controversial results on the level of differentiation might originate from the different subtypes of the SH-SY5Y cell line, as well as from the BDNF concentrations used. In the light of the current knowledge, further

examinations of the properties of BDNF are needed before considering its use as a therapeutic agent for clinical use.

Ultimately, the level of differentiation was determined by combining all the above substances, including RA, E_2, CHOL, and BDNF (RCBE). RCBE combination treatment showed neurite outgrowth, the branching of neurites, neuron-neuron interactions, synaptic vesicle recycling, and a cell network structure. RCBE showed results of functional differentiation, with the ability to produce functional synaptic vesicle recycling and network formation. RCBE has potential advantages over traditional treatments. However, the efficacy of BDNF in arresting the population growth rate of human neuroblastoma cells should be further researched to ensure its ability to differentiate. A recent study examined the electrophysiological properties of undifferentiated SH-SY5Y cells, and the cells differentiated with RA, RB, and RBCE treatments by performing whole-cell patch-clamp recordings (Sahin et al., 2021). Their results showed that the Na^+ currents existed in all differentiated cells, but not in the undifferentiated cells. However, the Na^+ currents became the most pronounced in the differentiated RB cells. In addition, they found that undifferentiated cells had significantly larger K^+ currents. They suggested RA with BDNF as the best differentiation protocol, since they did not find any statistically significant difference between RB and RBCE in electrophysiological comparison (Sahin et al., 2021). In the future, it would be interesting to study the possible emergence of the network-wide activity of differentiated human neuroblastoma cells with the MEA technique.

In the future, it would be important to continue research on the impact of E_2, CHOL, BDNF, and RA in human neuroblastoma cell differentiation for a number of reasons: **1)** Only in a few cases can the results of animal experiments be directly and reliably compared to humans; **2)** for ethical reasons, it is desirable to have alternatives to primary cells from animal experimentation; **3)** the knowledge of how to increase the level of neuronal differentiation of human neuroblastoma cells towards neuronal phenotypes can be seen as an improvement in cancer cell therapies; and **4)** basic research on the differentiation of human cancer cells is crucial to understand, as they can be utilized in the study of different pathological disease models. The differentiation of human neuroblastoma cells can be compared also to stem cells in health and pathology.

The results of the differentiation of human SH-SY5Y cells discussed above have great importance since I provided a functional combination of agents that effectively induced human cell differentiation towards a neuronal phenotype and neural network. The outcome of the neuroblastoma remains poor, and the development of

novel therapeutic approaches is needed. Despite active research aim at improving the prognosis of neuroblastoma patients in recent decades, only a few patients become survivors. Therefore, therapies such as the induced differentiation of cancer cells are important. I suggest to further study the role of E_2, CHOL, and RA in differentiation of neuroblastoma cells to possibly promote better prognosis in children with neuroblastoma. A well-validated process of differentiation of cell cultures prepared from individual patients may help to develop personalized treatments for neuroblastoma in the future.

6 CONCLUSIONS

This thesis highlights the importance of excitatory and inhibitory synaptic receptors in initiating, propagating, and terminating network burst activity in postnatal rat cortical networks *in vitro*. The thesis presents how AMPA receptors affect the onset of network bursts by rapidly recruiting neurons into network-wide activity and ultimately also affect the diversity of spatio-temporal structures and the termination of network bursts along with inhibitory $GABA_A$ receptors. These results provide new insights into how synaptic receptors alone and in interaction influence the dynamics of cortical network activity *in vitro*. The results presented in this thesis may also provide new hypotheses for future studies in living animals *in vivo*.

It is known from the previous studies that cortical processing depends on the excitation-inhibition balance and that the altered balance contributes to impaired cortical sensory processing, which in turn can lead to various neurological disorders and pathogenesis such as autism spectrum disorder, epilepsy, ischemia, and schizophrenia. However, it has not been known how the excitatory-inhibitory balance in the level of synaptic receptors affects the spontaneous activity in postnatal cortical networks, as this is technically very challenging to study in living animal *in vivo*. This thesis presents NMDA and $GABA_A$ receptor-mediated superburst activity under gradual AMPA receptor blockade in dissociated cortical networks *in vitro*. The result indicates that gradual elimination of AMPA receptors and excessive NMDA and $GABA_A$ receptor-mediated synaptic transmission may underlie conditions like epileptic-type activity in the brain. This result of the thesis challenges the prevailing view that only disinhibition or immature cortical network activity would lead to superburst-type activity. The results of this thesis are a significant contribution to understanding the role of synaptic transmission in the dynamics of cortical network activity, as they suggest that impaired regulation of the excitation-inhibition balance results in superbursts activity in cortical networks *in vitro*. The results presented in this thesis increase the molecular and cellular level understanding of spontaneous activity and the importance of synaptic receptors in the network burst activity during postnatal stage.

This thesis also examined the ability of human neuroblastoma cells to morphologically differentiate into neuronal phenotypes and networks. The thesis

work succeeded in creating neuronal network of human neuroblastoma cell line on a dish, in which proliferation arrest, neurite outgrowth and branching, and synaptic vesicle recycling were observed. The development of differentiation protocols is important because new knowledge of the protocol presented here can be used as a basis for the future development of individual cancer cell therapies for neuroblastoma patients. The thesis also provides basic neurobiological information about human neuroblastoma cells, their differentiation, and network formation with differentiation substances and surface coating agents. The **Publication IV** related to human neuroblastoma differentiation has already been cited more than 70 times.

Ultimately, the thesis promotes the interface between experimental and computational neurosciences by developing multiunit time-series spike data analysis so that the data analysis supports the construction of data-driven network modeling. The data-driven *in silico* models can be used to test the significance of different model parameter sets, fine-tuned based on MEA data such as the data recorded and analyzed in this thesis. Such an integration of experimental and theoretical models will continue to assist in the development and setting of experimental *in vitro* and *in vivo* research questions and hypotheses. Appropriate, systematized data curation and analysis for modeling can also increase the reproducibility, comparability, and replicability of scientific studies.

REFERENCES

Adelsberger, H., Garaschuk, O., & Konnerth, A. (2005). Cortical calcium waves in resting newborn mice. *Nature Neuroscience, 8*(8), 988-990. doi:nn1502 [pii]

Agholme, L., Lindstrom, T., Kagedal, K., Marcusson, J., & Hallbeck, M. (2010). An in vitro model for neuroscience: Differentiation of SH-SY5Y cells into cells with morphological and biochemical characteristics of mature neurons. *Journal of Alzheimer's Disease, 20*(4), 1069-1082. doi:10.3233/JAD-2010-091363 [doi]

Aguilo, A., Schwartz, T. H., Kumar, V. S., Peterlin, Z. A., Tsiola, A., Soriano, E., & Yuste, R. (1999). Involvement of cajal-retzius neurons in spontaneous correlated activity of embryonic and postnatal layer 1 from wild-type and reeler mice. *The Journal of Neuroscience, 19*(24), 10856-10868.

Allene, C., Cattani, A., Ackman, J. B., Bonifazi, P., Aniksztejn, L., Ben-Ari, Y., & Cossart, R. (2008). Sequential generation of two distinct synapse-driven network patterns in developing neocortex. *The Journal of Neuroscience, 28*(48), 12851-12863. doi:10.1523/JNEUROSCI.3733-08.2008

Aronoff, R., Matyas, F., Mateo, C., Ciron, C., Schneider, B., & Petersen, C. C. (2010). Long-range connectivity of mouse primary somatosensory barrel cortex. *The European Journal of Neuroscience, 31*(12), 2221-2233. doi:10.1111/j.1460-9568.2010.07264.x [doi]

Babayan, A. H., & Kramar, E. A. (2013). Rapid effects of oestrogen on synaptic plasticity: Interactions with actin and its signalling proteins. *Journal of Neuroendocrinology, 25*(11), 1163-1172. doi:10.1111/jne.12108 [doi]

Bahl, A., Stemmler, M. B., Herz, A. V., & Roth, A. (2012). Automated optimization of a reduced layer 5 pyramidal cell model based on experimental data. *Journal of Neuroscience Methods, 210*(1), 22-34. doi:S0165-0270(12)00129-X [pii]

Baltz, T., de Lima, A. D., & Voigt, T. (2010). Contribution of GABAergic interneurons to the development of spontaneous activity patterns in cultured neocortical networks. *Frontiers in Cellular Neuroscience, 4*, 15. doi:10.3389/fncel.2010.00015 [doi]

Baltz, T., Herzog, A., & Voigt, T. (2011). Slow oscillating population activity in developing cortical networks: Models and experimental results. *Journal of Neurophysiology, 106*(3), 1500-1514. doi:10.1152/jn.00889.2010 [doi]

Baltz, T., & Voigt, T. (2015). Interaction of electrically evoked activity with intrinsic dynamics of cultured cortical networks with and without functional fast GABAergic synaptic transmission. *Frontiers in Cellular Neuroscience, 9*, 272. doi:10.3389/fncel.2015.00272 [doi]

Bando, Y., Irie, K., Shimomura, T., Umeshima, H., Kushida, Y., Kengaku, M., . . . Tagawa, Y. (2016). Control of spontaneous Ca2+ transients is critical for neuronal maturation in the developing neocortex. *Cerebral Cortex (New York, N.Y.: 1991), 26*(1), 106-117. doi:10.1093/cercor/bhu180 [doi]

Baker, R.E., & Van Pelt, J., (1997). Cocultured, but not isolated, cortical explants display normal dendritic development: a long-term quantitative study. *Developmental Brain Research*, 98(1), 21-29. doi:10.1016/S0165-3806(96)00163-0

Barral, J., & Reyes, A.D., (2016). Synaptic scaling rules preserves excitatory/inhibitory balance and salient neuronal dynamics. *Nature Neuroscience* 19, 1690-1690. doi:10.1038/nn.4415

Bazargani, N., & Attwell, D. (2016). Astrocyte calcium signaling: The third wave. *Nature Neuroscience, 19*(2), 182-189. doi:10.1038/nn.4201 [doi]

Ben-Ari, Y. (2001). Developing networks play a similar melody. *Trends in Neurosciences, 24*(6), 353-360. doi:S0166-2236(00)01813-0 [pii]

Ben-Ari, Y., Gaiarsa, J. L., Tyzio, R., & Khazipov, R. (2007). GABA: A pioneer transmitter that excites immature neurons and generates primitive oscillations. *Physiological Reviews, 87*(4), 1215-1284. doi:87/4/1215 [pii]

Ben-Ari, Y., & Spitzer, N. C. (2010). Phenotypic checkpoints regulate neuronal development. *Trends in Neurosciences, 33*(11), 485-492. doi:10.1016/j.tins.2010.08.005 [doi]

Benveniste, M., & Mayer, M. L. (1991). Kinetic analysis of antagonist action at N-methyl-D-aspartic acid receptors. two binding sites each for glutamate and glycine. *Biophysical Journal, 59*(3), 560-573. doi:S0006-3495(91)82272-X [pii]

Biedler, J. L., Helson, L., & Spengler, B. A. (1973). Morphology and growth, tumorigenicity, and cytogenetics of human neuroblastoma cells in continuous culture. *Cancer Research, 33*(11), 2643-2652.

Blankenship, A. G., & Feller, M. B. (2010). Mechanisms underlying spontaneous patterned activity in developing neural circuits. *Nature Reviews.Neuroscience, 11*(1), 18-29. doi:10.1038/nrn2759 [doi]

Bonetti, C., & Surace, E. M. (2010). Mouse embryonic retina delivers information controlling cortical neurogenesis. *PLoS One, 5*(12), e15211. doi:10.1371/journal.pone.0015211 [doi]

Brewer, G. J., Boehler, M. D., Jones, T. T., & Wheeler, B. C. (2008). NbActiv4 medium improvement to neurobasal/B27 increases neuron synapse densities and network spike rates on multielectrode arrays. *Journal of Neuroscience Methods, 170*(2), 181-187. doi:10.1016/j.jneumeth.2008.01.009 [doi]

Brewer, G. J., Boehler, M. D., Pearson, R. A., DeMaris, A. A., Ide, A. N., & Wheeler, B. C. (2009). Neuron network activity scales exponentially with synapse density. *Journal of Neural Engineering, 6*(1), 014001-2560/6/1/014001. Epub 2008 Dec 22. doi:10.1088/1741-2560/6/1/014001 [doi]

Brunel, N., & Wang, X. J. (2003). What determines the frequency of fast network oscillations with irregular neural discharges? I. synaptic dynamics and

excitation-inhibition balance. *Journal of Neurophysiology, 90*(1), 415-430. doi:10.1152/jn.01095.2002 [doi]

Burgess, A., Vigneron, S., Brioudes, E., Labbe, J. C., Lorca, T., & Castro, A. (2010). Loss of human greatwall results in G2 arrest and multiple mitotic defects due to deregulation of the cyclin B-Cdc2/PP2A balance. *Proceedings of the National Academy of Sciences of the United States of America, 107*(28), 12564-12569. doi:10.1073/pnas.0914191107 [doi]

Carroll, R. C., & Zukin, R. S. (2002). NMDA-receptor trafficking and targeting: Implications for synaptic transmission and plasticity. *Trends in Neurosciences, 25*(11), 571-577. doi:S0166-2236(02)02272-5 [pii]

Cernaianu, G., Brandmaier, P., Scholz, G., Ackermann, O. P., Alt, R., Rothe, K., . . . Trobs, R. B. (2008). All-trans retinoic acid arrests neuroblastoma cells in a dormant state. subsequent nerve growth factor/brain-derived neurotrophic factor treatment adds modest benefit. *Journal of Pediatric Surgery, 43*(7), 1284-1294. doi:10.1016/j.jpedsurg.2008.01.007 [doi]

Chamniansawat, S., & Chongthammakun, S. (2009). Estrogen stimulates activity-regulated cytoskeleton associated protein (arc) expression via the MAPK- and PI-3K-dependent pathways in SH-SY5Y cells. *Neuroscience Letters, 452*(2), 130-135. doi:10.1016/j.neulet.2009.01.010 [doi]

Chao, Z. C., Bakkum, D. J., & Potter, S. M. (2008). Shaping embodied neural networks for adaptive goal-directed behavior. *PLoS Computational Biology, 4*(3), e1000042. doi:10.1371/journal.pcbi.1000042 [doi]

Chen, X., & Dzakpasu, R. (2010). Observed network dynamics from altering the balance between excitatory and inhibitory neurons in cultured networks. *Physical Review E, Statistical, Nonlinear, and Soft Matter Physics, 82*(3 Pt 1), 031907. doi:10.1103/PhysRevE.82.031907 [doi]

Chen, Y., & Ghosh, A. (2005). Regulation of dendritic development by neuronal activity. *Journal of Neurobiology, 64*(1), 4-10. doi:10.1002/neu.20150 [doi]

Cheung, Y. T., Lau, W. K., Yu, M. S., Lai, C. S., Yeung, S. C., So, K. F., & Chang, R. C. (2009). Effects of all-trans-retinoic acid on human SH-SY5Y neuroblastoma as in vitro model in neurotoxicity research. *Neurotoxicology, 30*(1), 127-135. doi:10.1016/j.neuro.2008.11.001 [doi]

Chiappalone, M., Bove, M., Vato, A., Tedesco, M., & Martinoia, S. (2006). Dissociated cortical networks show spontaneously correlated activity patterns during in vitro development. *Brain Research, 1093*(1), 41-53. doi:S0006-8993(06)00801-8 [pii]

Chiappalone, M., Novellino, A., Vajda, I., Vato, A., Martinoia, S., & van Pelt, J., (2005). Burst detection algorithms for the analysis of spatio-temporal patterns in cortical networks of neurons. *Neurocomputing*, 65–66, 653–662. doi:10.1016/j.neucom.2004.10.094

Chiu, C., & Weliky, M. (2001). Spontaneous activity in developing ferret visual cortex in vivo. *The Journal of Neuroscience, 21*(22), 8906-8914. doi:21/22/8906 [pii]

Compte, A., Brunel, N., Goldman-Rakic, P. S., & Wang, X. J. (2000). Synaptic mechanisms and network dynamics underlying spatial working memory in a cortical network model. *Cerebral Cortex (New York, N.Y.: 1991), 10*(9), 910-923. doi:10.1093/cercor/10.9.910 [doi]

Corlew, R., Bosma, M. M., & Moody, W. J. (2004). Spontaneous, synchronous electrical activity in neonatal mouse cortical neurones. *The Journal of Physiology, 560*(Pt 2), 377-390. doi:10.1113/jphysiol.2004.071621 [doi]

Cornell-Bell, A. H., Finkbeiner, S. M., Cooper, M. S., & Smith, S. J. (1990). Glutamate induces calcium waves in cultured astrocytes: Long-range glial signaling. *Science (New York, N.Y.), 247*(4941), 470-473. doi:10.1126/science.1967852 [doi]

Corner, M. A., Baker, R.E., & van Pelt, J., (2008) Physiological consequences of selective suppression of synaptic transmission in developing cerebral cortical networks in vitro: Differential effects on intrinsically generated bioelectric discharges in a living 'model' system for slow-wave sleep activity. *Neuroscience and Biobehavioral Reviews* 32, 1569–1600. doi: 10.1016/j.neubiorev.2008.06.008

Corner, M. A., van Pelt, J., Wolters, P. S., Baker, R. E., & Nuytinck, R. H. (2002). Physiological effects of sustained blockade of excitatory synaptic transmission on spontaneously active developing neuronal networks--an inquiry into the reciprocal linkage between intrinsic biorhythms and neuroplasticity in early ontogeny. *Neuroscience and Biobehavioral Reviews, 26*(2), 127-185. doi:S0149763401000628 [pii]

Cotterill, E., Charlesworth, P., Thomas, C. W., Paulsen, O., & Eglen, S. J. (2016). A comparison of computational methods for detecting bursts in neuronal spike trains and their application to human stem cell-derived neuronal networks. *Journal of Neurophysiology.* 116, 306–321. doi: 10.1152/jn.00093.2016

Craig, A. M., & Banker, G. (1994). Neuronal polarity. *Annual Review of Neuroscience, 17*, 267-310. doi:10.1146/annurev.ne.17.030194.001411 [doi]

Crochet, S., Chauvette, S., Boucetta, S., & Timofeev, I. (2005). Modulation of synaptic transmission in neocortex by network activities. *The European Journal of Neuroscience, 21*(4), 1030-1044. doi:EJN3932 [pii]

Croft, B. G., Fortin, G. D., Corera, A. T., Edwards, R. H., Beaudet, A., Trudeau, L. E., & Fon, E. A. (2005). Normal biogenesis and cycling of empty synaptic vesicles in dopamine neurons of vesicular monoamine transporter 2 knockout mice. *Molecular Biology of the Cell, 16*(1), 306-315. doi:E04-07-0559 [pii]

Czarnecki, A., Magloire, V., & Streit, J. (2008). Local oscillations of spiking activity in organotypic spinal cord slice cultures. *The European Journal of Neuroscience, 27*(8), 2076-2088. doi:10.1111/j.1460-9568.2008.06171.x [doi]

D'Angelo, E., De Filippi, G., Rossi, P., & Taglietti, V. (1998). Ionic mechanism of electroresponsiveness in cerebellar granule cells implicates the action of a persistent sodium current. *Journal of Neurophysiology, 80*(2), 493-503. doi:10.1152/jn.1998.80.2.493 [doi]

D'Angelo, E., Nieus, T., Maffei, A., Armano, S., Rossi, P., Taglietti, V., . . . Naldi, G. (2001). Theta-frequency bursting and resonance in cerebellar granule cells: Experimental evidence and modeling of a slow k+-dependent mechanism. *The Journal of Neuroscience, 21*(3), 759-770. doi:21/3/759 [pii]

Darbon, P., Yvon, C., Legrand, J. C., & Streit, J. (2004). INaP underlies intrinsic spiking and rhythm generation in networks of cultured rat spinal cord neurons. *The European Journal of Neuroscience, 20*(4), 976-988. doi:10.1111/j.1460-9568.2004.03565.x [doi]

de Lima, A. D., Merten, M. D., & Voigt, T. (1997). Neuritic differentiation and synaptogenesis in serum-free neuronal cultures of the rat cerebral cortex. *The Journal of Comparative Neurology, 382*(2), 230-246. doi:10.1002/(SICI)1096-9861(19970602)382:23.0.CO;2-4 [pii]

Dehghani, N., Peyrache, A., Telenczuk, B., Le Van Quyen, M., Halgren, E., Cash, S. S., . . . Destexhe, A. (2016). Dynamic balance of excitation and inhibition in human and monkey neocortex. *Scientific Reports, 6*, 23176. doi:10.1038/srep23176 [doi]

Demerens, C., Stankoff, B., Logak, M., Anglade, P., Allinquant, B., Couraud, F., . . . Lubetzki, C. (1996). Induction of myelination in the central nervous system by electrical activity. *Proceedings of the National Academy of Sciences of the United States of America, 93*(18), 9887-9892. doi:10.1073/pnas.93.18.9887 [doi]

Dichter, M. A. (1978). Rat cortical neurons in cell culture: Culture methods, cell morphology, electrophysiology, and synapse formation. *Brain Research, 149*(2), 279-293.

Dingledine, R., Borges, K., Bowie, D., & Traynelis, S. F. (1999). The glutamate receptor ion channels. *Pharmacological Reviews, 51*(1), 7-61.

Duckett, J. W., & Koop, C. E. (1977). Neuroblastoma. *The Urologic Clinics of North America, 4*(2), 285-295.

Dzieran, J., Rodriguez Garcia, A., Westermark, U. K., Henley, A. B., Eyre Sanchez, E., Trager, C., . . . Arsenian-Henriksson, M. (2018). MYCN-amplified neuroblastoma maintains an aggressive and undifferentiated phenotype by deregulation of estrogen and NGF signaling. *Proceedings of the National Academy of Sciences of the United States of America, 115*(6), E1229-E1238. doi:10.1073/pnas.1710901115 [doi]

Egert, U., Knott, T., Schwarz, C., Nawrot, M., Brandt, A., Rotter, S., & Diesmann, M. (2002). MEA-tools: An open source toolbox for the analysis of multi-electrode data with MATLAB. *Journal of Neuroscience Methods, 117*(1), 33-42. doi:S0165027002000456 [pii]

Egorov, A. V., & Draguhn, A. (2013). Development of coherent neuronal activity patterns in mammalian cortical networks: Common principles and local hetereogeneity. *Mechanisms of Development, 130*(6-8), 412-423. doi:10.1016/j.mod.2012.09.006 [doi]

Encinas, M., Iglesias, M., Liu, Y., Wang, H., Muhaisen, A., Cena, V., . . . Comella, J. X. (2000). Sequential treatment of SH-SY5Y cells with retinoic acid and brain-

derived neurotrophic factor gives rise to fully differentiated, neurotrophic factor-dependent, human neuron-like cells. *Journal of Neurochemistry, 75*(3), 991-1003.

Eytan, D., & Marom, S. (2006). Dynamics and effective topology underlying synchronization in networks of cortical neurons. *The Journal of Neuroscience, 26*(33), 8465-8476. doi:26/33/8465 [pii]

Fanti, Z., De-Miguel, F. F., & Martinez-Perez, M. E. (2008). A method for semiautomatic tracing and morphological measuring of neurite outgrowth from DIC sequences. *Conference Proceedings: Annual International Conference of the IEEE Engineering in Medicine and Biology Society, 2008*, 1196-1199. doi:10.1109/IEMBS.2008.4649377 [doi]

Feller, M. B. (1999). Spontaneous correlated activity in developing neural circuits. *Neuron, 22*(4), 653-656. doi:S0896-6273(00)80724-2 [pii]

Fong, M. F., Newman, J. P., Potter, S. M., & Wenner, P. (2015). Upward synaptic scaling is dependent on neurotransmission rather than spiking. *Nature Communications, 6*, 6339. doi:10.1038/ncomms7339 [doi]

French, D. A., & Gruenstein, E. I. (2006). An integrate-and-fire model for synchronized bursting in a network of cultured cortical neurons. *Journal of Computational Neuroscience, 21*(3), 227-241. doi:10.1007/s10827-006-7815-5 [doi]

Funahashi, S. (2017). Working memory in the prefrontal cortex. *Brain Sciences, 7*(5), 10.3390/brainsci7050049. doi:E49 [pii]

Fuster, J. M. (2000). Prefrontal neurons in networks of executive memory. *Brain Research Bulletin, 52*(5), 331-336. doi:S0361-9230(99)00258-0 [pii]

Fuster, J. M., Bauer, R. H., & Jervey, J. P. (1985). Functional interactions between inferotemporal and prefrontal cortex in a cognitive task. *Brain Research, 330*(2), 299-307. doi:0006-8993(85)90689-4 [pii]

Gandolfo, M., Maccione, A., Tedesco, M., Martinoia, S., & Berdondini, L. (2010). Tracking burst patterns in hippocampal cultures with high-density CMOS-MEAs. *Journal of Neural Engineering, 7*(5), 056001-2560/7/5/056001. Epub 2010 Aug 18. doi:10.1088/1741-2560/7/5/056001 [doi]

Garaschuk, O., Linn, J., Eilers, J., & Konnerth, A. (2000). Large-scale oscillatory calcium waves in the immature cortex. *Nature Neuroscience, 3*(5), 452-459. doi:10.1038/74823 [doi]

Gavet, O., & Pines, J. (2010). Progressive activation of CyclinB1-Cdk1 coordinates entry to mitosis. *Developmental Cell, 18*(4), 533-543. doi:10.1016/j.devcel.2010.02.013 [doi]

Giugliano, M., Darbon, P., Arsiero, M., Luscher, H. R., & Streit, J. (2004). Single-neuron discharge properties and network activity in dissociated cultures of neocortex. *Journal of Neurophysiology, 92*(2), 977-996. doi:10.1152/jn.00067.2004 [doi]

Golbs, A., Nimmervoll, B., Sun, J. J., Sava, I. E., & Luhmann, H. J. (2011). Control of programmed cell death by distinct electrical activity patterns. *Cerebral Cortex (New York, N.Y.: 1991), 21*(5), 1192-1202. doi:10.1093/cercor/bhq200 [doi]

Goldie, B. J., Barnett, M. M., & Cairns, M. J. (2014). BDNF and the maturation of posttranscriptional regulatory networks in human SH-SY5Y neuroblast differentiation. *Frontiers in Cellular Neuroscience, 8*, 325. doi:10.3389/fncel.2014.00325 [doi]

Goldman-Rakic, P. S. (1988). Topography of cognition: Parallel distributed networks in primate association cortex. *Annual Review Neuroscience, 11*, 137-156. doi:10.1146/annurev.ne.11.030188.001033 [doi]

Goldman-Rakic, P. S. (1994). Working memory dysfunction in schizophrenia. *The Journal of Neuropsychiatry and Clinical Neurosciences, 6*(4), 348-357.

Gritsun, T. A., Le Feber, J., Stegenga, J., & Rutten, W. L. (2010). Network bursts in cortical cultures are best simulated using pacemaker neurons and adaptive synapses. *Biological Cybernetics, 102*(4), 293-310. doi:10.1007/s00422-010-0366-x [doi]

Gullo, F., Mazzetti, S., Maffezzoli, A., Dossi, E., Lecchi, M., Amadeo, A., . . . Wanke, E. (2010). Orchestration of "presto" and "largo" synchrony in up-down activity of cortical networks. *Frontiers in Neural Circuits, 4*, 11. doi:10.3389/fncir.2010.00011 [doi]

Guo, Y., Zou, G., Qi, K., Jin, J., Yao, L., Pan, Y., & Xiong, W. (2021). Simvastatin impairs hippocampal synaptic plasticity and cognitive function in mice. *Molecular Brain, 14*(1), 41-x. doi:10.1186/s13041-021-00758-x [doi]

Gutfreund, Y., Yarom, Y., & Segev, I. (1995). Subthreshold oscillations and resonant frequency in guinea-pig cortical neurons: Physiology and modelling. *The Journal of Physiology, 483*, 621-640. doi:10.1113/jphysiol.1995.sp020611 [doi]

Harrill, J. A., Chen, H., Streifel, K. M., Yang, D., Mundy, W. R., & Lein, P. J. (2015). Ontogeny of biochemical, morphological and functional parameters of synaptogenesis in primary cultures of rat hippocampal and cortical neurons. *Molecular Brain., 8*(10) doi:10.1186/s13041-015-0099-9

Harsch, A., & Robinson, H. P. (2000). Postsynaptic variability of firing in rat cortical neurons: The roles of input synchronization and synaptic NMDA receptor conductance. *The Journal of Neuroscience, 20*(16), 6181-6192. doi:20/16/6181 [pii]

Hokenson, R. E., Short, A. K., Chen, Y., Pham, A. L., Adams, E. T., Bolton, J. L., Baram, T. Z. (2021). Unexpected role of physiological estrogen in acute stress-induced memory deficits. *The Journal of Neuroscience, 41*(4), 648-662. doi:10.1523/JNEUROSCI.2146-20.2020 [doi]

Hollmann, M., & Heinemann, S. (1994). Cloned glutamate receptors. *Annual Review of Neuroscience, 17*, 31-108. doi:10.1146/annurev.ne.17.030194.000335 [doi]

Ichikawa, M., Muramoto, K., Kobayashi, K., Kawahara, M., & Kuroda, Y. (1993). Formation and maturation of synapses in primary cultures of rat cerebral

cortical cells: An electron microscopic study. *Neuroscience Research, 16*(2), 95-103. doi:0168-0102(93)90076-3 [pii]

Izhikevich, E. M. (2003). Simple model of spiking neurons. *IEEE Transactions on Neural Networks, 14*(6), 1569-1572. doi:10.1109/TNN.2003.820440 [doi]

Jaboin, J., Kim, C. J., Kaplan, D. R., & Thiele, C. J. (2002). Brain-derived neurotrophic factor activation of TrkB protects neuroblastoma cells from chemotherapy-induced apoptosis via phosphatidylinositol 3'-kinase pathway. *Cancer Research, 62*(22), 6756-6763.

Jenkins, M. A., & Traynelis, S. F. (2012). PKC phosphorylates GluA1-Ser831 to enhance AMPA receptor conductance. *Channels (Austin, Tex.)*, 6(1), 60–64. doi:10.4161/chan.18648

Jimbo, Y., Kawana, A., Parodi, P., & Torre, V. (2000). The dynamics of a neuronal culture of dissociated cortical neurons of neonatal rats. *Biological Cybernetics, 83*(1), 1-20. doi:10.1007/PL00007970 [doi]

Jones, K. A., & Baughman, R. W. (1991). Both NMDA and non-NMDA subtypes of glutamate receptors are concentrated at synapses on cerebral cortical neurons in culture. *Neuron, 7*(4), 593-603.

Kaiser, M., & Hilgetag, C. C. (2010). Optimal hierarchical modular topologies for producing limited sustained activation of neural networks. *Frontiers in Neuroinformatics, 4*, 8. doi:10.3389/fninf.2010.00008 [doi]

Kamioka, H., Maeda, E., Jimbo, Y., Robinson, H. P., & Kawana, A. (1996). Spontaneous periodic synchronized bursting during formation of mature patterns of connections in cortical cultures. *Neuroscience Letters, 206*(2-3), 109-112.

Kanold, P. O., & Luhmann, H. J. (2010). The subplate and early cortical circuits. *Annual Review of Neuroscience, 33*, 23-48. doi:10.1146/annurev-neuro-060909-153244 [doi]

Kato-Negishi, M., Muramoto, K., Kawahara, M., Kuroda, Y., & Ichikawa, M. (2004). Developmental changes of GABAergic synapses formed between primary cultured cortical neurons. *Developmental Brain Research, 152*(2), 99-108. doi:10.1016/j.devbrainres.2004.05.013

Kavalali, E. T. (2007). Multiple vesicle recycling pathways in central synapses and their impact on neurotransmission. *The Journal of Physiology, 585*, 669-679. doi:jphysiol.2007.137745 [pii]

Kilb, W., Ikeda, M., Uchida, K., Okabe, A., Fukuda, A., & Luhmann, H. J. (2002). Depolarizing glycine responses in cajal-retzius cells of neonatal rat cerebral cortex. *Neuroscience, 112*(2), 299-307. doi:S0306452202000714 [pii]

Kilb, W., Kirischuk, S., & Luhmann, H. J. (2011). Electrical activity patterns and the functional maturation of the neocortex. *The European Journal of Neuroscience, 34*(10), 1677-1686. doi:10.1111/j.1460-9568.2011.07878.x [doi]

Kirkby, L. A., Sack, G. S., Firl, A., & Feller, M. B. (2013). A role for correlated spontaneous activity in the assembly of neural circuits. *Neuron, 80*(5), 1129-1144. doi:10.1016/j.neuron.2013.10.030 [doi]

Kleppe, I. C., & Robinson, H. P. (1999). Determining the activation time course of synaptic AMPA receptors from openings of colocalized NMDA receptors. *Biophysical Journal, 77*(3), 1418-1427. doi:S0006-3495(99)76990-0 [pii]

Kolk, S. M., & Rakic, P. (2021). Development of prefrontal cortex. *Neuropsychopharmacology,* doi:10.1038/s41386-021-01137-9 [doi]

Korinek, M., Gonzalez-Gonzalez, I. M., Smejkalova, T., Hajdukovic, D., Skrenkova, K., Krusek, J., . . . Vyklicky, L. (2020). Cholesterol modulates presynaptic and postsynaptic properties of excitatory synaptic transmission. *Scientific Reports, 10*(1), 12651-5. doi:10.1038/s41598-020-69454-5 [doi]

Kovalevich, J., & Langford, D. (2013). Considerations for the use of SH-SY5Y neuroblastoma cells in neurobiology. *Methods in Molecular Biology (Clifton, N.J.), 1078*, 9-21. doi:10.1007/978-1-62703-640-5_2 [doi]

Kriegstein, A. R., & Dichter, M. A. (1983). Morphological classification of rat cortical neurons in cell culture. *The Journal of Neuroscience, 3*(8), 1634-1647.

Krishek, B. J., Moss, S. J., & Smart, T. G. (1996). A functional comparison of the antagonists bicuculline and picrotoxin at recombinant GABAA receptors. *Neuropharmacology, 35*(9-10), 1289-1298.

Krishna, A., Biryukov, M., Trefois, C., Antony, P. M., Hussong, R., Lin, J., . . . May, P. (2014). Systems genomics evaluation of the SH-SY5Y neuroblastoma cell line as a model for parkinson's disease. *BMC Genomics, 15*, 1154-1154. doi:10.1186/1471-2164-15-1154 [doi]

Kuramoto, T., Werrbach-Perez, K., Perez-Polo, J. R., & Haber, B. (1981). Membrane properties of a human neuroblastoma II: Effects of differentiation. *Journal of Neuroscience Research, 6*(4), 441-449. doi:10.1002/jnr.490060402 [doi]

Kuroda, Y., Ichikawa, M., Muramoto, K., Kobayashi, K., Matsuda, Y., Ogura, A., & Kudo, Y. (1992). Block of synapse formation between cerebral cortical neurons by a protein kinase inhibitor. *Neuroscience Letters, 135*(2), 255-258.

Latham, P. E., Richmond, B. J., Nelson, P. G., & Nirenberg, S. (2000). Intrinsic dynamics in neuronal networks. I. theory. *Journal of Neurophysiology, 83*(2), 808-827. doi:10.1152/jn.2000.83.2.808 [doi]

Latham, P. E., Richmond, B. J., Nirenberg, S., & Nelson, P. G. (2000). Intrinsic dynamics in neuronal networks. II. experiment. *Journal of Neurophysiology, 83*(2), 828-835.

Le Bon-Jego, M., & Yuste, R. (2007). Persistently active, pacemaker-like neurons in neocortex. *Frontiers in Neuroscience, 1*(1), 123-129. doi:10.3389/neuro.01.1.1.009.2007 [doi]

Li, C., & Gulledge, A. T. (2021). NMDA receptors enhance the fidelity of synaptic integration. *eNeuro, 8*(2), 10.1523/ENEURO.0396-Apr. doi:ENEURO.0396-20.2020 [pii]

Lin, Y. C., Huang, Z. H., Jan, I. S., Yeh, C. C., Wu, H. J., Chou, Y. C., & Chang, Y. C. (2002). Development of excitatory synapses in cultured neurons dissociated from the cortices of rat embryos and rat pups at birth. *Journal of Neuroscience Research, 67*(4), 484-493.

Linne, M. L., Jalonen, T. O., Saransaari, P., & Oja, S. S. (1996). Taurine-induced single-channel currents in cultured rat cerebellar granule cells. *Advances in Experimental Medicine and Biology, 403*, 455-462.

Linne, M. L., Oja, S. S., & Jalonen, T. O. (1996). Simultaneous detection of action potential current waveforms and single ion channel openings in rat cerebellar granule cells. *International Journal of Neural Systems, 7*(4), 377-384.

Liu, F., Day, M., Muniz, L. C., Bitran, D., Arias, R., Revilla-Sanchez, R., . . . Brandon, N. J. (2008). Activation of estrogen receptor-beta regulates hippocampal synaptic plasticity and improves memory. *Nature Neuroscience, 11*(3), 334-343. doi:10.1038/nn2057 [doi]

Lonardoni, D., Amin, H., Di Marco, S., Maccione, A., Berdondini, L., & Nieus, T. (2017). Recurrently connected and localized neuronal communities initiate coordinated spontaneous activity in neuronal networks. *PLoS Computational Biology, 13*(7), e1005672. doi:10.1371/journal.pcbi.1005672 [doi]

Low, W. C., Rujitanaroj, P. O., Wang, F., Wang, J., & Chew, S. Y. (2015). Nanofiber-mediated release of retinoic acid and brain-derived neurotrophic factor for enhanced neuronal differentiation of neural progenitor cells. *Drug Delivery and Translational Research, 5*(2), 89-100. doi:10.1007/s13346-013-0131-5 [doi]

Luhmann, H. J., Sinning, A., Yang, J. W., Reyes-Puerta, V., Stuttgen, M. C., Kirischuk, S., & Kilb, W. (2016). Spontaneous neuronal activity in developing neocortical networks: From single cells to large-scale interactions. *Frontiers in Neural Circuits, 10*, 40. doi:10.3389/fncir.2016.00040 [doi]

Maeda, E., Robinson, H. P., & Kawana, A. (1995). The mechanisms of generation and propagation of synchronized bursting in developing networks of cortical neurons. *The Journal of Neuroscience, 15*(10), 6834-6845.

Manninen, T., Acimovic, J., Havela, R., Teppola, H., & Linne, M. L. (2018). Challenges in reproducibility, replicability, and comparability of computational models and tools for neuronal and glial networks, cells, and subcellular structures. *Frontiers in Neuroinformatics, 12*, 20. doi:10.3389/fninf.2018.00020 [doi]

Mao, T., Kusefoglu, D., Hooks, B. M., Huber, D., Petreanu, L., & Svoboda, K. (2011). Long-range neuronal circuits underlying the interaction between sensory and motor cortex. *Neuron, 72*(1), 111-123. doi:10.1016/j.neuron.2011.07.029 [doi]

Marom, S. (2009). Adaptive transition rates in excitable membranes. *Frontiers in Computational Neuroscience, 3*, 2. doi:10.3389/neuro.10.002.2009 [doi]

Marom, S., & Shahaf, G. (2002). Development, learning and memory in large random networks of cortical neurons: Lessons beyond anatomy. *Quarterly Reviews of Biophysics, 35*(1), 63-87.

Martin, D., Thompson, M. A., & Nadler, J. V. (1993). The neuroprotective agent riluzole inhibits release of glutamate and aspartate from slices of hippocampal area CA1. *European Journal of Pharmacology, 250*(3), 473-476. doi:0014-2999(93)90037-I [pii]

Martinez-Banaclocha, M. (2018). Ephaptic coupling of cortical neurons: Possible contribution of astroglial magnetic fields? *Neuroscience, 370*, 37-45. doi:S0306-4522(17)30558-4 [pii]

Martinoia, S., Bonzano, L., Chiappalone, M., & Tedesco, M. (2005). Electrophysiological activity modulation by chemical stimulation in networks of cortical neurons coupled to microelectrode arrays: A biosensor for neuropharmacological applications. *Sensors & Actuators: B. Chemical, 108*(1), 589-596. doi:10.1016/j.snb.2004.11.041

Mastroeni, D., Grover, A., Leonard, B., Joyce, J. N., Coleman, P. D., Kozik, B., . . . Rogers, J. (2009). Microglial responses to dopamine in a cell culture model of parkinson's disease. *Neurobiology of Aging, 30*(11), 1805-1817. doi:10.1016/j.neurobiolaging.2008.01.001 [doi]

Matsumoto, K., Wada, R. K., Yamashiro, J. M., Kaplan, D. R., & Thiele, C. J. (1995). Expression of brain-derived neurotrophic factor and p145TrkB affects survival, differentiation, and invasiveness of human neuroblastoma cells. *Cancer Research, 55*(8), 1798-1806.

Matsumoto, N., Hoshiko, M., Sugo, N., Fukazawa, Y., & Yamamoto, N. (2016). Synapse-dependent and independent mechanisms of thalamocortical axon branching are regulated by neuronal activity. *Developmental Neurobiology, 76*(3), 323-336. doi:10.1002/dneu.22317 [doi]

Mauch, D. H., Nagler, K., Schumacher, S., Goritz, C., Muller, E. C., Otto, A., & Pfrieger, F. W. (2001). CNS synaptogenesis promoted by glia-derived cholesterol. *Science (New York, N.Y.), 294*(5545), 1354-1357. doi:10.1126/science.294.5545.1354 [doi]

McEwen, B. S., Coirini, H., & Schumacher, M. (1990). Steroid effects on neuronal activity: When is the genome involved? *Ciba Foundation Symposium, 153*, 3-21.

Meier, R., Egert, U., Aertsen, A., & Nawrot, M. P. (2008). FIND--a unified framework for neural data analysis. *Neural Networks, 21*(8), 1085-1093. doi:10.1016/j.neunet.2008.06.019 [doi]

Micheva, K. D., & Beaulieu, C. (1996). Quantitative aspects of synaptogenesis in the rat barrel field cortex with special reference to GABA circuitry. *The Journal of Comparative Neurology, 373*(3), 340-354. doi:10.1002/(SICI)1096-9861(19960923)373:33.0.CO;2-2 [pii]

Minlebaev, M., Colonnese, M., Tsintsadze, T., Sirota, A., & Khazipov, R. (2011). Early gamma oscillations synchronize developing thalamus and cortex. *Science (New York, N.Y.), 334*(6053), 226-229. doi:10.1126/science.1210574 [doi]

Molnar, Z., & Clowry, G. (2012). Cerebral cortical development in rodents and primates. *Progress in Brain Research, 195*, 45-70. doi:10.1016/B978-0-444-53860-4.00003-9 [doi]

Molnar, Z., Luhmann, H. J., & Kanold, P. O. (2020). Transient cortical circuits match spontaneous and sensory-driven activity during development. *Science (New York, N.Y.), 370*(6514), 10.1126/science.abb2153. doi:eabb2153 [pii]

Moody, W. J., & Bosma, M. M. (2005). Ion channel development, spontaneous activity, and activity-dependent development in nerve and muscle cells. *Physiological Reviews, 85*(3), 883-941. doi:85/3/883 [pii]

Moriya, F., Shimba, K., Kotani, K., & Jimbo, Y. (2021). Modulation of dynamics in a pre-existing hippocampal network by neural stem cells on a microelectrode array. *Journal of Neural Engineering, 18*(4), 10.1088/1741-2552/ac1c88. doi:10.1088/1741-2552/ac1c88 [doi]

Moutaux, E., Christaller, W., Scaramuzzino, C., Genoux, A., Charlot, B., Cazorla, M., & Saudou, F. (2018). Neuronal network maturation differently affects secretory vesicles and mitochondria transport in axons. *Scientific Reports, 8*(1), 13429-x. doi:10.1038/s41598-018-31759-x [doi]

Muramoto, K., Ichikawa, M., Kawahara, M., Kobayashi, K., & Kuroda, Y. (1993). Frequency of synchronous oscillations of neuronal activity increases during development and is correlated to the number of synapses in cultured cortical neuron networks. *Neuroscience Letters, 163*(2), 163-165.

Murphy, T. H., Blatter, L. A., Wier, W. G., & Baraban, J. M. (1992). Spontaneous synchronous synaptic calcium transients in cultured cortical neurons. *The Journal of Neuroscience, 12*(12), 4834-4845.

Murphy, T. H., Blatter, L. A., Wier, W. G., & Baraban, J. M. (1993). Rapid communication between neurons and astrocytes in primary cortical cultures. *The Journal of Neuroscience, 13*(6), 2672-2679.

Nakamura, K., Martin, K. C., Jackson, J. K., Beppu, K., Woo, C. W., & Thiele, C. J. (2006). Brain-derived neurotrophic factor activation of TrkB induces vascular endothelial growth factor expression via hypoxia-inducible factor-1alpha in neuroblastoma cells. *Cancer Research, 66*(8), 4249-4255. doi:66/8/4249 [pii]

Nakanishi, K., & Kukita, F. (1998). Functional synapses in synchronized bursting of neocortical neurons in culture. *Brain Research, 795*(1-2), 137-146.

Namiki, S., Norimoto, H., Kobayashi, C., Nakatani, K., Matsuki, N., & Ikegaya, Y. (2013). Layer III neurons control synchronized waves in the immature cerebral cortex. *The Journal of Neuroscience, 33*(3), 987-1001. doi:10.1523/JNEUROSCI.2522-12.2013 [doi]

O'Donovan, M. J. (1999). The origin of spontaneous activity in developing networks of the vertebrate nervous system. *Current Opinion in Neurobiology, 9*(1), 94-104. doi:S0959-4388(99)80012-9 [pii]

Okujeni, S., & Egert, U. (2019a). Inhomogeneities in network structure and excitability govern initiation and propagation of spontaneous burst activity. *Frontiers in Neuroscience, 13*, 543. doi:10.3389/fnins.2019.00543 [doi]

Okujeni, S., & Egert, U. (2019b). Self-organization of modular network architecture by activity-dependent neuronal migration and outgrowth. *eLife, 8*, 10.7554/eLife.47996. doi:10.7554/eLife.47996 [doi]

Okujeni, S., Kandler, S., & Egert, U. (2017). Mesoscale architecture shapes initiation and richness of spontaneous network activity. *The Journal of Neuroscience, 37*(14), 3972-3987. doi:10.1523/JNEUROSCI.2552-16.2017 [doi]

Opitz, T., De Lima, A. D., & Voigt, T. (2002). Spontaneous development of synchronous oscillatory activity during maturation of cortical networks in vitro. *Journal of Neurophysiology, 88*(5), 2196-2206. doi:10.1152/jn.00316.2002

Orlandi, J. G., Soriano, J., Alvarez-Lacalle, E., Teller, S., & Casademunt, J. (2013). Noise focusing and the emergence of coherent activity in neuronal cultures . *Nature Physics, 9,* 582-590. doi:10.1038/nphys2686

Owens, D. F., Flint, A. C., Dammerman, R. S., & Kriegstein, A. R. (2000). Calcium dynamics of neocortical ventricular zone cells. *Developmental Neuroscience, 22*(1-2), 25-33. doi:17424 [pii]

Ozawa, S., Kamiya, H., & Tsuzuki, K. (1998). Glutamate receptors in the mammalian central nervous system. *Progress in Neurobiology, 54*(5), 581-618. doi:S0301-0082(97)00085-3 [pii]

Pahlman, S., Ruusala, A. I., Abrahamsson, L., Mattsson, M. E., & Esscher, T. (1984). Retinoic acid-induced differentiation of cultured human neuroblastoma cells: A comparison with phorbolester-induced differentiation. *Cell Differentiation, 14*(2), 135-144.

Palmer, L. M., Shai, A. S., Reeve, J. E., Anderson, H. L., Paulsen, O., & Larkum, M. E. (2014). NMDA spikes enhance action potential generation during sensory input. *Nature Neuroscience, 17*(3), 383-390. doi:10.1038/nn.3646; 10.1038/nn.3646

Parri, H. R., Gould, T. M., & Crunelli, V. (2001). Spontaneous astrocytic Ca2+ oscillations in situ drive NMDAR-mediated neuronal excitation. *Nature Neuroscience, 4*(8), 803-812. doi:10.1038/90507 [doi]

Parsons, C. G., Gruner, R., & Rozental, J. (1994). Comparative patch clamp studies on the kinetics and selectivity of glutamate receptor antagonism by 2,3-dihydroxy-6-nitro-7-sulfamoyl-benzo(F)quinoxaline (NBQX) and 1-(4-amino-phenyl)-4-methyl-7,8-methyl-endioxyl-5H-2,3-benzodiaze pine (GYKI 52466). *Neuropharmacology, 33*(5), 589-604.

Pfrieger, F. W. (2003). Role of cholesterol in synapse formation and function. *Biochimica Et Biophysica Acta, 1610*(2), 271-280. doi:S0005273603000245 [pii]

Preis, P. N., Saya, H., Nadasdi, L., Hochhaus, G., Levin, V., & Sadee, W. (1988). Neuronal cell differentiation of human neuroblastoma cells by retinoic acid plus herbimycin A. *Cancer Research, 48*(22), 6530-6534.

Presgraves, S. P., Ahmed, T., Borwege, S., & Joyce, J. N. (2004). Terminally differentiated SH-SY5Y cells provide a model system for studying neuroprotective effects of dopamine agonists. *Neurotoxicity Research, 5*(8), 579-598.

Pyle, J. L., Kavalali, E. T., Choi, S., & Tsien, R. W. (1999). Visualization of synaptic activity in hippocampal slices with FM1-43 enabled by fluorescence quenching. *Neuron, 24*(4), 803-808. doi:S0896-6273(00)81028-4 [pii]

Raichman, N., & Ben-Jacob, E. (2008). Identifying repeating motifs in the activation of synchronized bursts in cultured neuronal networks. *Journal of Neuroscience Methods, 170*(1), 96-110. doi:10.1016/j.jneumeth.2007.12.020 [doi]

Ramakers, G. J., Corner, M. A., & Habets, A. M. (1990). Development in the absence of spontaneous bioelectric activity results in increased stereotyped burst firing in cultures of dissociated cerebral cortex. *Experimental Brain Research, 79*(1), 157-166.

Ramakers, G. J., Corner, M. A., & Habets, A. M. (1991). Abnormalities in the spontaneous firing patterns of cultured rat neocortical neurons after chronic exposure to picrotoxin during development in vitro. *Brain Research Bulletin, 26*(3), 429-432.

Ramakers, G. J., de Wit, C., Wolters, P. S., & Corner, M. A. (1993). A developmental decrease in NMDA-mediated spontaneous firing in cultured rat cerebral cortex. *International Journal of Developmental Neuroscience, 11*(1), 25-32.

Reincke, S. A., & Hanganu-Opatz, I. L. (2017). Early-life stress impairs recognition memory and perturbs the functional maturation of prefrontal-hippocampal-perirhinal networks. *Scientific Reports, 7*, 42042. doi:10.1038/srep42042 [doi]

Renner, M., Choquet, D., & Triller, A. (2009). Control of the postsynaptic membrane viscosity. *The Journal of Neuroscience, 29*(9), 2926-2937. doi:10.1523/JNEUROSCI.4445-08.2009 [doi]

Rivera, C., Voipio, J., & Kaila, K. (2005). Two developmental switches in GABAergic signalling: The K+-cl- cotransporter KCC2 and carbonic anhydrase CAVII. *The Journal of Physiology, 562*(Pt 1), 27-36. doi:jphysiol.2004.077495 [pii]

Robinson, H. P., Kawahara, M., Jimbo, Y., Torimitsu, K., Kuroda, Y., & Kawana, A. (1993). Periodic synchronized bursting and intracellular calcium transients elicited by low magnesium in cultured cortical neurons. *Journal of Neurophysiology, 70*(4), 1606-1616.

Romanos, J., Benke, D., Saab, A. S., Zeilhofer, H. U., & Santello, M. (2019). Differences in glutamate uptake between cortical regions impact neuronal NMDA receptor activation. *Communications Biology*, 2, 127. https://doi.org/10.1038/s42003-019-0367-9

Rubenstein, J. L. (2011). Annual research review: Development of the cerebral cortex: Implications for neurodevelopmental disorders. *Journal of Child Psychology and Psychiatry, and Allied Disciplines, 52*(4), 339-355. doi:10.1111/j.1469-7610.2010.02307.x [doi]

Saarinen, A., Linne, M. L., & Yli-Harja, O. (2008). Stochastic differential equation model for cerebellar granule cell excitability. *PLoS Computational Biology, 4*(2), e1000004. doi:10.1371/journal.pcbi.1000004 [doi]

Sahin, M., Oncu, G., Yilmaz, M. A., Ozkan, D., & Saybasili, H. (2021). Transformation of SH-SY5Y cell line into neuron-like cells: Investigation of electrophysiological and biomechanical changes. *Neuroscience Letters, 745*, 135628. doi:S0304-3940(21)00006-9 [pii]

Sanchez-Vives, M. V., & McCormick, D. A. (2000). Cellular and network mechanisms of rhythmic recurrent activity in neocortex. *Nature Neuroscience, 3*(10), 1027-1034. doi:10.1038/79848 [doi]

Sarkanen, J. R., Nykky, J., Siikanen, J., Selinummi, J., Ylikomi, T., & Jalonen, T. O. (2007). Cholesterol supports the retinoic acid-induced synaptic vesicle formation in differentiating human SH-SY5Y neuroblastoma cells. *Journal of Neurochemistry, 102*(6), 1941-1952. doi:JNC4676 [pii]

Schneider, C. A., Rasband, W. S., & Eliceiri, K. W. (2012). NIH image to ImageJ: 25 years of image analysis. *Nature Methods, 9*(7), 671-675.

Schreurs, B. G. (2010). The effects of cholesterol on learning and memory. *Neuroscience and Biobehavioral Reviews, 34*(8), 1366-1379. doi:10.1016/j.neubiorev.2010.04.010 [doi]

Schwartz, T. H., Rabinowitz, D., Unni, V., Kumar, V. S., Smetters, D. K., Tsiola, A., & Yuste, R. (1998). Networks of coactive neurons in developing layer 1. *Neuron, 20*(3), 541-552. doi:S0896-6273(00)80993-9 [pii]

Selinummi, J., Seppala, J., Yli-Harja, O., & Puhakka, J. A. (2005). Software for quantification of labeled bacteria from digital microscope images by automated image analysis. *BioTechniques, 39*(6), 859-863. doi:000112018 [pii]

Sengupta, D. C., Lantz, C. L., Rumi, M. A. K., & Quinlan, E. M. (2019). 17alpha estradiol promotes plasticity of spared inputs in the adult amblyopic visual cortex. *Scientific Reports, 9*(1), 19040-y. doi:10.1038/s41598-019-55158-y [doi]

Shahaf, G., & Marom, S. (2001). Learning in networks of cortical neurons. *The Journal of Neuroscience, 21*(22), 8782-8788. doi:21/22/8782 [pii]

Shein, M., Volman, V., Raichman, N., Hanein, Y., & Ben-Jacob, E. (2008). Management of synchronized network activity by highly active neurons. *Physical Biology, 5*(3), 036008-3975/5/3/036008. doi:10.1088/1478-3975/5/3/036008 [doi]

Sheng, M., & Lee, S. H. (2001). AMPA receptor trafficking and the control of synaptic transmission. *Cell, 105*(7), 825-828. doi:S0092-8674(01)00406-8 [pii]

Smith, C. C., & McMahon, L. L. (2005). Estrogen-induced increase in the magnitude of long-term potentiation occurs only when the ratio of NMDA transmission to AMPA transmission is increased. *The Journal of Neuroscience, 25*(34), 7780-7791. doi:25/34/7780 [pii]

Smith-Swintosky, V. L., Gozes, I., Brenneman, D. E., D'Andrea, M. R., & Plata-Salaman, C. R. (2005). Activity-dependent neurotrophic factor-9 and NAP promote neurite outgrowth in rat hippocampal and cortical cultures. *Journal of Molecular Neuroscience : MN, 25*(3), 225-238. doi:JMN:25:3:225 [pii]

Soriano, J., Rodriguez Martinez, M., Tlusty, T., & Moses, E. (2008). Development of input connections in neural cultures. *Proceedings of the National Academy of Sciences of the United States of America, 105*(37), 13758-13763. doi:10.1073/pnas.0707492105 [doi]

Sukenik, N., Vinogradov, O., Weinreb, E., Segal, M., Levina, A., & Moses, E. (2021) Neuronal circuits overcome imbalance in excitation and inhibition by adjusting connection numbers. *Proceedings of the National Academy of Sciences of the United States of America*. 118, (12). doi: 10.1073/pnas.2018459118

Sun, J. J., Kilb, W., & Luhmann, H. J. (2010). Self-organization of repetitive spike patterns in developing neuronal networks in vitro. *The European Journal of Neuroscience, 32*(8), 1289-1299. doi:10.1111/j.1460-9568.2010.07383.x [doi]

Sun, J. J., & Luhmann, H. J. (2007). Spatio-temporal dynamics of oscillatory network activity in the neonatal mouse cerebral cortex. *The European Journal of Neuroscience, 26*(7), 1995-2004. doi:EJN5819 [pii]

Suresh, J., Radojicic, M., Pesce, L. L., Bhansali, A., Wang, J., Tryba, A. K., . . . van Drongelen, W. (2016). Network burst activity in hippocampal neuronal cultures: The role of synaptic and intrinsic currents. *Journal of Neurophysiology, 115*(6), 3073-3089. doi:10.1152/jn.00995.2015 [doi]

Taxier, L. R., Gross, K. S., & Frick, K. M. (2020). Oestradiol as a neuromodulator of learning and memory. *Nature Reviews.Neuroscience, 21*(10), 535-550. doi:10.1038/s41583-020-0362-7 [doi]

Tetzlaff, C., Okujeni, S., Egert, U., Worgotter, F., & Butz, M. (2010). Self-organized criticality in developing neuronal networks. *PLoS Computational Biology, 6*(12), e1001013. doi:10.1371/journal.pcbi.1001013 [doi]

Thivierge, J. P. (2009). How does non-random spontaneous activity contribute to brain development? *Neural Networks, 22*(7), 901-912. doi:10.1016/j.neunet.2009.01.001 [doi]

Toib, A., Lyakhov, V., & Marom, S. (1998). Interaction between duration of activity and time course of recovery from slow inactivation in mammalian brain na+ channels. *The Journal of Neuroscience, 18*(5), 1893-1903.

Toselli, M., Tosetti, P., & Taglietti, V. (1996). Functional changes in sodium conductances in the human neuroblastoma cell line SH-SY5Y during in vitro differentiation. *Journal of Neurophysiology, 76*(6), 3920-3927.

Tsodyks, M. V., & Markram, H. (1997). The neural code between neocortical pyramidal neurons depends on neurotransmitter release probability. *Proceedings of the National Academy of Sciences of the United States of America, 94*(2), 719-723. doi:10.1073/pnas.94.2.719 [doi]

Tsodyks, M., Uziel, A., & Markram, H. (2000). Synchrony generation in recurrent networks with frequency-dependent synapses. *The Journal of Neuroscience, 20*(1), RC50.

van Drongelen, W., Koch, H., Elsen, F. P., Lee, H. C., Mrejeru, A., Doren, E., . . . Ramirez, J. M. (2006). Role of persistent sodium current in bursting activity of mouse neocortical networks in vitro. *Journal of Neurophysiology, 96*(5), 2564-2577. doi:00446.2006 [pii]

van Huizen, F., Romijn, H. J., Habets, A. M. M. C., & van den Hooff, P. (1987). Accelerated neural network formation in rat cerebral cortex cultures chronically disinhibited with picrotoxin. *Experimental Neurology, 97*(2), 280-288. doi:https://doi.org/10.1016/0014-4886(87)90089-6

van Huizen, F., Romijn, H. J., & Habets, A. M. (1985). Synaptogenesis in rat cerebral cortex cultures is affected during chronic blockade of spontaneous bioelectric

activity by tetrodotoxin. *Brain Research, 351*(1), 67-80. doi:10.1016/0165-3806(85)90232-9 [doi]

Van Ooyen, A., Van Pelt, J., & Corner, M. A. (1995). Implications of activity dependent neurite outgrowth for neuronal morphology and network development. *Journal of Theoretical Biology, 172*(1), 63-82. doi:https://doi.org/10.1006/jtbi.1995.0005

van Pelt, J., Vajda, I., Wolters, P. S., Corner, M. A., & Ramakers, G. J. (2005). Dynamics and plasticity in developing neuronal networks in vitro. *Progress in Brain Research, 147*, 173-188. doi:S0079612304470137 [pii]

Van Pelt, J., Corner, M.A., Wolters, P.S., Rutten, W.L.C., & Ramakers, G.J.A. (2004a). Longterm stability and developmental changes in spontaneous network burst firing patterns in dissociated rat cerebral cortex cell cultures on multielectrode arrays. *Neuroscience Letters* 361, 86–89. doi: 10.1016/j.neulet.2003.12.062

van Pelt, J., Wolters, P. S., Corner, M. A., Rutten, W. L., & Ramakers, G. J. (2004b). Long-term characterization of firing dynamics of spontaneous bursts in cultured neural networks. *IEEE Transactions on BioMedical Engineering, 51*(11), 2051-2062. doi:10.1109/TBME.2004.827936 [doi]

Verwer, R.W.H., Hermens, W.T.J.M.C., Dijkhuizen, P.A., Brake, O.T., Baker, R.E., Salehi, A., Sluiter, A.A., Kok, M.J.M., Müller, L.J., Verhaagen, J., Swaab, D.F., (2002). Cells in human postmortem brain tissue slices remain alive for several weeks in culture. *The FASEB Journal* 16(1), 54-60. doi.org/10.1096/fj.01-0504com

Volman, V., Baruchi, I., & Ben-Jacob, E. (2005). Manifestation of function-follow-form in cultured neuronal networks. *Physical Biology, 2*(2), 98-110. doi:S1478-3975(05)91632-4 [pii]

Wagenaar, D. A., Pine, J., & Potter, S. M. (2004). Effective parameters for stimulation of dissociated cultures using multi-electrode arrays. *Journal of Neuroscience Methods, 138*(1-2), 27-37. doi:10.1016/j.jneumeth.2004.03.005 [doi]

Wagenaar, D. A., Pine, J., & Potter, S. M. (2006). An extremely rich repertoire of bursting patterns during the development of cortical cultures. *BMC Neuroscience, 7*, 11. doi:1471-2202-7-11 [pii]

Wang, D. D., & Kriegstein, A. R. (2011). Blocking early GABA depolarization with bumetanide results in permanent alterations in cortical circuits and sensorimotor gating deficits. *Cerebral Cortex (New York, N.Y.: 1991), 21*(3), 574-587. doi:10.1093/cercor/bhq124 [doi]

Wang, M., & Arnsten, A. F. (2015). Contribution of NMDA receptors to dorsolateral prefrontal cortical networks in primates. *Neuroscience Bulletin, 31*(2), 191-197. doi:10.1007/s12264-014-1504-6 [doi]

Wang, X. J. (1999). Synaptic basis of cortical persistent activity: The importance of NMDA receptors to working memory. *The Journal of Neuroscience, 19*(21), 9587-9603.

Weihberger, O., Okujeni, S., Mikkonen, J. E., & Egert, U. (2013). Quantitative examination of stimulus-response relations in cortical networks in vitro. *Journal of Neurophysiology, 109*(7), 1764-1774. doi:10.1152/jn.00481.2012 [doi]

Weissman, T. A., Riquelme, P. A., Ivic, L., Flint, A. C., & Kriegstein, A. R. (2004). Calcium waves propagate through radial glial cells and modulate proliferation in the developing neocortex. *Neuron, 43*(5), 647-661. doi:10.1016/j.neuron.2004.08.015 [doi]

Wilson, N.R., Ty, M.T., Ingber, D.E., Sur, M., Liu, G., (2007). Synaptic Reorganization in Scaled Networks of Controlled Size. *Journal of Neuroscience*, 27 (50), 13581-13589; doi.org/10.1523/JNEUROSCI.3863-07.2007

Wong, M., & Moss, R. L. (1992). Long-term and short-term electrophysiological effects of estrogen on the synaptic properties of hippocampal CA1 neurons. *The Journal of Neuroscience, 12*(8), 3217-3225.

Xicoy, H., Brouwers, J. F., Kalnytska, O., Wieringa, B., & Martens, G. J. M. (2020). Lipid analysis of the 6-hydroxydopamine-treated SH-SY5Y cell model for parkinson's disease. *Molecular Neurobiology, 57*(2), 848-859. doi:10.1007/s12035-019-01733-3 [doi]

Xu, J., & Wu, L. G. (2005). The decrease in the presynaptic calcium current is a major cause of short-term depression at a calyx-type synapse. *Neuron, 46*(4), 633-645. doi:S0896-6273(05)00306-5 [pii]

Yamamoto, H., Kubota, S., Chida, Y., Morita, M., Moriya, S., Akima, H., . . . Niwano, M. (2016). Size-dependent regulation of synchronized activity in living neuronal networks. *Physical Review E, 94*(1-1), 012407. doi:10.1103/PhysRevE.94.012407 [doi]

Yamamoto, N., & Lopez-Bendito, G. (2012). Shaping brain connections through spontaneous neural activity. *The European Journal of Neuroscience, 35*(10), 1595-1604. doi:10.1111/j.1460-9568.2012.08101.x; 10.1111/j.1460-9568.2012.08101.x

Yang, J. W., Hanganu-Opatz, I. L., Sun, J. J., & Luhmann, H. J. (2009). Three patterns of oscillatory activity differentially synchronize developing neocortical networks in vivo. *The Journal of Neuroscience, 29*(28), 9011-9025. doi:10.1523/JNEUROSCI.5646-08.2009

Yang, W., Miller, J. E., Carrillo-Reid, L., Pnevmatikakis, E., Paninski, L., Yuste, R., & Peterka, D. S. (2016). Simultaneous multi-plane imaging of neural circuits. *Neuron, 89*(2), 269-284. doi:10.1016/j.neuron.2015.12.012 [doi]

Yarom, Y., & Hounsgaard, J. (2011). Voltage fluctuations in neurons: Signal or noise? *Physiological Reviews, 91*(3), 917-929. doi:10.1152/physrev.00019.2010 [doi]

Yuste, R., & Katz, L. C. (1991). Control of postsynaptic Ca2+ influx in developing neocortex by excitatory and inhibitory neurotransmitters. *Neuron, 6*(3), 333-344. doi:0896-6273(91)90243-S [pii]

PUBLICATIONS

Publication I Teppola, H., Okujeni, S., Linne, M.-L., & Egert, U. (2011). AMPA, NMDA and $GABA_A$ Receptor Mediated Network Burst Dynamics in Cortical Cultures *in vitro*. In *Proceedings of the 8th International Workshop on Computational Systems Biology (WCSB2011)*, 8:181-184

Publication II Teppola, H., Aćimović, J., & Linne, M.-L. (2019). Unique Features of Network Bursts Emerge from the Complex Interplay of Excitatory and Inhibitory Receptors in Rat Neocortical Networks. *Frontiers in Cellular Neuroscience*, 13(377). doi:10.3389/fncel.2019.00377

Publication III Aćimović, J., Mäki-Marttunen, T., Teppola, H., & Linne, M.-L (2021). Analysis of Cellular and Synaptic Mechanisms behind Spontaneous Cortical Activity *in vitro*: Insights from Optimization of Spiking Neuronal Network Models. Submitted Manuscript. Available in: doi:10.1101/2021.10.28.466340

Publication IV Teppola, H., Sarkanen, J.-R., Jalonen, T.O., & Linne, M.-L. (2016). Morphological Differentiation Towards Neuronal Phenotype of SH-SY5Y Neuroblastoma Cells by Estradiol, Retinoic Acid, and Cholesterol. *Neurochemical Research*, 41(4):731–747. doi:10.1007/s11064-015-1743-6

Publication V Teppola, H., Sarkanen, J.-R., Jalonen, T.O., & Linne, M.-L. (2018). Impacts of Laminin and Polyethyleneimine Surface Coatings on Morphology of Differentiating Human SH-SY5Y Cells and Networks. In *Proceedings of the International Federation of Medical and Biological Engineering (IFMBE)*, 65:298-231. doi:10.1007/978-981-10-5122-7_75

PUBLICATION I

AMPA, NMDA, and $GABA_A$ Receptor Mediated Network Burst Dynamics in Cortical Cultures *in vitro*

Teppola H, Okujeni S, Linne M-L, Egert U

In Proceedings of the 8th International Workshop on
Computational Systems Biology, 2011; 8:181-184

AMPA, NMDA AND $GABA_A$ RECEPTOR MEDIATED NETWORK BURST DYNAMICS IN CORTICAL CULTURES *IN VITRO*

H. Teppola[1,2], S. Okujeni[2], M.-L. Linne[1], and U. Egert[2]

[1] Department of Signal Processing, Tampere University of Technology, Tampere, Finland
[2] Bernstein Center Freiburg & Department of Microsystems Engineering, IMTEK, Albert-Ludwig University of Freiburg, Freiburg, Germany

heidi.teppola@tut.fi, okujeni@bcf.uni-freiburg.de, marja-leena.linne@tut.fi, egert@imtek.uni-freiburg.de

ABSTRACT

In this work we study the excitatory AMPA, and NMDA, and inhibitory $GABA_A$ receptor mediated dynamical changes in neuronal networks of neonatal rat cortex *in vitro*. Extracellular network-wide activity was recorded with 59 planar electrodes simultaneously under different pharmacological conditions. We analyzed the changes of overall network activity and network-wide burst frequency between baseline and AMPA receptor (AMPA-R) or NMDA receptor (NMDA-R) driven activity, as well as between the latter states and disinhibited activity. Additionally, spatiotemporal structures of pharmacologically modified bursts and recruitment of electrodes during the network bursts were studied. Our results show that AMPA-R and NMDA-R receptors have clearly distinct roles in network dynamics. AMPA-Rs are in greater charge to initiate network wide bursts. Therefore NMDA-Rs maintain the already initiated activity. $GABA_A$ receptors ($GABA_A$-Rs) inhibit AMPA-R driven network activity more strongly than NMDA-R driven activity during the bursts.

1. INTRODUCTION

Synchronous patterns of activity, accompanied with intracellular Ca^{2+}-transients, are considered to play an essential role in the development of neuronal networks in a wide range of brain structures [4], including networks of dissociated cortical neurons *in vitro* [3]. Synchronous activity in form of network-wide bursts (NB) is thought to be generated by recurrent excitatory pathways. The inhibitory pathways suppressing excitation are also considered important in network burst dynamics.

As in native cortical tissue, glutamatergic AMPA-Rs (expressing fast ion channel kinetics) and NMDA-Rs (expressing slow ion channel kinetics, and both voltage and Mg^{2+}-dependency) are the main mediators of excitatory synaptic transmission among neurons *in vitro*. Fast inhibition is mediated through GABAergic transmission via $GABA_A$-Rs. Despite the solid biophysical characterization of AMPA, NMDA, and $GABA_A$ receptors at the monosynaptic level, their complex interplay on the network level is still not fully understood.

Simultaneous multi-unit recordings from neuronal networks of an intact brain *in vivo* are challenging to conduct with the existing technology. Therefore, microelectrode array (MEA) measurement systems have been developed for simultaneous extracellular recordings of many neurons in *in vitro* networks. These recordings allow spontaneous and stimulus evoked NB activity to be recorded over hours of time [5]. Previous spontaneous recordings of neural activity at 21 days *in vitro* (DIV) with MEA have shown, similarly to this work, that networks posses stable dynamics following synapse formation and maturation. The characteristic network-wide bursting in these previous studies consists of around 0.5 to 1 second long periods of simultaneous high spiking activity on many electrodes followed by 0.5 to 20 seconds quiescence periods [3], [6], [7].

Pharmacological studies of stimulus evoked network activity in cortical cultures have shown that the late component of NBs (25ms after stimulus, lasting several hundred milliseconds) was reduced or abolished by NMDA-R antagonist, such as APV and high Mg^{2+}, without affecting to the early component (first 25ms after stimulus). When inhibitory $GABA_A$-Rs were blocked by bicuculline (BIC) the opposite effect was obtained, the late component of evoked responses was increased [1]. Another study in dissociated spinal cord cultures has shown that the duration of AMPA-R driven bursts decreased compared to the baseline, suggesting the role of NMDA-Rs in the maintenance of high network activity during bursting. In addition, NMDA-R antagonist has been found to reduce the burst rate indicating a contribution of NMDA-Rs in network activation. By silencing AMPA-R at the presence of disinhibition (BIC), the burst rate was reduced and burst onset was slowed down and in some experiments bursting ceased completely by AMPA-R antagonist [2].

In this work, we study for first time the coordinated interplay between excitation and inhibition in

network dynamics in dissociated neurons of rat neonatal cortex. First, we obtained spontaneous baseline activity with MEA from six different densely cultured networks at 21 DIV **(Figure 1)**. Then, we silenced each of the excitatory pathways by blocking either AMPA-Rs or NMDA-Rs with NBQX or D-AP5, respectively, both in three different cultures. Finally, we disinhibited the networks with $GABA_A$-R antagonist PTX. This protocol allows us to investigate the temporal and spatial patterns of network dynamics, produced by fast and slow excitatory and fast inhibitory transmission.

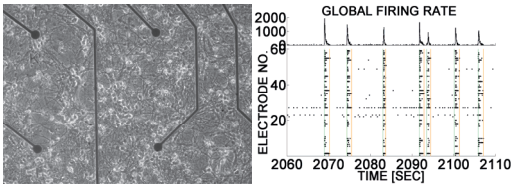

Figure 1. Left: Cultured network of cortical neurons on MEA plate at 21 DIV. **Right:** Spontaneous synchronized patterns of activity. The upper plot shows array wide firing rate (Hz) and the raster plot at the bottom shows the activity (spikes) recorded with 59 electrodes during a time period of 50 seconds.

2. MATERIALS AND METHODS

Primary cell cultures: Cortical cells were extracted from neonatal Wistar rats' frontal lobes and enzymatically and mechanically dissociated. 200 000 cells were seeded on 0.1% polyethyleneimine coated microelectrode arrays (60 TiN electrodes Ø 30µM, 500µM electrode pitch, Multi Channel Systems Ltd.). Cells were cultured in 2ml minimum essential medium supplemented with 5% heat inactivated horse serum, 20mmol/l glucose, 1% gentamycine and 0.5mmol/l L-glutamine in 5% CO_2 humidified incubator at 37°C. One third of the medium were changed twice a week and recordings were done between 21-23 DIV.

Pharmacology: The following agents were used for suppressing ionotropic receptors: 10µM D-(-)-2-Amino-5-phosphonopentanoic acid (**D-AP5**) to competitively block the glutamate site of NMDA-Rs, 10µM 2.3-Dioxo-6-nitro-1,2,3,4 tetrahydrobenzo-[f]quinoxaline-7-sulfonamide (**NBQX**) to competitively block AMPA-Rs and 10µM Picrotoxin (**PTX**) to non-competitively block $GABA_A$-R. All drugs were applied to medium with a pipette.

Electrophysiological recordings and analysis: Spontaneous network activity was recorded with MEA-1060 amplifier (Multi Channel Systems Ltd.) in normal culture conditions and after applying each of the drugs for one hour. Raw signals from each electrode were digitally high-pass filtered at 200Hz and extracellular activity of neurons (spikes) were detected based on voltage threshold, -5 times of standard deviation from mean noise baseline of each electrode using MC-Rack software (Multi Channel Systems Ltd.).

For further analysis the initial 600s of recorded data after drug application were discarded and the following 3000s were analyzed. Artifacts and electrodes with firing rates (FR) lower than 9% of the average FR on electrodes with spike activity were removed. NBs were detected according to following criteria: first inter spike interval < 100ms defines onset time of NB and first inter spike interval > 100ms defines offset of NB, in addition, minimum 8 electrodes should be active during the NB.

3. RESULTS

We pharmacologically blocked the excitatory AMPA-R and NMDA-R separately. Upon monitoring network activity, we additionally blocked $GABA_A$-R to observe the interplay between inhibition and each excitatory pathway.

First, we calculated the overall network activity (spikes/sec) and burst frequency (bursts/min) over whole analysis period of 3000s. Recordings from networks under AMPA-R blockage (n=3) and under NMDA-R blockage (n=3) were compared to the baseline recordings. As expected, overall firing rate decreased upon suppression of either AMPA-R or NMDA-R driven excitation and increased when networks were disinhibited as shown in **Table1**. When comparing the ratio of overall firing rate and burst frequency between baseline and NMDA-R suppressed excitation the results showed that the overall firing rate and burst frequency decreased by a factor of 10 and 2, respectively. However, blocking AMPA-Rs decreased overall firing rate only 3 fold and burst frequency 21 fold **(Table1)**.

When the excitatory pathway was driven by AMPA-Rs and the inhibitory pathway was simultaneously suppressed, the overall network activity increased 14 fold (n=3) but burst frequency decreased 2 fold (n=2) in two out of three cultures and increased 3 fold (n=1) in one out of three cultures. Disinhibition during NMDA-R driven activity caused overall network activity to increase only 2 fold and burst frequency to increase 5 fold **(Table1)**.

Burst firing rate profiles in **Figure 2** show how the temporal structure of bursts are modified following each drug application at single electrode level and at average over all electrodes. AMPA-R driven bursts became shorter, contained fewer spikes, the peak FR was reached earlier (~20-40 ms) in the bursts and late phase was diminished. Contrarily, NMDA-R driven bursts became longer, contained more spikes, the peak FR was achieved later in the course of the burst (~ 90-200 ms)

and the late phase of NBs was more pronounced. Disinhibition increased the early and late phases of bursts in comparison to control and AMPA-R driven bursts but, interestingly, in comparison to NMDA-R driven bursts the late phase squeezed after disinhibition **(Figure 2)**.

The recruitment of electrodes during NBs was significantly decreased during AMPA-R driven activity. In contrast, networks were widely recruited over 200ms time periods with disinhibition of AMPA-R driven activity as shown in **Figure 3**. Approximately the same number of electrodes was recruited when NMDA-R driven NBs were compared to control case. However, after disinhibition, the recruitment of electrodes a bit increased but more importantly recruitment was much faster than during NMDA-R driven or baseline activity, indicating that NMDA-R driven inhibition slows down the propagation of network-wide activity at the beginning of bursts **(Figure 3)**.

4. CONCLUSIONS

Our results show that AMPA-R driven NBs are initiated more often than NMDA-R driven ones contributing over ten times more to the initiation of network activity compared to NMDA-Rs. By blocking NMDA-Rs, the overall firing rate was lowered three times more compared to AMPA-R blockage, which indicates the importance of NMDA-Rs in maintaining network activity during the bursts.

Nearly ten times higher overall firing rates were observed during disinhibited AMPA-R driven activity compared to the NMDA-R driven one. This indicates the $GABA_A$-Rs primary role for inhibiting especially AMPA-R driven network activity. The connection between the roles of $GABA_A$-Rs and AMPA-Rs is also indicated by the fact that NMDA-R driven activity displays higher firing rates compared to the control case, where both NMDA-Rs and AMPA-R are active **(Figure 2)**.

Contradictory behavior of both decreasing and increasing burst frequencies during disinhibition of AMPA-R driven activity could be explained by two different underlying mechanisms: 1. There are more bursts, due to lower firing threshold, to initiate AMPA-R driven NBs when inhibition is suppressed; 2. There are less bursts because AMPA-R driven neurons are more excited, thus lengthening network bursts and, hence, recovery times.

We additionally found out that disinhibition, in general, increases the early and late phase of bursts due to decreased threshold for excitation. Suprisingly, the late phase of NMDA driven bursts shortened and burst frequency increased by disinhibition. This can be explained by our finding that $GABA_A$-R slows down the recruitment of NMDA driven NBs, thus by blocking $GABA_A$-Rs in such a network, the recruitment of NBs speeds up and further, the duration of bursts shortens.

Our results further indicate that the dynamics of cortical networks *in vitro* incorporate a complex interplay between excitatory and inhibitory transmission. NMDA-R and AMPA-R driven activities are both able to initiate network-wide bursting. However, AMPA-Rs role for initiation is much more important. The main role of NMDA-Rs is to maintain already initiated activity. $GABA_A$-Rs inhibit AMPA-R driven network excitation more strongly than the NMDA-R driven during bursts. However, $GABA_A$-R mediated inhibition slows down the propagation of NMDA-R mediated network activity more than AMPA-R mediated. Experimentally investigated interplay between excitatory and inhibitory transmission in cortical networks *in vitro* can further be studied using biologically plausible computational network models.

5. ACKNOWLEDGEMENTS

The authors would like to acknowledge the following funding: Graduate School of Tampere University of Technology, Tampere Graduate School in Information Science and Engineering (TISE), Academy of Finland Grant (213462, 129657, 106030, and 124615), German BMBF (FKZ 01GQ0830, 01GQ0420), and EC (NEURO, 12788).

6. REFERENCES

[1] Y. Jimbo, A. Kanawa, P. Parodi and V. Torre, “The dynamics of a neuronal culture of dissociated cortical neurons of neonatal rats”, Biol Cybern, vol. 83, pp. 1-20, 2000.

[2] J.- C. Legrand, P. Darbon and J. Streit, “Contributions of NMDA receptors to network recruitment and rhythm generation in spinal cord cultures”, Eur J Neurosci, vol. 19, pp. 521-532, 2004.

[3] H. P. C. Robinson, M. Kawahara, Y. Jimbo, K. Torimitsu, Y. Kuroda and A. Kawana, ”Periodic synchronized bursting and intracellular calcium transients elicited by low magnesium in cultured cortical neurons”, J Neurophys, vol. 70, pp. 1606-1616, 1993.

[4] C. J. Shatz, “Impulse activity and the patterning of connections during CNS development”, Neuron, vol. 5, pp. 745-756, 1990.

[5] Stett, U. Egert, E. Guenther, F. Hofmann, T. Meyer, W. Nisch and H. Haemmerle, “Biological applications of microelectrode arrays in drug discovery and basic research”, Anal Bioanal Chem, vol. 377, pp. 486-495, 2003.

[6] D. A. Wagenaar, J. Pine and S. M. Potter, ”An extremely rich repertoire of bursting patterns during the development of cortical cultures”, BMC Neurosci vol.7, no. 11, 2006.

[7] D. Eytan, and S. Marom,”Dynamics and effective topology underlying synchronization in networks of cortical neurons”, J Neurosci, vol. 26, no. 33, pp. 8465-8476, 2006.

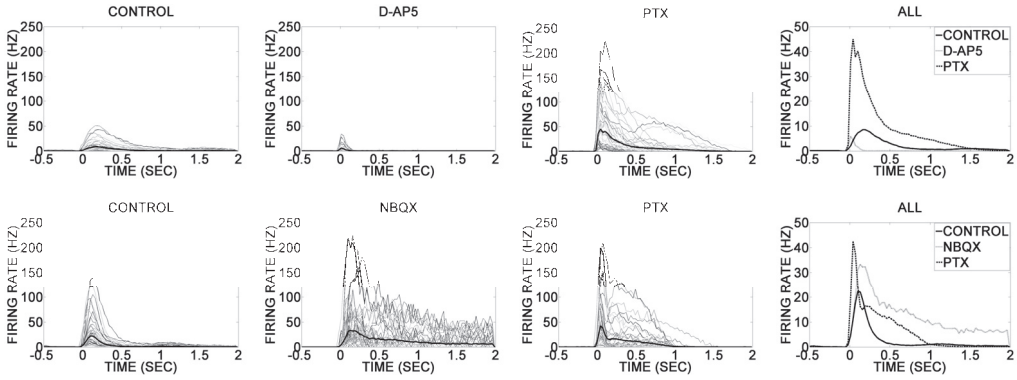

Figure 2. Burst firing rate profiles. Upper row corresponds to AMPA driven experiment and lower row to NMDA driven experiment. Columns from left: firing rate profiles during control, suppression of excitation, suppression of inhibition, and the average profiles for all three cases. D-AP5, NBQX, and PTX are the pharmacological agents for suppressing NMDA-Rs, AMPA-Rs, and $GABA_A$-Rs respectively. In the first three columns one single thin line corresponds to firing rate in one electrode averaged over all bursts (aligned to NB onsets). In all columns, thick lines correspond to overall average burst firing rates over all electrodes and over all bursts (bin width 30ms).

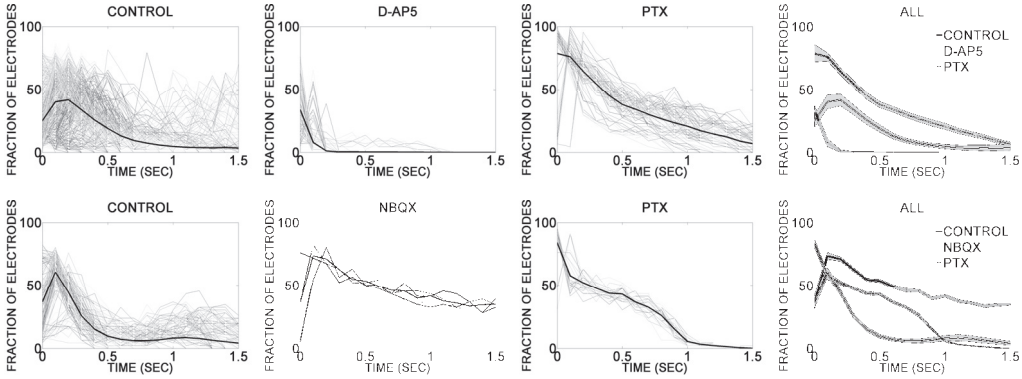

Figure 3. Network burst electrode fraction curves. Upper row corresponds to AMPA driven experiment and lower row to NMDA driven experiment. Columns from left: Percentage of the electrodes attending to the NBs for control, suppression of excitation, suppression of inhibition, and the average curves for all three cases. D-AP5, NBQX, and PTX are the pharmacological agents for suppressing NMDA-Rs, AMPA-Rs, and $GABA_A$-Rs respectively. In the first three columns, one single thin line corresponds to fraction of attending electrodes in one network burst. In all columns, thick lines correspond to average fraction of electrodes over all network bursts. In the most right column, shaded areas show the standard error of mean (bin width 100ms).

Pharmacological condition	AMPA driven activity	NMDA driven activity	Disinhibition for AMPA driven activity	Disinhibition for NMDA driven activity
Increase in overall firing rate	—	—	14.1±2.3(n=3)	1.8±0.5 (n=3)
Decrease in overall firing rate	9.8±2.9 (n=3)	3.2±1.7 (n=3)	—	—
Increase in burst frequency	—	—	3.2 (n=1)	4.6±2.0 (n=3)
Decrease in burst frequency	2.2±0.7 (n=3)	21.3±9.2(n=3)	2.4±1.3 (n=2)	—

Table1. Computed changes in overall firing rate (spikes/s) and burst frequency (bursts/min) compared to the previous pharmacological condition (mean ± standard deviation). Disinhibition chronologically follows the associated AMPA-R driven or NMDA-R driven activity.

PUBLICATION II

Unique Features of Network Bursts Emerge from the Complex Interplay of Excitatory and Inhibitory Receptors in Rat Neocortical Networks

Teppola H, Aćimović J, Linne M-L

Frontiers in Cellular Neuroscience, 2019; 13(377)
DOI:10.3389/fncel.2019.00377

frontiers in Cellular Neuroscience

ORIGINAL RESEARCH
published: 06 September 2019
doi: 10.3389/fncel.2019.00377

Unique Features of Network Bursts Emerge From the Complex Interplay of Excitatory and Inhibitory Receptors in Rat Neocortical Networks

Heidi Teppola, Jugoslava Aćimović and Marja-Leena Linne**

Computational Neuroscience Group, Faculty of Medicine and Health Technology, Tampere University, Tampere, Finland

OPEN ACCESS

Edited by:
Arianna Maffei,
Stony Brook University, United States

Reviewed by:
Thierry Ralph Nieus,
Luigi Sacco Hospital, Italy
David Gall,
Free University of Brussels, Belgium

****Correspondence:***
Heidi Teppola
heidi.teppola@tuni.fi
Marja-Leena Linne
marja-leena.linne@tuni.fi

Specialty section:
This article was submitted to Cellular Neurophysiology, a section of the journal Frontiers in Cellular Neuroscience

Received: *06 April 2019*
Accepted: *02 August 2019*
Published: *06 September 2019*

Citation:
Teppola H, Aćimović J and Linne M-L (2019) Unique Features of Network Bursts Emerge From the Complex Interplay of Excitatory and Inhibitory Receptors in Rat Neocortical Networks. Front. Cell. Neurosci. 13:377. doi: 10.3389/fncel.2019.00377

Spontaneous network activity plays a fundamental role in the formation of functional networks during early development. The landmark of this activity is the recurrent emergence of intensive time-limited network bursts (NBs) rapidly spreading across the entire dissociated culture *in vitro*. The main excitatory mediators of NBs are glutamatergic alpha-amino-3-hydroxy-5-methyl-4-isoxazolepropionic acid receptors (AMPARs) and *N*-Methyl-D-aspartic-acid receptors (NMDARs) that express fast and slow ion channel kinetics, respectively. The fast inhibition of the activity is mediated through gamma-aminobutyric acid type A receptors ($GABA_A$Rs). Although the AMPAR, NMDAR and $GABA_A$R kinetics have been biophysically characterized in detail at the monosynaptic level in a variety of brain areas, the unique features of NBs emerging from the kinetics and the complex interplay of these receptors are not well understood. The goal of this study is to analyze the contribution of fast $GABA_A$Rs on AMPAR- and NMDAR- mediated spontaneous NB activity in dissociated neonatal rat cortical cultures at 3 weeks *in vitro*. The networks were probed by both acute and gradual application of each excitatory receptor antagonist and combinations of acute excitatory and inhibitory receptor antagonists. At the same time, the extracellular network-wide activity was recorded with microelectrode arrays (MEAs). We analyzed the characteristic NB measures extracted from NB rate profiles and the distributions of interspike intervals, interburst intervals, and electrode recruitment time as well as the similarity of spatio-temporal patterns of network activity under different receptor antagonists. We show that NBs were rapidly initiated and recruited as well as diversely propagated by AMPARs and temporally and spatially maintained by NMDARs. $GABA_A$Rs reduced the spiking frequency in AMPAR-mediated networks and dampened the termination of NBs in NMDAR-mediated networks as well as slowed down the recruitment of activity in all networks. Finally, we show characteristic super bursts composed of slow NBs with highly repetitive spatio-temporal patterns in gradually AMPAR blocked networks.

To the best of our knowledge, this study is the first to unravel in detail how the three main mediators of synaptic transmission uniquely shape the NB characteristics, such as the initiation, maintenance, recruitment and termination of NBs in cortical cell cultures *in vitro*.

Keywords: AMPA receptor, cell culture, $GABA_A$ receptor, neocortical cells, neuronal network, NMDA receptor, microelectrode array, spontaneous network burst activity

INTRODUCTION

Spontaneous network activity plays a fundamental role in the formation of functional networks during early development of the central nervous system (Feller, 1999; O'Donovan, 1999; Ben-Ari, 2001; Blankenship and Feller, 2010; Egorov and Draguhn, 2013; Luhmann et al., 2016). Recurrent network bursts (NBs) are observed in cerebral cortex *in vivo* (Chiu and Weliky, 2001; Crochet et al., 2005; Minlebaev et al., 2007; Yang et al., 2009; Wang and Arnsten, 2015), in cortical brain slice preparations *in vitro* (Yuste and Katz, 1991; Garaschuk et al., 2000; Harsch and Robinson, 2000; Sanchez-Vives and McCormick, 2000; Corner et al., 2002; Corlew et al., 2004; Sun and Luhmann, 2007; Allene et al., 2008), as well as in dissociated *in vitro* cortical cell cultures (Dichter, 1978; Murphy et al., 1992; Muramoto et al., 1993; Maeda et al., 1995; Marom and Shahaf, 2002; Opitz et al., 2002; van Pelt et al., 2004; Chiappalone et al., 2006; Eytan and Marom, 2006; Wagenaar et al., 2006; Tetzlaff et al., 2010; Teppola et al., 2011; Weihberger et al., 2013; Okujeni et al., 2017). Considering that the bursting dynamics are an essential feature of the activity both *in vivo* and *in vitro* and that the complex underlying mechanisms that shape this activity are not well understood, their better characterization is highly important. Since *in vitro* networks are easy to control under several pharmacological conditions with simultaneous long-term recordings of the evolution of the extracellular network-wide activity with microelectrode arrays (MEAs), they provide a model system that ultimately helps to unravel and compare the receptor mechanisms that modulate the dynamics of cortical circuits *in vivo*. In this work we study how the spontaneous NBs are shaped by the underlying interplay of the excitatory and inhibitory receptors of synaptic transmission to modify excitation-inhibition balance in dissociated *in vitro* cultures extracted from both hemispheres of postnatal (P0) rats. The goal of the study is to analyze the contribution of fast gamma-aminobutyric acid type A receptors ($GABA_A$Rs) on alpha-amino-3-hydroxy-5-methyl-4-isoxazolepropionic acid receptor- (AMPAR-) and N-methyl-D-aspartate receptor- (NMDAR-) mediated spontaneous NB activity at 3 weeks *in vitro* cultures. The importance of the systematic analysis of data is emphasized throughout the study to enable efficient comparison of data obtained from different *in vitro* networks and the validation of future computational models.

In mature cortical cell cultures, spontaneous NBs consist of ∼0.5 s long period of extensive spiking across the culture separated by ∼7 s long silent steady interburst intervals (IBIs) (Kuroda et al., 1992; Muramoto et al., 1993; Robinson et al., 1993; Teppola et al., 2011). These NBs are shown to be driven by the excitatory synaptic transmission (Robinson et al., 1993; Jimbo et al., 2000) which is primarily mediated by the action of glutamate on two types of glutamatergic ionotropic receptors, AMPARs and NMDARs (Hollmann and Heinemann, 1994; Dingledine et al., 1999). It has been shown with patch-clamp technique that zero magnesium (Mg^{2+}) in the medium results in large slow excitatory postsynaptic currents (EPSCs) that occur simultaneously with the NB depolarization (Robinson et al., 1993). The NB depolarization is reversibly inhibited either with 100 μM NMDAR antagonist 2-amino-5-phosphovaleric acid (APV) or with 2 mM Mg^{2+}, producing large hyperpolarization in cortical cultures (Robinson et al., 1993). This inhibition indicates that the NMDAR-mediated component of EPSC is essential for the NB activity and that the NMDARs are tonically active at rest before inhibition. In addition, periodic activity can be blocked with 30 μM AMPAR antagonist 6-cyano-7-nitroquinoxaline-2,3-dione (CNQX), implying that there is also a significant AMPA component in the synaptic currents (Robinson et al., 1993). When the cultures are electrically stimulated, the evoked responses of the cortical cells are shown to be composed of the early and the late phases, which are produced by the activation of distinct synaptic pathways (Jimbo et al., 2000; Marom and Shahaf, 2002; Wagenaar et al., 2004). The early phase component includes early post-synaptic spikes that occur between 5 and 50 ms after the stimuli, and their temporal precision varies around 2 ms with low reliability (Wagenaar et al., 2004). The NMDARs are involved in the generation of the late phase since the time constant of late-phase (160 ms) is in the same order of magnitude as the decay time of NMDAR-mediated EPSC (Jimbo et al., 2000). Here, we start by showing that AMPARs play a greater role in the initiation of spontaneous NBs, while NMDARs are maintaining the already initiated activity in post-natal rat cortical dissociated cultures *in vitro*.

Inhibitory synaptic transmission is known to be mediated by the action of gamma-aminobutyric on gabaergic receptors (GABARs) in these networks (Ramakers et al., 1990; Baltz et al., 2010). GABAergic signaling and interneurons

Abbreviations: AMPA, alpha-amino-3-hydroxy-5-methyl-4-isoxazolepropionic acid; APV, 2-amino-5-phosphovaleric acid; BF, burst frequency; BIC, bicuculline; BL, burst length; BS, burst size; CC, correlation coefficient; CNQX, 6-cyano-7-nitroquinoxaline-2,3-dione; CO_2, carbon dioxide; CPP, (±)-3-(2-Carboxypiperazin-4-yl)propyl-1-phosphonic acid; CTRL, control, D-AP5, D-2-Amino-5-phosphonovaleric acid, DIV, days *in vitro*; E18, embryonic day 18; EPSC, excitatory postsynaptic current; FP, falling phase; FR, firing rate; GABA, gamma-aminobutyric acid; IBI, interburst interval; ISI, inter-spike interval; MEA, microelectrode array; MEM, minimum essential medium; MFR, maximal firing rate; Mg^{2+}, magnesium; NB, network burst; NBQX, 1,2,3,4-Tetrahydro-6-nitro-2,3-dioxo-benzo[f]quinoxaline-7-sulfonamide disodium salt hydrate; NMDA, *N*-Methyl-D-aspartic acid; OFR, overall firing rate; P0, postnatal day 0; PBS, phosphate-buffered saline; PKC, protein kinase C; PTX, picrotoxin; RC, electrode recruitment count; RP, rising phase; SB, super burst; SD, standard deviation.

are crucial in the spontaneous network activity of a developing neocortex (Moody and Bosma, 2005; Ben-Ari et al., 2007). Depolarizing GABAergic signaling has been implicated in the early morphological and functional maturation of neuronal networks (Owens and Kriegstein, 2002; Cancedda et al., 2007; Pfeffer et al., 2009; Wang and Kriegstein, 2011). The developmental GABA shift from depolarizing to hyperpolarizing signaling represents a hallmark in cortical network maturation. This shift closes the period of GABAR-driven network oscillations and sets the onset of mature GABAergic function (Rivera et al., 2005; Ben-Ari et al., 2007). The developmental alterations of the network activity and their correlates with the GABA shift are also shown in dissociated cortical cultures (Soriano et al., 2008; Baltz et al., 2010). Previous research has shown that less synchronized burst activity correlates with the gradual maturation of $GABA_A$ receptor signaling, which depends on the presence of large GABAergic neurons with widespread connections in cultured cortical networks (Baltz et al., 2010). Additionally, it has been demonstrated that the late phase substantially increases after the blockade of $GABA_A$Rs with their antagonists (10μM bicuculline (BIC), 5μM picrotoxin (PTX) or 20μM gabazine) which indicates that the intensity and duration of the late phase are controlled by inhibitory synapses among cortical neurons *in vitro* (Jimbo et al., 2000; Weihberger et al., 2013; Baltz and Voigt, 2015). Furthermore, GABAergic interneurons are shown to control the dynamic spatio-temporal pattern formation in neuronal networks by organizing spatially and temporally the network activity rather than only reducing firing probability (Whittington and Traub, 2003; Mann and Paulsen, 2007; Klausberger and Somogyi, 2008).

Although the excitatory and inhibitory synaptic transmission including the kinetics of AMPAR, NMDAR, and $GABA_A$R are biophysically well characterized at the monosynaptic level, their complex interplay and contribution to network activity dynamics are not well understood. Specifically, it is not known how $GABA_A$Rs separately shape AMPAR- and NMDAR-mediated NB dynamics. In this work, we study the contribution of fast AMPAR-, and slow NMDAR-mediated recurrent excitatory signaling and the contribution of fast $GABA_A$R-mediated inhibitory signaling to initiate, maintain, propagate and terminate NBs. Our focus is on how inhibitory $GABA_A$Rs individually shape the AMPAR- or NMDAR-mediated spontaneous network activity dynamics. To identify these receptor mechanisms and to determine how $GABA_A$Rs modify AMPAR- and NMDAR-mediated spontaneous NB dynamics, the extracellular activity was systematically recorded using the MEA technique under several combinations of receptor antagonists (see I–V) in P0 neocortical cultures at the end of the 3rd week *in vitro*. In addition, the recorded multiunit-spike data was quantitatively analyzed (see 1–11). In brief, the following five conditions were studied: I mature control (CTRL) cultures without pharmacology, II cultures with AMPAR blockade (NBQX, 1,2,3,4-Tetrahydro-6-nitro-2,3-dioxo-benzo[f]quinoxaline-7-sulfonamide disodium salt hydrate), i.e., NMDAR-mediated synaptic transmission, III cultures with NMDAR blockade (D-AP5, D-2-Amino-5-phosphonovaleric acid), i.e., AMPAR-mediated synaptic transmission, IV disinhibited cultures from II with $GABA_A$R blockade (PTX), and V disinhibited cultures from III with the $GABA_A$R blockade (PTX). These five conditions were used in two different types of experimental protocols. In the first, neurons were initially probed by acute application of a high concentration of either the AMPAR or NMDAR antagonist and then by acute application of a high concentration of the $GABA_A$R antagonist. In the second, an increasing concentration of either AMPAR or NMDAR antagonist was gradually applied, thus allowing neurons to adapt to the reduced synaptic transmission of each specific receptor type. We analyzed the multi-unit spike data with our focus being on the (1) overall firing rate (OFR [Hz]), (2) burst frequency (BF [NB/min]), (3) burst length (BL [s]), (4) falling phase (FP [s]), (5) rising phase (RP [s]), (6) maximum firing rate within the NB (MFR [Hz]), (7) burst size (BS [spikes]), and (8) electrode recruitment count (RC). We also analyzed (9) interspike intervals (ISI [s]) and (10) interburst intervals (IBI [s]) as well as (11) the network recruitment time of active electrodes at the beginning of the NBs and (12) the similarity of spatio-temporal patterns of NBs. The systematic analysis enables the efficient comparison of data and the validation of future computational models.

In this study, we show that the networks express NBs when either AMPARs or NMDARs are acutely blocked with as high a concentration as 10 μM of NBQX or D-AP5. We present that AMPARs facilitate the fast initiation and fast recruitment of neurons into the network activity and further increase the diversity of spatio-temporal patterns. Our results also confirm that NMDARs contribute temporally and spatially to maintain the highly repetitive spatio-temporal patterns. Furthermore, the results show that $GABA_A$Rs reduce the spiking frequency and coverage as well as slow down the recruitment of neurons into the network activity. In particular, $GABA_A$Rs prevented the spiking frequency in AMPAR-mediated networks and dampened the termination of NBs in NMDAR-mediated networks. In addition, $GABA_A$Rs further increased the diversity of spatio-temporal patterns in NMDAR-mediated networks. To the best of our knowledge, this study is the first to unravel in detail how the three main mediators of synaptic transmission uniquely shape the NB characteristics, such as the initiation, maintenance, propagation and termination of NBs in newborn rat dissociated neocortical cell cultures *in vitro*. Additionally, the study supports developing new computational models of cortical *in vitro* networks to understand their dynamics both in healthy and pathological conditions.

MATERIALS AND METHODS

We conducted a re-analysis of previously published results (Teppola et al., 2011), significantly expanded the set of employed data analysis methods and obtained entirely new findings using these methods. We particularly focused on the systematic quantitative characterization of various aspects of spontaneous network activity to support the future development of computational models.

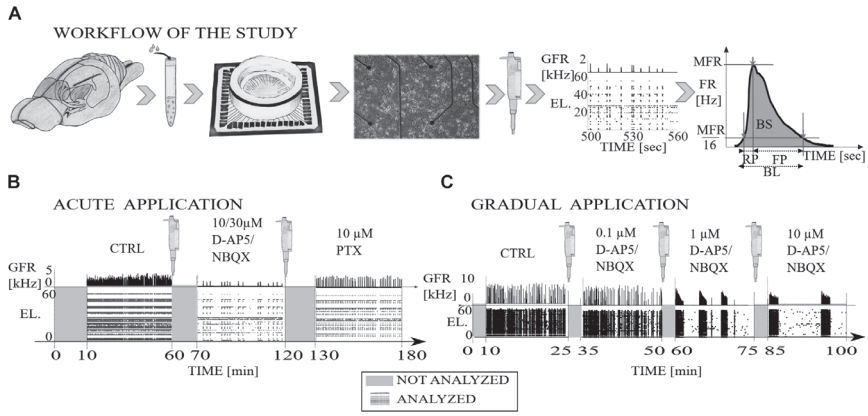

FIGURE 1 | Illustration of the workflow of the study and diagrams of the experimental recording protocols with pharmacological procedures. **(A)** The primary cell cultures were extracted from the prefrontal cortex of the postnatal brains of Wistar rats (yellow). The cortical cells were derived from the tissue by mechanical chopping, trypsinization and dissociation, the cells were seeded on polyethyleneimine coated MEA dishes and cultured until 3 weeks *in vitro*. Network-wide activity was recorded with MEA before and after either the gradual or acute application of excitatory or inhibitory synaptic receptor antagonists. Data analysis was performed on the multi-unit spike times, including NB detection, computation of the burst measures, such as BL, RP, FP, MFR, BS, and RC. Additionally, we computed interspike interval distributions (ISI), interburst-interval distributions (IBI) and cumulative time curves of electrode recruitment (see section "Materials and Methods"). **(B)** Timeline of a total of 180 min of recording in which excitatory synaptic transmission was probed by acute application of either AMPAR or NMDAR antagonist (NBQX and D-AP5, respectively both 10 µM), and inhibitory synaptic transmission was probed by acute application of $GABA_AR$ antagonist (PTX, 10 µM). After application of an antagonist the first ten minutes of the recording were not analyzed and the remaining 50 min of the recording were analyzed. **(C)** Timeline of a total of 100 min of recording in which excitatory synaptic transmission was probed by gradual application of AMPAR (NBQX, 0.1, 1, and 10 µM) or NMDAR (D-AP5 0.1, 1, and 10 µM) antagonist. The first ten minutes of the recording were not analyzed due to the transition phase (gray) and the remaining 15 min were analyzed (raster plot with global firing rate [kHz]). GFR denotes the global firing rate and EL the electrode numbers.

Preparation and Maintenance of Cell Cultures

In Teppola et al. (2011), the primary cortical cell cultures were prepared as described previously (Shahaf and Marom, 2001), and animal handling and tissue preparation were performed in accordance with guidelines for animal research at the University of Freiburg. No further preparation of cell cultures were required for the present study. The cells were derived from the prefrontal cortex of both hemispheres (**Figure 1A**) of postnatal (P0) Wistar rat pups of either sex. Cortical tissue was mechanically chopped with a scalpel in cold phosphate-buffered saline solution (PBS, all reagents from GIBCO, Invitrogen, Karlsruhe, Germany, unless otherwise stated) and enzymatically treated with 0.05% trypsin solution in a shaker for 15 min at 37°C. Trypsinization was stopped with 20% horse serum. DNase (Sigma-Aldrich, Steinheim, Germany) was added (type IV 50 µg/ml) to degrade deoxyribonuclease around cells. Cells were dissociated by gentle trituration with a serological pipette (10 ml; Becton Dickinson, Franklin Lakes, NJ, United States) in PBS, centrifuged (5 min 2000rcf, Rotofix 32A, Hettich, Tuttlingen, Germany) and re-suspended into minimum essential medium (MEM, supplemented with 5% heat-inactivated horse serum, 20 mM glucose, 0.5 mM L-glutamine, and 1% gentamicine, 1 ml MEM/rat). Cells were counted with an automated cell counter (CASY TT, Schärfe Systems GmbH, Reutlingen, Germany) and seeded at densities of 2,000 cells/mm^2 onto polyethyleneimine (PEI, 200 µl, 0,2%, Sigma-Aldrich, Steinheim, Germany) coated MEAs (MultiChannel Systems Ltd., Reutlingen, Germany). Cells were cultured in 2 ml MEM in 5% CO_2 humidified incubator at 37°C. One third of the medium was changed twice a week and recordings were done between 20–25 days *in vitro* (DIV). All the cultures were carefully prepared and validated in order to provide as stable and comparable recording conditions as possible for each protocol and culture. In particular, the cell density (2000 cells/mm^2) and the maturation point (20–25 DIV) were selected according to the literature (Wagenaar et al., 2006) to guarantee appropriate experimental model system to be combined with the standard MEA.

Pharmacology

In Teppola et al. (2011), the AMPAR-mediated ionotropic glutamatergic transmission was probed by competitive antagonist of the AMPARs 1,2,3,4-Tetrahydro-6-nitro-2,3-dioxo-benzo[f]quinoxaline-7-sulfonamide disodium salt hydrate (NBQX). The NMDAR-mediated ionotropic glutamatergic transmission was probed by competitive antagonist of the glutamate site of the NMDARs D-(-)-2-Amino-5-phosphonopentanoic acid (D-AP5). The ionotropic GABAergic transmission was probed by non-competitive $GABA_AR$ antagonist picrotoxin (PTX). These reagents were used for suppressing or blocking the function of each receptor type, allowing to study the contribution of the receptors for network activity dynamics during electrophysiological recordings. All drugs were directly applied with a pipette into the culture

medium inside the dry incubator. All pharmacological chemicals were purchased from Sigma-Aldrich, Steinheim, Germany.

Synaptic transmission was probed by both acute and gradual applications of AMPAR and NMDAR antagonists and by acute application of $GABA_AR$ antagonist. In the case of acute antagonist applications, higher concentrations of the drug were applied to simultaneously block all specific types of receptors in the whole cell culture. Acute application enabled the study of the acute influence of an antagonist, i.e., to induce the complete blockade of each receptor type on network activity dynamics. In the case of gradual antagonist applications, increasing concentrations of the drug were applied to the culture, thereby allowing neurons to briefly adapt to the reduced synaptic transmission of each specific receptor type. Gradual application enabled the study of the concentration-dependent effects of each excitatory antagonist on network dynamics.

The AMPARs were acutely antagonized with NBQX that was applied at concentrations completely blocking the AMPAR-mediated ionotropic glutamatergic transmission (for 10 μM, see **Figure 2A** and **Table 1**, Protocol id 1, and for 30 μM, see **Supplementary Figure S1C** and **Supplementary Table S1**). The concentration of 10 μM of NBQX has been shown to be sufficient to block the AMPA receptor mediated current (Parsons et al., 1994). The NMDARs were acutely antagonized

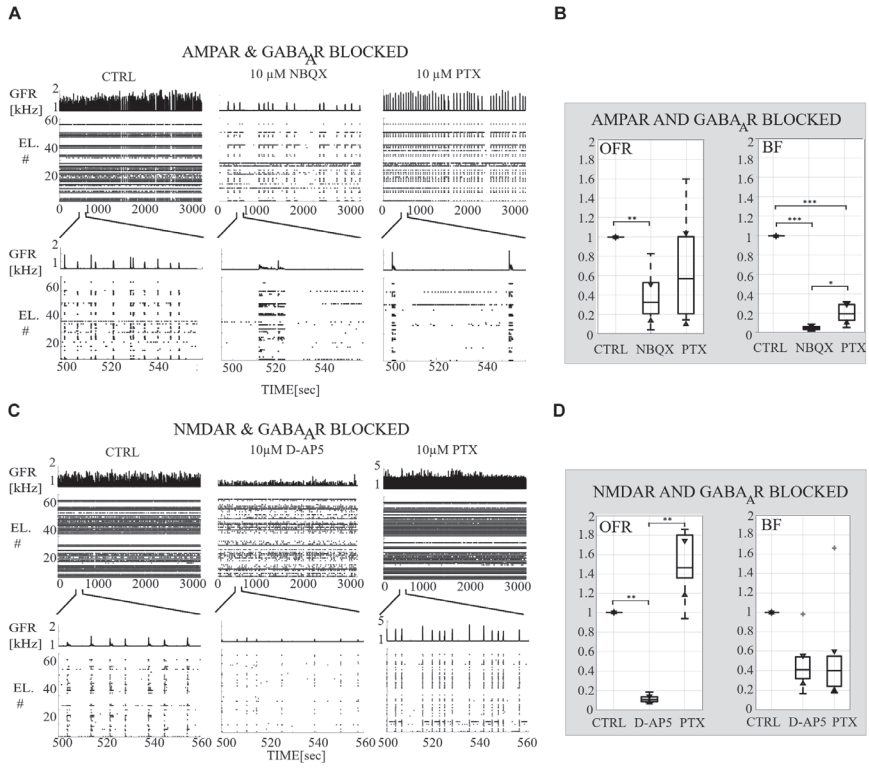

FIGURE 2 | Receptor-dependent network-wide activity probed by acute application of AMPA, NMDA and $GABA_A$ receptor antagonists, relative changes in OFR and in BF. **(A)** Raster plots of network-wide activity. In each subpanel, the global firing rates (GFR [kHz]) are displayed on top of raster plots of spike times (TIME [s]) from each electrode (EL #) in each condition. The first subpanel shows the CTRL recording, the second subpanel the activity after acute application of AMPAR antagonist (10 μM NBQX), and the third subpanel the activity after acute applications of both antagonists of AMPAR and $GABA_AR$ (10 μM PTX). The top row shows the complete analyzed recording of 3,000 s, and the bottom row enlargements of 60 s to display fine details of the activity. **(B)** Relative change in OFR and in BF are computed for each recording and then displayed as box plot representation of pooled rates of the CTRL recordings ($n = 7$), of the recordings when AMPARs are antagonized (NBQX, $n = 7$) and of the recordings when both AMPARs and $GABA_ARs$ (PTX, $n = 7$) are antagonized. **(C)** Same as **(A)** except that the CTRL recording is compared to the recording when NMDARs (10 μM D-AP5) and both NMDARs with $GABA_ARs$ (10 μM PTX) are acutely antagonized. **(D)** Same as **(B)** except that the CTRL recordings ($n = 6$) are compared to conditions when NMDARs are antagonized (D-AP5, $n = 6$) and to the conditions when both NMDARs and $GABA_ARs$ (PTX, $n = 6$) are antagonized. Both AMPAR and NMDAR antagonists significantly decreased the OFR ($p_{ranksum} < 0.01$) **(B,D)**. Disinhibition significantly increased the OFR in NMDAR blocked cultures ($p_{ranksum} < 0.01$), but not in AMPAR blocked cultures compared to the condition before disinhibition **(B,D)**. AMPAR blockade significantly decreased the network BF ($p_{ranksum} < 0.001$) and followed disinhibition slightly increased BF ($p_{ranksum} < 0.05$) compared to the condition before disinhibition. The box plots show the median, 25th and 75th percentiles and whiskers extending to the minimal and maximal values and the plus signs represent outliers. $^{***}p_{ranksum} < 0.001$, $^{**}p_{ranksum} < 0.01$, $^{*}p_{ranksum} < 0.05$.

TABLE 1 | List of experimental protocols including recording conditions, blocked and functional receptors and the number of used cultures.

Protocol id	Recording condition/Drug	Concentration of an antagonist	Blocked receptors	Functional receptors among the considered ones	Number of cultures
Acute application					
1	CTRL	–	None	All	7
	NBQX	10 μM	AMPA	NMDA, $GABA_A$	
	PTX	10 μM	$GABA_A$	NMDA	
2	CTRL	–	None	All	6
	D-AP5	10 μM	NMDA	AMPA, $GABA_A$	
	PTX	10 μM	$GABA_A$	AMPA	
Gradual application					
3	CTRL	–	None	All	2
	NBQX	0.1, 1, 10 μM (in total 11.1 μM)	AMPA	NMDA, $GABA_A$	
4	CTRL	–	None	All	2
	D-AP5	0.1, 1, 10 μM (in total 11.1 μM)	NMDA	AMPA, $GABA_A$	

with D-AP5 that was applied at concentrations of 10 or 30 μM (for 10 μM, see **Figure 2C** and **Table 1**, Protocol id 2, and for 30 μM, see **Supplementary Figure S1C** and **Supplementary Table S1**). Previous literature has shown that 10 μM of D-AP5 is sufficient to block 95% of the NMDA receptor mediated currents (Benveniste and Mayer, 1991). Additionally, we performed experiments where 30 μM of D-AP5 or NBQX was used to be confident that AMPA or NMDA receptor mediated currents were completely antagonized (see **Supplementary Material** section). The results were consistent with both concentrations (10 and 30 μM D-AP5 or NBQX). Therefore, we show in the manuscript only the results with 10 μM NBQX and in the **Supplementary Material** section the results with 30 μM. Cultures were disinhibited and $GABA_A$Rs acutely antagonized with PTX applied at a concentration of 10 μM which is shown to completely block ionotropic GABAergic transmission (Krishek et al., 1996) (**Figures 1B**, **2A,C** and **Table 1**, Protocol id 1, 2).

In the case of gradual application of the AMPAR antagonist, an increasing amount of NBQX was applied to first partially (0.1 and 1 μM) and then completely block the AMPAR-mediated transmission (10 μM, Parsons et al., 1994) (**Figures 1C**, **6A** and **Table 1**, Protocol id 3). In the gradual application of the NMDAR antagonist, the selected increasing amount of D-AP5 (0.1, 1, and 10 μM) was applied to gradually reduce the functioning of NMDAR-mediated ionotropic glutamatergic transmission (Benveniste and Mayer, 1991) (**Figures 1C**, **6C** and **Table 1**, Protocol id 4).

Experimental Protocols

A total of 20 cell cultures from seven different preparations were studied by recording the network activity of the cultures with MEAs. In the case of acute application of the excitatory receptor antagonists (AMPAR or NMDAR blockade) followed by the acute application of the inhibitory $GABA_A$R antagonist, a total of 13 cultures from three different preparations were studied. Seven cultures were used for experiments of acute AMPAR blockade (10 μM NBQX) followed by acute $GABA_A$R blockade (10 μM PTX). Six cultures were used for experiments of acute NMDAR blockade (10 μM D-AP5) followed by acute $GABA_A$R blockade (10 μM PTX). Each experiment consisted of the following steps: (1) one hour long CTRL recording, (2) application of 10 μM antagonist (NBQX in experiments with AMPAR blockade, D-AP5 in experiments with NMDAR blockade), (3) recording for one hour, (4) application of 10 μM PTX, and (5) recording for 1 h (**Figures 1B**, **2A,C** and **Table 1**, Protocol id 1, 2). After the application of the antagonist, the first ten minutes of the recording were not analyzed to avoid transition phases. The remaining 50 min of the recording were analyzed.

In the case of gradual application of the excitatory receptor antagonists (AMPAR or NMDAR blockade), a total of four cell cultures from two different preparations were studied. Two cultures were used for experiments with gradual AMPAR blockade (0.1, 1, and 10 μM NBQX) and two cultures for experiments with gradual NMDAR blockade (0.1, 1, and 10 μM D-AP5). Each experiment consisted of the following steps: (1) 25 min-long CTRL recording, (2) application of 0.1 μM antagonist (NBQX in experiments with AMPAR blockade, D-AP5 in experiments with NMDAR blockade), (3) recording for 25 min, (4) application of 1 μM antagonist, (5) recording for 25 min, (6) application of 10 μM antagonist, and (7) recording for 25 min (**Figures 1C**, **6A,C** and **Table 1**, Protocol id 3, 4). For each 25 min-long recording, the first 10 min were not analyzed to avoid transition phases. The remaining 15 min were analyzed as described below. A total of three cultures were used to study gradual disinhibition, see **Supplementary Material** section (**Supplementary Table S1** and **Supplementary Figures S1–S4**).

Extracellular Microelectrode Array Recording

In Teppola et al. (2011), the spontaneous extracellular bioelectrical activity was recorded from the cell cultures inside a dry incubator (37°C, 5% CO_2). The activity was collected using MEAs (MultiChannel Systems Ltd., Reutlingen, Germany). The 59 TiN electrodes, Ø 30 μM, were placed in rectangular pattern (6 × 10 grid with 500μm pitch distance). The recorded signals were amplified using MEA-1060-BC built-in system amplifier with 25 kHz sampling frequency. The recorded data was acquired using MC-Rack software (Multi Channel Systems

Ltd., versions 3.3–4.5). Raw signals from each electrode were digitally high-pass filtered at 200 Hz cutoff and with detection dead time of 2 ms (Butterworth, 2nd order high-pass filter). Finally, the signals were thresholded at −5 times of standard deviation (SD) from the mean noise baseline for each electrode. The times when the signals crossed this voltage threshold were detected as spike times for further analysis. The collection of spike times obtained from each electrode provides an estimation of NB activity, we will refer to it as NB spike times in what follows. In the case of gradual AMPAR blockade, we observed strong occurrence of superbursts (SBs), which lasted ∼100 s with 3–8 min silent steady period. Similar SBs occurring in short, sharply defined trains with several minutes of silent periods have been described previously in young cultures at 7–11 DIV (Wagenaar et al., 2006). The raw data from MEA recordings, i.e., spike times and electrode indices, were imported into MATLAB (version 2013b, The Mathworks Inc., MA, United States) using MEA-Tools (Egert et al., 2002) and the FIND-Toolbox (Meier et al., 2008). The NB detection and further advanced data analysis, statistics and image preparation were completed using our own Matlab (version 2013b, The Mathworks Inc., MA, United States) code.

Preprocessing of Data and Burst Detection

The initial 10 min of the recording after the application of an antagonist were not analyzed to avoid transient phases. The following 15 or 50 min, depending of the recording protocol, were then analyzed (**Figures 1B,C**). Electrodes with firing rate (FR) lower than 9% of the average FR on electrodes with spike activity were excluded. Spontaneous NBs were detected according to the following criteria: the first interspike interval $<$100 ms defined the onset time of the NB and the first interspike interval $>$100 ms defined the offset of the NB. In addition, the following criteria were included in the NB detection algorithm: a minimum of five electrodes must be active during the NB and a minimum of five spikes must be recorded per NB. Similar burst detection criteria has been previously presented in the literature, see for example (Chiappalone et al., 2006). All data was manually inspected to verify that the bursts were correctly and as accurately as possible identified when recorded with the standard 59 TiN electrode MEA technique. Standard MEA technique is a reliable and accepted recording technique for high-throughput screening of network dynamics in multiple cultures and protocols (Wagenaar et al., 2006). In addition to the standard MEA, the high-density MEAs have been used in the literature to obtain extra high accuracy and precision when detecting random spiking, burst duration, activity propagation and NB rates (Gandolfo et al., 2010; Maccione et al., 2010; Lonardoni et al., 2015).

Relative Overall Firing Rate and Burst Frequency Computations

The relative changes in OFR [Hz] and network BF [NB/min] were computed for each recording and then displayed as a box plot representation of pooled rates in the acute application of the excitatory/inhibitory receptor blockade (see **Table 1**, Protocol id 1, 2). The box plots show the median, 25th and 75th percentiles with whiskers extending to the minimal and maximal values. The plus signs represent outliers in **Figures 2B,D**. Statistical analysis was performed for pooled rates using Wilcoxon rank sum test. Differences were considered to be significant when $p_{\text{ranksum}} < 0.05$, $p_{\text{ranksum}} < 0.01$, or $p_{\text{ranksum}} < 0.001$, different significances are indicated with *, **, ***, respectively, in **Figures 2B,D**.

Relative changes in OFR and BF were computed for each recording and then displayed as separate graph representations of the rates in the cases of gradual application of the excitatory receptor blockade (see **Table 1**, Protocol id 3, 4, **Figures 6B,D**, and **Supplementary Figures S1B,D**). To compute the relative OFR, the number of all spikes was divided by the duration of the recording period in seconds. To compute the BF, the number of NBs was divided by the duration of the recording period in minutes. The values were normalized to CTRL condition by dividing the value with the CTRL value.

Characterization of Burst Measures

To analyze the characteristic burst measures, NB firing rate (FR [Hz]) profiles were calculated for each NB. NB rate profiles were calculated by smoothing the spike counts in the bins via convolution with a Gaussian kernel (SD of 15). NB measures were calculated from NB rate profiles as follows; (1) MFR [Hz] was defined as the peak of the profile, (2) the RP [s] starts at the time point when the FR reaches 1/16th of the MFR and ends when the FR reaches the time point of the MFR, (3) the FP [s] starts at the time point of MFR and ends when FR decreases back to 1/16th of the MFR, and (4) BL [s] is the sum of RP and FP (**Figure 1A**). In addition, we calculated (5) the BS [spikes], i.e., number of spikes per each NB, and (6) RC, i.e., the number of active electrodes during the NB. BS and RC were calculated from the start time point until the end time point of the detected NBs. We calculated the NB measures i.e., the peak of NB and the intervals between the time of the peak of NB and the time at 1/16th of the height of NB similar to Gritsun et al. (2010). The method reduces the variability and possible oscillating tails of NBs and also provides a systematic measure for comparing NB rate profiles under different pharmacology. Similar burst measures have been previously presented in the literature, see for example (Vajda et al., 2008; Bologna et al., 2010). However, the set of experimental protocols, burst measures and analysis tools in the presented work is extensive.

The MFR and BS were additionally divided by the recruitment count, i.e., the number of active electrodes, to have MFR per electrode and BS per electrode. Firstly, for each NB measure (except the maximum of RC) and each culture, we computed the median across all NBs recorded in that culture. Then we computed the mean and the SD across all medians obtained from all cultures. Secondly, we divided SD by the mean to calculate the coefficient of variation, i.e., relative SD. Thirdly, we normalized the mean of medians to CTRL. Fourthly, the relative values (mean and SD) of all NB measures were displayed as bars with error bars (**Figures 3B,D**, **7B,D**). Wilcoxon rank sum test and

p-values were computed for all burst measures in each condition and in each culture. If the tests showed a similar result for each culture, the significance was displayed as $^{***}p_{\text{ranksum}} < 0.001$, $^{**}p_{\text{ranksum}} < 0.01$, $^{*}p_{\text{ranksum}} < 0.05$ in **Figures 3B,D**, **7B,D**.

Interspike Interval and Interburst Interval Distributions

The distributions of ISI [s] within NB (i.e., the time difference between the consecutive spikes during NBs) were computed for each condition and for each culture. First the histograms were created using the following values for the edges of the bins: 10^{i}, where i is in $\{-10, -9.8, \ldots, 6\}$. The mean of ISI distributions from all cultures of the same condition were computed and the values of i were plotted on the x-axis with a logarithmic scale (log(TIME[s]). Statistical analysis was performed for all ISIs between each condition in the same culture using Wilcoxon rank sum test and *p*-values. If the tests showed a similar result for every culture when the same conditions were compared, the differences were considered significant and were displayed as $^{***}p_{\text{ranksum}} < 0.001$, $^{**}p_{\text{ranksum}} < 0.01$, $^{*}p_{\text{ranksum}} < 0.05$ in **Figures 4A**, **8A** and **Supplementary Figure S3A**.

The distributions of IBIs [s] (i.e., the time difference between the last spike of NB and the first spike of NB + 1) were computed for each condition and for each culture. First, IBI data matrices were smoothed using the Gaussian window method (matlab function *smooth*) with an integer scalar of five for the size of the window and a scalar of 0.65 for SD of the Gaussian window. Then the histograms were created using the following values for the edges of the bins: 10^{i}, where i is in $\{0, 0.05, \ldots, 5\}$. The mean of IBI distributions from all cultures of the same condition were computed and the values of i were plotted on the x-axis with a logarithmic scale. Statistical analysis was performed for all IBIs between each condition in the same culture using Wilcoxon rank sum test and *p*-values. If the tests showed a similar result for every culture when the same conditions were compared, the differences were considered significant and were displayed as $^{***}p_{\text{ranksum}} < 0.001$, $^{**}p_{\text{ranksum}} < 0.01$, $^{*}p_{\text{ranksum}} < 0.05$ in **Figures 4B**, **8B** and **Supplementary Figure S3B**.

Network Recruitment Time Computed as Cumulative Relative Number of Active Electrodes

Cumulative number of electrodes recruited at the onset of a NB, relative to the CTRL, was computed for each condition and each culture. For each NB, the timing of the first spike at each electrode was stored. These stored spike times were used to compute a time vector as follows. We discretized the NB duration, starting at 0.5 s after the onset of NB and using the 0.0001 s discretization time step. For each discrete time step we counted the number of electrodes activated until that time, the obtained cumulative number of electrodes was stored into the time vector. Next, we pooled all the time vectors representing all NBs recorded from the same culture and condition. The mean value of activated electrodes was computed for each time step, by averaging over all NBs. The obtained results illustrate the speed of electrode recruitment, and are shown in **Figures 4C**, **8C** and **Supplementary Figure S3C**.

Similarity Analysis of the Spatio-Temporal Patterns

A more detailed analysis revealed that each NB has a unique structure. The importance of characterizing NB structures has been emphasized in the literature. In Raichman and Ben-Jacob (2008), the NB structure is defined as "momentary spatio-temporal pattern in which neurons at different locations fire spike-trains at different delays relative to each other." We refer to these unique NB structures as spatio-temporal patterns. To analyze the similarity between each spatio-temporal pattern in different pharmacological conditions, NBs were characterized by the first spike time relative to the burst onset from each electrode, i.e., the rank order of the first spike from each electrode within the NB. Pairwise-spike-time-difference matrices were computed of the difference of the first spike times for each pair of electrodes within each NB. The similarities between NBs were computed as the correlation coefficient (CC) between their pairwise-spike-time-difference matrices. The CC is computed using Matlab implementation of the well-known expression. The CCs, that are close to one indicate similar spatio-temporal patterns between the NBs, CCs close to zero indicate no correlation and CCs close to minus one indicate anticorrelated spatio-temporal patterns. An alternative measure for analysis of spatio-temporal patterns in neuronal cultures has been proposed in the literature (Raichman and Ben-Jacob, 2008). To compare the results of multiple cultures, we computed the distributions of CCs in each condition and in each culture from the CC matrices in **Figures 5B,D**, **9B,D** and **Supplementary Figure S4B**. Statistical analysis was performed for all CCs between each condition in the same culture using Wilcoxon rank sum test and *p*-values. If the tests showed a similar result for every culture when the same conditions were compared, the differences were considered significant and was displayed as $^{***}p_{\text{ranksum}} < 0.001$, $^{**}p_{\text{ranksum}} < 0.01$, $^{*}p_{\text{ranksum}} < 0.05$ in **Figures 5B,D**, **9B,D** and **Supplementary Figure S4B**.

RESULTS

We studied quantitatively the contribution of slow (NMDA) and fast (AMPA) glutamatergic and fast gabaergic ($GABA_A$) receptors to the dynamics of spontaneous network activity in cortical cultures *in vitro* (see **Figure 1A** for illustration). The kinetics of these receptors are known at the single cell and synapse levels, but how their complex interplay affects the network-level activity is not well understood. Our goal was to examine to what extend the fast and slow kinetics of receptor openings play a role in the network activity dynamics. The data studied in this work spontaneously exhibit stereotypical NBs, the periods of intensive activity engaging the majority of neurons and followed by longer silent periods of sparse activity of single spikes. The NBs were characterized by a fast spread of activity across the culture, followed by a slower interval of activity termination. We analyzed the data collected using an *in vitro* experimental

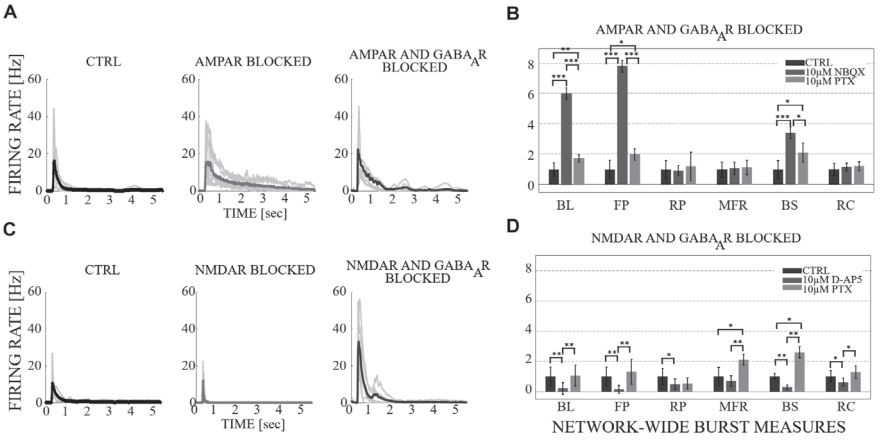

FIGURE 3 | The influence of acute application of the excitatory and inhibitory receptor antagonists on NB profiles and measures. **(A)** The top row shows the NB profiles [Hz] from six congruent experiments where the data of the CTRL recording (1st subpanel) is compared to the data of the recording conditions when AMPARs (2nd subpanel), and AMPARs with $GABA_A$Rs (3rd subpanel) are antagonized. The thin gray lines represent the average NB profiles of each culture, whereas the thick line represents the average over all cultures. The profiles are aligned with each other at the time point when the rate is reached. The presented profiles are computed using the spike-data from **Figure 2**, processed as described in section "Materials and Methods". **(B)** The relative change of characteristic burst measures including, BL, FP, RP, MFR, BS and RC are extracted from NB profiles (see section "Materials and Methods"). Each bar represents the mean ± SD of the medians from all cultures. The values were normalized to the CTRL condition. The panel shows the relative change in AMPAR (10 μM NBQX) blocked networks, followed by $GABA_A$R (10 μM PTX) blockade (n = 7). **(C)** Shows the same as **(A)**, except the data of the CTRL recording (1st subpanel) is compared to the data of the recording conditions when NMDARs (2nd subpanel) and NMDARs with $GABA_A$Rs (3rd subpanel) are antagonized. **(D)** Shows the same as **(B)**, except that the relative change is computed in NMDAR blocked networks (10 μM D-AP5), followed by $GABA_A$R (10 μM PTX) blockade (n = 6). BL, FP and BS increased significantly ($p_{ranksum} < 0.001$) when applying acute AMPAR blockade compared to CTRL **(B)**. BL ($p_{ranksum} < 0.001$), FP ($p_{ranksum} < 0.001$) and BS ($p_{ranksum} < 0.05$) decreased significantly when acutely disinhibited, and compared to previous AMPAR blocked condition **(B)**. In contrast, BL ($p_{ranksum} < 0.01$), FP ($p_{ranksum} < 0.01$), RP ($p_{ranksum} < 0.05$), BS ($p_{ranksum} < 0.01$) and RC ($p_{ranksum} < 0.05$) significantly decreased when NMDARs were blocked **(D)**. Furthermore, BL ($p_{ranksum} < 0.01$), FP ($p_{ranksum} < 0.01$), MFR ($p_{ranksum} < 0.01$), BS ($p_{ranksum} < 0.01$) and RC ($p_{ranksum} < 0.05$) significantly increased when disinhibited and compared to the previous NMDAR blocked condition **(D)**. $^{***}p_{ranksum} < 0.001$, $^{**}p_{ranksum} < 0.01$, $^{*}p_{ranksum} < 0.05$.

setup that simultaneously enabled the precise pharmacological manipulation of synaptic receptor activation and the long-term monitoring of network activity with the MEA technique. We focused on how the excitatory and inhibitory receptors modulate the overall network activity as well as the initiation, maintenance, propagation and termination of NBs. In particular, we assessed how the inhibition mediated by $GABA_A$ receptors uniquely shapes the spontaneous NBs guided by AMPA and NMDA receptor transmission.

Our long-term goal is to better understand the complex interplay and mechanisms between the excitatory and inhibitory receptors using both experimental and computational modeling techniques. We contributed to our goal by analyzing a rich set of data recorded under different pharmacological conditions, including the acute and gradual application of each excitatory receptor antagonist and the acute application of inhibitory receptor antagonist to shed light on the network activity dynamics. Four different pharmacological protocols were selected to comprehensively study the contribution of AMPA, NMDA and $GABA_A$ receptors to network dynamics (see **Table 1**). In the first two pharmacological protocols, the immediate acute effects of higher concentrations of NBQX and D-AP5 on spontaneous activity and NBs were studied. One of the ionotropic glutamatergic receptor types was acutely blocked, either AMPARs or NMDARs, and, furthermore, acutely disinhibited the network with $GABA_A$ receptor antagonist (see **Figure 1B** for illustration). In the other two protocols, the network was gradually probed by increasing the concentration of each ionotropic glutamatergic receptor antagonist (see **Figure 1C** for illustration). The influence of AMPARs on spontaneous network activity dynamics was probed by a NBQX, and the effects of NMDARs were examined by applying D-AP5. We present a quantitative characterization of the complex interplay between NMDAR-, and AMPAR-mediated excitation and $GABA_A$R-mediated inhibition. We systematically analyze and compare different measures, including the OFR, the BF, the characteristic NB measures of NB profiles, the ISIs, the IBIs, the recruitment time of active electrodes in the network as well as the similarity of spatio-temporal patterns, computed from multi-unit spike data recorded with MEA under each pharmacological condition.

Quantifying the Nature of Spontaneous Activity in Cortical Cultures *in vitro*

Spontaneous network-wide activity developed already at the end of the first week *in vitro* and continued until 20–25 DIV, when the presented experimental recordings were collected.

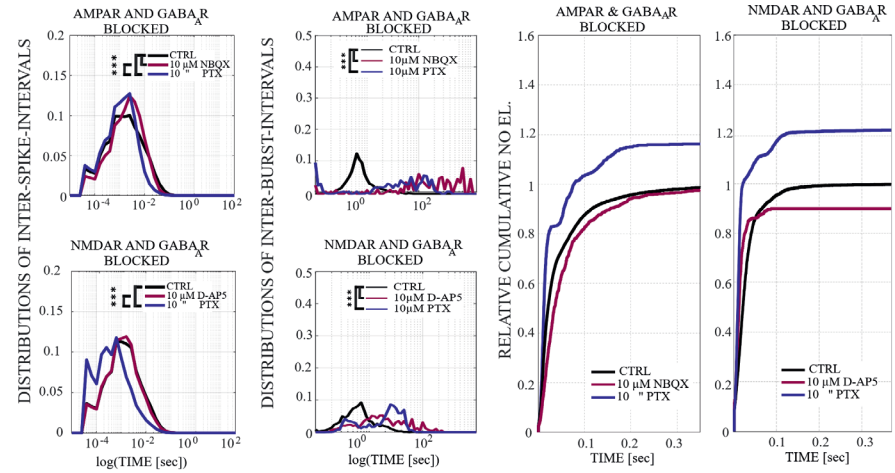

FIGURE 4 | The influence of acute application of the excitatory and inhibitory receptor antagonists on ISIs, IBIs and network-wide electrode recruitment speed at the beginning of the bursts. **(A)**The excitatory and inhibitory receptor dependence on ISIs within NBs. ISI distributions shifted to higher fractions in acutely AMPAR blocked networks (n = 7), meaning significantly longer distances between spikes within NBs in neurons probed by 10 μM NBQX ($p_{ranksum}$ < 0.001) and, contrariwise, the ISI distribution shifted to lower fractions in disinhibited AMPAR blocked networks (n = 7), meaning significantly shorter distances between spikes within NBs in neurons probed by 10 μM PTX ($p_{ranksum}$ < 0.001) **(top panel)**. ISI distribution did not differ in an acutely NMDAR blocked network (10 μM D-AP5) (n = 6), but disinhibition with 10 μM PTX significantly shifted the ISI distributions toward lower fractions in an NMDAR and GABA$_A$R blocked network (n = 6), meaning significantly shorter distances between spikes within NBs in neurons without functional NMDARs and GABA$_A$Rs ($p_{ranksum}$ < 0.001) **(bottom panel)**. **(B)** IBI distributions revealed mainly longer fractions of intervals between NBs in acutely AMPAR blocked condition (10 μM NBQX) ($p_{ranksum}$ < 0.001), as well as in acutely AMPAR and GABA$_A$R blocked condition (10 μM PTX) ($p_{ranksum}$ < 0.001) in comparison to the CTRL condition. Disinhibited networks had shorter IBIs than before disinhibition ($p_{ranksum}$ < 0.001) **(top panel)**. IBI distributions shifted toward lower fractions for disinhibited AMPAR-mediated NBs in comparison to the CTRL condition or previous condition ($p_{ranksum}$ < 0.001) **(bottom panel)**. Wilcoxon rank sum test and p-values were computed for all ISIs and IBIs in each condition and in each culture. If the tests showed similar results and p-values for every culture, the results were displayed in **(A,B)**. $^{***}p_{ranksum}$ < 0.001, $^{**}p_{ranksum}$ < 0.01, $^{*}p_{ranksum}$ < 0.05. The x-scale is logarithmic. **(C)** A change in the excitatory and inhibitory receptor balance modulates network-wide electrode recruitment speed at the beginning of the bursts. Network recruitment slowed down by acute AMPAR blockade (10 μM NBQX) and sped up with an increased number of active electrodes by disinhibition (10 μM PTX) in comparison to the CTRL condition **(left panel)**. On contrary, the recruitment of the network sped up with the acute application of NMDAR antagonist (10 μM D-AP5) with less active electrodes and sped up, including more active electrodes in the networks, after acute disinhibition (10 μM PTX) in comparison to the CTRL condition **(right panel)**. The disinhibition of the network by the GABA$_A$R antagonist by acute application increased the recruitment speed even more than the NMDAR blockade. Values were normalized to the CTRL conditions. Bin width is 0.1 ms.

Firstly, the spontaneous activity of CTRL condition consisted of stereotypical NBs that upon initiation rapidly spread across the network with the median of the RP being 88.93 ± 47.10 ms (mean ± std, n = 20). Secondly, the observed peak of activity, the MFR in a burst, had median value of 1.90 ± 1.75 Hz (mean ± std, n = 20). Thirdly, after reaching the peak, the NBs entered the termination phase which lasted significantly longer, with the median of the FP being 257.24 ± 193.66 ms (mean ± std, n = 20). In total, the median of the BL of NBs was 373.17 ± 248.23 ms (mean ± std, n = 20), and was followed by relatively long periods of random firing of low intensity with the median of the IBIs being 7.18 ± 4.71 s (mean ± std, n = 20). The median number of spikes in NBs (BS) was 204.60 ± 166.22 spikes (mean ± std, n = 20) and the median number of active electrodes (RC) in NBs was 26.9 ± 13.52 (mean ± std, n = 20) out of the 60 electrodes available in the MEA dishes. Distinct NBs were observed in all the considered experimental conditions. The NBs occurred even in the presence of 30 μM AMPAR (NBQX) or NMDAR (D-AP5) antagonists (see **Supplementary Material** section). Furthermore, various quantitative measures of NBs significantly changed under different protocols.

Quantitative Characterization of AMPAR Contribution to Fast Initiation of NBs, Fast Recruitment of Neurons, and Diversity of Spatio-Temporal Patterns

Fast glutamatergic AMPARs are the main mediator of excitatory activity. They play a critical role in the fast initiation of NBs, the fast recruitment of neurons into NBs as well as in the fast activity propagation at the beginning of the NBs. In addition, AMPA and GABA$_A$ receptors contributed in decreasing the similarity between spatio-temporal patterns. These functions of AMPARs were studied using two complementary experimental protocols, the acute and gradual blocking of AMPARs. Moreover, we showed differences between the acute and gradual protocols. The gradual application of AMPAR blockade induced SBs, which were not observed in acutely AMPAR blocked networks. We

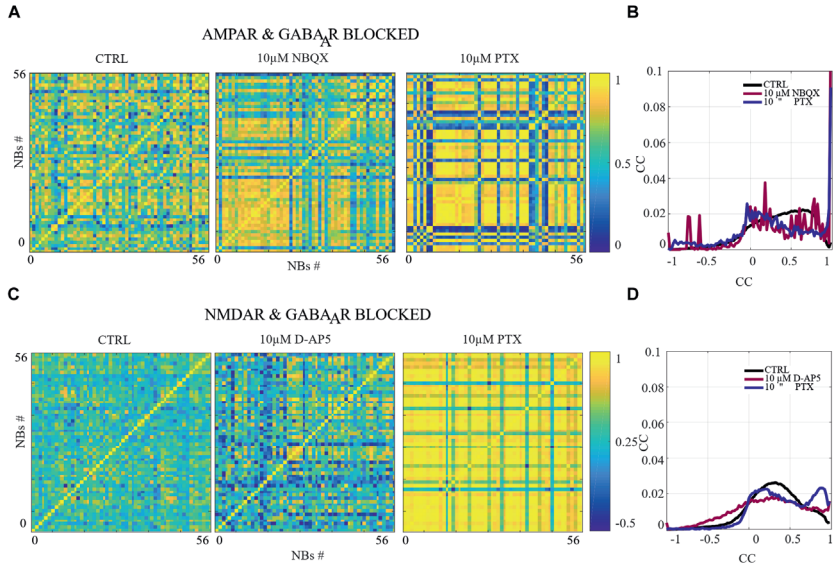

FIGURE 5 | The excitation-inhibition balance changes the spatio-temporal patterns. **(A,C)** CC matrices computed for pairwise-spike-time-difference matrices between each NB in each condition of acute applications. **(B,D)** Mean distributions of CC across the NBs and networks are shown. **(A,B)** The acute AMPAR blockade with 10 μM NBQX changed the distribution of the similarity of spatio-temporal patterns significantly ($p_{ranksum} < 0.001$) in three out of seven networks in comparison to the CTRL condition. However, the number of NBs was too low to evaluate statistical significance in the other four AMPAR blocked networks. The acute disinhibition with 10 μM PTX in AMPAR blocked networks significantly increased ($p_{ranksum} < 0.001$) the similarity of spatio-temporal patterns in four out of seven cultures in comparison to the CTRL condition ($N = 56$ NBs, 7 networks per condition). **(C,D)** The acute NMDAR blockade with 10 μM D-AP5 did not significantly change the CC matrices/diversity of spatio-temporal patterns. The acute $GABA_AR$ blockade with 10 μM PTX of NMDAR blocked networks significantly increased ($p_{ranksum} < 0.001$) the similarity between spatio-temporal patterns in four out of six cultures in comparison to the CTRL condition ($N = 56$ NBs 6 network per condition). $^{***}p_{ranksum} < 0.001$, $^{**}p_{ranksum} < 0.01$, $^{*}p_{ranksum} < 0.05$.

compare the major differences between the gradual and acute applications in the last paragraph of the section "Results." In what follows, we present the data obtained using acute protocol quantified using a versatile set of activity measures (see section "Materials and Methods").

The network dynamics were probed by applying acutely high concentrations of 10 μM (the results obtained when applying 30 μM of NBQX are shown in **Supplementary Material** section) of NBQX to explore the immediate acute effects of AMPAR antagonists on network dynamics. The results were consistent with both concentrations. Therefore, we show here only the results with 10 μM NBQX and in the **Supplementary Material** section the results with 30 μM; the raster plots of network activity demonstrate characteristic long bursts (**Figures 2A**, **3A**, middle subpanels) with significantly longer IBI ($p_{ranksum} < 0.001$; **Figure 4B**, top panel) in comparison to the CTRL condition. The OFR ($p_{ranksum} < 0.01$) and BF ($p_{ranksum} < 0.001$) significantly decreased with acute NBQX application (**Figure 2B**) when compared to CTRL. The BF decreased more than the OFR (**Figure 2B**), meaning that NBs occurred less frequently compared to CTRL. The burst measure analysis showed that BL, FP and BS significantly increased ($p_{ranksum} < 0.001$) in comparison to the CTRL condition (**Figure 3B**). The fraction of ISI distributions significantly increased ($p_{ranksum} < 0.001$), meaning longer ISIs with complete AMPAR blockade (**Figure 4A**, top panel). This confirms that AMPARs are needed for fast spiking within the NBs. The IBI distributions shifted toward higher values, meaning significantly less frequent NBs than in the CTRL condition ($p_{ranksum} < 0.001$) (**Figure 4B**, top panel). This observation shows that AMPARs have an important role in the initiation of NBs. The network-wide electrode recruitment time increased also after acute AMPAR blockade, meaning slower network recruitment (**Figure 4C**, left panel). The acute AMPAR blockade significantly ($p_{ranksum} < 0.001$) increased the similarity of spatio-temporal patterns in three out of seven networks in comparison to the CTRL condition (**Figures 5A,B**). However, the number of NBs was too low to evaluate statistical tests for the other four acutely AMPAR blocked networks.

Quantitative Characterization of NMDAR Contribution to Spatial and Temporal Maintenance of the Propagating Network Bursts

The slower glutamate receptors, the NMDARs, contributed to the overall network excitability via manipulation of spatio-temporal patterns of network activity. In the temporal domain, their contribution maintained the network activity particularly during

the termination phase of the NBs. In the spatial domain, the blocking of NMDARs reduced the number of active electrodes. NMDAR blockade reduced also the time needed for activity to recruit all the electrodes, indicating that NMDARs or another mechanism influencing NMDARs, e.g., the inhibition, slowed down the activity recruitment in these networks.

The role of NMDARs on spontaneous NB dynamics were studied probing the culture by acute application of 10 μM of NMDAR antagonist D-AP5. The consistent findings were obtained when probing the cultures with a higher concentration of 30 μM D-AP5, these results are presented in the **Supplementary Material** section. The raster plots of network activity demonstrate characteristic short NBs (**Figure 2C**, middle subpanels). The results confirmed that the OFR significantly decreased ($p_{\text{ranksum}} < 0.01$) and BF also slightly decreased when acutely blocking the NMDARs (**Figure 2D**). The OFR decreased more in the NMDARs blocked networks than in the AMPARs blocked networks in comparison to the CTRL condition in all acute applications (**Figures 2B**, left panel, **D**, left panel). On the contrary, the BF decreased more in AMPAR blocked networks than in NMDAR blocked networks in comparison to the CTRL condition (**Figures 2B**, right panel, **D**, right panel), indicating that NMDARs do not contribute as much to the BF as AMPARs. The BL ($p_{\text{ranksum}} < 0.01$), FP ($p_{\text{ranksum}} < 0.01$), RP ($p_{\text{ranksum}} < 0.05$), BS ($p_{\text{ranksum}} < 0.01$) and RC ($p_{\text{ranksum}} < 0.05$) significantly decreased when acute 10 μM D-AP5 was applied (**Figures 3C,D**). This means that NMDARs are responsible for maintaining NBs in these networks. Intriguingly, the blockade of NMDARs reduced the RC in all applications, which suggests that the NMDARs have an important spatial role in overall NB activity. The ISI distributions were not modulated by acute NMDAR blockade (**Figure 4A**, bottom panel). On the contrary, the IBI distributions shifted toward higher fractions, indicating significantly longer ($p_{\text{ranksum}} < 0.001$) intervals between NBs in the NMDAR blocked condition than in the CTRL condition (**Figure 4B**, bottom panel). Moreover, in the NMDAR blocked condition the IBIs intervals were shorter than in the AMPAR blocked condition (**Figure 4B**) which stressed the dependence of AMPARs for the initiation of NBs. The recruitment time shortened when the NMDARs were antagonized (**Figure 4C**, right panel), meaning that either NMDARs or, e.g., the interplay between NMDARs and inhibition slow down the activity propagation. The results of the similarity analysis of the spatio-temporal patterns indicate that the acute NMDAR blockade did not significantly change the similarity between spatio-temporal patterns, indicating that AMPARs facilitate the diversity ($p_{\text{ranksum}} < 0.001$) of the activity propagation and that NMDARs do not diversify the spatio-temporal patterns (**Figures 5C,D**).

$GABA_A$Rs Dampen the Termination Phase of Network Bursts and Decrease the Burst Frequency in the NMDAR-Mediated Networks

So far, we described the changes in network-wide dynamics when blocking individual excitatory receptors through acute application of a receptor antagonist. In what follows, we examine the combined contributions of pairs of receptors. This is done first by acute blocking of one of the considered glutamatergic receptors described above and then by acute disinhibition. In this section we present the quantitative characterization of a combined contribution of AMPAR and $GABA_A$R blockade to the network activity. The ionotropic $GABA_A$Rs play a critical role in the fast inhibition of neurons. In the presence of NMDARs, $GABA_A$Rs contributed particularly to the inhibition of the termination phase of NBs as well as to NB frequency in NMDAR-mediated networks. Finally, the overall spiking frequency in NMDAR-mediated networks was not as strongly inhibited by $GABA_A$Rs as the spiking frequency in AMPAR-mediated networks.

To assess how $GABA_A$ receptors shape the NMDAR-mediated spontaneous NB dynamics, first the AMPARs were acutely blocked (10 μM NBQX, i.e., NMDAR-mediated networks), and then the networks were acutely disinhibited by applying 10 μM PTX. Disinhibition did not change the OFR, but it significantly increased ($p < 0.05$, $n = 7$) the BF in comparison to the solely AMPAR blocked condition (**Figure 2B**). However, the BF remained significantly lower after disinhibition when compared to the CTRL condition ($p < 0.001$, $n = 7$) (**Figure 2B**, right panel), meaning that $GABA_A$Rs inhibited the NMDAR-mediated NB frequency. Disinhibited NMDAR-mediated (AMPAR and $GABA_A$R blocked) burst profiles were truncated in comparison to long NMDAR-mediated profiles (**Figure 3A**), meaning that $GABA_A$Rs slow down the termination phase of the NMDAR-mediated NBs. A detailed burst measure analysis showed that the BL ($p < 0.001$, $n = 7$), FP ($p < 0.001$ $n = 7$) and BS ($p < 0.05$, $n = 7$) significantly decreased by disinhibition in comparison to the previous AMPAR blocked condition (**Figure 3B**). However, the BL ($p < 0.01$ $n = 7$), FP ($p < 0.05$, $n = 7$) and BS ($p < 0.05$, $n = 7$) significantly increased in comparison to the CTRL condition (**Figure 3B**). The ISI distribution shifted significantly ($p < 0.001$, $n = 7$) toward lower values in NMDAR-mediated networks by acute disinhibition when compared to the CTRL condition or the solely AMPAR blocked conditions, meaning that $GABA_A$Rs inhibit NMDAR-mediated spiking (**Figure 4A**, top panel). However, the shift in ISI distributions was not as profound as for the ISI distributions in networks with dominantly AMPAR-mediated synaptic transmission (**Figure 4A**). The IBI distributions were significantly higher ($p < 0.001$) in disinhibited AMPAR blocked networks when compared to the CTRL condition (**Figure 4B**, top panel). IBIs significantly decreased ($p < 0.01$) in four out of seven cultures and did not change in three out of seven cultures when compared to the previous AMPAR blocked condition. This indicates that disinhibition shortens IBIs in NMDAR-mediated networks (**Figure 4B**, top panel). The network recruitment time decreased in all cultures ($n = 7$) (**Figure 4C**, left panel), indicating that $GABA_A$Rs contribute by inhibiting the network recruitment at the beginning of the NMDAR-mediated NBs as well. The acute disinhibition of NMDAR-mediated networks significantly increased ($p_{\text{ranksum}} < 0.001$) the similarity of spatio-temporal patterns in four out of seven cultures (three cultures contained

too few NBs to reliably compute statistical significance) (**Figures 5A**, right panel, **B**).

$GABA_A$Rs Contribute to Inhibiting the Spiking Frequency and Preventing the Fast Spread of Activity Propagation in the AMPAR-Mediated Networks

In this section, we present the quantitative characterization of a combined contribution of NMDAR and $GABA_A$R blockade to the network activity. The blocking of $GABA_A$Rs significantly increased the number of active electrodes in AMPAR-mediated networks. $GABA_A$Rs dampened the initiation phase of the NB activity and slowed down the network recruitment in AMPAR-mediated networks. In the presence of AMPARs, $GABA_A$Rs contributed particularly to the inhibition of spiking frequency. $GABA_A$Rs balanced the AMPAR-mediated activity to maintain the dynamics of activity, suggesting crucial interplay between fast $GABA_A$Rs-mediated inhibition and fast AMPAR-mediated spiking.

In order to study the influence of $GABA_A$ receptors on shaping the AMPAR-mediated NB activity dynamics we first acutely blocked NMDARs using 10 μM D-AP5, and then acutely disinhibited the networks by applying 10 μM of PTX. The results showed that the disinhibition significantly increased ($p < 0.01$, $n = 6$) the OFR, but not BF in comparison to the NMDAR blocked condition (**Figure 2D**). The BL ($p < 0.01$, $n = 6$), FP ($p < 0.01$, $n = 6$), MFR ($p < 0.01$, $n = 6$), BS ($p < 0.01$, $n = 6$) and RC ($p < 0.05$, $n = 6$) significantly increased in comparison to the previous NMDAR blocked condition, meaning that $GABA_A$Rs strongly inhibited the spiking frequency within the NBs (**Figure 3D**). In addition, disinhibition increased the spatial spread of extracellular activity in AMPAR-mediated networks, meaning that $GABA_A$Rs effectively inhibited the AMPAR-mediated activity across the cultures (**Figure 3D**, RC). Contrary to the NMDAR-mediated networks, in AMPAR-mediated networks the distributions of ISIs did not significantly deviate from the one recorded under the CTRL condition (**Figure 4A**). Interestingly, disinhibition significantly reduced ($p < 0.001$) the ISIs when compared to both the CTRL and the AMPAR-mediated condition (**Figure 4A**, bottom panel). Although, in NMDAR-mediated networks, the mean of the ISI distribution also shifted toward a lower value after disinhibition, the change was not as significant as in the AMPAR-mediated networks (**Figure 4A**). This means that $GABA_A$Rs strongly inhibited the spiking frequency in AMPAR-mediated networks and suggest important interplay between the $GABA_A$Rs-mediated inhibition and the AMPAR-mediated fast spiking. The IBIs were significantly increased ($p < 0.001$, $n = 6$) in disinhibited AMPAR-mediated networks in comparison to the CTRL condition and the condition before disinhibition (**Figure 4B**, bottom panel). The IBIs were significantly reduced ($p < 0.001$) by disinhibition in half of the networks and significantly increased ($p < 0.01$) in the other half in comparison to the solely AMPAR-mediated condition (notice the bidmodal distribution in **Figure 4B**, bottom panel). Disinhibition decreased the recruitment time of electrodes in all cultures ($n = 6$) compared to the CTRL condition and the AMPAR-mediated condition (**Figure 4C**, right panel). This means that disinhibition significantly accelerated the recruitment of neurons in these networks while $GABA_A$Rs tended to maintain the steady speed of recruitment. The acute disinhibition of AMPAR-mediated networks significantly increased ($p_{\text{ranksum}} < 0.001$) the similarity of spatio-temporal patterns in four out of six cultures (**Figures 5C,D**).

Gradual AMPAR Blockade Induced Super Bursts That Share Similar Spatio-Temporal Patterns

In order to gradually study the influence of AMPARs on spontaneous network dynamics, the networks were also gradually blocked in a concentration-dependent manner using 0.1, 1, and 10 μM of NBQX (the total added NBQX concentration was 11.1 μM). Intriguingly, these networks exhibited a very strong occurrence of SBs (see section "Materials and Methods") when using 1 and 10 μM of NBQX ($n = 2$) (**Figure 6A**). The SBs lasted ∼100 s and were separated by longer silent periods. The duration of these silent periods was dependent on the concentration of applied antagonist, i.e., when applying 1 μM of NBQX the duration was ∼3 min, and when applying 10 μM of NBQX it was ∼6 min (**Figure 6A**). The gradual application of the AMPAR antagonist increased the OFR when applying 1 and 10 μM of NBQX and increased the BF when applying 1 μM of NBQX in comparison to the CTRL condition ($n = 2$) (**Figure 6B**). At the end of the gradual application protocol (11,1 μM NBQX), the NBs lasted longer with the median BL being 305.75 ± 80.26 ms (mean ± std, $n = 2$) in comparison to the CTRL condition with the median of the BL being 137.25 ± 9.56 ms (mean ± std, $n = 2$) (**Figure 7B**). Additionally, the intervals between NBs became shorter with the median of IBIs being 645.86 ± 302.00 ms (mean ± std, $n = 2$) in comparison to the CTRL median value of 5916 ± 686.00 ms (mean ± std, $n = 2$) (**Figure 8B**, top panel).

A more detailed analysis of NB measures showed that the increase in OFR results from the significant increase in BL, FP, RP and BS ($p_{\text{ranksum}} < 0.001$) (**Figure 7B**). MFRs and RC significantly decreased (**Figure 7B**) and the MFR was reached later by concentration-dependent manner (**Figure 7A**, the inset). The median ISI significantly increased when using 1 and 10 μM of NBQX ($p_{\text{ranksum}} < 0.001$) (**Figure 8A**, top panel), indicating longer distances between spikes within NBs. In experiments where the gradual blocking of AMPARs was performed, the long SBs disintegrated into a number of shorter NBs, separated by visible but shorter IBIs. The median IBIs were significantly shorter ($p_{\text{ranksum}} < 0.001$) in comparison to the CTRL condition (**Figure 8B**, top panel). The recruitment time of neurons in a network increased when gradually applying the AMPAR antagonist (**Figure 8C**, left panel), meaning that the fast recruitment of neurons attending to NBs is dependent on AMPARs. The results of the similarity analysis of the spatio-temporal patterns indicate that the gradual AMPAR blockade significantly increased the similarity between spatio-temporal patterns, meaning that AMPARs support the diversity ($p_{\text{ranksum}} < 0.001$) of the activity propagation (**Figures 9A,B**).

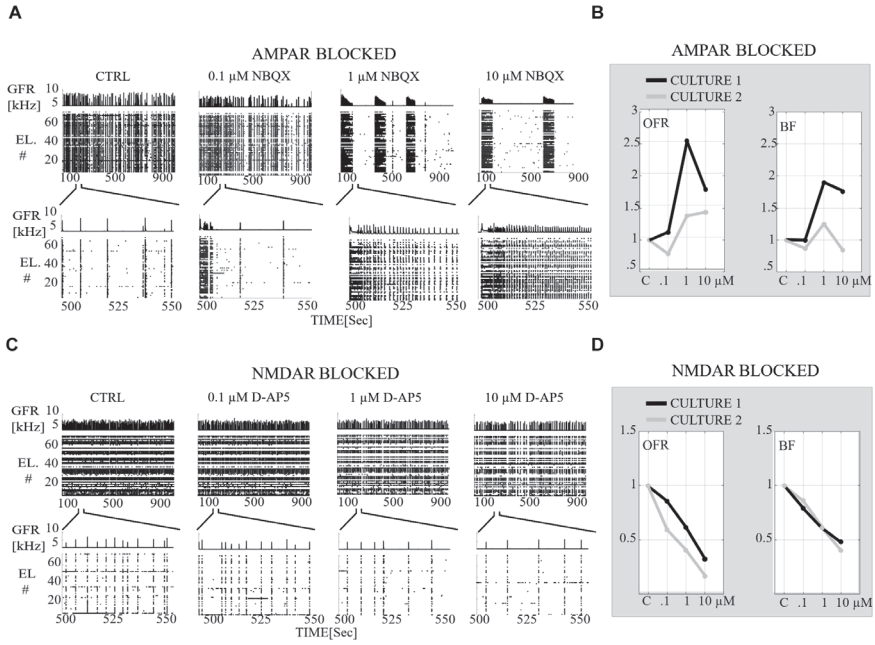

FIGURE 6 | Receptor-dependent network-wide activity probed by gradual application of AMPA and NMDA receptor antagonists, relative changes in OFR [Hz] and in BF [NB/min]. **(A)** Raster plots of network activity of the CTRL recording probed by gradual application of AMPAR antagonist (0.1, 1, and 10 μM NBQX). In each subpanel, the global firing rates (GFR [kHz]) are displayed on top of the raster plots of spike times [s] from electrodes (EL #) in each condition. Top row shows the completely analyzed recording of 900 s, and the bottom row enlargements of the 60 s to display fine details of the activity. **(B)** Relative change in OFR and BF with respect to those obtained from the CTRL condition as shown for each recording (n = 2 cultures). This relative change is computed as described in the section "Materials and Methods". The values of the applied NBQX concentrations are shown on the x-axis. **(C)** Same as **(A)** except that a CTRL recording is probed by gradual application of NMDARs antagonists (0.1, 1, and 10 μM D-AP5). **(D)** Same as **(B)** except that the CTRL recordings are compared to condition when NMDARs are gradually antagonized with 0.1, 1, and 10 μM D-AP5. Gradual AMPAR blockade increased the OFR in both cultures in comparison to the CTRL condition **(B)**. Gradual application of NMDAR antagonist gradually decreased the OFR and BF in comparison to the CTRL condition **(D)**.

The role of NMDARs on spontaneous network dynamics was also assessed with the gradual blockade of NMDARs in a concentration-dependent manner using 0.1, 1, and 10 μM D-AP5 (the total added D-AP5 concentration was 11.1 μM). The results showed that the OFR and BF decreased when applying an increased concentration of the excitatory antagonist (D-AP5) (**Figures 6C,D**). A more detailed analysis of burst measures showed that the BL, FP, RP, BS and RC significantly decreased ($p_{\text{ranksum}} < 0.001$) when applying 10 μM D-AP5 (**Figure 7D**). The comparison of burst profiles and zooming into the first 200 ms showed that the BL, in particular the FP of the NBs, diminished when using 10 μM D-AP5 (**Figure 7C**, the inset). IBIs significantly increased ($p_{\text{ranksum}} < 0.001$) with 1, and 10 μM D-AP5 (**Figure 8B**, bottom panel). In addition, our results showed that these networks were recruiting neurons faster to the NBs than the CTRL networks, meaning that NMDARs or related mechanisms slow down the recruitment of neurons at the beginning of NBs (**Figure 8C**, right panel). Finally, we show that there are no changes in the similarity measures of the spatio-temporal patterns in NMDAR-blocked cultures, indicating that the NMDARs do not diversify spatio-temporal patterns of NBs (**Figures 9C,D**). However, we show that NMDARs contribute characteristic SBs composed of tens of slow NBs with highly repetitive spatio-temporal patterns in gradually AMPAR blocked networks (**Figures 9A,B**).

In what follows, we compare the major differences between the results of gradual and acute blockades. Intriguingly, the gradual application of an AMPAR blockade induced SBs (**Figure 6A**), which were not observed in acutely AMPAR blocked networks (**Figure 2A**, middle panel). Although there were long silent periods between the SBs, the OFR significantly increased in comparison to the CTRL condition in the case of gradual AMPAR blockade (**Figures 6A,B**). In contrast, the OFR significantly decreased in comparison to CTRL in the case of acute AMPAR blockade (**Figure 2B**, left panel). In the case of acute AMPAR blockade also the BF significantly decreased when compared to the CTRL condition (**Figure 2B**, right panel), which we did not observe in the networks probed by a gradual AMPAR blockade (**Figure 6B**, right panel). However, the BL, FP, BS and ISIs increased in both experimental protocols (**Figures 3B**, **7B**, **4A**, top panel, **8A**, top panel). Furthermore, the IBIs decreased in networks with a gradual AMPAR blockade (**Figure 8B**, top

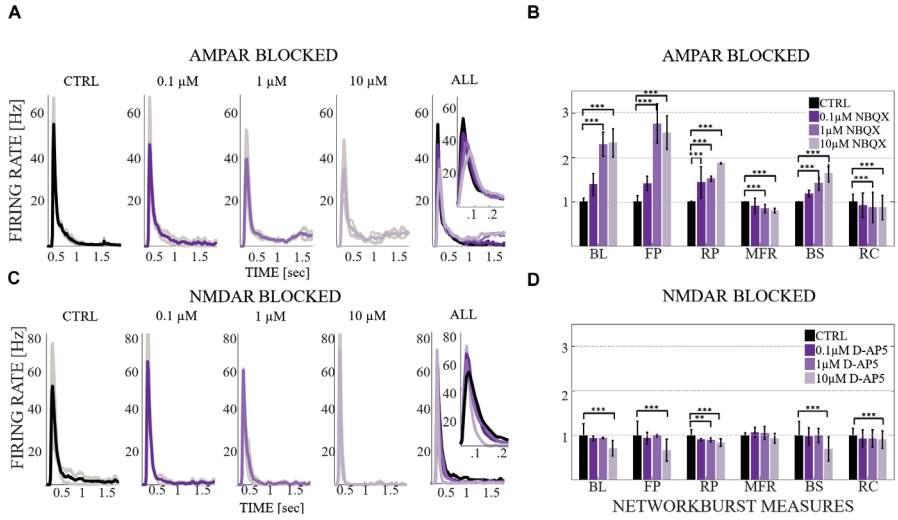

FIGURE 7 | The influence of gradual application of the excitatory receptor antagonists on NB profiles and burst measures. **(A)** The burst profiles [Hz] from two congruent experiments where the data of the CTRL recording (1st subpanel) is compared to the data of the recording conditions when AMPARs (2nd, 3rd, and 4th subpanels) are antagonized with 0.1, 1, and 10 µM NBQX. Thin gray lines represent the average NB profiles of each culture in each condition, whereas the thick line represents the average over both cultures. The profiles are aligned with each other at the time point when the MFR is reached. The presented profiles are computed using the spike-data from **Figure 6**, processed as described in section "Materials and Methods". The 1st, 2nd, 3rd, and 4th subpanels show the first 1.5 s of burst profiles. The 5th subpanel shows all four average NB profiles in the same panel and enlargement of the first 300 ms of all four profiles to display the fine details at the beginning of the NBs. Bin width is 0.01 s. **(B)** The relative change of characteristic burst measures extracted from burst profiles, including BL, FP, RP, MFR, BS and RC (see section "Materials and Methods"). Each bar represents the mean of the medians ± SD divided by mean, i.e., coefficient of variation from both cultures. The top panel shows the relative change in networks probed by a gradual blockade of AMPARs (0.1, 1, and 10 µM NBQX). **(C)** Same as **(A)** except that the data of the CTRL recording (1st subpanel) is compared to the data of the recording conditions when NMDARs (2nd, 3rd, and 4th subpanels) are antagonized with 0.1, 1, and 10 µM D-AP5. **(D)** Same as **(B)** except that the relative change in networks is probed by a gradual blockade of NMDARs (0.1, 1, and 10 µM D-AP5). Wilcoxon rank sum test and *p*-values were computed for all burst measures in each condition and in each culture. If the tests showed a similar result for both cultures, the significance was displayed in **(B,D)**. BL, FP, RP and BS gradually increased by a gradual AMPAR blockade **(B)** and gradually decreased by a gradual NMDAR blockade **(D)**. MFR gradually decreased by AMPAR blockade **(B)**. RC decreased by both AMPAR and NMDAR blockades **(B,D)**. $^{***}p_{\text{ranksum}} < 0.001$, $^{**}p_{\text{ranksum}} < 0.01$, $^{*}p_{\text{ranksum}} < 0.05$.

panel), but increased in networks with an acute AMPAR blockade (**Figure 4B**, top panel) in comparison to the CTRL condition. The recruitment time increased similarly in both gradual and acute applications of the AMPAR blockade (**Figures 4C**, left panel, **8C**, left panel). The spatio-temporal patterns became similar when gradually blocking the AMPARs (**Figures 9A,B**). However, the acute blocking of AMPARs gave rather small number of NBs. Thus for this experimental condition we could not to evaluate the similarity of NBs with sufficient statistical significance (**Figures 4A,B**). Finally, there were no differences when gradually and acutely blocking the NMDARs nor the $GABA_A$Rs.

DISCUSSION

We systematically analyzed the unique features of NBs, including the initiation, maintenance, propagation and termination of NBs, which emerge from a complex interplay between fast AMPA and slow NMDA glutamatergic and fast $GABA_A$ gabaergic receptors when embedded into a self-organized network. We analyzed the data collected from P0 rat cortical neurons between 20–25 DIV using the MEA recording technique with receptor antagonists. The kinetics of the receptors are known at the single cell and synapse levels, but their contribution to NBs is not well understood. We show how the spontaneous NBs are modified by the distinctive kinetics of each of the ionotropic excitatory and inhibitory receptors in these networks. In particular, (1) AMPARs contributed to the fast initiation of NBs, the fast recruitment of network activity and more versatile spatio-temporal patterns of network activity; (2) NMDARs maintained the NBs temporally and spatially as well as slowed down the spread of activity propagation; (3) $GABA_A$Rs inhibited the spiking frequency and prevented the fast spread of activity propagation in the AMPAR-mediated networks; (4) $GABA_A$Rs further dampened the termination phase of the NBs and the NB frequency in the NMDAR-mediated networks; in addition, (5) the NMDAR- and $GABA_A$R-mediated networks exhibited characteristic SBs composed of slow NBs with highly repetitive spatio-temporal patterns in the presence of a gradual AMPAR blockade. To the best of our knowledge, all these unique features of the NBs emerging from the interplay between excitatory and inhibitory

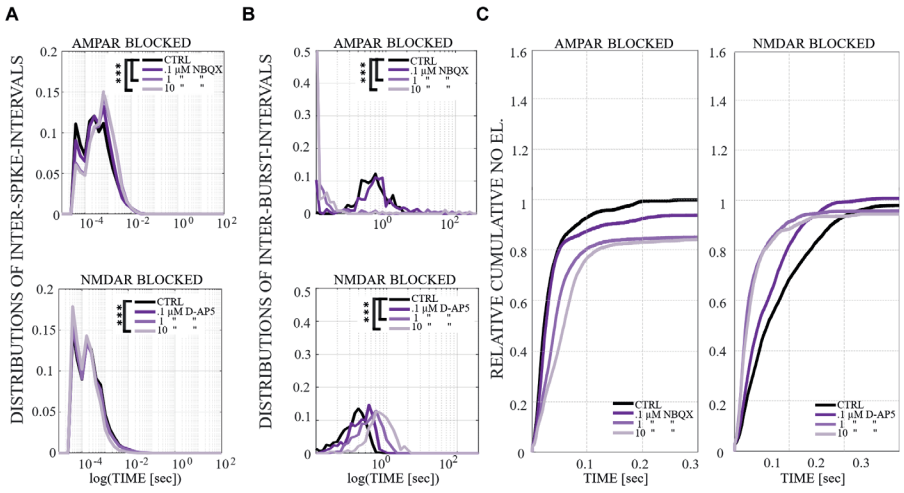

FIGURE 8 | The influence of gradual application of the excitatory receptor antagonists on ISIs, IBIs and network-wide electrode recruitment speed at the beginning of the bursts. **(A)** The excitatory receptor dependence on ISIs within NBs. Average ISI distribution gradually shifts toward higher fractions in gradually AMPAR blocked networks (n = 2) (top panel), meaning significantly longer distances between spikes within NBs in neurons probed by 1 and 10 μM NBQX ($p_{ranksum} < 0.001$). In contrast, the average ISI distribution shifts toward slightly lower fractions in gradually NMDAR blocked networks (n = 2) (bottom panel), meaning significantly shorter distances between spikes within NBs in neurons probed by 10 μM D-AP5 ($p_{ranksum} < 0.001$). **(B)** A change in the excitatory receptor balance modulates the duration of IBIs and thus the frequency of NB events. Neurons in gradually AMPAR blocked networks with 1 and 10 μM NBQX expressed bimodal distributions with significantly shorter and longer IBIs than neurons in CTRL or in 0.1 μM NBQX blocked networks ($p_{ranksum} < 0.001$) (top panel). The IBI distributions gradually shifted toward higher fractions in gradually NMDAR blocked networks (bottom panel), meaning significantly longer distances between NBs in neurons probed by 1 and 10 μM D-AP5 in comparison to the CTRL condition ($p_{ranksum} < 0.001$). Wilcoxon rank sum test and p-values were computed for all ISIs and IBIs in each condition and in each culture. If the tests showed similar results and p-values for every culture, the results were displayed in **(A,B)**. $^{***}p_{ranksum} < 0.001$, $^{**}p_{ranksum} < 0.01$, $^{*}p_{ranksum} < 0.05$. The x-scale is logarithmic. **(C)** A change in the excitatory receptor modulates network-wide electrode recruitment speed at the beginning of the NBs (left panel). The network recruitment speed slowed down gradually with gradual AMPAR blockade (0.1, 1, and 10 μM NBQX) (left panel) and sped up gradually with gradual NMDAR blockade (0.1, 1, and 10 μM D-AP5) (right panel). Values were normalized to the CTRL conditions. Bin width is 0.1 ms.

receptors have not been previously reported using the MEA recording technique, pharmacological protocols and rat P0 cortical cell cultures referred to herein.

Dissociated *in vitro* cell cultures have been previously used as model systems to study cortical network activity with MEA technique. The MEA technique is a widely used, reliable and feasible recording technique for high-throughput screening of network dynamics, particularly when multiple cell cultures and experimental protocols are considered similarly to this study. The network activity has been studied in cell cultures obtained from the neocortex of P0 (Shahaf and Marom, 2001; Eytan and Marom, 2006; Teppola et al., 2011; Weihberger et al., 2013; Reinartz et al., 2014; Haroush and Marom, 2015; Okujeni et al., 2017) and E17-18 (Robinson et al., 1993; Maeda et al., 1995; Kamioka et al., 1996; Jimbo et al., 2000; Opitz et al., 2002; van Pelt et al., 2004; Chiappalone et al., 2006; Wagenaar et al., 2006; Baltz et al., 2010; Fong et al., 2015) rats. In addition, network activity has been studied in cultures prepared from other areas of the rodent central nervous system, including hippocampus (Arnold et al., 2005; Mazzoni et al., 2007; Chen and Dzakpasu, 2010; Niedringhaus et al., 2013; Eisenman et al., 2015; Slomowitz et al., 2015; Suresh et al., 2016; Lonardoni et al., 2017) and spinal cord (Keefer et al., 2001; Gramowski et al., 2004; Legrand et al., 2004; Ham et al., 2008). In this study, we analyzed the activity recorded from rat P0 networks under a rich set of pharmacological protocols. In these protocols excitatory (AMPA, NMDA) and inhibitory ($GABA_A$) receptors were systematically blocked, and consequently the excitation-inhibition balance was modified. The impact of changes in excitation-inhibition balance to NB dynamics was addressed. We used an extensive set of data analysis methods to quantitatively explain the observed mechanisms. This approach allowed us to not only closely inspect the data and the studied mechanisms but also to present the data in a format that facilitates the computational modeling of the system.

The adopted *in vitro* experimental setup enables the precise manipulation of pharmacological conditions in the extracellular environment while recording the spatio-temporal evolution of network activity with the MEA technique over many hours. The MEA technique allows the robust monitoring of the uniformly sampled extracellular network activity for several hours (Egert et al., 2002). Precise pharmacological manipulations combined with long-term activity recordings are difficult *in vivo* (Yang et al., 2016). In turn, the main drawbacks of *in vitro* models are the lack of architecture and sensory inputs from other brain areas, which lead to the formation of the network without natural function after development. Although this reduced approach

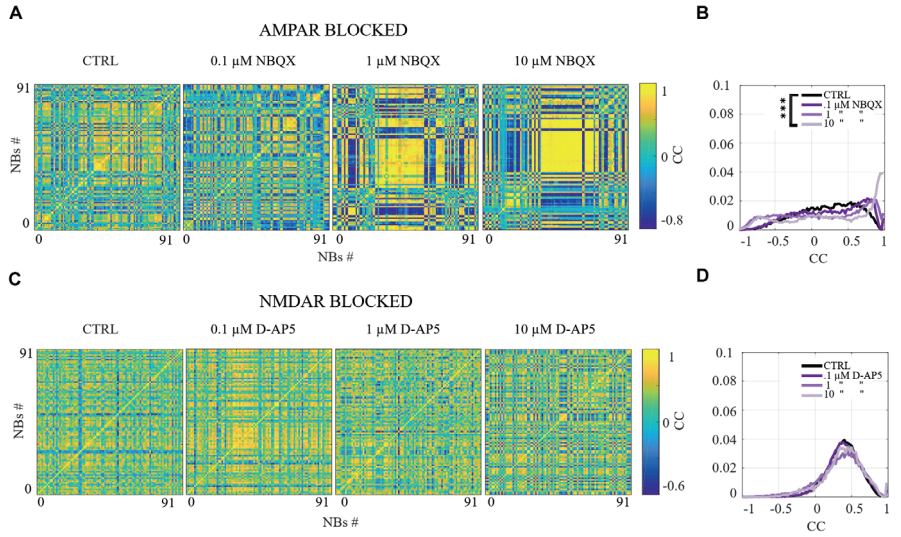

FIGURE 9 | The gradual AMPA receptor blockade changes the spatio-temporal patterns which is not seen in the gradual NMDA receptor blockade. **(A,C)** CC matrices computed for pairwise-spike-time-difference matrices between each NB in each condition of gradual applications. **(B,D)** Mean distributions of CC across the NBs and networks are shown. **(A)** The spatio-temporal patterns became less diverse with gradual 10 µM AMPAR blockade (N = 91 NBs). **(B)** The distribution of CC in AMPAR blocked condition (10 µM NBQX) obtained an increased tail around one in addition to another lower peak around minus one, this indicates polarization among the NBs with respect to spatio-temporal patterns of activity in cultures treated with gradual AMPAR blockade (N = 91 NBs). **(C,D)** The gradual NMDAR blockade did not have an effect on the similarity of spatio-temporal patterns in comparison to the CTRL condition (N = 91 NBs). The gradual AMPAR blockade with 10 µM NBQX significantly decreased ($p_{ranksum} < 0.001$) the diversity of spatio-temporal patterns in comparison to the CTRL condition **(A,B)**. The gradual NMDAR blockade did not significantly change the diversity of spatio-temporal patterns **(C,D)**. $^{***}p_{ranksum} < 0.001$, $^{**}p_{ranksum} < 0.01$, $^{*}p_{ranksum} < 0.05$.

yields differences in observations between network properties *in vitro* and *in vivo,* general phenomena, such as cell homeostasis and synaptic transmission, have been found both *in vitro* and *in vivo*. In addition, *in vitro* cell cultures are conventionally used in pharmacological testing and design. To address the central question of this study, the quantitative analysis of NB features emerging from the complex interplay of excitatory and inhibitory receptors, *in vitro* cultures combined with the MEA recording technique provide an optimal setup.

The same experimental setup has been used to demonstrate a number of properties of spontaneous and evoked activity. Previous studies show that the network activity appears in the form of uncorrelated firing of spikes at the end of the first week *in vitro* (Shahaf and Marom, 2001; Marom and Shahaf, 2002). Consistent with previous research (Linne et al., 1996), we also observed uncorrelated spikes in networks used in this study during the first week *in vitro* (data not shown). At the 2nd week *in vitro*, the stereotypical NBs became prominent in the network activity and persisted throughout the lifetime of the cultures (data not shown) similarly to previous studies (Maeda et al., 1995; Kamioka et al., 1996; Nakanishi and Kukita, 1998; Marom and Shahaf, 2002; Wagenaar et al., 2006; Baltz et al., 2010). During the 3rd week *in vitro*, we observed that the NBs were more variable and the NB frequency had increased in comparison to previous weeks similar to others (Marom and Shahaf, 2002; Wagenaar et al., 2006; Baltz et al., 2010). The overall level of activity as well as the structure and frequency of NB properties have been shown to depend on the used animal species, brain location, age of the donor rats (Lin et al., 2002), seeding density (Wagenaar et al., 2006) and the age of the culture (Wagenaar et al., 2006). Denser cultures are shown to exhibit bursting more actively and earlier than sparser cultures (Wagenaar et al., 2006). According to the definition from Wagenaar et al. (2006), we used data from cultures that provide dense (2000 cells/mm^2) and mature (20–25 DIV) networks in order to provide as stable and comparable recording conditions as possible for every culture (Wagenaar et al., 2006). These recording conditions allowed us to systematically and quantitatively characterize the measures extracted from each NB. Finally, our control networks showed a steady occurrence of network bursting (NB) with frequency of 0.120 ± 0.079 Hz (mean ± std, n = 20) with the results being consistent with previous studies of similar neocortical postnatal preparations (Weihberger et al., 2013; Okujeni et al., 2017), see also (Teppola et al., 2011). Next, we discuss the unique features of the network activity that emerged from the contributions of the main mediators of synaptic transmission in rat postnatal cortical cultures *in vitro*.

We first assessed the contribution of fast glutamatergic AMPARs. These receptors play a critical role in the initiation of NBs and in the fast recruitment of neurons into the NBs. In the section "Results," we carefully evaluated these contributions using a number of suitable quantitative measures. Our results

are consistent with previous studies which showed the critical contribution of AMPARs to the early phase (∼0–25 ms) of NBs in cortical cell cultures *in vitro* (Jimbo et al., 2000; Wagenaar et al., 2004) as well as with recent studies which demonstrated that the NMDAR blockade [with 50 μM APV/20 μM CPP ((±)-3-(2-Carboxypiperazin-4-yl)propyl-1-phosphonic acid)] significantly reduced the duration of spontaneous NBs compared to the control condition in embryonic cortical and hippocampal cultures (Fong et al., 2015; Suresh et al., 2016). In organotypic neonatal visual cortex explants network activity has been shown to be strongly suppressed after applying a selective NMDA receptor blocker (20 μM APV) and began again to rise after 30 min or more exposure in 1- and 2-weeks old explants, whereas the activity levels did not rise after initial suppression in 3-weeks old explants (Corner et al., 2002). Similarly to Corner et al., 2002, we did not observe any rise in the network activity during the 1 h recording period after acute application of the NMDA receptor blocker D-AP5 in the 3 week-old networks. Furthermore, we showed that the interplay between AMPARs and $GABA_A$Rs significantly increases the diversity of spatio-temporal patterns. This important contribution has not been shown before in *in vitro* preparations, to the best of our knowledge. Jointly, the presented results suggest the complex contribution of fast AMPARs and fast $GABA_A$Rs in the spatiotemporal organization of network activity, rather than only exciting or reducing the overall level of activity.

Next, we addressed the contribution of NMDARs to the network activity. We showed that the NBs persist even in the presence of a high concentration of AMPAR antagonists, such as 30 μM of NBQX. Further analysis of the recorded NBs showed that NMDARs maintain the elevated network activity particularly during the late phase of the NBs. Together with $GABA_A$Rs, the NMDARs contribute to slowing down the recruitment of neurons into the NBs. A body of literature supports our findings by showing that AMPAR blocking (by 40/50/100 μM of CNQX) only partially reduced the FR in cortical cultures taken from E18 rats (Ramakers et al., 1993; Martinoia et al., 2005; Fong et al., 2015). This reduction was primarily obtained through reduction in the NB frequency while the level of spiking during NBs remained the same or even increased compared to the control condition (Ramakers et al., 1993; Martinoia et al., 2005; Fong et al., 2015). In addition, Jimbo et al. (2000) showed that in evoked NBs the slower termination phase lasted approximately 25–300 ms (Jimbo et al., 2000). All of these studies showed that the application of an AMPAR antagonist increases the NB duration while the application of an NMDAR antagonist reduces the termination phase (Ramakers et al., 1993; Jimbo et al., 2000; Martinoia et al., 2005; Fong et al., 2015). These findings support our results. Previous studies using dissociated hippocampal cultures taken from E18 rats showed complete abolishing of NBs in the presence of a selective AMPAR antagonist CNQX already at the concentration of 20 μM, different to our findings (Suresh et al., 2016; Lonardoni et al., 2017). The deviations in results can emerge from differences in the data-analysis methods applied to data collected using high-density MEA in Mazzoni et al. (2007) (as opposed to the standard 59 TiN electrode MEA used here), from a relatively short recording period (15 min, compared to our 50 min long recordings) or from the embryonic origin of these cell cultures (Suresh et al., 2016; Lonardoni et al., 2017). It has been demonstrated that the use of higher electrode density may affect the statistics of network activity measures in dissociated cultures (Gandolfo et al., 2010; Maccione et al., 2010; Lonardoni et al., 2015). Furthermore, the age of the donor animal affects the properties of the excitatory synapses in cultured neurons (Lin et al., 2002). More precisely, Lin et al. (2002) compared the EPSCs in two *in vitro* preparations, in dissociated cultures extracted from rat embryos (E18) and in dissociated cultures from P0 donors. At 7 DIV, the EPSCs in E18 cultures were small and almost exclusively mediated by AMPARs, whereas the EPSCs in P0 cultures were larger and mediated by both AMPARs and NMDARs. These results suggest a stronger contribution of NMDARs in P0 cultures and support our observation that NBs remain present in the network activity even after blocking AMPARs. We present here and in the upcoming paragraphs crucial contributions of slow glutamatergic NMDARs to the network activity. These roles have been previously underestimated and thus require futher attention in the future.

In addition to addressing the roles of slow and fast excitatory receptors, we characterized the contribution of fast ionotropic $GABA_A$Rs. In networks mediated by both AMPARs and NMDARs, $GABA_A$Rs reduced the overall spiking by inhibiting both the initiation and termination phases of NBs. Fast inhibition modulated the spatio-temporal propagation of NBs by reducing the number of active electrodes and at the same time increased the time needed to recruit them into NBs. In order to better understand the mechanisms of interaction between $GABA_A$Rs and each type of the considered excitatory receptors, the contribution of $GABA_A$Rs was characterized in dominantly AMPAR-mediated and in dominantly NMDAR-mediated networks. In NMDAR-mediated networks, $GABA_A$Rs contributed to the dampening of the termination phase of NBs while at the same time reducing the frequency of NB occurrences. In AMPAR-mediated networks, the $GABA_A$Rs reduced the overall firing, inhibited the initiation phase of NBs and slowed down the recruitment of electrodes into NBs. The observed changes were more pronounced than those found in NMDAR-mediated networks, suggesting a profound interplay between AMPAR and $GABA_A$R receptors, possibly arising from similar fast kinetics. Furthermore, we showed that $GABA_A$Rs reduced the overall spiking activity of NBs during both the early and late phases of the NBs, slowed down the network recruitment and spiking during the NBs as well as reduced the number of active electrodes attending to NBs (see **Supplementary Figures S1–S3**). Some aspects of $GABA_A$Rs contribution have been shown previously in cortical *in vitro* networks. It has been shown that the termination phase of NBs substantially increases in intensity and duration after $GABA_A$R blocking with known antagonists (including 10 μM BIC, 5/10 μM PTX or 20 μM gabazine) (Jimbo et al., 2000; Weihberger et al., 2013; Baltz and Voigt, 2015; Okujeni et al., 2017). This finding is consistent with our results. However, to the best of our knowledge, the role of $GABA_A$Rs in solely AMPAR-mediated or solely NMDAR-mediated networks has not been addressed before *in vitro*.

The striking property of NMDAR- and $GABA_AR$-mediated (gradual AMPARs blocked) networks is the emergence of SBs carrying tens of NBs confined within the duration of a SB. The SBs were observed exclusively in the experiments with gradual AMPAR blocking but not in the experiments with acute AMPAR blocking, which suggests different biophysical mechanisms engaged by different blocking protocols. The presence of SBs affected both the global properties of network activity and the fine structure of the spatio-temporal patterns. The overall NB frequency, which significantly decreased in networks probed by acute AMPAR blocking, was rescued due to the high occurrence of NBs within a SB. The similarity in spatio-temporal patterns within NBs increased after gradual blocking of AMPARs and the emergence of SBs. This increased similarity in spatio-temporal patterns might be due to the fine tuning of inhibition-excitation balance in networks with gradual AMPAR blocking. Compared to acute blocking, the gradual blocking protocols provided more flexibility in manipulating the activation of synaptic receptors and allowed progressive changing of the excitation-inhibition balance. Thus, it is possible that the gradual protocol left a sufficient amount of active AMPARs that further activated inhibitory receptors and increased the overall inhibition to excitation ratio. This is supported by studies where the inhibition-excitation balance was manipulated through an increase in the total number of interneurons in cultures and identified the same type of SBs in network activity (Chen and Dzakpasu, 2010). Another mechanism capable of reducing the variability in spatio-temporal patterns is a reduction in the number of burst initiation zones. Previous studies have demonstrated that cortical and hippocampal networks *in vitro* tend to develop a number of localized areas that promote NB initiation (Soriano et al., 2008; Okujeni et al., 2017). Gradual AMPAR blocking reduces the number of these burst initiation zones (according to the preliminary data analysis done to quantify NB similarity) which effectively increases the similarity between observed NBs. An analogous increase in NB similarity was seen in the study that effectively reduced the number of burst initiation zones by inhibiting the protein kinase C (PKC) in postnatal cortical cultures (Okujeni et al., 2017). Additionally, PKC is known to enhance AMPAR conductance via phosphorylation of the AMPAR subunit (Jenkins and Traynelis, 2012). Therefore, the modulations of overall network activity seen after the inhibition of PKC most likely correlate with the effects obtained by AMPAR blocking. Various other cellular mechanisms and phenomena may also have an influence on the observed SB dynamics *in vitro*, including synaptic scaling (Fong et al., 2015) and AMPAR/NMDAR trafficking (Sheng and Lee, 2001; Carroll and Zukin, 2002), extrasynaptic receptors (Parri et al., 2001), astrocytes (Bazargani and Attwell, 2016), dendritic properties and NMDA spikes (Palmer et al., 2014) and even ephaptic coupling (Martinez-Banaclocha, 2018). Further addressing of these mechanisms is beyond the scope of our study.

We presented an extensive collection of experimental protocols designed to carefully manipulate the balance of excitatory and inhibitory receptors by blocking specific synaptic mechanisms and thereby analyze the consequences on network-level activity. Further research on the mechanisms behind NBs will benefit from combining experimental with computational techniques. For instance, with computational models we can further study the cellular and synaptic mechanisms as well as the structural organization of neuronal networks that best reproduce the experimental data. In addition, a well-defined data-driven computational model could reduce the amount of biological experiments and thus accelerate scientific progress. Several computational studies have addressed selected mechanisms affecting the characteristic features of MEA-recorded NBs (Giugliano et al., 2004; Baltz et al., 2011; Gigante et al., 2015; Lonardoni et al., 2017; Manninen et al., 2018). Typically, these studies rely on phenomenological network models and show qualitative agreement with network-level experimental data. Recent advances in neuroinformatics tools (Davison et al., 2009; Denker and Grün, 2016) and infrastructure (Amunts et al., 2016) provide an opportunity to expand these studies by constructing more complex models incorporating details of underlying biophysical mechanisms. Such models can be carefully constrained using multiple modalities of experimental data (e.g., patch-clamp recordings in addition to the MEA recordings considered here) and computationally intensive data-driven modeling protocols. However, the majority of experimental studies are not designed to support computational modeling. Experimental results are often not presented in a manner that supports easy extraction of quantitative values needed for computational modeling. The presented results are compressed and often lack crucial information. In this paper we would like to suggest a different, model friendly manner for presenting experimental data: we carefully quantified different phases and aspects of network activity, provided statistics for them, and listed the obtained quantitative values. Information about the extensive data analysis that we performed is used to support ongoing modeling efforts (Aćimović et al., manuscript in preparation).

This study concludes that the fast AMPARs have a dominant role in the initiation of NBs by rapidly recruiting neurons and that the slow NMDARs maintain the elevated NBs. $GABA_ARs$ strongly inhibit the AMPAR-mediated spiking and further dampen the NMDAR-mediated termination phase. According to our study, there is an active interplay between the fast $GABA_AR$- and fast AMPAR-mediated activities. In the gradual blocking of AMPARs, the contribution of the network activity is dominated by the SBs that are composed of tens of slow NMDAR-mediated NBs with highly repetitive spatio-temporal patterns. This phenomenon that has been for the first time shown and carefully quantified in this study requires further attention. Combining experimental wet-lab and *in silico* modeling are required to unravel the roles of the considered mechanisms and their contribution to the network level activity.

DATA AVAILABILITY

The datasets for this study will be available in https://github.com/HTeppola/Front_Cell_Neurosci_Network_Burst_Analysis. Requests to access the datasets should be directed to the

corresponding author, M-LL. Any use and subsequent publication of the data presented in this publication and repository must be cited accordingly (i.e., include citation to this article and to the GitHub repository).

AUTHOR CONTRIBUTIONS

HT and M-LL conceived the study presented in this manuscript. HT organized the data that she previously recorded, analyzed, and presented in Teppola et al. (2011), reprocessed and re-analyzed the data to support better fitting of computational modeling of cell culture dynamics, performed data-analysis, prepared the figures, and drafted the manuscript. HT, JA, and M-LL selected the data analysis procedures and new code implementing those procedures, jointly interpreted and discussed the results and their implications, revised the manuscript, and approved the final version of the manuscript. JA and M-LL reviewed the measures, statistical analysis, and result presentation to select those that best support data-driven computational modeling.

FUNDING

This work was supported by the Academy of Finland through grants 297893 and 318879 (ERA-NET NEURON project "SYNSCHIZ") awarded to M-LL. HT acknowledges the support from the Graduate School of Tampere University of Technology, Tampere Graduate School in Information Science and Engineering, Finnish Foundation for Technology Promotion, Finnish Cultural Foundation (Central and Pirkanmaa Regional funds), and Finnish Brain Foundation sr. This research received funding from the European Union's Horizon 2020 Framework Programme for Research and Innovation under the Specific Grant Agreement No. 785907 (Human Brain Project SGA2).

SUPPLEMENTARY MATERIAL

The Supplementary Material for this article can be found online at: https://www.frontiersin.org/articles/10.3389/fncel.2019.00377/full#supplementary-material

REFERENCES

Allene, C., Cattani, A., Ackman, J. B., Bonifazi, P., Aniksztejn, L., Ben-Ari, Y., et al. (2008). Sequential generation of two distinct synapse-driven network patterns in developing neocortex. *J. Neurosci.* 28, 12851–12863. doi: 10.1523/JNEUROSCI.3733-08.2008

Amunts, K., Ebell, C., Muller, J., Telefont, M., Knoll, A., and Lippert, T. (2016). The human brain project: creating a european research infrastructure to decode the human brain. *Neuron* 92, 574–581. doi: 10.1016/j.neuron.2016.10.046

Arnold, F. J., Hofmann, F., Bengtson, C. P., Wittmann, M., Vanhoutte, P., and Bading, H. (2005). Microelectrode array recordings of cultured hippocampal networks reveal a simple model for transcription and protein synthesis-dependent plasticity. *J. Physiol.* 564, 3–19. doi: 10.1113/jphysiol.2004.077446

Baltz, T., de Lima, A. D., and Voigt, T. (2010). Contribution of GABAergic interneurons to the development of spontaneous activity patterns in cultured neocortical networks. *Front. Cell Neurosci.* 4:15. doi: 10.3389/fncel.2010.00015

Baltz, T., Herzog, A., and Voigt, T. (2011). Slow oscillating population activity in developing cortical networks: models and experimental results. *J. Neurophysiol.* 106, 1500–1514. doi: 10.1152/jn.00889.2010

Baltz, T., and Voigt, T. (2015). Interaction of electrically evoked activity with intrinsic dynamics of cultured cortical networks with and without functional fast GABAergic synaptic transmission. *Front. Cell Neurosci.* 9:272. doi: 10.3389/fncel.2015.00272

Bazargani, N., and Attwell, D. (2016). Astrocyte calcium signaling: the third wave. *Nat. Neurosci.* 19, 182–189. doi: 10.1038/nn.4201

Ben-Ari, Y. (2001). Developing networks play a similar melody. *Trends Neurosci.* 24, 353–360. doi: 10.1016/s0166-2236(00)01813-0

Ben-Ari, Y., Gaiarsa, J. L., Tyzio, R., and Khazipov, R. (2007). GABA: a pioneer transmitter that excites immature neurons and generates primitive oscillations. *Physiol. Rev.* 87, 1215–1284. doi: 10.1152/physrev.00017.2006

Benveniste, M., and Mayer, M. L. (1991). Kinetic analysis of antagonist action at N-methyl-D-aspartic acid receptors. Two binding sites each for glutamate and glycine. *Biophys. J.* 59, 560–573. doi: 10.1016/s0006-3495(91)82272-x

Blankenship, A. G., and Feller, M. B. (2010). Mechanisms underlying spontaneous patterned activity in developing neural circuits. *Nat. Rev. Neurosci.* 11, 18–29. doi: 10.1038/nrn2759

Bologna, L. L., Nieus, T., Tedesco, M., Chiappalone, M., Benfenati, F., and Martinoia, S. (2010). Low-frequency stimulation enhances burst activity in cortical cultures during development. *Neuroscience* 165, 692–704. doi: 10.1016/j.neuroscience.2009.11.018

Cancedda, L., Fiumelli, H., Chen, K., and Poo, M. M. (2007). Excitatory GABA action is essential for morphological maturation of cortical neurons *in vivo*. *J. Neurosci.* 27, 5224–5235. doi: 10.1523/jneurosci.5169-06.2007

Carroll, R. C., and Zukin, R. S. (2002). NMDA-receptor trafficking and targeting: implications for synaptic transmission and plasticity. *Trends Neurosci.* 25, 571–577. doi: 10.1016/s0166-2236(02)02272-5

Chen, X., and Dzakpasu, R. (2010). Observed network dynamics from altering the balance between excitatory and inhibitory neurons in cultured networks. *Phys. Rev. E Stat. Nonlin. Soft Matter Phys.* 82:031907. doi: 10.1103/PhysRevE.82.031907

Chiappalone, M., Bove, M., Vato, A., Tedesco, M., and Martinoia, S. (2006). Dissociated cortical networks show spontaneously correlated activity patterns during *in vitro* development. *Brain Res.* 1093, 41–53. doi: 10.1016/j.brainres.2006.03.049

Chiu, C., and Weliky, M. (2001). Spontaneous activity in developing ferret visual cortex in vivo. *J. Neurosci.* 21, 8906–8914. doi: 10.1523/jneurosci.21-22-08906.2001

Corlew, R., Bosma, M. M., and Moody, W. J. (2004). Spontaneous, synchronous electrical activity in neonatal mouse cortical neurones. *J. Physiol.* 560, 377–390. doi: 10.1113/jphysiol.2004.071621

Corner, M. A., van Pelt, J., Wolters, P. S., Baker, R. E., and Nuytinck, R. H. (2002). Physiological effects of sustained blockade of excitatory synaptic transmission on spontaneously active developing neuronal networks–an inquiry into the reciprocal linkage between intrinsic biorhythms and neuroplasticity in early ontogeny. *Neurosci. Biobehav. Rev.* 26, 127–185. doi: 10.1016/s0149-7634(01)00062-8

Crochet, S., Chauvette, S., Boucetta, S., and Timofeev, I. (2005). Modulation of synaptic transmission in neocortex by network activities. *Eur. J. Neurosci.* 21, 1030–1044. doi: 10.1111/j.1460-9568.2005.03932.x

Davison, A. P., Brüderle, D., Eppler, J., Kremkow, J., Muller, E., Pecevski, D., et al. (2009). PyNN: a common interface for neuronal network simulators. *Front. Neuroinform.* 2:11. doi: 10.3389/neuro.11.011.2008

Denker, M., and Grün, S. (2016). "Designing workflows for the reproducible analysis of electrophysiological data," in *Brain-Inspired Computing*, eds K. Amunts, L. Grandinetti, T. Lippert, and N. Petkov (Springer: Springer International Publishing), 58–72. doi: 10.1007/978-3-319-50862-7_5

Dichter, M. A. (1978). Rat cortical neurons in cell culture: culture methods, cell morphology, electrophysiology, and synapse formation. *Brain Res.* 149, 279–293. doi: 10.1016/0006-8993(78)90476-6

Dingledine, R., Borges, K., Bowie, D., and Traynelis, S. F. (1999). The glutamate receptor ion channels. *Pharmacol. Rev.* 51, 7–61.

Egert, U., Knott, T., Schwarz, C., Nawrot, M., Brandt, A., Rotter, S., et al. (2002). MEA-Tools: an open source toolbox for the analysis of multi-electrode data with MATLAB. *J. Neurosci. Methods* 117, 33–42. doi: 10.1016/S0165-0270(02)00045-6

Egorov, A. V., and Draguhn, A. (2013). Development of coherent neuronal activity patterns in mammalian cortical networks: common principles and local hetereogeneity. *Mech. Dev.* 130, 412–423. doi: 10.1016/j.mod.2012.09.006

Eisenman, L. N., Emnett, C. M., Mohan, J., Zorumski, C. F., and Mennerick, S. (2015). Quantification of bursting and synchrony in cultured hippocampal neurons. *J. Neurophysiol.* 114, 1059–1071. doi: 10.1152/jn.00079.2015

Eytan, D., and Marom, S. (2006). Dynamics and effective topology underlying synchronization in networks of cortical neurons. *J. Neurosci.* 26, 8465–8476. doi: 10.1523/jneurosci.1627-06.2006

Feller, M. B. (1999). Spontaneous correlated activity in developing neural circuits. *Neuron* 22, 653–656. doi: 10.1016/s0896-6273(00)80724-2

Fong, M. F., Newman, J. P., Potter, S. M., and Wenner, P. (2015). Upward synaptic scaling is dependent on neurotransmission rather than spiking. *Nat. Commun.* 6:6339. doi: 10.1038/ncomms7339

Gandolfo, M., Maccione, A., Tedesco, M., Martinoia, S., and Berdondini, L. (2010). Tracking burst patterns in hippocampal cultures with high-density CMOS-MEAs. *J. Neural. Eng.* 7:056001. doi: 10.1088/1741-2560/7/5/056001

Garaschuk, O., Linn, J., Eilers, J., and Konnerth, A. (2000). Large-scale oscillatory calcium waves in the immature cortex. *Nat. Neurosci.* 3, 452–459. doi: 10.1038/74823

Gigante, G., Deco, G., Marom, S., and Del Giudice, P. (2015). Network events on multiple space and time scales in cultured neural networks and in a stochastic rate model. *PLoS Comput. Biol.* 11:e1004547. doi: 10.1371/journal.pcbi.1004547

Giugliano, M., Darbon, P., Arsiero, M., Luscher, H. R., and Streit, J. (2004). Single-neuron discharge properties and network activity in dissociated cultures of neocortex. *J. Neurophysiol.* 92, 977–996. doi: 10.1152/jn.00067.2004

Gramowski, A., Jugelt, K., Weiss, D. G., and Gross, G. W. (2004). Substance identification by quantitative characterization of oscillatory activity in murine spinal cord networks on microelectrode arrays. *Eur. J. Neurosci.* 19, 2815–2825. doi: 10.1111/j.0953-816X.2004.03373.x

Gritsun, T. A., Le Feber, J., Stegenga, J., and Rutten, W. L. (2010). Network bursts in cortical cultures are best simulated using pacemaker neurons and adaptive synapses. *Biol. Cybern.* 102, 293–310. doi: 10.1007/s00422-010-0366-x

Ham, M. I., Bettencourt, L. M., McDaniel, F. D., and Gross, G. W. (2008). Spontaneous coordinated activity in cultured networks: analysis of multiple ignition sites, primary circuits, and burst phase delay distributions. *J. Comput. Neurosci.* 24, 346–357. doi: 10.1007/s10827-007-0059-1

Haroush, N., and Marom, S. (2015). Slow dynamics in features of synchronized neural network responses. *Front. Comput. Neurosci.* 9:40. doi: 10.3389/fncom.2015.00040

Harsch, A., and Robinson, H. P. C. (2000). Postsynaptic variability of firing in rat cortical neurons: the roles of input synchronization and synaptic NMDA receptor conductance. *J. Neurosci.* 20, 6181–6192. doi: 10.1523/jneurosci.20-16-06181.2000

Hollmann, M., and Heinemann, S. (1994). Cloned glutamate receptors. *Annu. Rev. Neurosci.* 17, 31–108. doi: 10.1146/annurev.ne.17.030194.000335

Jenkins, M. A., and Traynelis, S. F. (2012). PKC phosphorylates GluA1-Ser831 to enhance AMPA receptor conductance. *Channels* 6, 60–64. doi: 10.4161/chan.18648

Jimbo, Y., Kawana, A., Parodi, P., and Torre, V. (2000). The dynamics of a neuronal culture of dissociated cortical neurons of neonatal rats. *Biol. Cybern.* 83, 1–20. doi: 10.1007/PL00007970

Kamioka, H., Maeda, E., Jimbo, Y., Robinson, H. P. C, and Kawana, A. (1996). Spontaneous periodic synchronized bursting during formation of mature patterns of connections in cortical cultures. *Neurosci. Lett.* 206, 109–112. doi: 10.1016/s0304-3940(96)12448-4

Keefer, E. W., Gramowski, A., and Gross, G. W. (2001). NMDA receptor-dependent periodic oscillations in cultured spinal cord networks. *J. Neurophysiol.* 86, 3030–3042. doi: 10.1152/jn.2001.86.6.3030

Klausberger, T., and Somogyi, P. (2008). Neuronal diversity and temporal dynamics: the unity of hippocampal circuit operations. *Science* 321, 53–57. doi: 10.1126/science.1149381

Krishek, B. J., Moss, S. J., and Smart, T. G. (1996). A functional comparison of the antagonists bicuculline and picrotoxin at recombinant GABAA receptors. *Neuropharmacology* 35, 1289–1298. doi: 10.1016/s0028-3908(96)00089-5

Kuroda, Y., Ichikawa, M., Muramoto, K., Kobayashi, K., Matsuda, Y., Ogura, A., et al. (1992). Block of synapse formation between cerebral cortical neurons by a protein kinase inhibitor. *Neurosci. Lett.* 135, 255–258. doi: 10.1016/0304-3940(92)90449-h

Legrand, J. C., Darbon, P., and Streit, J. (2004). Contributions of NMDA receptors to network recruitment and rhythm generation in spinal cord cultures. *Eur. J. Neurosci.* 19, 521–532. doi: 10.1111/j.0953-816x.2003.03143.x

Lin, Y-. C., Huang, Z.-H., Jan, I-. S., Yeh, C-. C., Wu, H-. J., Chou, Y-. C., et al. (2002). Development of excitatory synapses in cultured neurons dissociated from the cortices of rat embryos and rat pups at birth. *J. Neurosci. Res.* 67, 484–493.

Linne, M.-L, Oja, S. S., and Jalonen, T. O. (1996). Simultaneous detection of action potential current waveforms and single ion channel openings in rat cerebellar granule cells. *Int. J. Neural Syst.* 7, 377–384. doi: 10.1142/s0129065796000348

Lonardoni, D., Amin, H., Di Marco, S., Maccione, A., Berdondini, L., and Nieus, T. (2017). Recurrently connected and localized neuronal communities initiate coordinated spontaneous activity in neuronal networks. *PLoS Comput. Biol.* 13:e1005672. doi: 10.1371/journal.pcbi.1005672

Lonardoni, D., Di Marco, S., Amin, H., Maccione, A., Berdondini, L., and Nieus, T. (2015). "High-density MEA recordings unveil the dynamics of bursting events in Cell Cultures," in *Proceedings of the 37th Annual International Conference of the IEEE Engineering in Medicine and Biology Society (EMBC)*, (Milan: IEEE), 3763–3766. doi: 10.1109/EMBC.2015.7319212

Luhmann, H. J., Sinning, A., Yang, J. W., Reyes-Puerta, V., Stüttgen, M. C., Kirischuk, S., et al. (2016). Spontaneous neuronal activity in developing neocortical networks: from single cells to large-scale interactions. *Front. Neural Circuits* 10:40. doi: 10.3389/fncir.2016.00040

Maccione, A., Gandolfo, M., Tedesco, M., Nieus, T., Imfeld, K., Martinoia, S., et al. (2010). Experimental investigation on spontaneously active hippocampal cultures recorded by means of high-density MEAs: analysis of the spatial resolution effects. *Front. Neuroeng.* 3:4. doi: 10.3389/fneng.2010.00004

Maeda, E., Robinson, H. P., and Kawana, A. (1995). The mechanisms of generation and propagation of synchronized bursting in developing networks of cortical neurons. *J. Neurosci.* 15, 6834–6845. doi: 10.1523/jneurosci.15-10-06834.1995

Mann, E. O., and Paulsen, O. (2007). Role of GABAergic inhibition in hippocampal network oscillations. *Trends Neurosci.* 30, 343–349. doi: 10.1016/j.tins.2007.05.003

Manninen, T., Aćimović, J., Havela, R., Teppola, H., and Linne, M.-L. (2018). Challenges in reproducibility, replicability, and comparability of computational models and tools for neuronal and glial networks, cells, and subcellular structures. *Front. Neuroinform.* 12:20. doi: 10.3389/fninf.2018.00020

Marom, S., and Shahaf, G. (2002). Development, learning and memory in large random networks of cortical neurons: lessons beyond anatomy. *Q. Rev. Biophys.* 35, 63–87. doi: 10.1017/s0033583501003742

Martinez-Banaclocha, M. (2018). Ephaptic coupling of cortical neurons: possible contribution of astroglial magnetic fields? *Neuroscience* 370, 37–45. doi: 10.1016/j.neuroscience.2017.07.072

Martinoia, S., Bonzano, L., Chiappalone, M., and Tedesco, M. (2005). Electrophysiological activity modulation by chemical stimulation in networks of cortical neurons coupled to microelectrode arrays: a biosensor for neuropharmacological applications. *Sens. Actuators B. Chem.* 108, 589–596. doi: 10.1016/j.snb.2004.11.041

Mazzoni, A., Broccard, F. D., Garcia-Perez, E., Bonifazi, P., Ruaro, M. E., and Torre, V. (2007). On the dynamics of the spontaneous activity in neuronal networks. *PLoS One* 2:e439. doi: 10.1371/journal.pone.0000439

Meier, R., Egert, U., Aertsen, A., and Nawrot, M. P. (2008). FIND–a unified framework for neural data analysis. *Neural Netw.* 21, 1085–1093. doi: 10.1016/j.neunet.2008.06.019

Minlebaev, M., Ben-Ari, Y., and Khazipov, R. (2007). Network mechanisms of spindle-burst oscillations in the neonatal rat barrel cortex in vivo. *J. Neurophysiol.* 97, 692–700. doi: 10.1152/jn.00759.2006

Moody, W. J., and Bosma, M. M. (2005). Ion channel development, spontaneous activity, and activity-dependent development in nerve and muscle cells. *Physiol. Rev.* 85, 883–941. doi: 10.1152/physrev.00017.2004

Muramoto, K., Ichikawa, M., Kawahara, M., Kobayashi, K., and Kuroda, Y. (1993). Frequency of synchronous oscillations of neuronal activity increases during development and is correlated to the number of synapses in cultured cortical neuron networks. *Neurosci. Lett.* 163, 163–165. doi: 10.1016/0304-3940(93)90372-r

Murphy, T. H., Blatter, L. A., Wier, W. G., and Baraban, J. M. (1992). Spontaneous synchronous synaptic calcium transients in cultured cortical neurons. *J. Neurosci.* 12, 4834–4845. doi: 10.1523/jneurosci.12-12-04834.1992

Nakanishi, K., and Kukita, F. (1998). Functional synapses in synchronized bursting of neocortical neurons in culture. *Brain Res.* 795, 137–146. doi: 10.1016/s0006-8993(98)00283-2

Niedringhaus, M., Chen, X., Conant, K., and Dzakpasu, R. (2013). Synaptic potentiation facilitates memory-like attractor dynamics in cultured in vitro hippocampal networks. *PLoS One* 8:e57144. doi: 10.1371/journal.pone.0057144

O'Donovan, M. J. (1999). The origin of spontaneous activity in developing networks of the vertebrate nervous system. *Curr. Opin. Neurobiol.* 9, 94–104. doi: 10.1016/s0959-4388(99)80012-9

Okujeni, S., Kandler, S., and Egert, U. (2017). Mesoscale Architecture Shapes Initiation and Richness of Spontaneous Network Activity. *J. Neurosci.* 37, 3972–3987. doi: 10.1523/JNEUROSCI.2552-16.2017

Opitz, T., De Lima, A. D., and Voigt, T. (2002). Spontaneous development of synchronous oscillatory activity during maturation of cortical networks in vitro. *J. Neurophysiol.* 88, 2196–2206. doi: 10.1152/jn.00316.2002

Owens, D. F., and Kriegstein, A. R. (2002). Is there more to GABA than synaptic inhibition? *Nat. Rev. Neurosci.* 3, 715–727. doi: 10.1038/nrn919

Palmer, L. M., Shai, A. S., Reeve, J. E., Anderson, H. L., Paulsen, O., and Larkum, M. E. (2014). NMDA spikes enhance action potential generation during sensory input. *Nat. Neurosci.* 17, 383–390. doi: 10.1038/nn.3646

Parri, H. R., Gould, T. M., and Crunelli, V. (2001). Spontaneous astrocytic Ca2+ oscillations in situ drive NMDAR-mediated neuronal excitation. *Nat. Neurosci.* 4, 803–812. doi: 10.1038/90507

Parsons, C. G., Gruner, R., and Rozental, J. (1994). Comparative patch clamp studies on the kinetics and selectivity of glutamate receptor antagonism by 2,3-dihydroxy-6-nitro-7-sulfamoyl-benzo(F)quinoxaline (NBQX) and 1-(4-amino-phenyl)-4-methyl-7,8-methyl-endioxyl-5H-2,3-benzodiaze pine (GYKI 52466). *Neuropharmacology* 33, 589–604. doi: 10.1016/0028-3908(94)90163-5

Pfeffer, C. K., Stein, V., Keating, D. J., Maier, H., Rinke, I., Rudhard, Y., et al. (2009). NKCC1-dependent GABAergic excitation drives synaptic network maturation during early hippocampal development. *J. Neurosci.* 29, 3419–3430. doi: 10.1523/JNEUROSCI.1377-08.2009

Raichman, N., and Ben-Jacob, E. (2008). Identifying repeating motifs in the activation of synchronized bursts in cultured neuronal networks. *J. Neurosci. Methods* 170, 96–110. doi: 10.1016/j.jneumeth.2007.12.020

Ramakers, G. J., Corner, M. A., and Habets, A. M. (1990). Development in the absence of spontaneous bioelectric activity results in increased stereotyped burst firing in cultures of dissociated cerebral cortex. *Exp. Brain Res.* 79, 157–166.

Ramakers, G. J., de Wit, C., Wolters, P. S., and Corner, M. A. (1993). A developmental decrease in NMDA-mediated spontaneous firing in cultured rat cerebral cortex. *Int. J. Dev. Neurosci.* 11, 25–32. doi: 10.1016/0736-5748(93)90032-9

Reinartz, S., Biro, I., Gal, A., Giugliano, M., and Marom, S. (2014). Synaptic dynamics contribute to long-term single neuron response fluctuations. *Front. Neural Circuits* 8:71. doi: 10.3389/fncir.2014.00071

Rivera, C., Voipio, J., and Kaila, K. (2005). Two developmental switches in GABAergic signalling: the K+-Cl- cotransporter KCC2 and carbonic anhydrase CAVII. *J. Physiol.* 562, 27–36. doi: 10.1113/jphysiol.2004.077495

Robinson, H. P., Kawahara, M., Jimbo, Y., Torimitsu, K., Kuroda, Y., and Kawana, A. (1993). Periodic synchronized bursting and intracellular calcium transients elicited by low magnesium in cultured cortical neurons. *J. Neurophysiol.* 70, 1606–1616. doi: 10.1152/jn.1993.70.4.1606

Sanchez-Vives, M. V., and McCormick, D. A. (2000). Cellular and network mechanisms of rhythmic recurrent activity in neocortex. *Nat. Neurosci.* 3, 1027–1034. doi: 10.1038/79848

Shahaf, G., and Marom, S. (2001). Learning in networks of cortical neurons. *J. Neurosci.* 21, 8782–8788. doi: 10.1523/jneurosci.21-22-08782.2001

Sheng, M., and Lee, S. H. (2001). AMPA receptor trafficking and the control of synaptic transmission. *Cell* 105, 825–828. doi: 10.1016/s0092-8674(01)00406-8

Slomowitz, E., Styr, B., Vertkin, I., Milshtein-Parush, H., Nelken, I., Slutsky, M., et al. (2015). Interplay between population firing stability and single neuron dynamics in hippocampal networks. *eLife* 4:04378. doi: 10.7554/eLife.04378

Soriano, J., Rodriguez Martinez, M., Tlusty, T., and Moses, E. (2008). Development of input connections in neural cultures. *Proc. Natl. Acad. Sci. U.S.A.* 105, 13758–13763. doi: 10.1073/pnas.0707492105

Sun, J. J., and Luhmann, H. J. (2007). Spatio-temporal dynamics of oscillatory network activity in the neonatal mouse cerebral cortex. *Eur. J. Neurosci.* 26, 1995–2004. doi: 10.1111/j.1460-9568.2007.05819.x

Suresh, J., Radojicic, M., Pesce, L. L., Bhansali, A., Wang, J., Tryba, A. K., et al. (2016). Network burst activity in hippocampal neuronal cultures: the role of synaptic and intrinsic currents. *J. Neurophysiol.* 115, 3073–3089. doi: 10.1152/jn.00995.2015

Teppola, H., Okujeni, S., Linne, M.-L., and Egert, U. (2011). "AMPA, NMDA and GABAA receptor mediated network burst dynamics in cortical cultures *in vitro*," in *Proceedings of the 8th International Workshop on Computational Systems Biology (WCSB 2011)*, eds H. Koeppl, J. Aćimović, J. Kesseli, T. Mäki-Marttunen, A. Larjo, and O. Yli-Harja (Zürich: TICSP series), 181–184. arxiv.org/abs/1802.00217

Tetzlaff, C., Okujeni, S., Egert, U., Worgotter, F., and Butz, M. (2010). Self-organized criticality in developing neuronal networks. *PLoS Comput. Biol.* 6:e1001013. doi: 10.1371/journal.pcbi.1001013

Vajda, I., van Pelt, J., Wolters, P., Chiappalone, M., Martinoia, S., van Someren, E., et al. (2008). Low-frequency stimulation induces stable transitions in stereotypical activity in cortical networks. *Biophys. J.* 94, 5028–5039. doi: 10.1529/biophysj.107.112730

van Pelt, J., Wolters, P. S., Corner, M. A., Rutten, W. L. C., and Ramakers, G. J. A. (2004). Long-term characterization of firing dynamics of spontaneous bursts in cultured neural networks. *IEEE Trans. Biomed. Eng.* 51, 2051–2062. doi: 10.1109/TBME.2004.827936

Wagenaar, D. A., Pine, J., and Potter, S. M. (2004). Effective parameters for stimulation of dissociated cultures using multi-electrode arrays. *J. Neurosci. Methods* 138, 27–37. doi: 10.1016/j.jneumeth.2004.03.005

Wagenaar, D. A., Pine, J., and Potter, S. M. (2006). An extremely rich repertoire of bursting patterns during the development of cortical cultures. *BMC Neurosci.* 7:11. doi: 10.1186/1471-2202-7-11

Wang, D. D., and Kriegstein, A. R. (2011). Blocking early GABA depolarization with bumetanide results in permanent alterations in cortical circuits and sensorimotor gating deficits. *Cereb. Cortex* 21, 574–587. doi: 10.1093/cercor/bhq124

Wang, M., and Arnsten, A. F. T. (2015). Contribution of NMDA receptors to dorsolateral prefrontal cortical networks in primates. *Neurosci. Bull.* 31, 191–197. doi: 10.1007/s12264-014-1504-6

Weihberger, O., Okujeni, S., Mikkonen, J. E., and Egert, U. (2013). Quantitative examination of stimulus-response relations in cortical networks in vitro. *J. Neurophysiol.* 109, 1764–1774. doi: 10.1152/jn.00481.2012

Whittington, M. A., and Traub, R. D. (2003). Interneuron diversity series: inhibitory interneurons and network oscillations in vitro. *Trends Neurosci.* 26, 676–682. doi: 10.1016/j.tins.2003.09.016

Yang, J. W., Hanganu-Opatz, I. L., Sun, J. J., and Luhmann, H. J. (2009). Three patterns of oscillatory activity differentially synchronize developing neocortical networks in vivo. *J. Neurosci.* 29, 9011–9025. doi: 10.1523/JNEUROSCI.5646-08.2009

Yang, W., Miller, J. E., Carrillo-Reid, L., Pnevmatikakis, E., Paninski, L., Yuste, R., et al. (2016). Simultaneous multi-plane imaging of neural circuits. *Neuron* 89, 269–284. doi: 10.1016/j.neuron.2015.12.012

Yuste, R., and Katz, L. C. (1991). Control of postsynaptic Ca2+ influx in developing neocortex by excitatory and inhibitory neurotransmitters. *Neuron* 6, 333–344. doi: 10.1016/0896-6273(91)90243-s

Conflict of Interest Statement: The authors declare that the research was conducted in the absence of any commercial or financial relationships that could be construed as a potential conflict of interest.

Materials and Methods in *Supplementary material* section:

Pharmacology:

In pure gradual disinhibition the selected amount of PTX (0.1μM, 0.2μM, 0.3μM, 1μM, 2μM, 3μM) was applied to antagonize the $GABA_AR$-mediated ionotropic GABAergic transmission (Figure S1A, S1B, Table S1, Protocol id s1). In the case of gradual disinhibition after the acute application of excitatory receptor antagonist (AMPAR or NMDAR complete blockade), an increasing amount of PTX was gradually applied to first partially (0.1μM, 1μM) and then completely block the $GABA_AR$-mediated transmission (10μM, 40μM) (Figure S1C, S1D, Table S1, Protocol id s2, s3).

Experimental protocol:

In the case of gradual disinhibition ($GABA_AR$ blockade), a total of three cell cultures from two different preparations were studied. One culture was used solely for performing experiments on the gradual disinhibition of $GABA_AR$ (0.1, 0.2, 0.3, 1, 2, 3μM PTX). Two cultures were used for performing experiments on the gradual disinhibition of $GABA_AR$ (0.1, 1, 10, 40μM PTX) either after the acute AMPAR blockade (30μM NBQX) or the acute NMDAR blockade (30μM D-AP5). The experiments consisted of the following steps: **(1)** 25 min-long CTRL recording, **(2)** acute application of 30μM excitatory antagonist (NBQX in experiments with AMPAR blockade, D-AP5 in experiments with NMDAR blockade), **(3)** recording for 25min, **(4)** application of 0.1μM $GABA_AR$ antagonist (PTX), **(5)** recording for 25min, **(6)** application of 1μM PTX, **(7)** recording for 25min, **(8)** application of 10μM PTX, **(9)** recording for 25min, **(10)** application of 40μM PTX, and **(11)** recording for 25min (Figure S1C, Table s1, Protocol id s2, s3). After the application of the antagonist, the first ten minutes of the recording were not analyzed to avoid transition phases. The remaining 15 minutes of the recording were analyzed.

Relative overall firing rate and burst frequency computations:

The relative overall firing rate (OFR, [Hz]) and network burst frequency (BF, (NB/min)) were computed for each recording and then displayed as separate graph representations of the rates in in the cases of gradual application of the inhibitory receptor blockade (see Table s1, Protocol id s1, s2, s3) (Figures S1B, S1D). To compute the relative OFR, the number of all spikes was divided by the duration of the recording period in seconds. To compute the BF, the number of NBs was divided by the duration of the recording period in minutes. The values were normalized to CTRL condition by dividing the value with the CTRL value.

Characterization of burst measures:

For gradual disinhibition, burst measures were not normalized to CTRL and were displayed as a box plot representation of the pooled measures. Box plots show the median, 25^{th} and 75^{th} percentiles with whiskers extending to the minimal and maximal values, and the plus signs represent outliers (Figure S2B). Wilcoxon rank sum test and p-values were computed for all pooled burst measures between CTRL and each condition. Differences were considered to be significant when $p_{ranksum} < 0.001$. This significance is indicated with * in Figure S2B.

Interspike interval and interburst interval distributions:

The mean of ISI distributions from all cultures of the same condition were computed and the values of i were plotted on the x-axis with a logarithmic scale (log(TIME[sec]). Statistical analysis was performed for all ISIs between each condition in the same culture using Wilcoxon rank sum test and p-values. If the tests showed a similar result for the culture the differences were considered significant and were displayed as ***$p_{ranksum} < 0.001$, **$p_{ranksum} < 0.01$, *$p_{ranksum} < 0.05$ in Figure S3A.

The IBI distributions were computed and the values of i were plotted on the x-axis with a logarithmic scale. Statistical analysis was performed for all IBIs between each condition in the same culture using Wilcoxon rank sum test and p-values. If the tests showed a similar result for the culture, the differences were considered significant and were displayed as ***$p_{ranksum} < 0.001$, **$p_{ranksum} < 0.01$, *$p_{ranksum} < 0.05$ in Figures S3B.

Network recruitment time computed as cumulative relative number of active electrodes:

Cumulative number of electrodes recruited at the onset of a NB, relative to the CTRL, was computed for each condition and each culture. For each NB, the timing of the first spike at each electrode was stored. These stored spike times were used to compute a time vector as follows. We discretized the NB duration, starting at 0.5 s after the onset of NB and using the 0.0001 s discretization time step. For each discrete time step we counted the number of electrodes activated until that time, the obtained cumulative number of electrodes was stored into the time vector. Next, we pooled all the time vectors representing all NBs recorded from the same culture and condition. The mean value of activated electrodes was computed for each time step, by averaging over all NBs. The obtained results illustrate the speed of electrode recruitment, and are shown in Supplementary Figure S3C.

Similarity analysis of the activity propagation patterns:

Statistical analysis was performed for all CCs between each condition in the same culture using Wilcoxon rank sum test and p-values. If the tests showed a similar result for the culture the differences were considered significant and was displayed as ***$p_{ranksum} < 0.001$, **$p_{ranksum} < 0.01$, *$p_{ranksum} < 0.05$ in Figures S4B.

Results in *Supplementary material* section:

Quantitative characterization of $GABA_A$Rs: reduced overall spiking and slowing down the activity propagation

The fast ionotropic $GABA_A$Rs are the main mediator of the inhibitory activity in neuronal networks beside the metabotropic $GABA_B$Rs. The $GABA_A$Rs contributed to the overall network excitability via reduction of network activity. In the temporal domain, the $GABA_A$Rs reduced the overall spiking activity of NBs during both the early and late phases of the NBs as well as slowed down the activity propagation and spiking during the NBs. In the spatial domain, $GABA_A$Rs effectively reduced the number of active electrodes attending to NBs.

In order to study the influence of $GABA_A$Rs on network activity dynamics, the networks were gradually disinhibited in a concentration-dependent manner by applying increasing concentrations of picrotoxin (0.1, 0.2, 0.3, 1, 2, and 3μM PTX, the total added PTX concentration was 6.6μM). Our results showed that the OFR gradually increased to almost four-fold while BF increased only mildly in comparison to the CTRL condition (Figure S1B). When applying 2μM (the total concentration was 3.6μM) and 3μM (in total 6.6μM) of PTX, the NB measures including the BL, FP, MFR, BS and RC significantly increased ($p < 0.001$) when compared to the CTRL condition (Figure S2B (**top row**)). The rising phase significantly decreased ($p < 0.001$) when applying 0.3, 1, 2 and 3μM PTX in comparison to the CTRL condition (Figure S2B (**top row**)). The duration of ISIs significantly decreased ($p < 0.001$) with the PTX in comparison to the CTRL condition (Figure S3A (**left panel**)), indicating more frequent spiking activity in disinhibited networks. The recruitment time of neurons at the beginning of the NBs gradually decreased by disinhibition, meaning faster recruitment of activity (Figure S3C (**leftmost panel**)). The results of a similarity analysis of the activity propagation patterns indicate that the gradual $GABA_A$R blockade significantly increased ($p_{ranksum} < 0.001$) the similarity (Figure S4A, S4B).

$GABA_A$Rs dampen the termination phase of network bursts and decrease the burst frequency in the NMDAR-mediated networks:

To assess how $GABA_A$ receptors shape the NMDAR-mediated spontaneous NB dynamics, first the AMPARs were acutely blocked (30μM NBQX, i.e. NMDAR-mediated networks), and then the networks were gradually disinhibited by applying 0.1, 1, 10 and 40μM PTX (the total added PTX concentration was 51.1μM). After AMPAR blocking (30μM of NBQX), the OFR dropped to about half of the control value and BF almost to zero in comparison to the CTRL condition. Further gradual disinhibition (with 0.1, 1, 10 and 40μM of PTX) brings the OFR to levels comparable to or higher than the CTRL condition, reaching about 1.7 of the CTRL value when disinhibited with the highest concentration of PTX. In addition, disinhibition restored the BF to about half of the control value (Figure S1D). However, disinhibition did not increase the OFR or BF in the NMDAR-mediated networks as much as in the AMPAR-mediated networks (30μM D-AP5) or in the solely disinhibited networks (Figures S1B, S1D). The results indicate that AMPARs are crucial for the higher firing rate within the NBs when networks were disinhibited and that NMDAR-mediated spiking was not similarly inhibited as AMPAR-mediated spiking by $GABA_A$Rs (Figure S1B, S1D). A more detailed analysis of the burst measures showed that the NMDAR-mediated BL, FP and BS decreased when networks were disinhibited in comparison to inhibited networks, meaning that $GABA_A$Rs dampened the termination of NBs (Figures S2A, S2B (**middle row)**). The number of active electrodes significantly increased ($p < 0.001$) by disinhibition in NMDAR-mediated networks in comparison to the CTRL condition. This result indicates that the disinhibition increased the spatial coverage of network activity in NMDAR-mediated networks (Figure S2B (**rightmost panel in middle row)**). The AMPAR blockade (30μM NBQX) significantly prolonged the ISIs (Figure S3A (**middle panel)**). Although the disinhibition shortened the ISIs in comparison to the AMPAR blocked condition, the ISIs were still significantly longer ($p < 0.001$) after disinhibition when compared to the CTRL condition (Figure S3A (**middle panel)**). These results demonstrate that disinhibition is not able to significantly increase spiking frequency within the NMDAR-mediated NBs (Figure S3A (**middle panel)**). The gradual disinhibition significantly shortened ($p < 0.001$) the IBIs when compared to the AMPAR blocked condition (Figure S3B (**middle panel)**). The recruitment time of neurons increased in NMDAR-

mediated networks and began to decrease when the networks were further disinhibited (Figure S3C (**middle panel**)). However, disinhibition in NMDAR-mediated NBs did not shorten the recruitment time to the level of the CTRL condition, assuring that AMPARs are crucial for the fast activity propagation at the beginning of the NBs.

$GABA_A$Rs contribute to inhibiting the spiking frequency and preventing the fast spread of activity propagation in the AMPAR-mediated networks:

In order to study the influence of $GABA_A$ receptors on shaping the AMPAR-mediated NB activity dynamics, the NMDARs (30µM D-AP5) were acutely blocked and continued to gradually disinhibit the networks by applying 0.1, 1, 10 and 40µM of PTX (the total added PTX concentration was 51.1µM). The results showed that the total gradual disinhibition in the AMPAR-mediated networks (30µM D-AP5) increased the OFR over threefold and BF only mildly, similarly to solely disinhibited cultures (Figure S1D (**black lines**)). A more detailed analysis of the burst measures demonstrated that the BL, FP, RP, MFR, BS and RC significantly decreased ($p < 0.001$) in AMPAR-mediated networks in comparison to the CTRL condition (Figure S2B (**bottom row**)). The gradual disinhibition did not significantly increase the BL, FP or RP in the AMPAR-mediated networks in comparison to the CTRL condition (Figure S2B (**bottom row**)). The antagonist of the NMDARs effectively removed the late phase of network burst profiles. The late phase was not restored by subsequent disinhibition (Figure S2A (**bottom row**), S2B (**bottom row**)). Furthermore, disinhibition significantly increased ($p < 0.001$) the MFR, BS and RC in AMPAR-mediated networks in comparison to the CTRL condition, meaning that $GABA_A$Rs strongly inhibited the AMPAR-mediated spiking within the NBs (Figure S2B (**bottom row**)). The ISI distributions did not change by NMDAR blockade (30µM D-AP5) (Figure S3A (**left panel**)). Disinhibition significantly shortened ($p < 0.001$) the ISIs only when using as high concentrations as 10µM and 40µM of PTX (Figure S3A (**left panel**)), suggesting important interplay between the $GABA_A$Rs-mediated inhibition and the AMPAR-mediated fast spiking. The NMDAR blockade (30µM D-AP5) increased the IBIs, but disinhibition did not change them in AMPAR-mediated networks in comparison to the CTRL condition (Figure S3B (**left panel**)). The recruitment time of neurons decreased when blocking the NMDARs and continued to decrease when gradually applying increasing concentrations of PTX (Figure S3C (**rightmost panel**)), meaning that NMDARs and $GABA_A$Rs slow down the network recruitment.

Table S1. List of supplemental protocols including recording conditions, blocked and functional receptors and the number of used cultures.

Protocol id	Recording condition/ Drug	Concentration of an antagonist	Blocked receptors	Functional receptors among the considered ones	Number of cultures
Gradual disinhibition					
s1	CTRL PTX	- .1, .2, .3, 1, 2, 3μM (in total 6.6μM)	None $GABA_A$	All AMPA, NMDA	1
Gradual disinhibition after the acute application of the excitatory receptor antagonists					
s2	CTRL NBQX PTX	- 30μM .1, 1, 10, 40μM (in total 51.1μM)	None AMPA $GABA_A$	All NMDA, $GABA_A$ NMDA	1
S3	CTRL D-AP5 PTX	- 30μM .1, 1, 10, 40μM (in total 51.1μM)	None NMDA $GABA_A$	All AMPA, $GABA_A$ AMPA	1

Supplementary Figures:

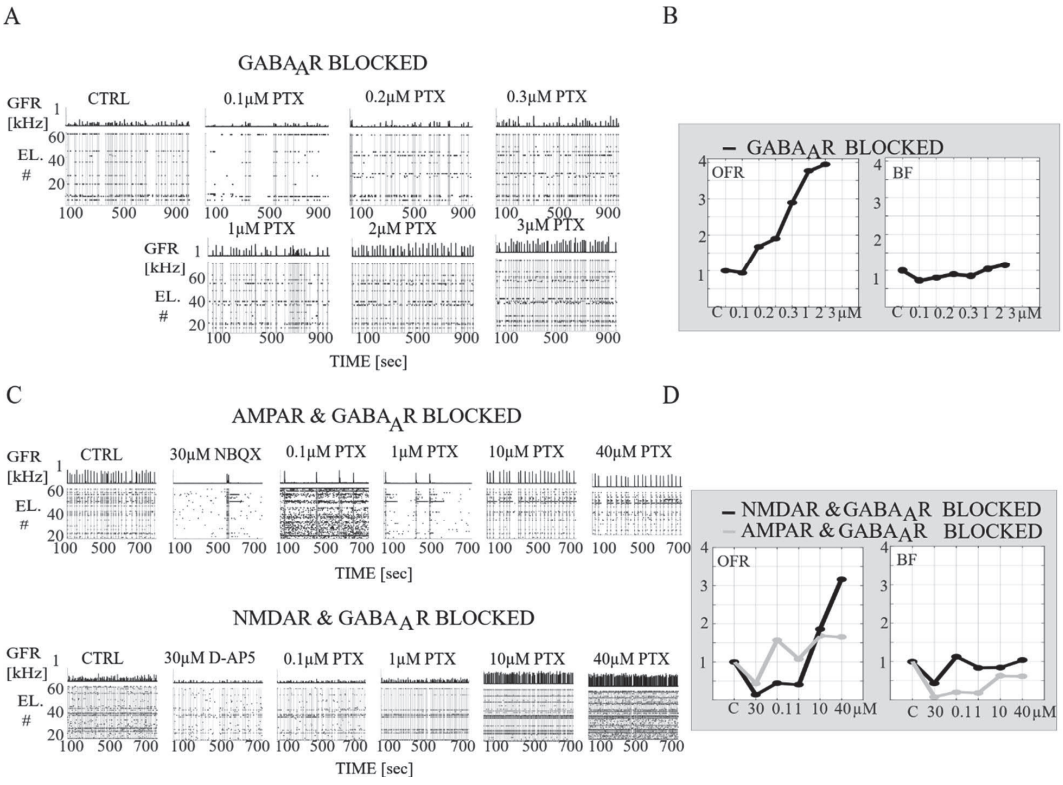

S1. Receptor-dependent network-wide activity probed by **gradual disinhibition**, relative changes in OFR [Hz] and in BF (NB/min). **(A)** and **(C)** Raster plots of network activity of the CTRL recording probed by three different types of gradual application of GABA$_A$Rs antagonist (PTX). In each subpanel, the global firing rates (GFR, [kHz]) are displayed on top of raster plots of spike times [sec] from electrodes (EL #) in each condition. **(A)** The recording period of 900 seconds from network probed by a gradual application of GABA$_A$R antagonist (0.1, 0.2, 0.3, 1, 2, and 3μM PTX). **(C)** The top row shows the recording from the network that is probed first by an acute application of AMPAR antagonist (30μM NBQX) and then by a gradual application of GABA$_A$R antagonist (0.1, 1, 10, and 40μM PTX). The bottom row shows the recording from the network that is probed first by an acute application of NMDAR antagonist (30μM D-AP5), and then by a gradual application of GABA$_A$R antagonist (0.1, 1, 10, and 40μM PTX). **(B)** and **(D)** Relative changes in OFR and in BF with respect to those obtained from the CTRL condition as shown for each recording. The relative change is computed as described in the *Materials and Methods* section. The values of the applied concentrations of each antagonist are shown on the x-axis. The disinhibition of the CTRL culture increased the OFR, but only slightly the BF **(B)**. Acute 30μM AMPAR and NMDAR antagonists decreased the OFR and BF **(D)**. An acute application of AMPAR antagonist decreased the BF more than the NMDAR antagonist **(D)**. In contrast, an acute application of NMDAR antagonist decreased the OFR more than AMPAR antagonist **(D)**. Pure disinhibition increased the OFR four fold **(B)**. The disinhibition of the NMDAR blocked culture

increased the OFR more than three fold **(black line in D)** similarly to pure disinhibition **(B)**. However, the disinhibition of the AMPAR blocked culture increased the OFR only 1.6 fold **(grey line in D)**.

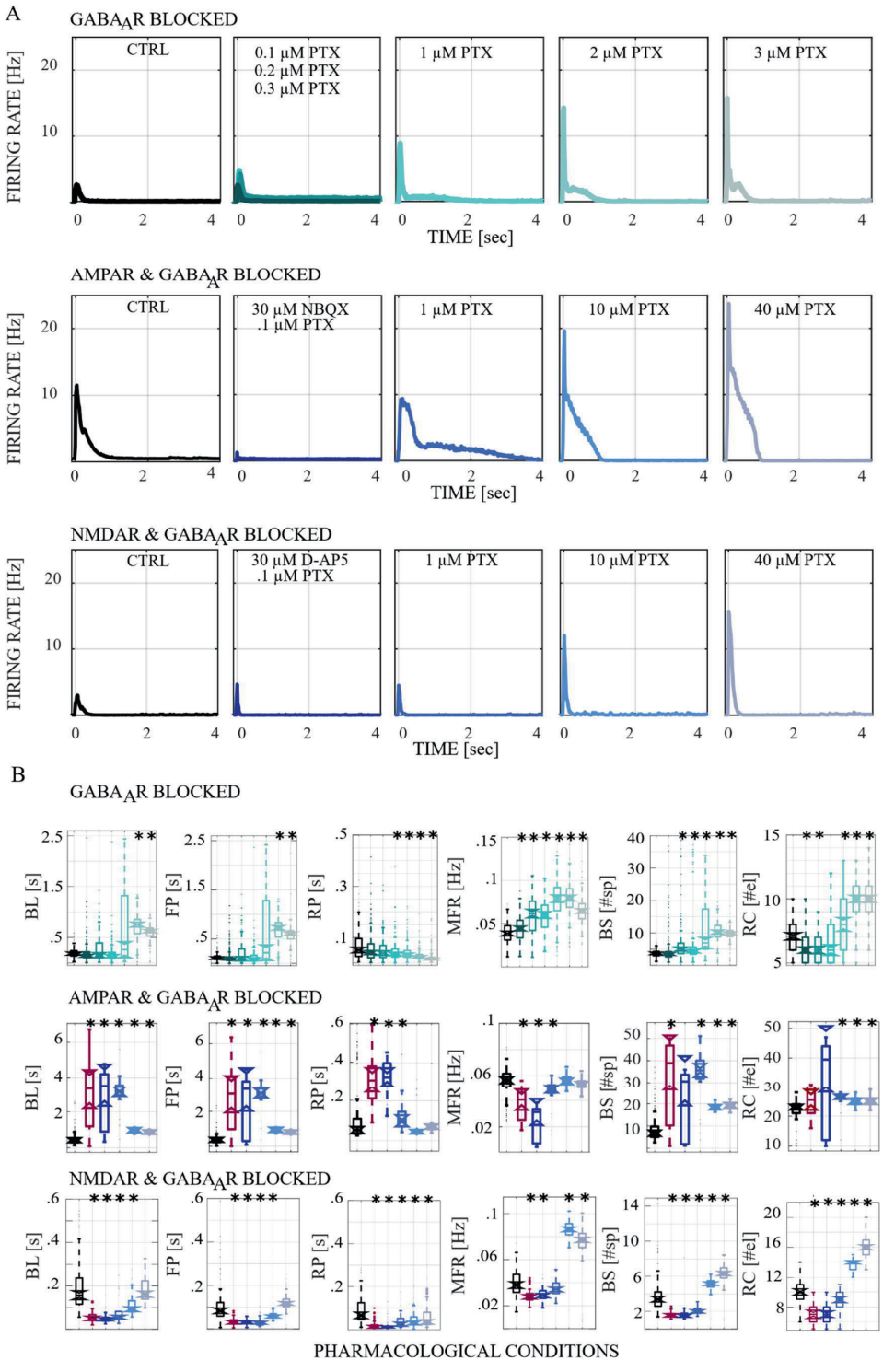
A
GABA$_A$R BLOCKED
CTRL
0.1 µM PTX
0.2 µM PTX
0.3 µM PTX
1 µM PTX
2 µM PTX
3 µM PTX
FIRING RATE [Hz]
TIME [sec]
AMPAR & GABA$_A$R BLOCKED
CTRL
30 µM NBQX
.1 µM PTX
1 µM PTX
10 µM PTX
40 µM PTX
NMDAR & GABA$_A$R BLOCKED
CTRL
30 µM D-AP5
.1 µM PTX
1 µM PTX
10 µM PTX
40 µM PTX
B
GABA$_A$R BLOCKED
AMPAR & GABA$_A$R BLOCKED
NMDAR & GABA$_A$R BLOCKED
BL [s]
FP [s]
RP [s]
MFR [Hz]
BS [#sp]
RC [#el]
PHARMACOLOGICAL CONDITIONS

S2. The influence of **gradual disinhibition** on network burst profiles and burst measures. **(A)** The top row compares the burst profiles [Hz] of CTRL data to the data collected after blocking $GABA_A$Rs with .1, .2, .3, 1, 2 and 3μM PTX. The middle row compares the CTRL with the data collected after acutely antagonized AMPARs (30μM NBQX) and gradually antagonizing $GABA_A$Rs (.1, 1, 10 and 40μM PTX). The bottom row shows the similar comparison as the middle row, except that in this case NMDARs are acutely antagonized (30μM D-AP5) and $GABA_A$Rs are again gradually antagonized (.1, 1, 10, and 40μM PTX). The presented profiles are computed using the spike-data from Figure S.1. The colors on the A and B panels corresponds to each condition and indicates the applied concentration of an antagonist. **(B)** The changes of characteristic burst measures computed from burst profiles are shown in **(A)**, including BL, FP, RP, MFR, BS and RC (see *Materials and Methods*). The top row shows the data from the experiment where the $GABA_A$Rs are gradually blocked, the middle row shows acute AMPAR blockade with gradual $GABA_A$R blockade and the bottom row acute NMDAR blockade with gradual $GABA_A$R blockade, similar to **(A)**. Each box plot represents the median, 25^{th} and 75^{th} percentiles and whiskers extending to minimal and maximal values. **Top row**; BL, FP and BS significantly increased ($p_{\text{ranksum}} < 0.001$) when using 2 and 3μM PTX compared to CTRL. RP significantly decreased ($p_{\text{ranksum}} < 0.001$) when applying .3, 1, 2 and 3μM PTX, MFR significantly increased ($p_{\text{ranksum}} < 0.001$) with all concentrations of PTX and RC first significantly decreased ($p_{\text{ranksum}} < 0.001$) when using .1 and .2μM PTX and then significantly increased ($p_{\text{ranksum}} < 0.001$) when applying 1, 2 and 3μM PTX. **Middle row**; BL, and FP significantly increased ($p_{\text{ranksum}} < 0.001$) first when using 30μM NBQX and then when applying .1, 1, 10 or 40μM PTX compared to CTRL. However, BL, FP, RP and BS remarkably decreased with 10 and 40μM PTX when compared to lower PTX concentrations. RP significantly increased and MFR significantly decreased ($p_{\text{ranksum}} < 0.001$) when using 30μM NBQX and when applying .1 and 1μM PTX. BS significantly increased ($p_{\text{ranksum}} < 0.001$) when using 30μM NBQX and when applying 1, 10 and 40μM PTX. RC significantly increased when using 1, 2 and 3μM PTX. **Bottom row**: BL and FP significantly decreased after 30μM D-AP5 and after .1, 1 and 10μM disinhibition. However, in contrast to the AMPAR and $GABA_A$R blocked case BL and FP increased by growing disinhibition with NMDAR antagonist. RP also significantly decreased ($p_{\text{ranksum}} < 0.001$) in all conditions compared to CTRL. MFR, BS and RC significantly decreased ($p_{\text{ranksum}} < 0.001$) when applying 30μM D-AP5 and when using .1μM PTX. On the contrary, MFR, BS and RC significantly increased ($p_{\text{ranksum}} < 0.001$) when PTX was increased to 10 and 40μM. Interestingly, burst measures change in opposite directions depending on whether AMPAR or NMDAR blockade is involved. In addition, disinhibition alters the burst measures in opposite directions depending on whether AMPARs or NMDARs are blocked first. *$p_{ranksum} < 0.001$.

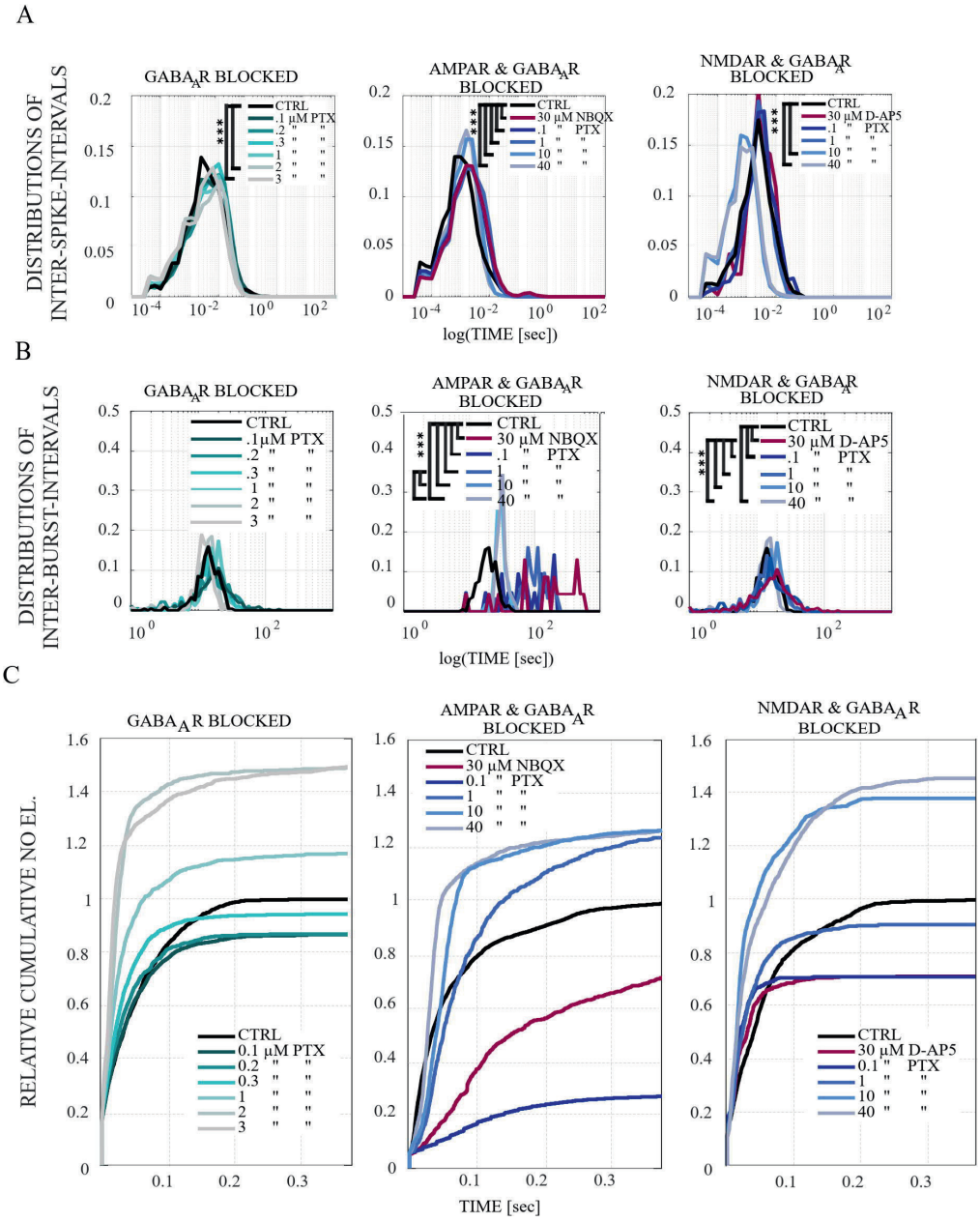

S3. (A) The excitatory and inhibitory receptor dependence on interspike intervals within NBs. Neurons in gradually disinhibited network first expressed significantly shorter ISIs when applying 2 and 3µM PTX ($p_{\text{ranksum}} < 0.001$) compared to CTRL **(left panel).** The acute application of 30µM NBQX significantly increased ISIs ($p_{\text{ranksum}} < 0.001$) similarly to the gradual blockade of AMPARs in comparison to the CTRL condition. Gradual disinhibition with .1, 1, 10 and 40 µM PTX

gradually decreased ISIs in comparison to the condition with AMPAR blockade (30µM NBQX). However, the fractions of ISI distributions were still significantly higher in comparison to the CTRL condition ($p_{ranksum} < 0.001$) **(middlet panel).** ISI distribution did not differ in an acutely NMDAR blocked network (30µM D-AP5). Interestingly, disinhibition with 10 and 40µM PTX clearly shifts ISI distributions towards the lower fractions in a NMDAR and $GABA_AR$ blocked network, meaning significantly shorter distances between spikes within NBs in neurons without functional NMDARs and $GABA_ARs$ ($p_{ranksum} < 0.001$) **(right panel)**. **(B)** A change in the excitatory and inhibitory receptor balance modulates the duration of interburst intervals and thus the frequency of NB events. Neurons in gradually disinhibited networks expressed significantly shorter IBIs than in CTRL networks when the concentration of PTX was 3µM ($p_{ranksum} < 0.05$) **(left panel)**. A significantly longer fraction of intervals was computed after acute AMPAR blockade (30µM NBQX) and with all concentrations of PTX (.1, 1, 10 and 40µM) compared to CTRL ($p_{ranksum} < 0.001$) **(middle panel)**. Disinhibition with 10 and 40µM PTX after acute NMDAR blockade (30µM D-AP5) shifted the IBI distributions to lower fractions compared to CTRL ($p_{ranksum} < 0.001$), meaning shorter distances between NBs **(right panel)**. Wilcoxon rank sum test and p-values were computed for all ISIs and IBIs in each condition and in each culture. If the tests showed similar results and p-values for every culture, the results were displayed in **(A)**, and **(B)**. $***p_{ranksum} < 0.001$, $**p_{ranksum} < 0.01$, $*p_{ranksum} < 0.05$. The x-scale is logarithmic. **(C)** A change in the excitatory and inhibitory receptor balance modulates network-wide electrode recruitment speed at the beginning of the bursts. Gradual disinhibition by $GABA_AR$ blockade remarkably sped up the network recruitment speed as well as increased the number of active electrodes in all three cultures with increasing concentrations of the $GABA_AR$ antagonist PTX. The first example on the left shows the increasing influence of the gradual application of the $GABA_ARs$ antagonist (0.1, 0.2, 0.3, 1, 2, 3µM PTX) on the electrode recruitment speed **(left panel)**. The second, middle example shows that the acute AMPAR blockade (30µM NBQX) first slows down the electrode recruitment speed with less active electrodes, and the gradual disinhibition with PTX (0.1, 1, 10, 40µM) accelerated it, starting with 1µM PTX in comparison to the AMPAR blocked condition (middle panel). An acute NMDAR blockade with D-AP5 (30µM) sped up the electrode recruitment speed with less active electrodes in comparison to the CTRL condition. The gradual disinhibition with PTX (0.1, 1, 10, 40µM) gradually increased the number of active electrodes and further accelerated the recruitment speed **(right panel).** The disinhibition of the network by the $GABA_AR$ antagonist by gradual **(C)** application increased the recruitment speed even more than the NMDAR blockade. Values were normalized to the CTRL conditions. Bin width is 0.1ms.

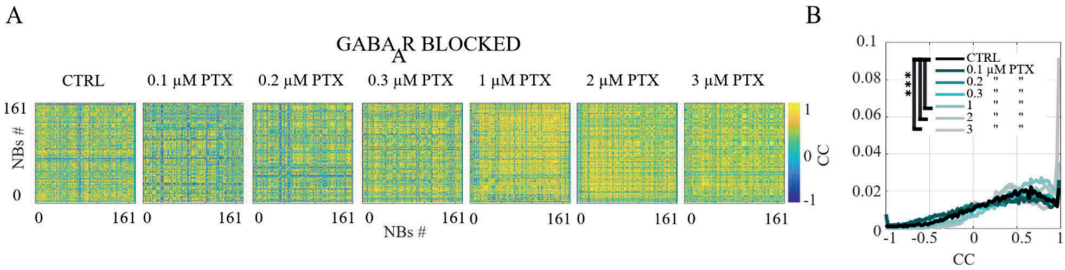

S4. (A) Correlation coefficient (CC) matrices computed for pairwise-spike-time-difference matrices between each NB in each condition of gradual applications. **(B)** Mean distributions of CC across the NBs and networks are shown. The gradual $GABA_AR$ blockade changed slightly the CC matrices ($N = 161$ NBs). The gradual $GABA_AR$ blockade with 1, 2, and 3µM PTX significantly increased ($p_{ranksum} < 0.001$) the similarity between spatio-temporal patterns in comparison to the CTRL condition**.**

PUBLICATION III

Analysis of Cellular and Synaptic Mechanisms behind Spontaneous Cortical Activity *in vitro*: Insights from Optimization of Spiking Neuronal Network Models

Aćimović J, Mäki-Marttunen T, Teppola H, Linne M-L

Submitted Manuscript, 2021
DOI:10.1101/2021.10.28.466340

PUBLICATION IV

Morphological Differentiation Towards Neuronal Phenotype of SH-SY5Y Neuroblastoma Cells by Estradiol, Retinoic Acid, and Cholesterol

Teppola H, Sarkanen J-R, Jalonen TO, Linne M-L

Neurochemical Research, 2016; 41(4):731–747
DOI:10.1007/s11064-015-1743-6A

Neurochem Res
DOI 10.1007/s11064-015-1743-6

ORIGINAL PAPER

Morphological Differentiation Towards Neuronal Phenotype of SH-SY5Y Neuroblastoma Cells by Estradiol, Retinoic Acid and Cholesterol

Heidi Teppola[1] · Jertta-Riina Sarkanen[2] · Tuula O. Jalonen[3] · Marja-Leena Linne[1]

Received: 19 July 2015 / Revised: 16 October 2015 / Accepted: 17 October 2015

Abstract Human SH-SY5Y neuroblastoma cells maintain their potential for differentiation and regression in culture conditions. The induction of differentiation could serve as a strategy to inhibit cell proliferation and tumor growth. Previous studies have shown that differentiation of SH-SY5Y cells can be induced by all-*trans*-retinoic-acid (RA) and cholesterol (CHOL). However, signaling pathways that lead to terminal differentiation of SH-SY5Y cells are still largely unknown. The goal of this study was to examine in the RA and CHOL treated SH-SY5Y cells the additive impacts of estradiol (E_2) and brain-derived neurotrophic factor (BDNF) on cell morphology, cell population growth, synaptic vesicle recycling and presence of neurofilaments. The above features indicate a higher level of neuronal differentiation. Our data show that treatment for 10 days in vitro (DIV) with RA alone or when combined with E_2 (RE) or CHOL (RC), but not when combined with BDNF (RB), significantly ($p < 0.01$) inhibited the cell population growth. Synaptic vesicle recycling, induced by high-K^+ depolarization, was significantly increased in all treatments where RA was included (RE, RC, RB, RCB), and when all agents were added together (RCBE). Specifically, our results show for the first time that E_2 treatment can alone increase synaptic vesicle recycling in SH-SY5Y cells. This work contributes to the understanding of the ways to improve suppression of neuroblastoma cells' population growth by inducing maturation and differentiation.

Keywords Brain-derived neurotrophic factor · Cholesterol · Differentiation · Estradiol · Retinoic acid · SH-SY5Y

Abbreviations

AChE	Acetylcholinesterase
Arc	Activity-regulated cytoskeleton associated protein
BDNF	Brain-derived neurotrophic factor
CHOL	Cholesterol
CO_2	Carbon dioxide
CTNF	Corrected total neurofilament fluorescence
DIV	Days in vitro
E_2	Estradiol
ER	Estrogen receptor
LTP	Long-term potentiation
NF-68	Neurofilament 68 kD
PBS	Phosphate-buffered saline
RA	All-*trans* retinoic acid
RB	All-*trans* retinoic acid with BDNF
RC	All-*trans* retinoic acid with CHOL
RCB	All-*trans* retinoic acid with CHOL and BDNF
RCBE	All-*trans* retinoic acid with CHOL, BDNF and E_2
RE	All-*trans* retinoic acid with E_2
RT	Room temperature
TrkB	Tropomyosin-related kinase B

Tuula O. Jalonen and Marja-Leena Linne are Co-senior authors.

✉ Heidi Teppola
heidi.teppola@tut.fi

[1] Department of Signal Processing, Tampere University of Technology, P.O. Box 553, 33101 Tampere, Finland

[2] Department of Cell Biology, School of Medicine, University of Tampere, Tampere, Finland

[3] Department of Physiology and Neuroscience, St. George's University School of Medicine, St. George's, Grenada, West Indies

Published online: 30 October 2015

Introduction

Neuroblastoma is the most common extra-cranial solid malignant tumor of sympathetic nervous system in infants and young children [1]. Regardless of its stage, until today, there is no cure or treatment, which could offer good prognosis for patients [2, 3]. Human SH-SY5Y cell line, used in this study, is a subclone of SK-N-SH cell line which was isolated from a bone marrow of a 4 year-old female patient [4]. SH-SY5Y cells maintain their potential for regression, which results in aggressive proliferation of these cells [5]. Novel therapeutic treatments inducing differentiation into neuronal cell types could help to improve the prognosis of children suffering from neuroblastoma [6]. The induction of differentiation could serve as a strategy to inhibit cell population growth and eventually stop the tumor growth, as well as induce healthy mature neurons in patients.

Previous studies have presented that differentiation of SH-SY5Y cells can be induced by dibutyryl cyclic AMP [5, 7], 12-*o*-tetradecanoyl-phorbol-13-acetate [8–13], all-*trans*-retinoic-acid (RA) [9, 14–16], brain-derived neurotrophic factor (BDNF) [17–19], vanadate [20], nerve growth factor [21, 22], cholesterol (CHOL) [23], vitamin D3, and neuregulin beta1 [24]. The signaling pathways that lead to terminal differentiation of SH-SY5Y cells, however, are still largely unknown.

The retinoic acid (RA) is a potent cell differentiating factor, which through its nuclear receptors affects a vast range of promoter sites in the neuronal and glial cells in every step of embryonic and postnatal life [25]. RA-induced differentiation has been shown to inhibit cell proliferation [9], change cellular sodium conductance [15], enhance the outgrowth of neurites [16], increase the acetylcholinesterase (AChE) activity [26, 27], and enhance the synaptic vesicle recycling [23]. However, clinical trials have demonstrated that treatment with RA alone, or in combination with interferon alpha, is not enough against recurrent neuroblastoma in children [28, 29]. Therefore, new alternative resources for more effective neuronal differentiation are needed.

Cholesterol (CHOL) is a necessary component in cell membranes and important for synaptic structure and function [30]. It is synthesized by neurons themselves for their survival and growth. The development of active synapses requires additional amount of cholesterol that is shown to be secreted by glial cells (specifically astrocytes) in the central nervous system [30–32] and by Schwann cells in the peripheral nervous system [33]. The glia-derived cholesterol has also been shown to be crucial for differentiation of dendrites, synaptogenesis, increase in synaptic protein expression (synapsin-1) and neuronal activity, and for transmitter release [30, 32, 34, 35]. In pure human SH-SY5Y cell cultures, the glia-derived cholesterol is non-existing, and addition of cholesterol is needed in order to achieve conditions resembling normal neuronal environment with surrounding glial cells [23].

The brain-derived neurotrophic factor (BDNF) has been shown to support the survival of neurons and stimulate the growth and differentiation of new neurons and synapses [36]. BDNF is a ligand for tropomyosin-related kinase B (TrkB) receptor, expression of which is lacking in naïve neuroblastoma cells. However, TrkB receptor expression and responsiveness to BDNF is induced by RA [37]. The activation of TrkB by BDNF has been suggested to enhance neuroblastoma cell survival and resistance to chemotherapy [38]. BDNF has also been shown to expose only a modest benefit for RA-induced arrest in a dormant state [6]. However, the sequential treatment of SH-SY5Y cells with RA and BDNF has been reported to induce differentiated, neurotrophic factor-dependent neuron-like cells [18] and sustained treatment has been reported to enhance neuronal differentiation of neural progenitor cells [39]. Moreover, RA-BDNF treatment induces significant increase in the expression of synaptic genes, brain miRNA, miRNA biogenesis machinery, and AChE activity, in comparison to sole RA treatment [19]. These studies stimulate the interest to further examine the potential therapeutic competence of BDNF for RA-induced SH-SY5Y cell differentiation and for treatment of neuroblastoma. Disruption of BDNF and its downstream signaling pathways have been observed in many neurodegenerative diseases such as Alzheimer's, Parkinson's and Huntington's diseases [40–42], underlining the importance of BDNF. However, the results of the role of added exogenous BDNF for differentiation of RA treated SH-SY5Y cells are still controversial.

Estradiol (17-beta-estradiol, E_2), a form of estrogen hormone, has both acute and long-term effects on a variety of neuronal cell types. Increase in the number of dendritic spines and number of excitatory synapses, which are the slow long-term effects of estradiol, were first detected [43–45]. The acute effects, which alter the intrinsic and synaptic physiology of neurons within minutes (reversible depolarization and increased input resistance with a latency of <1 min in 19.8 % of CA1 neurons tested) were detected later [46, 47]. Several studies have shown that estrogen enhances synaptogenesis and synaptic plasticity [48–55], which properties may be crucial for example in enhancing memory consolidation [43, 56]. Additionally, estrogen has been demonstrated to induce synaptic connectivity [52], enhance NMDA receptor expression and activity [57–66], and long-term potentiation (LTP) [58, 59, 64, 67]. Several earlier studies have addressed possible signaling

mechanisms associated with estrogen-induced cellular functions. Estrogen activates these functions through the activation of estrogen receptors (ERs), ERα and ERβ, which serve as transcription factors modifying the activity of target genes [68, 69]. Estrogen has been shown to increase the key synaptic proteins, e.g. PSD-95, via either activation of ERα [70], ERβ [51], or both [71]. Estrogen is thought to use both nuclear ERs and plasma membrane ERs which are usually referred to as classical genomic and non-genomic pathways [69]. In classical genomic action, ERs are thought to translocate into nucleus in ligand-dependent manner and acting as a transcription factor of target genes after prolonged estrogen exposure [72]. In non-genomic action, estrogen has been shown to activate the membrane ERs, which rapidly stimulate the membrane-associated signaling molecules such as PI-3K and MAPK, resulting in quick increase in protein expression [73, 74]. SH-SY5Y cells have been shown to express both ERα and ERβ [75]. Estrogen has also been shown to stimulate the activity-regulated cytoskeleton associated protein (Arc) expression via the MAPK and PI-3K dependent pathway in SH-SY5Y cells [48]. Arc is known to be induced by neuronal activity and playing a key role in activity-dependent synaptic plasticity [76]. Its knockdown has been shown to lead to impairment of long-term memory [77, 78]. However, the specific role of E_2 for inducing differentiation in human SH-SY5Y neuroblastoma cells is still unknown.

The main goal of the current study was to find a functional combination of substances for effective induction of differentiation of the SH-SY5Y cells. Based on our earlier studies, we used RA and CHOL as primary differentiation treatments [23]. We further investigated the ability of E_2 and BDNF to support, and possible enhance, the RA and CHOL induced neuronal differentiation. We quantified the individual and additive impacts of BDNF and E_2 on the RA and CHOL-induced neurite outgrowth, presence of neurofilament 68, synaptic vesicle recycling and arrest in the population growth rate of SH-SY5Y neuroblastoma cells in vitro.

Methods

Maintenance and Differentiation of Cell Cultures

The human SH-SY5Y neuroblastoma cell line (CRL-2266; American Type Culture Collection, Manassas, VA, USA) was cultured as previously described [23]. Briefly, the cells were plated at passage 29–30 with density of 5000 cells/cm^2 on 48-well culture dishes. Cells were cultured and maintained in 5 % CO_2 humidified incubator at 37 °C in 1:1 nutrient mixture F-12K Kaighn's modification, and minimum essential medium supplemented with 10 % fetal bovine serum, 2 mM/L L-glutamine, 1 % antibiotic–antimycotic mixture and 1 % non-essential amino acids (all reagents from GIBCO, Invitrogen, Carlsbad, CA, USA, unless otherwise stated). Cell differentiation was induced with 10 μM/L all-*trans* retinoid-acid (RA), 1 nM/L 17-beta-estradiol (E_2), 50 ng/mL brain-derived neurotrophic factor (BDNF), 10 μg/mL cholesterol (3β-hydroxy-5-cholestene, CHOL), or with combinations such as (i) 5 μM/L RA with 5 μg/mL CHOL (RC), (ii) 5 μM/L RA with 50 ng/mL BDNF (RB), (iii) 5 μM/L RA with 1 nM/L E_2 (RE), (iv) 5 μM/L RA with 5 μg/mL CHOL, and 50 ng/mL BDNF (RCB), and (v) 5 μM/L RA with 5 μg/mL CHOL, 50 ng/mL BDNF, and 1 nM/L E_2 (RCBE) for 10 DIV (all differentiation reagents from Sigma-Aldrich, St Louis, MO, USA, unless otherwise stated). Stock solutions of differentiation substances were diluted in 96 % ethanol; the final ethanol concentration never exceeded 0.1 % in cell culture. Control cells were treated with <0.1 % ethanol. All used substance concentrations were carefully evaluated according to already published literature. Suitable, least toxic concentrations, also used by other laboratories, were used to enable comparison of our results with others. All differentiation substances (except BDNF when used in combinations) were applied with medium exchange at 1, 3 and 7 DIV. BDNF was applied at 4 and 7 DIV when used together with RA (RB), RA and CHOL (RCB) or RA, CHOL and E_2 (RCBE). The cell growth, condition, and morphology were observed with culture microscope (Olympus CK40) and images were taken at 10 DIV DP10 microscope digital camera system (Olympus, Tokyo, Japan).

Neurofilament Staining

For detecting the level of differentiation in the neuroblastoma cell cultures, the cells were stained at 10 DIV with neuronal marker NF-68 for neurofilament light polypeptide (68 kDa, Sigma-Aldrich). Cells were first fixed for 20 min with 4 % paraformaldehyde (Sigma-Aldrich) in phosphate buffered saline solution (PBS), washed three times with PBS and permeabilized in 0.5 % Triton X-100 (J.T. Baker, Phillipsburg, NJ, USA) for 15 min. After washing with PBS, the non-specific antibody binding sites were blocked with 10 % bovine serum albumin (GIBCO) in PBS for 30 min to reduce the background. Cells were then incubated with the primary antibody mouse monoclonal anti-NF-68 1:200 for 1 h at room temperature (RT; +22 °C), rinsed three times with PBS, and then incubated with a secondary antibody FITC-conjugated goat anti-mouse IgG 1:100 (Sigma-Aldrich) for 30 min at RT. Fluorescence was visualized with Nikon Eclipse TS100 microscope equipped with Nikon DS Camera Control Unit DS L-1 and images were organized with Visio 2010 (Microsoft, WA, USA).

The intensity of total neurofilament fluorescence (NF-68) and the intensity of total background fluorescence were measured from each fluorescence image with ImageJ software (National Institute of Mental Health, Bethesda, Maryland, USA) [79]. Corrected total neurofilament fluorescence (CTNF) was calculated from the gathered data in Excel 2010 (Microsoft, WA, USA) with the method used previously [80, 81], as follows: The fluorescence of the neurofilaments of interest was selected using the selection tool. Area of interest, integrated density, and mean gray value were calculated from selected areas with ImageJ software. A region next to the selected neurofilament was selected as a background value. The CTNF was calculated by using the following equation CTNF = integrated density − (area of selected neurofilaments × mean fluorescence of background readings).

Quantification of Cell Population Growth

The substance-induced changes in the growth rate were quantified by counting the nuclei of 10 DIV cultured SH-SY5Y cells in each treatment group. Cell nuclei were stained with 10 μg/mL Hoechst 33258 (Sigma-Aldrich) for 5 min. Cultures were washed five times in PBS and mounted on cover slips. Fluorescence results were visualized with Nikon DS Camera Control Unit DS L-1. Images of each treatment group were analyzed with CellC analysis software [82], which corrects the image background for auto-fluorescence by fitting a two-dimensional quadratic polynomial to the image and subtracts the fitted polynomial surface from the original image. After this the algorithm separates the nuclei pixels from background pixels by global thresholding and produces a binarized image with white nuclei on a black background. It furthermore separates clustered nuclei from each other by marker-controlled watershed segmentation, which is based on nuclei intensity. Eventually the software removes artifacts, such as staining residues by discarding objects smaller than 1/10 of the mean size of all objects. Images were organized with Microsoft Visio 2010. The obtained nuclei counts and statistics (see section "Statistical Analysis") were analyzed and plotted in MATLAB (version 2013b, The Mathworks Inc., MA, USA).

Quantification of Neurite Length

The SH-SY5Y cells were cultured in CTRL, CHOL, E_2, BDNF, RA, RE, RB, RC and RCBE conditions at 10 DIV. Neurites were traced from phase contrast images of each treatment group with NeuronGrowth plugin [83] of the ImageJ software (National Institute of Mental Health, Bethesda, Maryland, USA) [79]. The NeuronGrowth automatically counts the length of traced neurites in pixels and exports the data. The gathered data and statistics were analyzed and plotted in MATLAB (version 2013b, The Mathworks Inc., MA, USA).

Synaptic Vesicle Recycling

The level of synaptic vesicle recycling was verified by measuring the number of fluorescence puncta in 10 DIV cultured SH-SY5Y cells. Cells were treated either with <0.1 % ethanol (CTRL), RA, CHOL, BDNF, E_2, or with their combinations. Cultures were stained with AM1-43 styryl dye (Biotium, Hayward, CA, USA) for detecting synaptic exo/endocytosis in cells. AM1-43 is a fixable nerve terminal probe. It is not able to pass through the membranes, but instead, when cells are depolarized with high potassium (K^+)-Tyrode solution, AM1-43 styryl dye attaches inside those vesicles, which are ongoing exocytosis. Staining was modified from method previously described [23, 84, 85]. In the current experiments, the cells were incubated for 1 min with 4 μmol/L AM1-43, according to manufacturer's protocol, with the depolarizing Tyrode solution including 80 mmol/L K^+ (80 mmol/L KCl, 29 mmol/L NaCl, 2 mmol/L $MgCl_2$, 30 mmol/L glucose, 25 mmol/L HEPES, 2 mmol/L $CaCl_2$). Cells were further washed several times with SCAS quencher solution (Biotium, Hayward, CA, USA) at RT to reduce background fluorescence. Cells were fixed for 20 min with 4 % paraformaldehyde (GIBCO), permeabilized in 0.01 % Triton X-100 (J.T. Baker) for 12 min and washed three times for 1 min in cold PBS. All reagents were from Sigma Aldrich unless otherwise stated. The fluorescence was visualized with Nikon Eclipse TS100 microscope equipped with Nikon DS Camera Control Unit DS L-1 and images were organized with Microsoft Visio 2010. Fluorescence images of each treatment group were analyzed with ImageJ analysis software [79] using the following procedural steps specifically designed to this study: background of the image was subtracted by setting a rolling ball radius to 50 pixels, after image was sharpened, and then the maxima of fluorescence puncta were found with noise tolerance of 20 and with the point selection style. This procedure was evaluated by visual inspection and it was found to be the best for finding the correct number of AM1-43 puncta from fluorescence images. The obtained counts of fluorescence puncta per image were divided by the obtained median nuclei number (see section "Quantification of Cell Population Growth") in particular culture in 10 DIV treatments. These obtained counts of fluorescence puncta per median nuclei number and statistics (see section "Statistical Analysis") were analyzed and plotted in MATLAB (version 2013b).

Table 1 Summary of differentiation

Treatment[†]	Neurite length	Total neurofilament fluorescence	Inhibition of cell population growth	Synaptic vesicle recycling
CTRL	−	−	−	−
CHOL	++**	−	−	−
E_2	+*	−	−	+*
BDNF	−	−	−	−
RA	+++**	+++**	+++**	++**
RE	+++**	++*	+++**	++**
RC	+++**	+++**	+++**	+++*
RB	+++**	+++**	++	++**
RCB	+++**	[‡]	[‡]	+++*
RCBE	+++**	+++**	[‡]	+++*

The criteria for categorizing the neurite length were as follows: − neurites similar to control, + short neurites without branching and significantly longer than in control [$p < 0.05$ (*)], ++ intermediate neurites without branching and significantly longer than in control [$p < 0.01$ (**)], +++ long neurites with branching and significantly longer than in control [$p < 0.01$ (**)] and in CHOL or E_2 treatment conditions [$p < 0.01$ (**)]. The criteria for categorizing the total neurofilament fluorescence were as follows: − no neurofilament fluorescence, ++ significantly [$p < 0.05$ (*)] increased neurofilament fluorescence compared to control, +++ significantly [$p < 0.01$ (**)] increased neurofilament fluorescence compared to control. The criteria for categorizing the inhibition of cell population growth were as follows: − the number of cells has not changed after the treatment, ++ the number of cells decreased (not significantly), +++ the number of cells significantly [$p < 0.01$ (**)] decreased. The criteria for categorizing the amount of synaptic vesicle recycling were as follows: − no significant change in the counts of puncta in comparison to control, + significant [$p < 0.05$ (*)] increase in the counts of fluorescence puncta in comparison to control, ++ significant [$p < 0.01$ (**)] increase in the counts of fluorescence puncta in comparison to control, +++ significant [$p < 0.05$ (*)] increase in the counts of fluorescence puncta in comparison to RE and RB

[†] Control (CTRL, <0.1 % ethanol), cholesterol (CHOL; 10 μg/ml), 17-beta-estradiol (E_2; 1 nM/L), brain derived neurotrophic factor (BDNF; 50 ng/mL), *all-trans* retinoic acid (RA; 10 μg/mL), RA with E_2 (RE; RA 5 μg/mL, E_2 1 nM/L), RA with CHOL (RC; RA 5 μg/mL, CHOL 5 μg/mL), RA with BDNF (RB; RA 5 μg/mL, BDNF 50 ng/mL), RA with CHOL and BDNF (RCB; RA 5 μg/mL, CHOL 5 μg/mL, BDNF 50 ng/mL), RA with CHOL, BDNF and E_2 (RCBE; RA 5 μg/mL, CHOL 5 μg/mL, BDNF 50 ng/mL, E_2 1 nM/L)

[‡] Conclusive data not available

Summary of the Level of Differentiation

Results are summarized in Table 1, which shows the level of differentiation induced by different treatments. The level of differentiation was assessed at least from three samples from two separate experiments by analyzing the following features; neurite length, presence of neurofilaments, inhibition in cell population growth rate and synaptic vesicle recycling. Neurite lengths were detected both visually and, by using automated methods to support the visual detection. Other features were defined according to the methods explained above (see sections "Neurofilament Staining, Quantification of Cell Population Growth and Synaptic Vesicle Recycling").

Statistical Analysis

Statistical analysis was performed using One-way ANOVA in MATLAB (version 2013b). Differences were considered to be significant when $p < 0.01$ or $p < 0.05$, different significances are indicated with ** or * in the figures, respectively.

Results

Morphology of Differentiated SH-SY5Y Cells

Phase contrast images of SH-SY5Y cultures at 10 DIV were first visually analyzed for morphological assessment. In the visual analysis, control cells showed no particular neurite outgrowth (Fig. 1a), whereas CHOL-treated cells had a number of short neurites (green arrows in Fig. 1b; see also Table 1). Cells treated with E_2 had very short neurites (Fig. 1c), which were both fewer and shorter than the CHOL-induced neurites. The morphology of BDNF treated SH-SY5Y was relatively polar and cells grew more spread in the culture dish (Fig. 1d). This differed from control cells, which grew in clusters (Fig. 1a). No significant outgrowth of neurites was observed after BDNF treatment. Treatment with RA alone (Fig. 1e) as well as with combinations such as RE, RB, RC, RCB or RCBE, induced branching of longer neurites and detectable network formation (Fig. 1f–j, respectively).

The data show other morphological differences between the treatments as well. The RE treated SH-SY5Y cells had

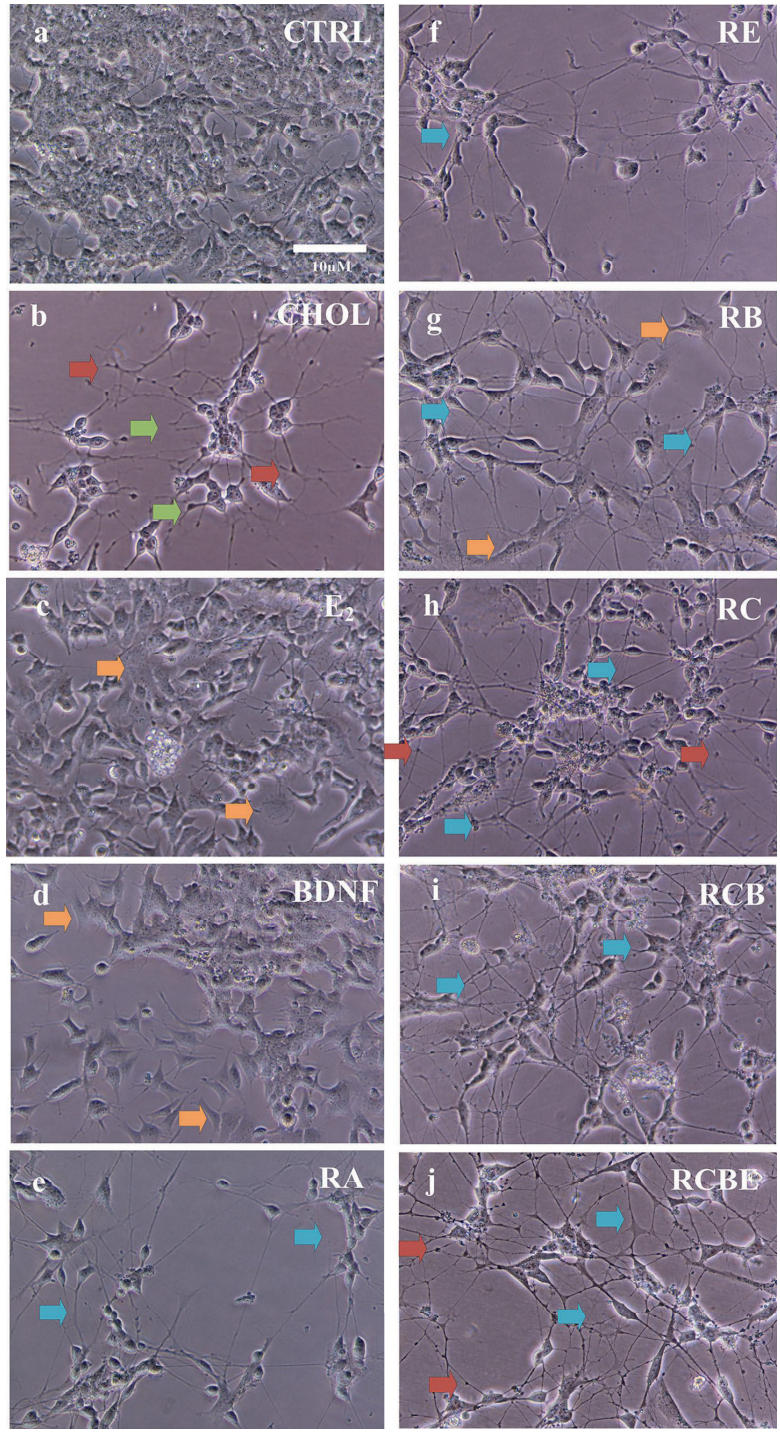

Fig. 1 Morphology and network formation of SH-SY5Y neuroblastoma cells at 10 DIV. **a** SH-SY5Y cells were grown for 10 DIV in control conditions (CTRL) and with **b** cholesterol (CHOL), **c** estradiol (E_2), **d** brain-derived neurotrophic factor (BDNF), **e** all-*trans* retinoic-acid (RA), or with their combinations **f**–**j** RE, RB, RC, RCB, RCBE, respectively. Data show that the CHOL treatment induced short neurites (*green arrows*) with many varicosities (*red arrows*) (**b**). E_2 induced few very short neurites in comparison to CHOL induced neurites (**c**). BDNF treatment did not induce significant growth of neurites or network formation (**d**). RA treatment generated thin branching neurites and promoted network formation (*blue arrows*, **e**). Networks of cells with cell-to cell contacts (*blue arrows*) were always detected when treated with RA together with **f** E_2 (RE), **g** BDNF (RB), **h** CHOL (RC), **i** CHOL and BDNF (RCB), and **j** CHOL, BDNF, and E_2 (RCBE). Flat substrate-adherent (S-type) cells were detected especially when cells were treated with E_2 or BDNF (*orange arrows*) (**c**, **d**) but also when cells were treated with RE (data not shown) or RB (*orange arrows*) (**g**). The RE treated cells (**f**) had thinner neurites than those treated with RCBE (**j**) (Color figure online)

networks of roundish cells with thin neurites without heavy branching (Fig. 1f). A small number of substrate-adherent (S-type) flat cells [86] were observed in cultures treated with RE (data not shown), RB (orange arrows in Fig. 1g) and RA (data not shown). The RB treatment induced networks that consisted of extended contacting neurites, as well as of cells in direct contact with each other without neurites. The neurites of the RB treated cells were thicker in comparison to RE induced neurites. The RC treatment induced cells with long, branching and connecting neurites (blue arrows in Fig. 1h). Other cholesterol treated cultures, such as RCB and RCBE, contained neurons with long branching neurites and network formation without S-type cells. More varicosities (red arrows in Fig. 1b) and small cell clusters (data not shown) were observed in CHOL treated cultures (CHOL, RC, RCB, RCBE) in comparison to the control, RE and RB treated groups, in which cells were more uniformly distributed (data not shown).

Inhibition of Cell Population Growth

The ability of a substance to inhibit the population growth of human SH-SY5Y cells is one of the indicators of increased level of differentiation. Therefore, we counted the numbers of the Hoechst 33258 stained nuclei at 10 DIV in RA, CHOL, BDNF, E_2, RE, RB, and RC treated cell cultures and compared the results to the number of nuclei in control conditions. The data demonstrated that CHOL, E_2 or BDNF treatments on their own did not inhibit the cell population growth (Fig. 2), which, however, was seen when treated with RA, as well as with RA together with CHOL (RC) [$p < 0.01$(**)] when compared to controls. Moreover, significant ($p < 0.01$ (**) inhibition was also detected with RA together with E_2 (RE) treatment, when compared to controls (Fig. 2). Interestingly, when cells were treated with RA and BDNF, no inhibition of growth was detected (Fig. 2).

Neurite Lengths

The neurites of SH-SY5Y cells were traced from phase contrast images taken from each experiment at 10 DIV with NeuronGrowth (see section "Methods"), which provides supportive information of the lengths in addition to the visual inspection of the cell morphology. In addition to RA [$p < 0.01$ (**)], also with CHOL alone [$p < 0.01$ (**)] and E_2 alone [$p < 0.05$ (*)] treatments, induced a significant increase in the length of neurites in comparison to control cells at 10 DIV (Fig. 3). Furthermore, the significant increase in the neurite length was seen in all

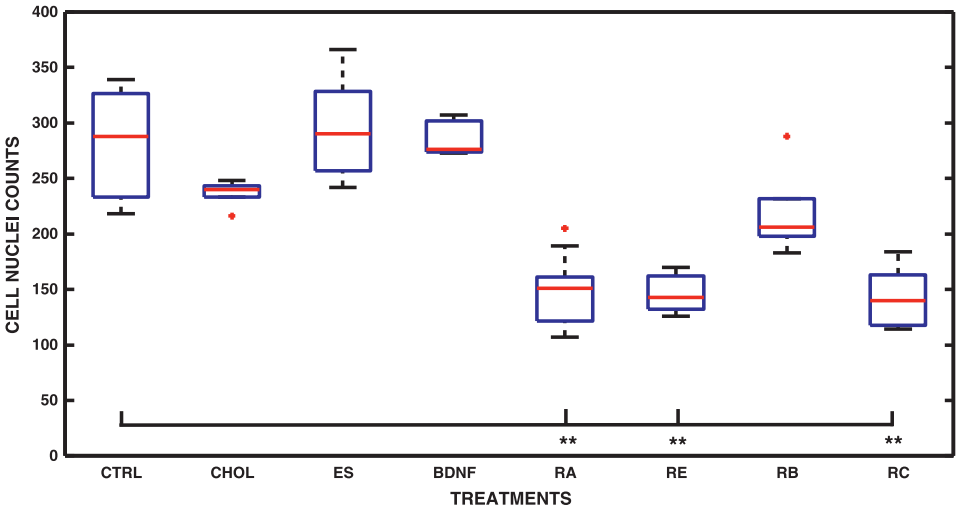

Fig. 2 Inhibition of cell population growth. Cells were cultured in control conditions [CTRL (n = 7)], and with CHOL (n = 6), E_2 (n = 6), BDNF (n = 6), RA (n = 6), RE (n = 6), RB (n = 6), and RC (n = 8) (n is the number of analyzed microscopy images) and the cell nuclei were counted at 10 DIV. In the *boxplot* representation the obtained median nuclei counts, 25th and 75th percentiles, extreme data points, and outliers of the data are shown with *red line*, *blue edges*, *black whiskers*, and *red asterisks*, respectively. Each differentiation agent is shown on the x-axis and the cell nuclei counts on the y-axis. The statistically significant differences ($p < 0.01$) are shown with *asterisks* (**). Significantly lower cell numbers were detected when cells were treated with RA, RE, or RC in comparison to CTRL data. Slight increase in cell numbers (nuclei counts) were observed when cells were treated with RB, in comparison to the cells treated solely with RA. The nuclei counts of RB treated cultures were not significantly lower in comparison to CTRL (Color figure online)

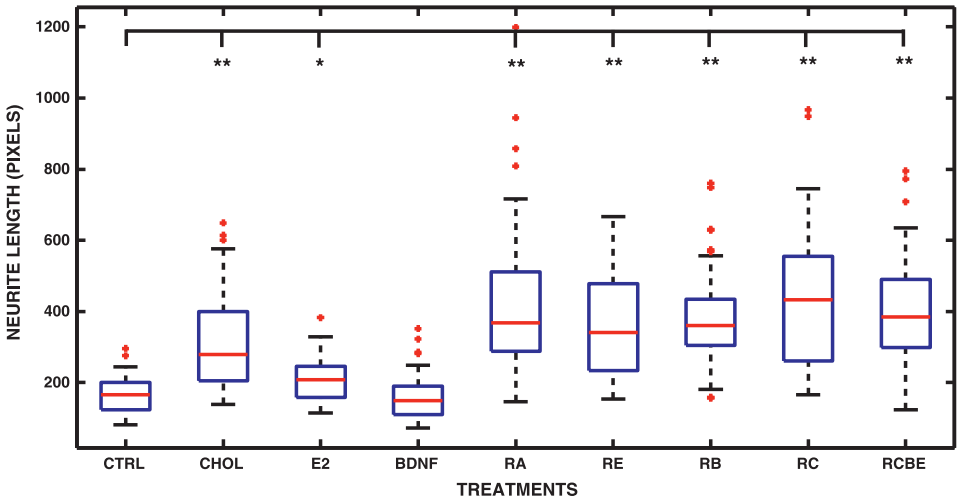

Fig. 3 Neurite lengths in SH-SY5Y cells. Cells were cultured in CTRL conditions, and with CHOL, E_2, BDNF, RA, or with their combinations; RE, RB, RC, RCBE. In the *boxplot* representation the obtained median of neurite lengths, the 25th and 75th percentiles, the extreme data points, and the outliers of the data are shown with *red line*, *blue edges*, *black whiskers* and *red asterisks*, respectively. Each treatment is shown on x-axis and the neurite lengths in pixels on y-axis. The statistically significant differences ($p < 0.01$) and ($p < 0.05$) are shown with *asterisks* (**) and (*), respectively. The neurite lengths were significantly longer when cells are treated with RA, CHOL, RE, RB, RC, and RCBE ($p < 0.01$). Interestingly, at 10 DIV, E_2 induces only short neurites, but the increase in the neurite length is still significant in comparison to controls ($p < 0.05$). Moreover, RA induces significantly longer neurites when compared to CHOL or E_2 induced neurite lengths ($p < 0.01$) (Color figure online)

combination treatments such as RE, RB, RC, RCBE [$p < 0.01$ (**)] relative to control conditions (Fig. 3). With the BDNF treatment alone no increase in the neurite length was detected.

Presence of Neurofilaments in SH-SY5Y Neuroblastoma Cells

The level of differentiation of the SH-SY5Y neuroblastoma cells at 10 DIV was further verified by imaging the NF-68 neurofilaments. The neurofilament fluorescence was defined by visual inspection and by measuring the intensity of CTNF, when cells were treated solely with RA, BDNF, CHOL, or E_2 (Fig. 4b–e, respectively) or in combination with RA and E_2 (RE), RA and BDNF (RB), RA and CHOL (RC), and RA, CHOL, BDNF, and E_2 (RCBE) (Fig. 4g–j, respectively). Both visual and automated image analyses showed that the presence of the NF-68 neurofilaments was clearly induced by RA (Fig. 4b). No major increase in NF-68 fluorescence levels was observed visually or automatically, when cells were treated with BDNF, CHOL or E_2 (Fig. 4c–e). However, the intensity of NF-68 fluorescence was significantly increased in all of the combination treatments relative to control cells, as shown in Fig. 4g–j, and in Fig. 5 for RA [$p < 0.01$ (**)], RE [$p < 0.05$(*)], RC [$p < 0.01$(**)], RB [$p < 0.01$(**)] and RCBE [$p < 0.01$(**)].

Differentiation-Induced Synaptic Vesicle Recycling

Our group has earlier shown that RA and RC treated human SH-SY5Y cells show intense Synaptophysin I (SypI) fluorescence in cell somata, along the neurites and at the sites of the cell-to-cell contacts. Furthermore, we have shown co-localization of SypI and AM1-43 at the end of the neurites at the cell-to-cell contacts of the RA and RC differentiated and high K^+ depolarized human SH-SY5Y cells [23]. It has been also shown elsewhere that the SH-SY5Y cells are capable of depolarization with high K^+ stimulation [87]. Therefore, high K^+ stimulation was used for studying the stimulation-related synaptic vesicle recycling also in this study. The SH-SY5Y neuroblastoma cells were incubated with E_2, CHOL, BDNF, or RA or with their combinations (RE, RB, RC, RCB and RCBE) and stained at 10 DIV with AM1-43, a fluorescent styryl dye (a nerve terminal probe) with the presence of depolarizing high K^+-Tyrode solution. The number of fluorescent puncta, reflecting the recycling synaptic vesicles, was counted after depolarization (see Fig. 6 and section "Methods"). Treatment with CHOL or BDNF alone does not increase the number of fluorescence puncta in comparison to CTRL. Our data show for the first time, that the treatment with E_2 alone [$p < 0.05$(*)], or RA together with E_2 (RE), BDNF (RB), BDNF and CHOL (RBC) or BDNF, CHOL and E_2 (RBCE), [$p < 0.01$(**)] significantly increases the number

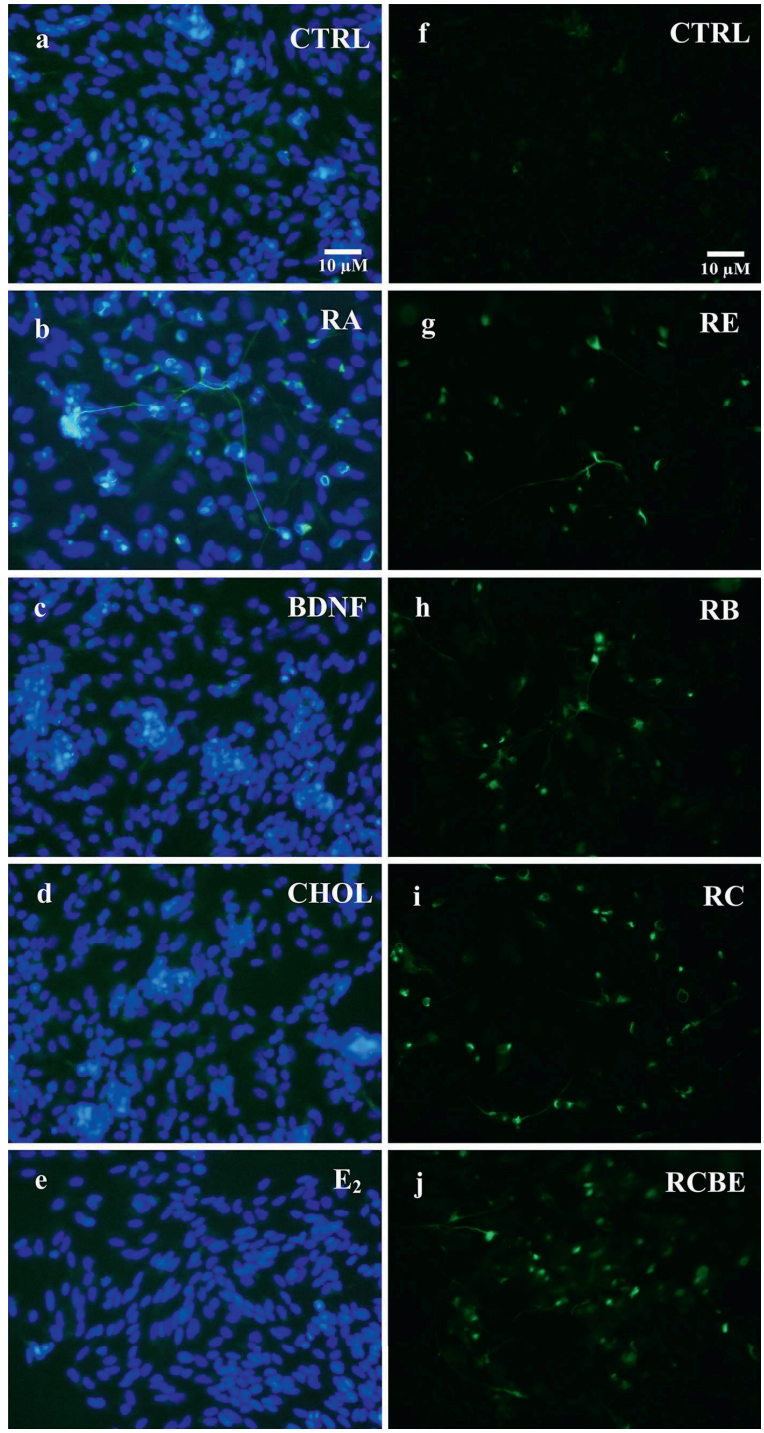

Fig. 4 The presence of NF-68 neurofilaments in SH-SY5Y neuroblastoma cells. Neurofilaments were detected at 10 DIV by immunostaining of NF-68 (*green*) and cell nuclei with Hoechst 33258 (*blue*). **a**–**e** Combined double staining of neurofilaments and nuclei in the SH-SY5Y cells in control conditions (CTRL), and when treated with RA, BDNF, CHOL and E_2, show that RA induces NF-68, seen also in the long branching neurites. **a**, **f** No NF-68 is seen in CTRL. **g**–**j** RE, RB, RC and RCBE treatments show presence of neurofilaments similar to those with RA alone (Color figure online)

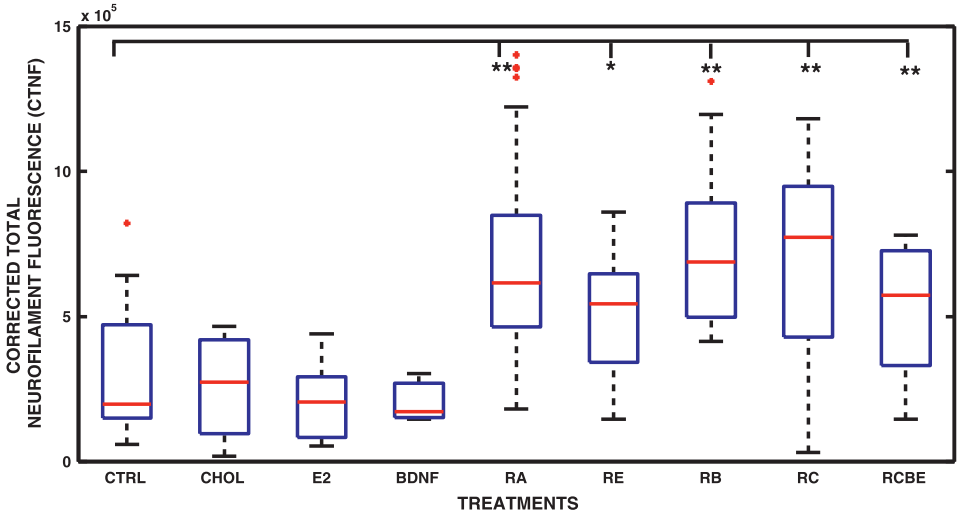

Fig. 5 Corrected total NF-68 neurofilament fluorescence (CTNF). CTNF was analyzed from the control (CTRL) SH-SY5Y cells (n = 19), and cells treated with RA (n = 38), BDNF (n = 6), CHOL (n = 6) and E_2 (n = 6) and RC (n = 9), RB (n = 14), RE (n = 13) and RCBE (n = 13) (n is the number of analyzed images). The obtained median of CTNF, the 25th and 75th percentiles, the extreme data points, and the outliers of the data are shown in the *boxplot* with *red line*, *blue edges*, *black whiskers* and *red asterisks*, respectively. Differentiation agents are shown on the x-axis and the CTNF on the y-axis. The statistical differences between the CTNF data and control values are shown with *asterisks* [$p < 0.05$(*), and $p < 0.01$(**)]. The automated analysis confirmed that the CTNF was significantly [$p < 0.01$(**)] increased in all other RA treated cultures (RA, RB, RC, RCB, and RCBE) in comparison to control cultures, except increased with less significance in the RE treated cultures [$p < 0.05$(*)]. This data show that NF-68 neurofilaments were induced by RA and further maintained by CHOL, BDNF and E_2 (Color figure online)

of fluorescence puncta when compared to controls. The results also confirm earlier results from our laboratory that RA alone, as well as together with CHOL, significantly [$p < 0.01$(**)] increases the number of AM1-43 fluorescence puncta in SH-SY5Y cells. This data also indicate a slight, however not significant, increase in fluorescence puncta in CHOL treated cultures, but not in BDNF treated cultures. In particular, we found a significant [$p < 0.05$(*)] increase in cells treated with RCB or RCBE relative to cultures treated without CHOL (such as RB or RE). These results demonstrate that in addition to RA and CHOL, also prolonged treatment with E_2 alone stimulates the synaptic vesicle recycling in SH-SY5Y cells. Highest numbers of fluorescence puncta were detected when all agents were combined (RCBE).

Discussion

Despite active research for improving the prognosis of high-risk neuroblastoma patients over the last decades, only a few patients become long-term survivors. Outcome of the stage 4 neuroblastoma remains poor, and the development of novel therapeutic approaches is needed [28, 88–91]. Therefore, therapies such as induced differentiation of cancer cells are important. Retinoic acid is one of the most prominent inducer of differentiation in clinical treatments [28, 90]. Therefore, in the current study, the level of differentiation of human SH-SY5Y cells towards neuronal type was followed by analyzing the additive impacts of estradiol (E_2/E) and brain-derived neurotrophic factor (BDNF/B) on cell morphology, neurite length, presence of neurofilaments, cell population growth and synaptic vesicle recycling in non-treated controls, as well as retinoic acid (RA/R) and cholesterol (CHOL/C) treated cells at 10 days in vitro.

We here confirm our earlier data [23] that the most potent inducer for differentiation is retinoic acid, especially with co-treatment with CHOL. Of the four markers of differentiation (cell population growth, neurite length, total NF-68 fluorescence and synaptic vesicle recycling) growth is inhibited only when RA is present. Estradiol (E_2), a predominant form of estrogen hormone, as well as CHOL, supports this inhibition. Growth rate of the cells treated with RA together with BDNF (RB) was higher than those, which were treated with RA alone. BDNF thus opposes the possibility of cells to undergo RA induced growth inhibition. Earlier results by other laboratories of the impact of BDNF, and in particular of the treatment together with RA, have given controversial results. While some studies show

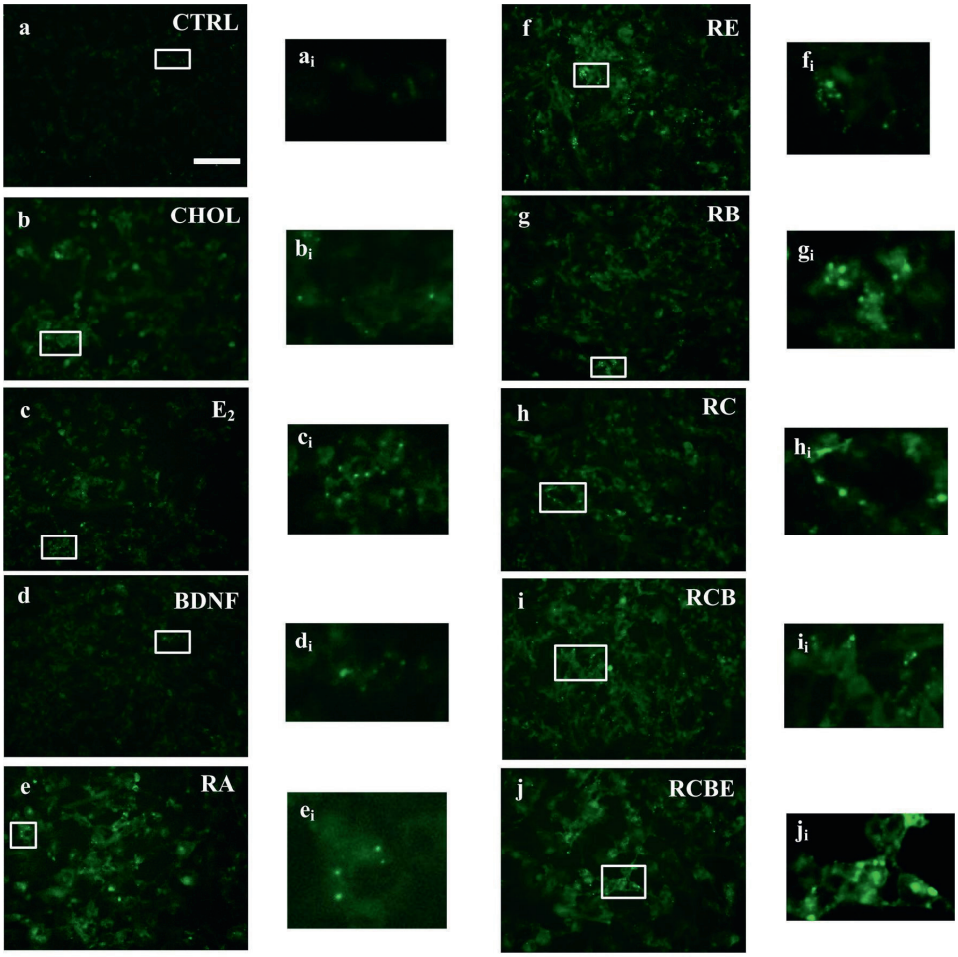
a
CTRL
a_i
f
RE
f_i
b
CHOL
b_i
g
RB
g_i
c
E_2
c_i
h
RC
h_i
d
BDNF
d_i
i
RCB
i_i
e
RA
e_i
j
RCBE
j_i

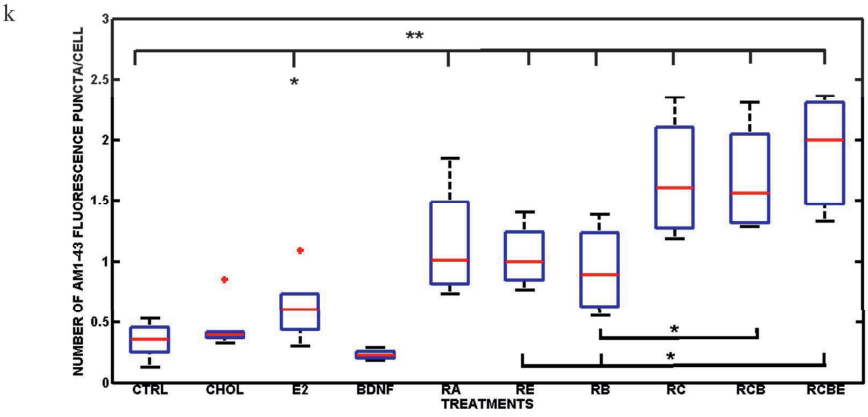
k
NUMBER OF AM1-43 FLUORESCENCE PUNCTA/CELL
TREATMENTS
CTRL
CHOL
E2
BDNF
RA
RE
RB
RC
RCB
RCBE
**
*
*
*
0
0.5
1
1.5
2
2.5
3

◀**Fig. 6** Synaptic vesicle recycling in SH-SY5Y neuroblastoma cells. **a–j** Synaptic vesicle recycling was measured by AM1-43 immunostaining in the presence of depolarizing high K^+ containing Tyrode solution from control cells [CTRL (n = 12)] and cells treated with CHOL (n = 6), E_2 (n = 6), BDNF (n = 6), RA (n = 6), or with their combinations such as RE (n = 6), RB (n = 6), RC (n = 6), RCB (n = 6), or RCBE, (n = 9) at 10 DIV (n is the number of analyzed images). $\mathbf{a_i}$–$\mathbf{j_i}$ Magnified examples of every treatment are shown. **k** Number of detected fluorescence puncta. In the *boxplot*, the obtained median number of fluorescence puncta, the 25th and 75th percentiles, the extreme data points, and the outliers of the data are shown with *red line*, *blue edges*, *black whiskers* and *red asterisks*, respectively. Differentiation agents are shown on the x-axis and the number of AM1-43 fluorescence puncta per obtained median nuclei number on the y-axis. The statistical differences between the data of interest and control values are shown as asterisks [$p < 0.05$(*), and $p < 0.01$(**)]. The number of fluorescence puncta did not significantly increase in comparison to CTRL group, when cells were treated solely with CHOL or BDNF (**b**, **d**, **k**). E_2 induced significant increase [$p < 0.05$(*)] in the number of AM1-43 puncta relative to control group (**c**, **k**). The results show that RA alone, as well as RE, RB, RC, RCB, and RCBE significantly [$p < 0.01$(**)] increased the number of AM1-43 puncta relative to control group (**e–j**). Additionally, the synaptic vesicle recycling was significantly [$p < 0.05$(*)] increased when cholesterol was present (in RCB and RCBE treated cultures) when compared to RB or RE treated groups without CHOL (**k**). The highest median of number of fluorescence puncta was detected when neuroblastoma cells were treated with all substances simultaneously (RCBE) (Color figure online)

that the RB treatment differentiated the SH-SY5Y cells [18, 19, 37], other studies show that the activation of TrkB-BDNF pathway, which is also activated by RB treatment, can lead to increased cell survival, invasion, metastasis, angiogenesis and drug resistance [92–96]. Our results of population growth of RB treated cells are in agreement with the study by Cernaianu et al. [6], showing that the effect on proliferation depends on the used concentration of BDNF, causing either significant inhibition (with 10 ng/mL BDNF) or no inhibition (with 50 or 100 ng/mL) and with the study by Nishida et al. [97], where they show that SH-SY5Y-A cells (American Type Culture Collection; also used in this study) differentiated in the presence of RA whereas RA treated SH-SY5Y-E cells (European Collection of Cell Cultures) require additional BDNF treatment for full differentiation. This is due to the defects in several signaling pathways in SH-SY5Y-E cells. In conclusion, the controversial results in the level of differentiation in some of the studies might originate from the different subtypes of SH-SY5Y, as well as from the used BDNF concentrations. In the light of the current knowledge further examinations of the properties of BDNF are needed, before considering the use of BDNF as a therapeutic agent for clinical use.

Long neurites, typical of neuronal morphology, are found with treatment by retinoic acid, as well as by cholesterol. We here show, that E_2 alone (at 1 nM concentration) is able to slightly increase the length of neurites, and when it is combined with RA (RE) or additionally with CHOL and BDNF (RCBE) neurites' length is even more enhanced involving also branching and network formation. It has been earlier demonstrated by Takahashi et al. [98], that 10 nM E_2 induces neurite outgrowth already after 2 DIV, which was not seen in this study. This difference in the presence of neurites may be explained by the 10 times difference in the E_2 concentrations used. With treatment by BDNF alone, no neurite outgrowth at 10 DIV was detected. This result is understandable based on other reports that 3–5 days' RA treatment is necessary to induce expression of TrkB receptors, which are crucial for BDNF induced neurite growth [18, 37]. Agholme et al. [24] have shown, that the RB and RCB treatments induced longer neurites than treatment with RA alone, which were not seen in our experiments. We additionally show, similarly to the results shown in previous studies, that RA alone [16, 23, 99] or when combined with CHOL (RC) [23], BDNF (RB) [100], or CHOL and BDNF (RCB) [24] induce considerable neurite outgrowth and neuronal networks.

Neurofilaments are major components of the neuronal cytoskeleton, providing structural support for the axons and regulating the axon's diameter. We here show that treatment with RA alone enhances the total light neurofilament (NF-68) fluorescence. Earlier study from Messi et al. [101] is in agreement with our results by showing that RA reduces cell migration and invasiveness and up regulates NF-68 expression. In addition, it has been shown that medium size neurofilaments (NF-145-160) are induced by RA in SH-SY5Y cells [102]. We detected that RA combined to E_2 enhanced the total NF-68 fluorescence, though less than the RC, RB, RCB or RCBE treatments. The enhancement of total NF-68 fluorescence in human SH-SY5Y cells by these treatments has not been previously reported.

Finally, we asked if RA, E_2, CHOL and BDNF or their combinations increase the synaptic vesicle recycling in SH-SY5Y cells. Results from the current study are interesting, as in addition to RA, also E_2, even when used alone, is able to significantly increase the number of detected vesicle recycling after depolarizing cells by high K^+-solution. Hu et al. [103] have shown in cultured neonatal rat cortical primary cells that E_2, produced and secreted by astrocytes, modulates synaptogenesis and synaptic function by increasing the synaptic vesicle recycling. In addition, they showed that added exogenic estradiol mimics this effect of astrocyte-conditioned medium on synaptic formation and transmission. Our results here are in agreement with this study. Chamniansawat and Chongthammakun [48] have shown that 48 h estrogen treatment significantly increases the expression of synapse related proteins, such as post-synaptic dense material 95 (PSD-95) and synaptophysin (SYP). As they did not see any estrogen induced immediate

or rapid effects on the PSD-95 and SYP mRNA expression in SH-SY5Y cells, they concluded that the expressions of PSD-95 and SYP requires translocalization across ER, as well as long period of time to activate the target gene expression in SH-SY5Y cells. This is called classical genomic action of estrogen, where estrogen partially acts through PI-3K signaling to activate PSD-95 and SYP expression. Our data support the hypothesis that prolonged treatment of E_2 enhances endo/exocytosis and thus promotes synaptic vesicle recycling in SH-SY5Y cells.

In the current study, synaptic vesicle recycling is significantly enhanced in all combination treatments, where cholesterol is present (RC, RCB and RCBE). Earlier it has been shown that the depolarized RC treated cells induced higher number of AM1-43 positive fluorescence puncta/cell in comparison to depolarized RA treated cells [23]. We now show for the first time that this same supra-additive effect can be observed in addition to depolarized RC treated cultures also in depolarized RCB and RCBE treated cultures. Sarkanen et al. [23] found that one aspect possibly explaining this effect of RA and CHOL is that the RA-induced fragmentation of Golgi apparatus is avoided by co-treatment with CHOL. In addition, it has been earlier shown that RA has antioxidant potential and, that RA isomers enhance the expression of genes linked with cholesterol efflux e.g. apoe, abca-1 and abcg-1 proteins in astrocytes [104]. We know also from other earlier studies that synaptogenesis is promoted by cholesterol [30], cholesterol influences multiple aspects of synaptic transmission [105], both presynaptically, by acting on neurotransmitter vesicle fusion [106–108] and postsynaptically, altering neurotransmitter receptor mobility in the membrane [109]. Moreover, it is known that retinoic acid has been shown to function in homeostatic plasticity as a signaling molecule that increases synaptic strength by a protein synthesis-dependent mechanism [110]. It is also known that homeostatic synaptic plasticity may manifest as altered presynaptic transmitter release and vesicle loading properties [111, 112]. All above mentioned studies support our current result of the supra-additive effect of cholesterol and retinoic acid on increasing the number of AM1-43 fluorescence puncta in SH-SY5Y cells when compared to cells treated without CHOL.

Earlier and our results indicate that the formation of new synapses is a complex process requiring the presence of multiple substances simultaneously. Cholesterol is especially important as a component of cellular membranes, regulating membrane structure, fluidity and permeability, and as a precursor for steroid hormones. The increased cholesterol efflux has been shown to impair the LTP at the hippocampal CA1 synapses [34]. This study, together with our results, indicates the importance of cholesterol in regulation of synaptic vesicle recycling, neurotransmission, and regeneration of synapses. Lately, research has also started to focus on the effects of estradiol (estrogen) on formation and activity of synapses. A recent study on adult male rat hippocampal slices shows that estradiol treatment enhances synaptic transmission and LTP via estradiol receptor beta (ERβ) stimulation. Estradiol activates the RhoA-GTPase signaling, which causes actin polymerization within dendritic spines. The study suggests that estradiol is able to increase the fast excitatory postsynaptic potentials and causes a reduction in the threshold for lasting synaptic changes. Results of the study further indicate that the estradiol (similarly to RA) activates the synaptic TrkB receptors needed for the effects of the BDNF [113].

It is important to review the capacity of neuroblastoma cells to differentiate into a neuronal cell type and link this differentiation to those factors, which are normally present in neuronal microenvironment. Amongst the various glial cells in central nervous system, astrocytes are known to release cholesterol and growth factors and thus promote different aspects of synapse development [30]. Neurons depend on import of cholesterol via lipoproteins [35] to effectively maintain development of new connections via dendrites, dendritic spines and synapses. The efficacy and stability of the pre-synaptic transmitter release largely depends on presence of cholesterol [32]. It is also known that neurons are able to convert glia-derived cholesterol to steroids, which then promotes synapse formation [114], and that astrocytes, in addition to cholesterol also produce and release estradiol, which enhances neurite growth [115] and increases synapse number and function [103, 116]. In this study, we investigated whether cholesterol or estradiol are able to increase synaptic vesicle recycling in human SH-SY5Y cells, and it was found that estradiol, even alone, is able to promote synaptic vesicle recycling in these cells. Cholesterol, in contrast, does that only when used together with retinoic acid. Our results indicate the importance of estradiol, cholesterol and retinoic acid in synaptic function.

The findings reported here have significance for understanding the effects of retinoic acid, cholesterol, estradiol and brain derived neurotrophic factor, either alone or in combinations in the process of SH-SY5Y neuroblastoma cell differentiation into neuronal cell type. More than one agent is clearly necessary to reach this goal in aim to benefit the differentiation induced therapies.

Acknowledgments The authors acknowledge the financial support from Tampere University of Technology President's Doctoral Programme, Finnish Foundation for Technology Promotion, Finnish Cultural Foundation, Pirkanmaa Regional fund, Tampere Doctoral Programme in Information Science and Engineering. The research leading to these results has received partial funding from the European Union Seventh Framework Programme (FP7) under grant agreement n° 604102 (HBP). Furthermore the authors want to thank

Professor Timo Ylikomi for providing research facilities, Ms. Mirja Hyppönen, Ms. Hilkka Mäkinen and Ms. Paula Helpiölä for their technical support.

Compliance with Ethical Standards

Conflict of Interest The authors declare that they have no conflict of interest.

Ethical Approval This article does not contain any studies with human participants or animals performed by any of the authors. For this type of study formal consent is not required.

References

1. Duckett JW, Koop CE (1977) Neuroblastoma. Urol Clin N Am 4:285–295
2. Franks LM, Bollen A, Seeger RC et al (1997) Neuroblastoma in adults and adolescents: an indolent course with poor survival. Cancer 79:2028–2035
3. Escobar MA, Grosfeld JL, Powell RL et al (2006) Long-term outcomes in patients with stage IV neuroblastoma. J Pediatr Surg 41:377–381
4. Biedler JL, Helson L, Spengler BA (1973) Morphology and growth, tumorigenicity, and cytogenetics of human neuroblastoma cells in continuous culture. Cancer Res 33:2643–2652
5. Kuramoto T, Werrbach-Perez K, Perez-Polo JR et al (1981) Membrane properties of a human neuroblastoma II: effects of differentiation. J Neurosci Res 6:441–449
6. Cernaianu G, Brandmaier P, Scholz G et al (2008) All-trans retinoic acid arrests neuroblastoma cells in a dormant state. Subsequent nerve growth factor/brain-derived neurotrophic factor treatment adds modest benefit. J Pediatr Surg 43:1284–1294
7. Tojima T, Kobayashi S, Ito E (2003) Dual role of cyclic AMP-dependent protein kinase in neuritogenesis and synaptogenesis during neuronal differentiation. J Neurosci Res 74:829–837
8. Pahlman S, Odelstad L, Larsson E et al (1981) Phenotypic changes of human neuroblastoma cells in culture induced by 12-O-tetradecanoyl-phorbol-13-acetate. Int J Cancer 28: 583–589
9. Pahlman S, Ruusala AI, Abrahamsson L et al (1984) Retinoic acid-induced differentiation of cultured human neuroblastoma cells: a comparison with phorbolester-induced differentiation. Cell Differ 14:135–144
10. Adem A, Mattsson ME, Nordberg A et al (1987) Muscarinic receptors in human SH-SY5Y neuroblastoma cell line: regulation by phorbol ester and retinoic acid-induced differentiation. Brain Res 430:235–242
11. Jalonen T, Akerman KE (1988) Single transient potassium channels in human neuroblastoma cells induced to differentiate in vitro. Neurosci Lett 86:99–104
12. Guarneri P, Cascio C, Piccoli T et al (2000) Human neuroblastoma SH-SY5Y cell line: neurosteroid-producing cell line relying on cytoskeletal organization. J Neurosci Res 60:656–665
13. Presgraves SP, Ahmed T, Borwege S et al (2004) Terminally differentiated SH-SY5Y cells provide a model system for studying neuroprotective effects of dopamine agonists. Neurotox Res 5:579–598
14. Preis PN, Saya H, Nadasdi L et al (1988) Neuronal cell differentiation of human neuroblastoma cells by retinoic acid plus herbimycin A. Cancer Res 48:6530–6534
15. Toselli M, Tosetti P, Taglietti V (1996) Functional changes in sodium conductances in the human neuroblastoma cell line SH-SY5Y during in vitro differentiation. J Neurophysiol 76:3920–3927
16. Cheung YT, Lau WK, Yu MS et al (2009) Effects of all-trans-retinoic acid on human SH-SY5Y neuroblastoma as in vitro model in neurotoxicity research. Neurotoxicology 30:127–135
17. Spina MB, Squinto SP, Miller J et al (1992) Brain-derived neurotrophic factor protects dopamine neurons against 6-hydroxydopamine and N-methyl-4-phenylpyridinium ion toxicity: involvement of the glutathione system. J Neurochem 59:99–106
18. Encinas M, Iglesias M, Liu Y et al (2000) Sequential treatment of SH-SY5Y cells with retinoic acid and brain-derived neurotrophic factor gives rise to fully differentiated, neurotrophic factor-dependent, human neuron-like cells. J Neurochem 75: 991–1003
19. Goldie BJ, Barnett MM, Cairns MJ (2014) BDNF and the maturation of posttranscriptional regulatory networks in human SH-SY5Y neuroblast differentiation. Front Cell Neurosci 8:325
20. Rogers MV, Buensuceso C, Montague F et al (1994) Vanadate stimulates differentiation and neurite outgrowth in rat pheochromocytoma PC12 cells and neurite extension in human neuroblastoma SH-SY5Y cells. Neuroscience 60:479–494
21. Lavenius E, Gestblom C, Johansson I et al (1995) Transfection of TRK-A into human neuroblastoma cells restores their ability to differentiate in response to nerve growth factor. Cell Growth Differ 6:727–736
22. Oe T, Sasayama T, Nagashima T et al (2005) Differences in gene expression profile among SH-SY5Y neuroblastoma subclones with different neurite outgrowth responses to nerve growth factor. J Neurochem 94:1264–1276
23. Sarkanen JR, Nykky J, Siikanen J et al (2007) Cholesterol supports the retinoic acid-induced synaptic vesicle formation in differentiating human SH-SY5Y neuroblastoma cells. J Neurochem 102:1941–1952
24. Agholme L, Lindstrom T, Kagedal K et al (2010) An in vitro model for neuroscience: differentiation of SH-SY5Y cells into cells with morphological and biochemical characteristics of mature neurons. J Alzheimers Dis 20:1069–1082
25. Szutowicz A, Bielarczyk H, Jankowska-Kulawy A et al (2015) Retinoic acid as a therapeutic option in Alzheimer's disease: a focus on cholinergic restoration. Expert Rev Neurother 15:239–249
26. Sidell N, Lucas CA, Kreutzberg GW (1984) Regulation of acetylcholinesterase activity by retinoic acid in a human neuroblastoma cell line. Exp Cell Res 155:305–309
27. Stio M, Celli A, Treves C (2001) Synergistic anti-proliferative effects of vitamin D derivatives and 9-cis retinoic acid in SH-SY5Y human neuroblastoma cells. J Steroid Biochem Mol Biol 77:213–222
28. Matthay KK, Reynolds CP, Seeger RC et al (2009) Long-term results for children with high-risk neuroblastoma treated on a randomized trial of myeloablative therapy followed by 13-cis-retinoic acid: a children's oncology group study. J Clin Oncol 27:1007–1013
29. Adamson PC, Matthay KK, O'Brien M et al (2007) A phase 2 trial of all-trans-retinoic acid in combination with interferon-alpha2a in children with recurrent neuroblastoma or wilms tumor: a pediatric oncology branch, NCI and children's oncology group study. Pediatr Blood Cancer 49:661–665
30. Mauch DH, Nagler K, Schumacher S et al (2001) CNS synaptogenesis promoted by glia-derived cholesterol. Science 294:1354–1357

31. Chen J, Costa LG, Guizzetti M (2011) Assessment of cholesterol homeostasis in astrocytes and neurons. Methods Mol Biol 758:403–414
32. Goritz C, Mauch DH, Pfrieger FW (2005) Multiple mechanisms mediate cholesterol-induced synaptogenesis in a CNS neuron. Mol Cell Neurosci 29:190–201
33. Ullian EM, Harris BT, Wu A et al (2004) Schwann cells and astrocytes induce synapse formation by spinal motor neurons in culture. Mol Cell Neurosci 25:241–251
34. Koudinov AR, Koudinova NV (2001) Essential role for cholesterol in synaptic plasticity and neuronal degeneration. FASEB J 15:1858–1860
35. Pfrieger FW (2003) Outsourcing in the brain: do neurons depend on cholesterol delivery by astrocytes? BioEssays 25:72–78
36. Huang EJ, Reichardt LF (2001) Neurotrophins: roles in neuronal development and function. Annu Rev Neurosci 24:677–736
37. Kaplan DR, Matsumoto K, Lucarelli E et al (1993) Induction of TrkB by retinoic acid mediates biologic responsiveness to BDNF and differentiation of human neuroblastoma cells. Eukaryotic signal transduction group. Neuron 11:321–331
38. Ho R, Eggert A, Hishiki T et al (2002) Resistance to chemotherapy mediated by TrkB in neuroblastomas. Cancer Res 62:6462–6466
39. Low WC, Rujitanaroj PO, Wang F et al (2015) Nanofiber-mediated release of retinoic acid and brain-derived neurotrophic factor for enhanced neuronal differentiation of neural progenitor cells. Drug Deliv Transl Res 5:89–100
40. Ferrer I, Goutan E, Marin C et al (2000) Brain-derived neurotrophic factor in huntington disease. Brain Res 866:257–261
41. Murer MG, Yan Q, Raisman-Vozari R (2001) Brain-derived neurotrophic factor in the control human brain, and in Alzheimer's disease and Parkinson's disease. Prog Neurobiol 63:71–124
42. Phillips HS, Hains JM, Armanini M et al (1991) BDNF mRNA is decreased in the hippocampus of individuals with Alzheimer's disease. Neuron 7:695–702
43. Gould E, Woolley CS, Frankfurt M et al (1990) Gonadal steroids regulate dendritic spine density in hippocampal pyramidal cells in adulthood. J Neurosci 10:1286–1291
44. McEwen BS, Coirini H, Schumacher M (1990) Steroid effects on neuronal activity: When is the genome involved? Ciba Found Symp 153:3–12 **(discussion 12–21)**
45. Woolley CS, Gould E, Frankfurt M et al (1990) Naturally occurring fluctuation in dendritic spine density on adult hippocampal pyramidal neurons. J Neurosci 10:4035–4039
46. Wong M, Moss RL (1992) Long-term and short-term electrophysiological effects of estrogen on the synaptic properties of hippocampal CA1 neurons. J Neurosci 12:3217–3225
47. Wong M, Moss RL (1991) Electrophysiological evidence for a rapid membrane action of the gonadal steroid, 17 beta-estradiol, on CA1 pyramidal neurons of the rat hippocampus. Brain Res 543:148–152
48. Chamniansawat S, Chongthammakun S (2009) Estrogen stimulates activity-regulated cytoskeleton associated protein (arc) expression via the MAPK- and PI-3K-dependent pathways in SH-SY5Y cells. Neurosci Lett 452:130–135
49. Chindewa R, Lapanantasin S, Sanvarinda Y et al (2008) Pueraria mirifica, phytoestrogen-induced change in synaptophysin expression via estrogen receptor in rat hippocampal neuron. J Med Assoc Thai 91:208–214
50. Jelks KB, Wylie R, Floyd CL et al (2007) Estradiol targets synaptic proteins to induce glutamatergic synapse formation in cultured hippocampal neurons: critical role of estrogen receptor-alpha. J Neurosci 27:6903–6913
51. Liu F, Day M, Muniz LC et al (2008) Activation of estrogen receptor-beta regulates hippocampal synaptic plasticity and improves memory. Nat Neurosci 11:334–343
52. Xu X, Zhang Z (2006) Effects of estradiol benzoate on learning-memory behavior and synaptic structure in ovariectomized mice. Life Sci 79:1553–1560
53. Babayan AH, Kramar EA (2013) Rapid effects of oestrogen on synaptic plasticity: interactions with actin and its signalling proteins. J Neuroendocrinol 25:1163–1172
54. Kretz O, Fester L, Wehrenberg U et al (2004) Hippocampal synapses depend on hippocampal estrogen synthesis. J Neurosci 24:5913–5921
55. Prange-Kiel J, Wehrenberg U, Jarry H et al (2003) Para/autocrine regulation of estrogen receptors in hippocampal neurons. Hippocampus 13:226–234
56. Woolley CS, McEwen BS (1994) Estradiol regulates hippocampal dendritic spine density via an N-methyl-D-aspartate receptor-dependent mechanism. J Neurosci 14:7680–7687
57. Weiland NG (1992) Estradiol selectively regulates agonist binding sites on the N-methyl-D-aspartate receptor complex in the CA1 region of the hippocampus. Endocrinology 131:662–668
58. Warren SG, Humphreys AG, Juraska JM et al (1995) LTP varies across the estrous cycle: enhanced synaptic plasticity in proestrus rats. Brain Res 703:26–30
59. Good M, Day M, Muir JL (1999) Cyclical changes in endogenous levels of oestrogen modulate the induction of LTD and LTP in the hippocampal CA1 region. Eur J Neurosci 11:4476–4480
60. Gazzaley AH, Weiland NG, McEwen BS et al (1996) Differential regulation of NMDAR1 mRNA and protein by estradiol in the rat hippocampus. J Neurosci 16:6830–6838
61. Cyr M, Ghribi O, Thibault C et al (2001) Ovarian steroids and selective estrogen receptor modulators activity on rat brain NMDA and AMPA receptors. Brain Res Brain Res Rev 37:153–161
62. Cyr M, Ghribi O, Di Paolo T (2000) Regional and selective effects of oestradiol and progesterone on NMDA and AMPA receptors in the rat brain. J Neuroendocrinol 12:445–452
63. Bi R, Foy MR, Vouimba RM et al (2001) Cyclic changes in estradiol regulate synaptic plasticity through the MAP kinase pathway. Proc Natl Acad Sci U S A 98:13391–13395
64. Cordoba Montoya DA, Carrer HF (1997) Estrogen facilitates induction of long term potentiation in the hippocampus of awake rats. Brain Res 778:430–438
65. Woolley CS, Weiland NG, McEwen BS et al (1997) Estradiol increases the sensitivity of hippocampal CA1 pyramidal cells to NMDA receptor-mediated synaptic input: correlation with dendritic spine density. J Neurosci 17:1848–1859
66. Rudick CN, Woolley CS (2001) Estrogen regulates functional inhibition of hippocampal CA1 pyramidal cells in the adult female rat. J Neurosci 21:6532–6543
67. Smith CC, McMahon LL (2005) Estrogen-induced increase in the magnitude of long-term potentiation occurs only when the ratio of NMDA transmission to AMPA transmission is increased. J Neurosci 25:7780–7791
68. Kuiper GG, Enmark E, Pelto-Huikko M et al (1996) Cloning of a novel receptor expressed in rat prostate and ovary. Proc Natl Acad Sci U S A 93:5925–5930
69. Levin ER (2005) Integration of the extranuclear and nuclear actions of estrogen. Mol Endocrinol 19:1951–1959
70. Akama KT, McEwen BS (2003) Estrogen stimulates postsynaptic density-95 rapid protein synthesis via the akt/protein kinase B pathway. J Neurosci 23:2333–2339
71. Waters EM, Mitterling K, Spencer JL et al (2009) Estrogen receptor alpha and beta specific agonists regulate expression of synaptic proteins in rat hippocampus. Brain Res 1290:1–11
72. Marino M, Galluzzo P, Ascenzi P (2006) Estrogen signaling multiple pathways to impact gene transcription. Curr Genomics 7:497–508

73. Ivanova T, Mendez P, Garcia-Segura LM et al (2002) Rapid stimulation of the PI3-kinase/akt signalling pathway in developing midbrain neurones by oestrogen. J Neuroendocrinol 14:73–79
74. Mannella P, Brinton RD (2006) Estrogen receptor protein interaction with phosphatidylinositol 3-kinase leads to activation of phosphorylated akt and extracellular signal-regulated kinase 1/2 in the same population of cortical neurons: a unified mechanism of estrogen action. J Neurosci 26:9439–9447
75. Bang OY, Hong HS, Kim DH et al (2004) Neuroprotective effect of genistein against beta amyloid-induced neurotoxicity. Neurobiol Dis 16:21–28
76. Steward O, Worley PF (2001) A cellular mechanism for targeting newly synthesized mRNAs to synaptic sites on dendrites. Proc Natl Acad Sci U S A 98:7062–7068
77. Guzowski JF, Lyford GL, Stevenson GD et al (2000) Inhibition of activity-dependent arc protein expression in the rat hippocampus impairs the maintenance of long-term potentiation and the consolidation of long-term memory. J Neurosci 20:3993–4001
78. Guzowski JF, Setlow B, Wagner EK et al (2001) Experience-dependent gene expression in the rat hippocampus after spatial learning: a comparison of the immediate-early genes arc, c-fos, and zif268. J Neurosci 21:5089–5098
79. Schneider CA, Rasband WS, Eliceiri KW (2012) NIH image to ImageJ: 25 years of image analysis. Nat Methods 9:671–675
80. Gavet O, Pines J (2010) Progressive activation of CyclinB1-Cdk1 coordinates entry to mitosis. Dev Cell 18:533–543
81. Burgess A, Vigneron S, Brioudes E et al (2010) Loss of human greatwall results in G2 arrest and multiple mitotic defects due to deregulation of the cyclin B-Cdc2/PP2A balance. Proc Natl Acad Sci U S A 107:12564–12569
82. Selinummi J, Seppala J, Yli-Harja O et al (2005) Software for quantification of labeled bacteria from digital microscope images by automated image analysis. Biotechniques 39:859–863
83. Fanti Z, De-Miguel FF, Martinez-Perez ME (2008) A method for semiautomatic tracing and morphological measuring of neurite outgrowth from DIC sequences. Conf Proc IEEE Eng Med Biol Soc 2008:1196–1199
84. Croft BG, Fortin GD, Corera AT et al (2005) Normal biogenesis and cycling of empty synaptic vesicles in dopamine neurons of vesicular monoamine transporter 2 knockout mice. Mol Biol Cell 16:306–315
85. Pyle JL, Kavalali ET, Choi S et al (1999) Visualization of synaptic activity in hippocampal slices with FM1-43 enabled by fluorescence quenching. Neuron 24:803–808
86. Biagiotti T, D'Amico M, Marzi I et al (2006) Cell renewing in neuroblastoma: electrophysiological and immunocytochemical characterization of stem cells and derivatives. Stem Cells 24:443–453
87. Daniele F, Di Cairano ES, Moretti S et al (2015) TIRFM and pH-sensitive GFP-probes to evaluate neurotransmitter vesicle dynamics in SH-SY5Y neuroblastoma cells: Cell imaging and data analysis. J Vis Exp (95). doi:10.3791/52267
88. Simon T, Berthold F, Borkhardt A et al (2011) Treatment and outcomes of patients with relapsed, high-risk neuroblastoma: results of german trials. Pediatr Blood Cancer 56:578–583
89. Berthold F, Boos J, Burdach S et al (2005) Myeloablative megatherapy with autologous stem-cell rescue versus oral maintenance chemotherapy as consolidation treatment in patients with high-risk neuroblastoma: a randomised controlled trial. Lancet Oncol 6:649–658
90. Matthay KK, Villablanca JG, Seeger RC et al (1999) Treatment of high-risk neuroblastoma with intensive chemotherapy, radiotherapy, autologous bone marrow transplantation, and 13-cis-retinoic acid. Children's cancer group. N Engl J Med 341:1165–1173
91. Pearson AD, Pinkerton CR, Lewis IJ et al (2008) High-dose rapid and standard induction chemotherapy for patients aged over 1 year with stage 4 neuroblastoma: a randomised trial. Lancet Oncol 9:247–256
92. Nakamura K, Martin KC, Jackson JK et al (2006) Brain-derived neurotrophic factor activation of TrkB induces vascular endothelial growth factor expression via hypoxia-inducible factor-1alpha in neuroblastoma cells. Cancer Res 66:4249–4255
93. Acheson A, Conover JC, Fandl JP et al (1995) A BDNF autocrine loop in adult sensory neurons prevents cell death. Nature 374:450–453
94. Jaboin J, Kim CJ, Kaplan DR et al (2002) Brain-derived neurotrophic factor activation of TrkB protects neuroblastoma cells from chemotherapy-induced apoptosis via phosphatidylinositol 3'-kinase pathway. Cancer Res 62:6756–6763
95. Matsumoto K, Wada RK, Yamashiro JM et al (1995) Expression of brain-derived neurotrophic factor and p145TrkB affects survival, differentiation, and invasiveness of human neuroblastoma cells. Cancer Res 55:1798–1806
96. Nakagawara A, Azar CG, Scavarda NJ et al (1994) Expression and function of TRK-B and BDNF in human neuroblastomas. Mol Cell Biol 14:759–767
97. Nishida Y, Adati N, Ozawa R et al (2008) Identification and classification of genes regulated by phosphatidylinositol 3-kinase- and TRKB-mediated signalling pathways during neuronal differentiation in two subtypes of the human neuroblastoma cell line SH-SY5Y. BMC Res. Notes 1:95-0500-1-95
98. Takahashi K, Piao S, Yamatani H et al (2011) Estrogen induces neurite outgrowth via rho family GTPases in neuroblastoma cells. Mol Cell Neurosci 48:217–224
99. Muley PD, McNeill EM, Marzinke MA et al (2008) The atRA-responsive gene neuron navigator 2 functions in neurite outgrowth and axonal elongation. Dev Neurobiol 68:1441–1453
100. Fryer RH, Kaplan DR, Kromer LF (1997) Truncated trkB receptors on nonneuronal cells inhibit BDNF-induced neurite outgrowth in vitro. Exp Neurol 148:616–627
101. Messi E, Florian MC, Caccia C et al (2008) Retinoic acid reduces human neuroblastoma cell migration and invasiveness: effects on DCX, LIS1, neurofilaments-68 and vimentin expression. BMC Cancer 8:30-2407-8-30
102. Rebhan M, Vacun G, Bayreuther K et al (1994) Altered ganglioside expression by SH-SY5Y cells upon retinoic acid-induced neuronal differentiation. NeuroReport 5:941–944
103. Hu R, Cai WQ, Wu XG et al (2007) Astrocyte-derived estrogen enhances synapse formation and synaptic transmission between cultured neonatal rat cortical neurons. Neuroscience 144:1229–1240
104. Sodhi RK, Singh N (2014) Retinoids as potential targets for Alzheimer's disease. Pharmacol Biochem Behav 120:117–123
105. Pfrieger FW (2003) Role of cholesterol in synapse formation and function. Biochim Biophys Acta 1610:271–280
106. Deutsch JW, Kelly RB (1981) Lipids of synaptic vesicles: relevance to the mechanism of membrane fusion. Biochemistry 20:378–385
107. Linetti A, Fratangeli A, Taverna E et al (2010) Cholesterol reduction impairs exocytosis of synaptic vesicles. J Cell Sci 123:595–605
108. Smith AJ, Sugita S, Charlton MP (2010) Cholesterol-dependent kinase activity regulates transmitter release from cerebellar synapses. J Neurosci 30:6116–6121
109. Renner M, Choquet D, Triller A (2009) Control of the postsynaptic membrane viscosity. J Neurosci 29:2926–2937
110. Aoto J, Nam CI, Poon MM et al (2008) Synaptic signaling by all-trans retinoic acid in homeostatic synaptic plasticity. Neuron 60:308–320

111. Davis GW (2006) Homeostatic control of neural activity: from phenomenology to molecular design. Annu Rev Neurosci 29:307–323
112. Rich MM, Wenner P (2007) Sensing and expressing homeostatic synaptic plasticity. Trends Neurosci 30:119–125
113. Kramar EA, Babayan AH, Gall CM et al (2013) Estrogen promotes learning-related plasticity by modifying the synaptic cytoskeleton. Neuroscience 239:3–16
114. Fester L, Zhou L, Butow A et al (2009) Cholesterol-promoted synaptogenesis requires the conversion of cholesterol to estradiol in the hippocampus. Hippocampus 19:692–705
115. Nilsen J, Mor G, Naftolin F (1998) Raloxifene induces neurite outgrowth in estrogen receptor positive PC12 cells. Menopause 5:211–216
116. Chen G, Li HM, Chen YR et al (2007) Decreased estradiol release from astrocytes contributes to the neurodegeneration in a mouse model of niemann-pick disease type C. Glia 55:1509–1518

PUBLICATION V

Impacts of Laminin and Polyethyleneimine Surface Coatings on Morphology of Differentiating Human SH-SY5Y Cells and Networks

Teppola H, Sarkanen J-R, Jalonen TO, Linne M-L

In Proceedings of the International Federation of
Medical and Biological Engineering, 2018; 65:298-231
DOI:10.1007/978-981-10-5122-7_75

Impacts of laminin and polyethyleneimine surface coatings on morphology of differentiating human SH-SY5Y cells and networks

H. Teppola[1], J.-R. Sarkanen[2], T.O. Jalonen[1] and M.-L. Linne[1]

[1] Faculty of Biomedical Sciences and Engineering and BioMediTech Institute, Tampere University of Technology, Tampere, Finland
[2] Faculty of Medicine and Life Sciences, University of Tampere, Tampere, Finland

Abstract— **The viability and morphological differentiation of the neuronal cells are often enhanced by attachment on surface coating proteins or polymers. Laminin is a basal membrane protein and one of the matrix components in the nervous system. Polyethyleneimine is a positively charged polymer widely used for improving attachment of cell cultures. The aim of this study was to find a favorable surface coating for cultures of differentiating human SH-SY5Y cells in order to promote homogenous cell adhesion, neurite sprouting and formation of the complete network structure. Two surface coatings were examined; laminin and polyethyleneimine alone or when used together. The impacts of the coatings on morphology of undifferentiated or retinoic-acid and cholesterol differentiated human SH-SY5Y cells and networks were then assessed. In addition, the influence of coatings on the number of cell nuclei at 10 days *in vitro* was quantified. The morphological analysis of the study shows that laminin enables homogenous attachment and oval cell nuclei formation, whereas polyethyleneimine induces clusters of cells in form of multicellular spheroids. Furthermore, laminin supports branching of long neurites and neuronal network formation, whereas polyethyleneimine induces straight neurite bundles between the spheroids of differentiated human cells.**

Keywords— **Human SH-SY5Y, Laminin, Neuronal network, Polyethyleneimine, Surface coatings**

I. Introduction

The human SH-SY5Y neuroblastoma cell line, used in this study, is a subclone of SK-N-SH cell line isolated from a bone marrow of a 4-year-old female patient [1]. This cell line has been used as a model for neurodegenerative diseases, such as Parkinson's disease [2]. Moreover, the cell line can also be used as a model platform for testing therapeutic treatments, which could help to improve the prognosis for patients suffering from neuroblastoma [3]. For understanding the properties of the SH-SY5Y cell models, in general, the molecular, cellular and electrophysiological experiments are performed [4]. These cells are cultured on plastic or glass surfaces, for example on microelectrode array plates [5]. However, when cells are cultured on negatively charged or hydrophobic surfaces, challenges such as poor attachment rate, poor viability, and heterogeneous distribution of SH-SY5Y cells appear. Therefore, coating of the culture plate is important for improving the survival and network formation of these cells [6,7]. Proteins (such as laminin (LAM), collagen, fibronectin) [6,7], organic polymers (such as polyethyleneimine (PEI)) [8, 9] or synthetic polymers (such as polylysine or polyornothine) [9] are widely used as coating agents for cell cultures. LAM produced by astrocytes or Schwann cells is basal lamina glycoprotein in both central and peripheral nervous system [10] and known to be beneficial for cell adhesion [6,7]. PEI is a positively charged cationic polymer, which is widely used for improving cell attachment [8]. It has been shown to improve adhesion, migration, survival and maturation of cells [9]. Despite the wide use of these coatings e.g. for primary cell cultures, their impacts on morphology of differentiating human SH-SY5Y cells and network structure are yet not known.

We have previously shown that cholesterol (CHOL) supports retinoic-acid (RA) in inducing neuronal differentiation of the SH-SY5Y cells [3,11]. Based on our earlier studies we here use RA together with CHOL [RA+CHOL; RC] to differentiate the cells towards neuronal phenotype. In this study our aim is to investigate the influence of two surface coatings, LAM and PEI, either alone or together (PEI + LAM) on the morphology of the human SH-SY5Y neuroblastoma cells and network structure, as well as number of the nuclei of cells with and without differentiating agents (RC) at 10 days *in vitro* (DIV). We examine the positive and negative impacts of culturing the undifferentiated and differentiated SH-SY5Y cells on LAM and PEI surfaces. Our final goal is to find the optimal coating, which allows the differentiated neuroblastoma cells to form long branching neurites and ultimately functional neuronal networks.

II. Materials and methods

A. Preparation of surface coatings for culture dishes

Surface coatings were tested in aim to achieve the best cell attachment and neuronal type morphology of the neuroblastoma cells. Culture dishes were coated either with 0.1% polyethyleneimine solution (PEI; Sigma-Aldrich,

Steinheim, Germany), 0.002% laminin (LAM; L2020 mouse, Sigma), 0.1% PEI with 0.002% LAM or not coated for control purpose (CTRL). All coating agents were diluted in sterile distilled (DI) water. For PEI + LAM culture dishes were first incubated overnight with the PEI coating agent at 4 °C, extra coating liquid was removed by pipetting, and the dishes were rinsed three times with DI water. LAM was added and incubated one hour in room temperature and the extra liquid was then removed with pipet. Culture dishes were then used immediately.

B. Maintenance and differentiation of cell cultures

The human SH-SY5Y neuroblastoma cell line (CRL-2266; American Type Culture Collection, Manassas, VA, USA) was cultured and differentiated for 10 days as previously described [3,11]. Differentiation substances were applied with medium exchange at 1, 3 and 7 DIV. The cell growth, condition and morphology were observed under culture microscope (Olympus CK40) and images were taken with DP10 microscope digital camera system (Olympus, Tokyo, Japan) at 1, 3, 7 and 10 DIV.

C. Quantification of cell population attachment and growth

The substance-induced changes for the growth of the cell population in each coating and differentiation treatment group were quantified by counting the cell nuclei at 10 DIV. The nuclei were stained with 10µg/mL Hoechst 33258 (Sigma) as previously described [3]. Fluorescence of the nuclei was visualized with Nikon DS Camera Control Unit DS L-1. Images of each treatment group were analyzed with CellC analysis software [12]. The obtained nuclei count and statistics (see statistical analysis) were analyzed and plotted by using the MATLAB software (version 2013b, The Mathworks Inc., MA, USA).

D. Statistical analysis

Statistical analysis was performed using the One-way ANOVA in MATLAB. Detected differences were considered to be significant when $p < 0.01$ with ** in Fig. 3.

III. Results

A. LAM enables homogenous attachment and PEI induces multicellular spheroids of human SH-SY5Y cells

In the first part of this study the phase contrast images of the human SH-SY5Y cells at 1, 3, 7 and 10 DIV were visually analyzed for validation of the attachment and morphology of the cells on different surface coatings. Cells were found to be attached in all tested conditions; without coating, with LAM, with PEI and with PEI + LAM at 1 DIV (Fig. 1).

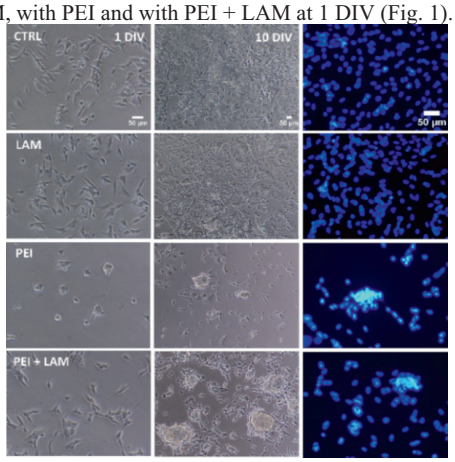

Fig. 1 Attachment and morphology of human SH-SY5Y cells on different surface coatings. Human cells attached in some extent without coating CTRL, with LAM, with PEI and with PEI+LAM on culture dishes at 1 DIV. Clusters of cells were observed when PEI or PEI + LAM coatings were used. The radii of MCSs increased over time and were greater when PEI + LAM were used. The cells covered homogenously the entire surface of CTRL and LAM coated dishes until 10 DIV. PEI and PEI + LAM induced uneven distribution of cell nuclei at 10 DIV (scale bar 50µM).

After 1 DIV attachment was more homogenous and widespread with LAM in comparison to PEI (Fig. 1). Multicellular spheroids (MCS) were observed with PEI alone or with PEI together with LAM coating beginning of the 3 DIV. MCSs were not observed with LAM coating or without coating, and cells were homogenously attached and with more triangular shape in comparison to cells cultured on PEI coated dishes (Fig. 1.).

B. LAM and PEI differently change the properties of neurites and multicellular spheroids of differentiated SH-SY5Y cells

In the second part of the study the morphology of the differentiated neuronal networks grown on surface coatings was assessed from phase contrast images of human SH-SY5Y cells and networks. Cells were grown on dishes without coating CTRL, with LAM, with PEI and with PEI+LAM and were treated with RA+CHOL (RC) and visually analyzed at 1, 3, 7 and 10 DIV. The impact of differentiation treatment with RC were seen in cultures grown on all surface coatings from beginning of the 3 DIV (Fig. 2). Long neurites growing between the cells and connecting cells to each other were observed in all conditions at 10 DIV (Fig. 2). LAM promoted branching of neurites with more varicosities in complete network

structures, in contrast to PEI, which induced straight bundles of neurites between MCS with no varicosities.

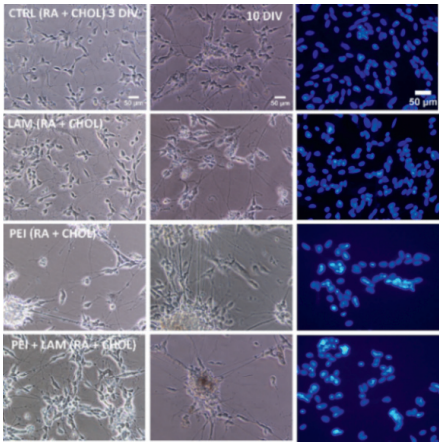

Fig. 2 The morphology of the differentiated human SH-SY5Y neuronal networks grown on different surface coatings. Cells were cultured and differentiated with RA+CHOL and grown in culture dishes without coating CTRL, with LAM, with PEI or with PEI+LAM until 10 DIV. Cells on CTRL and LAM dishes were well attached and had the appearance of healthy triangular cells with short neurites at 3 DIV. Cells grown on PEI coated dishes were more roundish in shape. Straight bundles of neurites grew between the MCS with PEI coating beginning of 3DIV. LAM promoted clear network structure with varicosities and branching neurites (scale bar 50µM).

C. LAM increases the level of differentiation, but does not eliminate the MCSs induced by PEI

In the third part of the study, the stained nuclei of both undifferentiated and differentiated human SH-SY5Y cell cultures were assessed at 10 DIV (Fig. 1 and 2). The undifferentiated nuclei were compact, roundish, and evenly distributed when grown on CTRL or on LAM coated dishes, though some nuclei with oval shape were also seen (Fig. 1). Oval nuclei shape indicates higher level of differentiation. PEI and PEI + LAM induced uneven distribution of nuclei (Fig. 1).

Data of cell nuclei grown in the presence of differentiation agents show that the RA and RA + CHOL treatments without coating and with LAM coating allow cells to form networks with long neurites and oval nuclei in shape, indicating neuronal differentiation. Furthermore, PEI or PEI + LAM coating induced uneven distribution of cells and often densely clustered nuclei (Fig. 2).

D. PEI, but not LAM, significantly decreases the number of nuclei

The capability of differentiation substances to inhibit the population growth of human SH-SY5Y cells and the inability of coating agents to induce attachment on culture surfaces can be measured as decreased nuclei number at 10 DIV. Differentiation and coating induced changes in the nuclei counts of cultures grown without coating and with RA, or RA + CHOL (RC), as well as of cultures with coatings and with RC in comparison to CTRL condition. Results of the differentiation study show that CHOL treatment alone did not inhibit cell population growth, which was seen when treated with RA, as well as with RC [$p < 0.01$ (**)] (Fig. 3). Interestingly, significant [$p < 0.01$ (**)] decrease in the number of cells was detected with PEI + RC and with PEI + LAM + RC, but not with LAM + RC when compared to RC treatment alone (Fig. 3). Results of coating show that significant [$p < 0.01$ (**)] decrease in the number of nuclei was detected when culture dishes were pretreated with PEI or with PEI + LAM in comparison to CTRL. With LAM this decrease was not detected (Fig. 3).

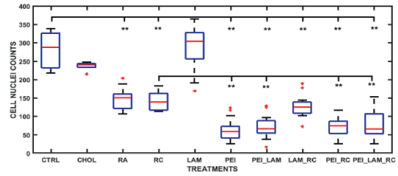

Fig. 3 PEI significantly decreases the number of nuclei with and without differentiation. Cells were cultured in CTRL condition (n = 7), and with CHOL (n = 6), RA (n = 23), RC (n = 11), and LAM (n = 19), LAM_RC (n = 18), PEI (n = 18), PEI_RC (n = 21), PEI_LAM (n = 18), and PEI_LAM_RC (n = 19) (n is the number of analyzed microscopy images) and the cell nuclei were counted at 10 DIV. Each differentiation agent is shown on the x-axis and the cell nuclei counts on the y-axis. The statistically significant differences ($p < 0.01$) are shown with *asterisks* (**).

IV. Discussion

In this study we show that in undifferentiated human SH-SY5Y cells at 10 DIV coating with LAM enabled homogenous and widespread attachment as well as partially oval cell nuclei. PEI coating induced multicellular spheroids (MCS) at the beginning of 3 DIV. The radii of MCSs increased over time and were greater in size when LAM was used together with PEI in comparison to PEI alone. This might be due to enhanced attachment by LAM. However, LAM was not capable to eliminate the PEI induced MCSs. In a recent study by Jung et al. (2013), MCSs have been induced by growing the RA-differentiated SH-SY5Y cells on an elastin-like polypeptide [13]. We here show for the first time the ability of PEI to induce MCSs in

the cultures of human SH-SY5Y cells. The MCS can be used as tools to assess the efficacy of e.g. chemo-, immuno-, and radio-therapy *in vitro* [13].

In addition to enhancing attachment LAM also promoted branching of long neurites and network structure. PEI, in contrast, induced straight neurite bundles between the MCSs of the RC differentiated human cells. These favorable coating results of LAM with RC differentiated SH-SY5Y cells are supported by an earlier study by Rossino et al. (1991), which shows, that RA induced up-regulation of the integrin alpha 1/beta 1 correlates with increased neurite extension in human neuroblastoma cells cultured on LAM coating [7]. This explains one of the possible mechanism for morphological differentiation of nerve cells. Interestingly, another study by Väänänen et al. (2006) shows that the tripeptide domain of gamma 1-LAM protects against 6-hydroxy-dopamine induced neurotoxicity by its inhibitory function on ionotropic glutamate receptors in rat model of Parkinson's disease [14]. All these results, together with our present study, suggest that LAM together with RC increases the neurite outgrowth. Also, these results support the suggestions of possible protection against neurotoxicity by LAM, particularly in the human SH-SY5Y model of Parkinson's disease [14]. In the future, electrophysiological characteristics of differentiated human SH-SY5Y cell networks grown on laminin coated surfaces could be studied with microelectrode array system as *in vitro* human cell model for neurodegenerative diseases.

V. Conclusions

This study shows that LAM enables homogenous and widespread attachment of undifferentiated human SH-SY5Y cells in culture. PEI when used alone or together with LAM induces MCSs which may be used as tools to assess the efficacy of e.g. chemo-, immuno-, and radio-therapy *in vitro*. LAM supports branching of long neurites and ideal network structure, in contrast to PEI, which induces straight neurite bundles between the MCSs of RA and CHOL differentiated human cells. Results indicate that LAM when used alone as coating agent increase the level of differentiation particularly of the RC differentiated human SH-SY5Y cells. When LAM is used together with PEI, it does not eliminate the MCSs.

Acknowledgment

The authors thank the Doctoral School of Tampere University of Technology, Finnish Foundation for Technology Promotion, Finnish Cultural Foundation and Pirkanmaa Regional Fund for financial support and Professor Timo Ylikomi for providing research facilities.

Conflict of Interest

The authors declare that they have no conflict of interest.

References

1. Biedler JL, Helson L, Spengler BA (1973) Morphology and growth, tumorigenicity, and cytogenetics of human neuroblastoma cells in continuous culture. Cancer Res. 33(11):2643-52.
2. Korecka JA, van Kesteren RE, Blaas E et al. (2013) Phenotypic characterization of retinoic acid differentiated SH-SY5Y cells by transcriptional profiling. PLoS One. 28;8(5):e63862. DOI 10.1371/journal.pone.0063862
3. Teppola H, Sarkanen J-R, Jalonen TO & Linne M-L (2016) Morphological differentiation towards neuronal phenotype of SH-SY5Y neuroblastoma cells by estradiol, retinoic acid and cholesterol. Neurochemical Research 41:731–747 DOI 10.1007/s11064-015-1743-6
4. Meyer R & Heinemann SH (1998) Characterization of an eag-like potassium channel in human neuroblastoma cells. *The Journal of Physiology*, *508*(Pt 1), 49–56 DOI 10.1111/j.1469-7793.1998.049br.x
5. Shenai MB, Putchakayala KG, Hessler JA et al. (2004) A novel MEA/AFM platform for measurement of real-time, nanometric morphological alterations of electrically stimulated neuroblastoma cells. IEEE Trans Nanobioscience 3(2):111-7
6. Jousimaa J, Merenmies J, Rauvala H (1984) Neurite outgrowth of neuroblastoma cells induced by proteins covalently coupled to glass coverslips. Eur J Cell Biol 35(1):55-61
7. Rossino P, Defilippi P, Silengo L et al. (1991) Up-regulation of the integrin alpha 1/beta 1 in human neuroblastoma cells differentiated by retinoic acid: correlation with increased neurite outgrowth response to laminin. Cell Regul. 2(12):1021-33
8. Vancha, AR, Govindaraju S, Parsa KV et al. (2004) Use of polyethyleneimine polymer in cell culture as attachment factor and lipofection enhancer. BMC Biotechnology, 4, 23. DOI 10.1186/1472-6750-4-23.
9. Lelong IH, Petegnief V, Rebel G (1992) Neuronal cells mature faster on polyethyleneimine coated plates than on polylysine coated plates. J Neurosci Res. 32(4):562-8
10. Liesi P (1985) Laminin-immunoreactive glia distinguish regenerative adult CNS systems from non-regenerative ones. EMBO J. 4(10):2505
11. Sarkanen J -R, Nykky J, Siikanen J et al. (2007) Cholesterol supports the retinoic acid-induced synaptic vesicle formation in differentiating human SH-SY5Y neuroblastoma cells. J Neurochem. 102(6):1941-52
12. Selinummi J, Sarkanen J-R, Niemistö A et al. (2006) Quantification of vesicles in differentiating human SH-SY5Y neuroblastoma cells by automated image analysis. Neurosci Lett. 27;396(2):102-7
13. Jung GS1, Lee KM, Park JK et al. (2013) Morphogenetic and neuronal characterization of human neuroblastoma multicellular spheroids cultured under undifferentiated and all-trans-retinoic acid-differentiated conditions. BMB Rep.46(5):276-8
14. Väänänen AJ, Rauhala P, Tuominen RK et al. (2006) KDI tripeptide of gamma1 laminin protects rat dopaminergic neurons from 6-OHDA induced toxicity. J Neurosci Res. 15;84(3):655-65.

Author: Heidi Teppola
Institute: Tampere University of Technology
Street: Korkeakoulunkatu 10, 33720
City: Tampere Country: Finland
Email: Heidi.teppola@tut.fi